Application of new crystallization approaches and serial crystallography to the structural study of enzyme/tRNA complexes

Raphaël de Wijn

UNIVERSITÉ DE STRASBOURG

ÉCOLE DOCTORALE DES SCIENCES DE LA VIE ET DE LA SANTÉ

CNRS – IBMC UPR 9002

THÈSE présentée par :

Raphaël DE WIJN

soutenue le : **14 décembre 2018**

pour obtenir le grade de : **Docteur de l'université de Strasbourg**

Discipline/ Spécialité : Biologie Structurale

Application des nouvelles approches de cristallisation et de cristallographie sérielle à l'étude structurale de complexes enzymes : ARNt

THÈSE dirigée par :

M SAUTER Claude	Directeur de recherches, Université de Strasbourg

RAPPORTEURS :

Mme CZJZEK Mirjam	Directrice de recherches, Sorbonne Université
Mme SCHMITT Emmanuelle	Directrice de recherches, École Polytechnique

---

AUTRES MEMBRES DU JURY :

M RENAUD Jean-Paul	Directeur de recherches, Université de Strasbourg

À mes parents, ma sœur et Teuteu qui aurait été fière...

Remerciements / acknowledgments

La fin de ma thèse c'est la fin d'une très belle période. C'est difficile de remercier correctement tous ceux qui ont contribué à ces trois ans et j'espère n'oublier personne. Tout d'abord parce que sans eux je n'aurai pas fait ma thèse et mon parcours universitaire à Strasbourg, Claude et Joern.

Claude merci de m'avoir fait découvrir le domaine formidable qu'est la biologie structurale. Tu as été génial en directeur de thèse (beaucoup de gens qui t'ont eu en cours et en travaux pratiques de par-delà le monde auraient aimé t'avoir XD). Tu m'as soutenu, laissé expérimenter, donné des responsabilités, confiance en moi, permis d'encadrer plusieurs stagiaires et d'énormément voyager :D. Merci beaucoup pour tout ça.

Joern, toi qui a commencé comme mon directeur de licence et qui est aujourd'hui mon ami, merci. Pour ces huit années de soutien, d'accompagnement, m'avoir permis de rencontrer tous ces autres étudiants franco-allemand et Erasmus, pour la confiance que tu as en moi et ces repas ensemble avec Joël et Valérie, merci beaucoup.

Maman, papa et frangine, avoir un soutien sans faille de votre part m'a été important pendant ces trois ans et plus généralement tout au long de mes études. Vous m'avez toujours motivé à en faire plus et été prêt à m'aider si j'en avais besoin. Merci. Bien sûr aussi le fort soutien familial plus général : Zina, Pascale, Gratata, Großvater, Ulrike, Monika und alle. Merci, danke. Pour notamment toutes les fois où je suis reparti de chez vous avec des tupperwares pleins de nourriture, car oui bien manger c'est important :D.

Marta et José, alalalalala notre trio de choc ! On est devenu si proche en deux ans ! On a atteint un niveau de confiance et de complicité assez exceptionnel, nos moments ensemble sont mémorables XD Vous m'avez aidé à arriver au bout de l'écriture, merci pour votre soutien et motivation sans faille ;).

Merci à beaucoup de personnes dans le labo et autour. Tout d'abord Magali pour m'avoir permis de m'intégrer à ton équipe si facilement en cours de thèse, Joëlle, Anne et Caroline pour vos conseils et votre aide (et j'en ai souvent eu besoin pour mes manips au 4ème, notamment pour mes purifs !), Bernard pour nos discussions sur tout et le puits de connaissance sans fond que tu es, Cédric depuis notre mission SAXS

ensemble, Elena et Tina pour la première année de ma thèse qu'on a passé ensembles, nos stagiaires Nicola, Justine, Léa et Kevin, même si toi c'est bon tu as « level up » (d'ailleurs je compte sur toi pour la relève ;)), qui vous êtes mélangés à nos soirées doctorantes.

Je veux aussi remercier nos supers collaborateurs qui sont impliqués dans une grande part de cette thèse. Oliver, Heike und Mario, danke für den schönen Aufenthalt in Leipzig und für alles, was wir zusammen geschafft haben! Jennifer R. pour nos formations passées ensemble, nos danses et ce run PX2. Sylvain et Eric pour m'avoir fait découvrir et permis d'expérimenter avec votre bébé, Xo4.

Enfin mes amis depuis tant d'années Tobias, Jenny, Marie, Marine, Paul, Caroline, Akira et tant d'autres, vous êtes géniaux ! Toujours présents quand j'en avais besoin, ou pour passer du bon temps ensembles. On a fait des trucs de fous, est partis à l'autre bout du monde ! Merci !

Pour terminer toutes les personnes de l'unité pour m'avoir accueilli toujours dans la bonne humeur dans cette grande maison qu'est l'IBMC et particulièrement Danièle et Léandra, pour votre aide administrative lors de cette thèse et tous ces ordres de mission que vous m'avez préparé XD.

Merci à tous !

Table of contents

Tables list

Figures list

I. Introduction

1 Macromolecular crystallography

1.1 History of crystallography

To start this historical introduction, the term “crystallography” should be defined. It was first introduced in the 18th century by the Swiss savant Maurice-Antoine Capeller as the study at the atomic scale of substances able to form crystals[1]. The word itself is based on the Latin *crystallus* for crystal and *graphie* for writing. The crystal order was later defined by the French physicist Auguste Bravais in the 19th century as a repetition, by translation, in three dimensions of an elementary motif. He is known for the conception of Bravais lattices and the formulation of Bravais law. The next major event was the discovery of a fundamental element of X-ray crystallography: X-rays, discovered by the German physicist Wilhelm Conrad Röntgen in 1895. The German physicist Max von Laue later discovered X-ray diffraction by crystals and was awarded a Nobel Prize in 1914. This event was commemorated in 2014 by the International Year of Crystallography (IYCr2014) by the United Nations to emphasize the importance of crystallography in physics, chemistry and medicine. Laue’s award was directly followed by the Nobel Prize to William Henry and William Lawrence Bragg in 1915 for “their services in the analysis of crystal structure by means of X-rays”. In a non-exhaustive list, several works in crystallography have contributed substantially to the biological field: the first diffraction pattern of a protein crystal (pepsin) by Dorothy Crowfoot Hodgkin and John Desmond Bernal in 1934 (Bernal & Crowfoot, 1934), the elucidation of the double-helix structure of DNA by Rosalind Franklin, Francis Crick and James Watson in 1953 (Watson & Crick, 1953) and the first protein structures (myoglobin and hemoglobin) elucidated by X-ray crystallography by John Kendrew and Max Perutz in 1958-60 (Kendrew et al. 1958; Perutz et al. 1960). In the field of protein synthesis or translation, crystallography also contributed to the understanding of the process by elucidating several important structures. Among them are the structure of the first tRNA, aminoacyl-tRNA synthetase and CCA-adding enzyme, a tRNA maturation enzyme. They were respectively solved by groups headed by Alexander

[1] https://www.afc.asso.fr/qu-est-ce-que-la-cristallographie/histoire

Rich and Aaron Klug in parallel in 1973-74 (Kim et al. 1973; Robertus et al. 1974), Irwin in 1976 (Irwin et al. 1976) and Thomas Steitz in 2002 (Li et al. 2002). More recently, the Nobel Prize 2009 was awarded for “studies of the structure and function of the ribosome” to Venkatraman Ramakrishnan, Thomas Steitz and Ada Yonath. All these discoveries are summarized in **Figure 1-1**.

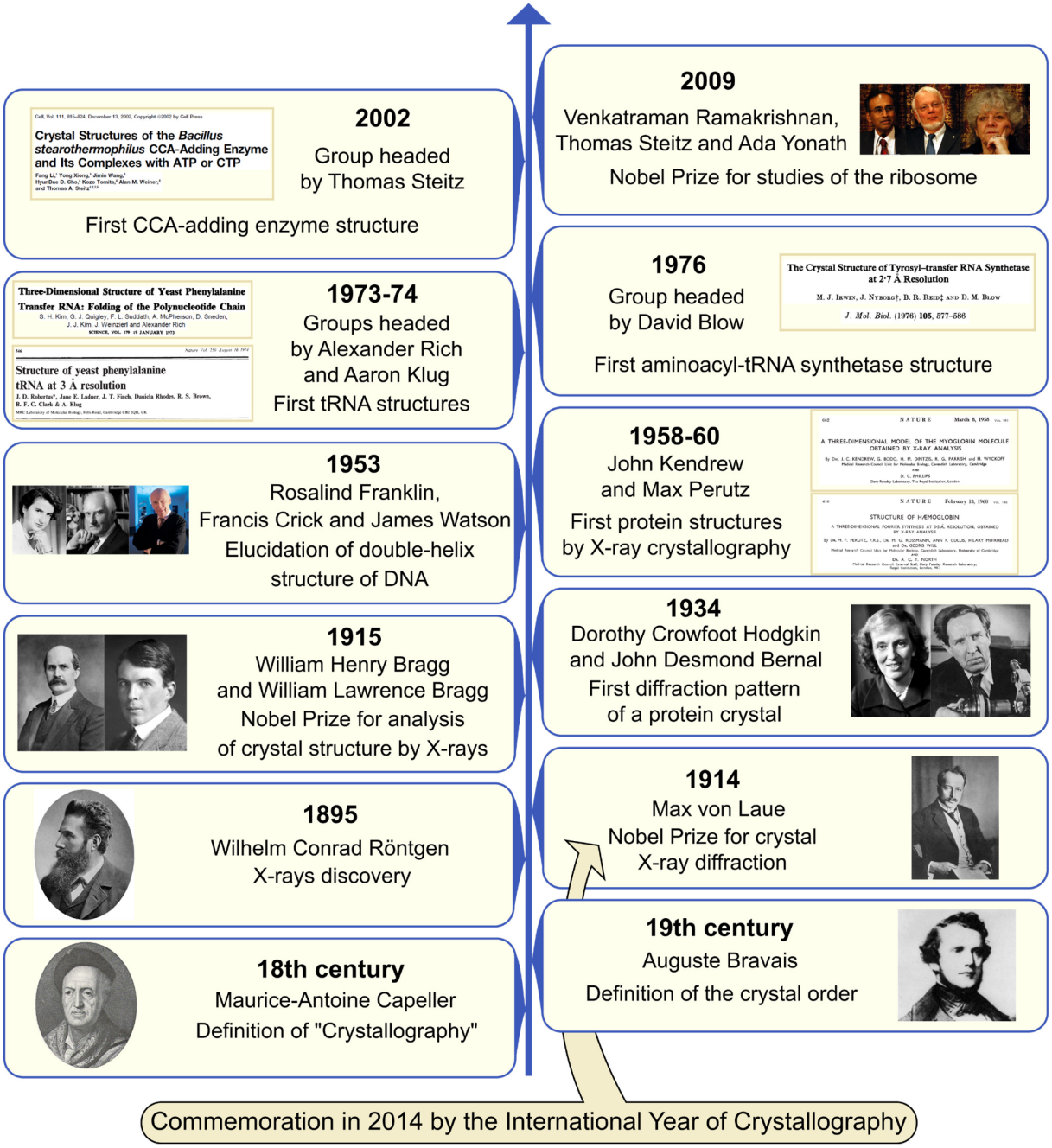

Figure 1-1 : Chronology of selected discoveries related to X-ray crystallography. Pictures are all in the public domain or from Wikipedia.

Since more than half a century, macromolecular crystallography is the method of choice for structural characterization of biological macromolecules, fundamental and applied research, such as drug development. At the end of summer 2018, the worldwide repository Protein Data Bank (PDB) contained more than 140,000 deposited structures of proteins and nucleic acids, with more than 80% determined by X-ray crystallography. As of today, crystallography is involved in a great variety of disciplines: physics, chemistry, mathematics, biophysics, biology, medicine, material sciences, metalworking industry and earth sciences. It finds applications in almost all scientific fields. When crystals are available, X-ray crystallography is the quickest and most powerful method for structural analysis. A complete dataset can nowadays be collected within minutes, if not seconds, resolutions down to 0.48 Å are accessible with proteins, as for crambin (Schmidt et al. 2011) or for an iron-sulfur protein (Hirano et al. 2016), and structures of high molecular weight macromolecules can be elucidated, such as the ribosome.

Crystallogenesis was recently introduced as the discipline which focuses on crystal growth. The aim of this discipline is not only to grow crystals for analysis but also to understand the processes involved behind crystal growth and nucleation, in order to better control them. This field is multidisciplinary and brings together specialists from various fields such as physicists, chemists and biologists. The fathers of crystallogenesis are Richard Giegé and Alexander McPherson, well known for their respective reference books, “Crystallization of Nucleic Acids and Proteins” (Ducruix and Giegé 1992) and “Introduction to Macromolecular Crystallography” (McPherson 2009).

1.2 Crystallographic analysis

The structural analysis by crystallography of a macromolecule, defined as proteins, nucleic acids and their complexes, includes several steps: purification, crystallization, X-ray analysis and 3D structure determination. As illustrated in **Figure 1-2**, the first step in a structural study of a biological macromolecule by crystallography is the production, purification and quality control of the sample of interest. By quality is meant the assessment of purity and integrity, homogeneity, activity and stability in solution, parameters which were shown to be critical in crystal formation (Giegé et al.

1986; Raynal et al. 2014). These are usually assessed by the use of diverse and complementary methods e.g. SDS-PAGE, Dynamic Light Scattering (DLS), Size Exclusion Chromatography (SEC) and activity assay. The way to obtain crystals is still nowadays mostly empirical and therefore the result of trial and error experiments. Hundreds of combinations of diverse crystallizing agents, buffers at different pH and additives, are tried in a variety of methods, from simple batch, vapor diffusion to counter-diffusion. But trying more crystallization conditions, beyond a few hundreds, does not necessarily increase in the number of useful hits (Newman et al. 2005; Newman 2011). Instead, complementary and/or advanced methods have been developed to facilitate crystal detection, to increase success rate at screening stage or to study the formation of nuclei to select conditions favoring crystallization, such as trace fluorescent labeling (TFL) (Pusey et al. 2015), microseed matrix screening (MMS) (D'Arcy et al. 2007, 2014), microfluidic chips (Pinker et al. 2013) or the use of Tb-Xo4 (Engilberge et al. 2017). These methods will be presented and discussed in this thesis.

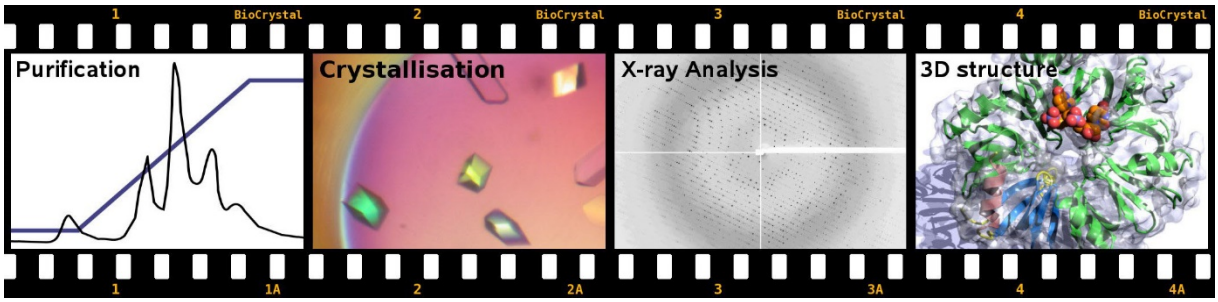

Figure 1-2 : Illustration of the four major steps in the structural study by crystallography of a biological macromolecule: purification, crystallization, X-ray analysis and 3D structure determination (adapted from Claude Sauter).

X-ray analysis of the crystals can then be performed with several types of instrumentations: laboratory diffractometers (in-house sources) using rotating-anodes, microfocus sealed tube or the metal-jet technology as X-ray sources (Skarzynski 2013) or bigger infrastructures like synchrotrons or X-ray free electron lasers (XFEL). This step consists of collecting hundreds to thousands of diffraction images while the crystal is rotated in the X-ray beam.

The final step, 3D structure determination, is then performed thanks to the use of a combination of program packages running on personal computers or web-servers, for example XDS (Kabsch 2010), PHENIX (Adams et al. 2010) or CCP4 (Winn et al. 2011) which enable the processing of diffraction data, then structure solution, refinement and analysis.

Two main bottlenecks in this workflow are first the determination of reproducible crystallization conditions and second the conditioning of crystals for X-ray analysis. Partial solutions and helps lie in the use of unconventional methods or devices. Some of them will be discussed in this thesis, and involve microfluidic chips ChipX, the Xtal Controller instrument, or advanced nucleation methods.

1.3 Phase diagram

The process of crystallization can easily be visualized using a phase diagram. The phase diagram shown **Figure 1-3** represents the state of a macromolecule in a solution and is usually represented by a 2D scheme, with the crystallizing agent concentration on the X-axis and the macromolecule concentration on the Y-axis. The diagram contains two areas separated by the solubility curve: the soluble zone under the curve where the macromolecule is undersaturated and fully soluble, and the supersaturated region above the curve, in which the macromolecule is in a thermodynamical unstable state being in excess and pushed to leave the solution. The latter region can be divided in three zones: (i) the metastable zone, where supersaturation is low, not high enough to cross the energy barrier and form nuclei (see section 1-4-1), (ii) the nucleation zone, where supersaturation is sufficient to induce ordered clusters, nuclei, of proteins to form in the solution, and (iii) the precipitation zone, where supersaturation reached such a high level that macromolecules will rapidly aggregate in a non-ordered manner. The actual pathway through the phase diagram for crystallization admitted by the scientific community consists in crossing the solubility curve to reach the nucleation zone, to form a nucleus, before driving the system back to the metastable zone for crystal growth.

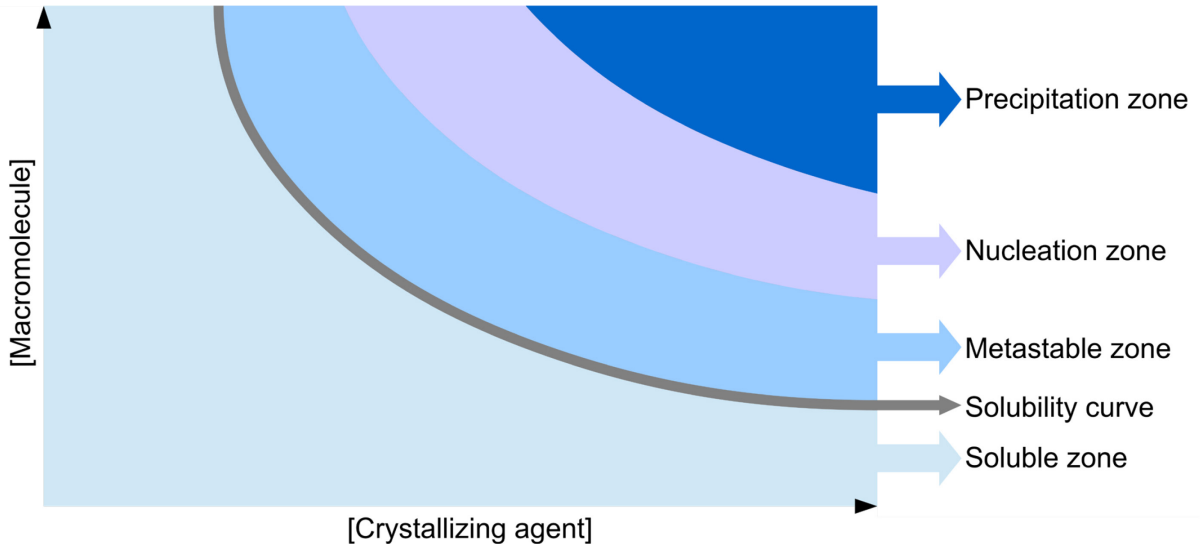

Figure 1-3 : Schematic representation of the salting-out phase diagram. The X and Y-axis represent the crystallizing agent and macromolecule concentrations, respectively. Each color represents a different zone indicated on the right, as well as the solubility curve.

The first condition needed for crystallization is to reach a supersaturation state by crossing the solubility curve. This is possible by increasing either molecule or crystallant concentrations, or both at the same time. The macromolecule solubility curve can be shifted by environmental conditions, such as pH, temperature or contaminants in solution. In the supersaturated state, the solution will not remain homogeneous (Asherie 2004). Small chemicals, e.g. inorganic salts, will crystallize after only an increase of supersaturation of few percents, in opposition to biological macromolecules, which need to exceed the solubility from hundred to a thousand percent (Chernov 1997), to reach high supersaturation and high nucleation rate probability to ensure crystallization in a reasonable amount of time. This fact is observable by the rapid and regular growth of salt crystals during crystallization trials with biological macromolecules. To avoid accumulation of a too high number of nuclei and no observable crystal (due to their small size), the solution then needs to enter back the metastable zone. This movement is made possible by the reduction of the number of molecules available in the solution following nucleation and the start of crystal growth. In this zone, a lower supersaturation prevents the formation of new nuclei but still allows the growth of existing nuclei in observable crystals.

In the following, the description of the phase diagram and of crystallization techniques will be limited to the ones which are relevant for biological macromolecules, such as proteins and nucleic acids.

1.4 Macromolecular crystallization process

1.4.1 Nucleation

Three steps in macromolecular crystals formation are widely accepted: nucleation, crystal growth and termination. The first often being considered as the most limiting, the second is important for crystal quality and the last for final crystal size (McPherson and Kuznetsov 2014). How nucleation occurs is still controversial and no unique model is applicable to every crystallization experiments. The first model is the classical nucleation theory, or one-step nucleation pathway (**Figure 1-4**), which was firstly described in 1926 (Volmer and Weber 1926) and adapted for macromolecule crystal nucleation in 1935 (Stranski and Kaischew 1935).

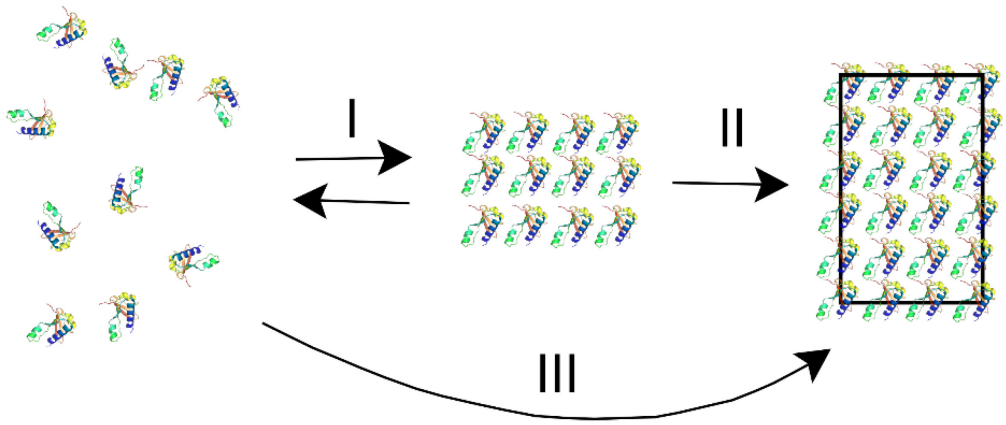

Figure 1-4 : Classical nucleation theory or one-step nucleation pathway for macromolecular crystals. The roman numerals represent state transitions, the box represents a growing crystal.

In this classical nucleation theory, small reversible clusters are formed in supersaturation conditions (I). As long as they do not exceed a certain critical size,

they remain transient and prone to dissolve. If they exceed this size, they will grow into crystals (II), alimented by soluble macromolecules (III) or even aggregates.

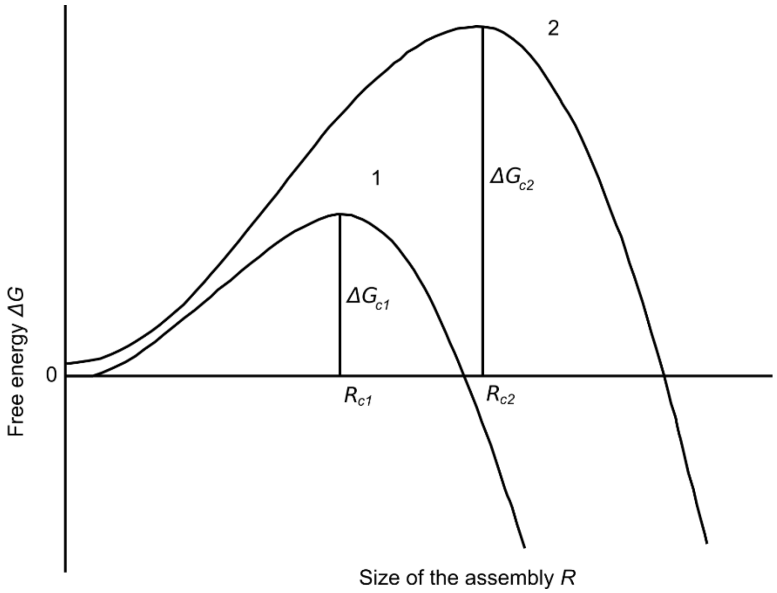

Figure 1-5 : Graphical representation of the supersaturation implication in the one-step nucleation process. The X-axis represents the radius R of the molecular assemblies forming in solution and the Y-axis the free energy ΔG for formation of the crystalline assembly. R_c represents the critical size for formation of a crystalline assembly at a given supersaturation, ΔG_c the free energy at R_c. At higher supersaturation (situation 1) the induction energy and critical nucleus size are smaller than at lower supersaturation (situation 2).

In the supersaturated zones, macromolecules will form assemblies of different types, which form and dissolve at different rates, depending on the supersaturation level. The radius R of these assemblies must reach a critical size, called here R_c, at which further assembly, and thus crystal growth, will be energetically more favorable than remaining in solution (**Figure 1-5**). Crystal formation is dependent on supersaturation state and speed in which supersaturation is reached (García-Ruiz 2003). To illustrate this dependency on the supersaturation level, a high supersaturation (1) and a low supersaturation states (2) are indicated in **Figure 1-5**. At higher supersaturation (1), a smaller minimum size R_{c1} and a lower free energy ΔG_{c1} is needed to transform an amorphous assembly, or cluster, into a crystalline one.

A second model is the two-step nucleation pathway (**Figure 1-6**). In this model, a metastable intermediate phase, or MIP (I), forms in the supersaturated solution before formation of a more ordered nucleus inside the MIP (II). This nucleus will then grow with the help of the surrounding macromolecules from the MIP (III) and from the soluble ones (IV).

This two-step pathway was observed in the nucleation of several protein crystals, among which are the lumazine synthase (Olga Gliko et al. 2005) or the beta-lactoglobulin (Sauter et al. 2015). Until now, there is no evidence that both theories could not coexist.

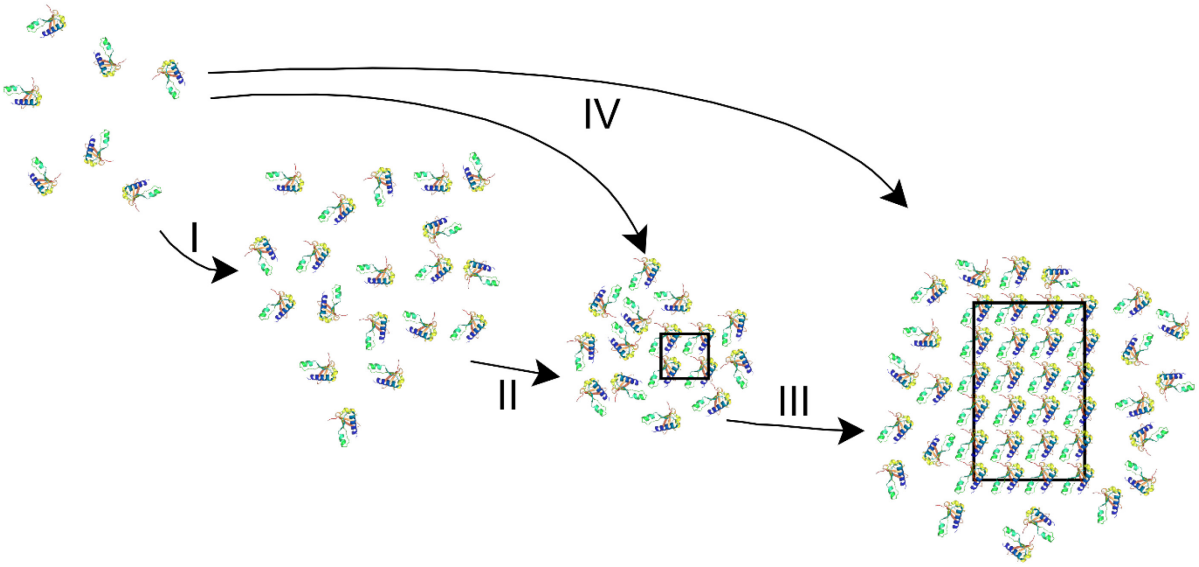

Figure 1-6 : Two-step nucleation pathway for macromolecular crystals. The roman numerals represent state transitions, boxes represent a nuclei or a growing crystal.

A method of choice to observe nucleation, early crystal growth and compare the effect of different crystallant solutions is dynamic light scattering and will be presented latter.

1.4.2 Growth and termination

Crystal growth and termination are more defined and accepted in the community. Atomic force microscopy (AFM) was introduced to study crystal growth *in situ*. It allowed the visualization of biological crystal growth in layers and revealed two

distinct mechanisms: tangential and face normal growth (**Figure 1-7**). Tangential growth occurs at the edge of existing layers and is responsible for their extension over the crystal surface. Face normal growth consists of the deposition or the formation of a new nucleus on an existing layer (or crystal face). This second mechanism must overcome an energy barrier, and thus, is limiting in comparison to tangential growth (reviewed in McPherson and Kuznetsov, 2014).

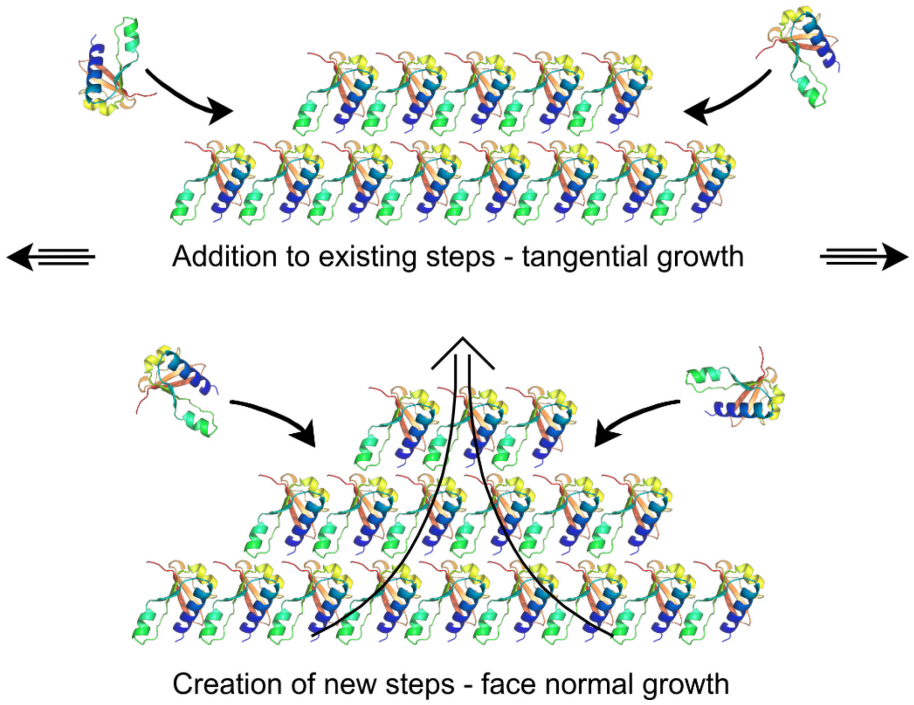

Figure 1-7 : Representation of the two crystal growth ways: tangential and face normal growth (adapted from McPherson and Kuznetsov, 2014).

An additional tangential growth mechanism was described and is called screw dislocation (McPherson et al. 2003). This mechanism is presented in **Figure 1-8** and based on the growth of an existing layer but in a circular manner due to a dislocation. This results in a continuous layer growing on itself.

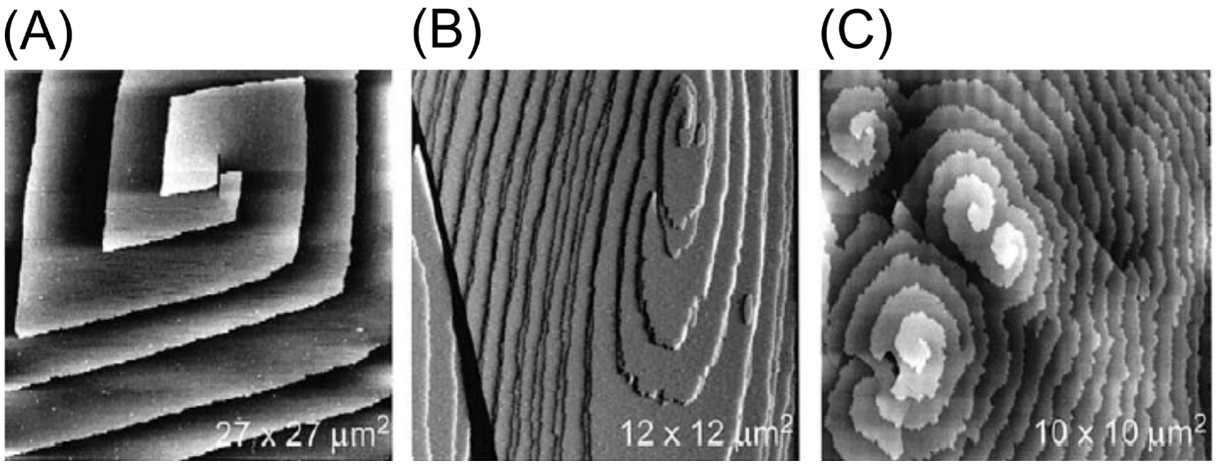

Two reasons are presented in the literature (McPherson et al. 2001) to explain termination of growth of a macromolecule crystal. First, the reduction of molecules available in solution as they are massively joining the growing crystal. Their concentration in solution drops to a point where it is no longer sufficient to sustain crystal growth. In other words, the system will leave the supersaturated zone and reach the thermodynamic equilibrium on the solubility curve. Second, the accumulation of impurities, in form of denatured molecules, aggregates or foreign molecules, at the surface of the growing crystals, a phenomenon known as face poisoning. The first case, the limited availability of macromolecules can be easily solved by constantly providing new macromolecules to the solution. In opposition, the second case is more difficult to solve, but it was shown by McPherson *et al*. in 2001 to be feasible by scraping the surface of a crystal and thus reviving its growth.

Macromolecule crystals are very fragile, they easily break when touching them and are sensible to temperature and pH. One of the main reasons for this is their high solvent content. Crystals of macromolecules exhibit solvent content between 30% and 80% in most cases, with the majority around 50% (Weichenberger et al. 2014, 2015). This solvent content is mostly due to the irregular form of macromolecules, not allowing a very tight crystal packing and the low amount of direct crystal stacking contacts between macromolecules. Additional contacts are performed via water molecule bridges.

1.5 Macromolecular crystallization methods

To induce crystal growth, several crystallization methods are available. The principle of the usual crystallization techniques and their expected pathways through the phase diagram are described in **Figure 1-9** and **Figure 1-10**.

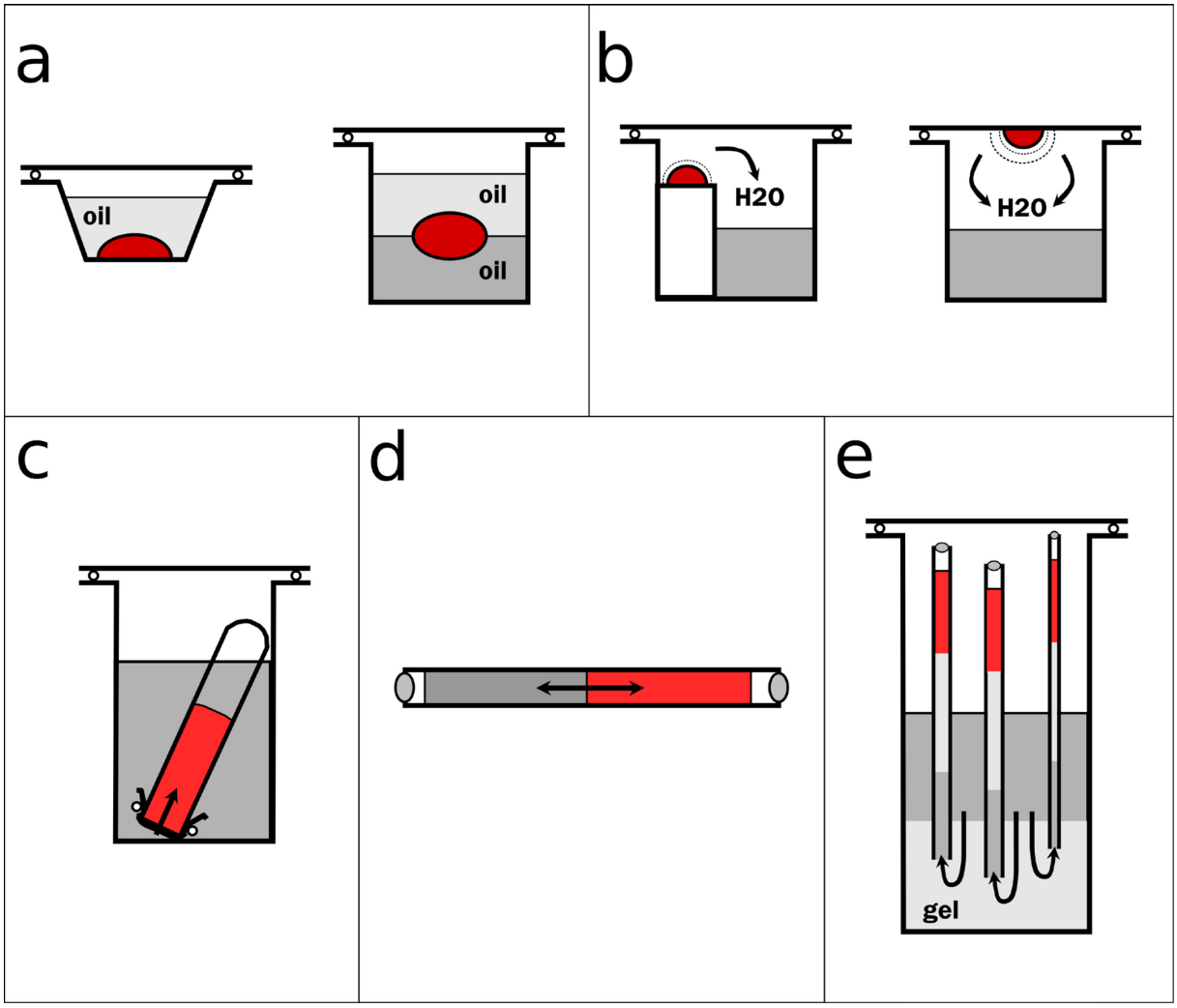

Figure 1-9 : Schematic representations of usual crystallization techniques: a) batch, b) vapor diffusion, c) dialysis, d) free-interface diffusion (FID) and e) counter-diffusion. The red compartments represent the macromolecular solutions, the grey ones the crystallizing agent solutions (excepted when indicated) (adapted from Sauter *et al.*, 2001).

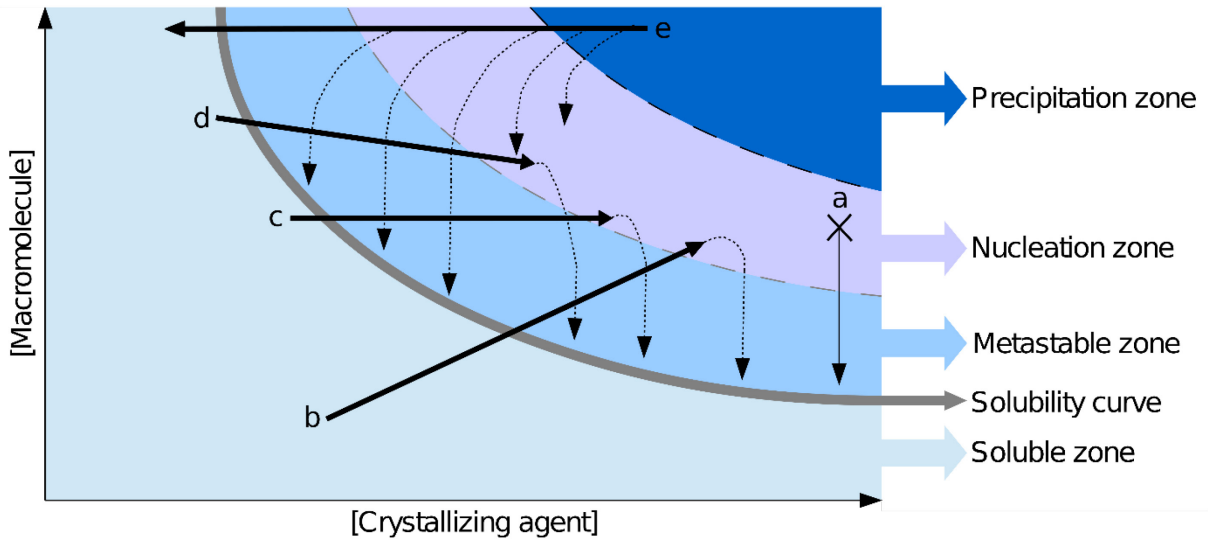

Figure 1-10 : Schematic representation of crystallization trajectories in the phase diagram. The X and Y-axis represent crystallizing agent and macromolecule concentrations, respectively. Colors represent different zones indicated on the right and the solubility curve separates the under- and supersaturated regions. Each pathway in the diagram is associated with a letter, which refers to a crystallization technique: a) batch, b) vapor diffusion, c) dialysis, d) free-interface diffusion and e) counter-diffusion.

The batch method (a) is the easiest one. It consists in mixing the macromolecule solution with the crystallization agent. The mix is incubated until crystal growth is observed. The associated pathway in the phase diagram is very simple: if the nucleation zone was reached by the mix, the solution will travel down the Y-axis as the drop volume remains constant but macromolecules will leave the soluble phase. If no supersaturated zone was reached, the mix will stay soluble and no evolution will occur. Vapor diffusion (b) is the most widely used method. It allows a gradual concentration of the drop, which is a mix of the macromolecule and crystallization agent solutions. This concentration occurs in a closed environment and is induced by the diffusion of water from the drop to the reservoir. This diffusion is explained by the differences of crystallization agent concentration (and related vapor surface tension) between the drop and the reservoir. In the phase diagram, this method will result in an increase along both X and Y-axis (as the drop volume goes down in most cases) and travel towards the supersaturated zones, where aggregates or nuclei will form. In dialysis (c), a membrane with calibrated pores only permeable to the crystallizing agent is used to separate the macromolecule and the reservoir solutions. As the solution volume

remains constant and only the crystallizing agent concentration can increase, the movement in the phase diagram will be horizontal until nucleation is reached. In the diffusion at the interface (d), or free interface diffusion (FID), both macromolecule and crystallizing agent solutions are brought into contact in a recipient small enough to avoid convection. In this condition, both solutions will gently mix by diffusing towards each other through a virtual interface. In opposition to dialysis, the macromolecule concentration will diminish (as the volume is increased) and crystallization agent concentration will increase. This will be characterized in the phase diagram by an increase in the X-axis and a decrease in the Y-axis into the supersaturation zones. The last method described here is counter diffusion (e). It requires a long capillary to create a gradient of crystallizing agent concentration and of supersaturation along the recipient by diffusion, thus continuously scanning different conditions. One capillary may be equivalent to many drops in batch or vapor diffusion. Several trajectories generated by the gradient along the capillary are represented in the phase diagram for this technique. Among counter-diffusion setups, one can mention crystallization chips including the microfluidic chips ChipX developed by Claude Sauter (Pinker et al. 2013) which will be described later in this thesis.

There are practical advantages that make some methods more widely used, such as vapor diffusion thanks to its easy up scaling in terms of number of assays. However, in some cases it is interesting to combine several of them and this case will be illustrated below in chapter III.

2 Advanced crystallization techniques

As presented above, crystallization of a macromolecular target is still nowadays the result of a trial and error experiments. In the history of bio-crystallography, methods were developed to increase crystallization success rate, crystal size and quality, and efforts were made to find a universal crystallizing agent. Some methods aim at favoring nucleation in solution, such as the use of the nucleant Tb-Xo4 (Engilberge et al. 2017), nanoporous materials (Shah et al. 2012) or crystallization assays exploiting an unconventional environment like agarose gel (Lorber et al. 2009), counterdiffusion (García-Ruiz 2003; Otálora et al. 2009), microfluidic (Sauter et al. 2007) or microgravity (Ng et al. 2002; Vergara et al. 2005). Other methods are based on the transfer of existing nuclei or crystal pieces in a fresh crystallization assay to favor crystal growth in the new solution, such as the use of animal hairs (cat, horse, human) or microseed matrix screening (MMS) (D'Arcy et al. 2007, 2014). In addition to favor nucleation or crystal growth, methods were also developed to make detection of nucleation events or crystals easier, such as depolarized dynamic light scattering (DDLS) (Schubert et al. 2015), as well as to facilitate discrimination between salt and protein crystals, for example by the use of trace fluorescent labeling (TFL) (Pusey et al. 2015).

2.1 Methods to favor nucleation and crystal growth

2.1.1 The Tb-Xo4 molecule

The lanthanide complex called "crystallophore" (Xo4) containing terbium (Tb) is a small molecule which presents several advantages in a crystallography study: it is a powerful phasing agent thanks to Tb anomalous properties, it acts as a nucleating agent by building bridges between proteins, and can be detected under UV-illumination to better distinguish macromolecule crystals (Engilberge et al. 2017).

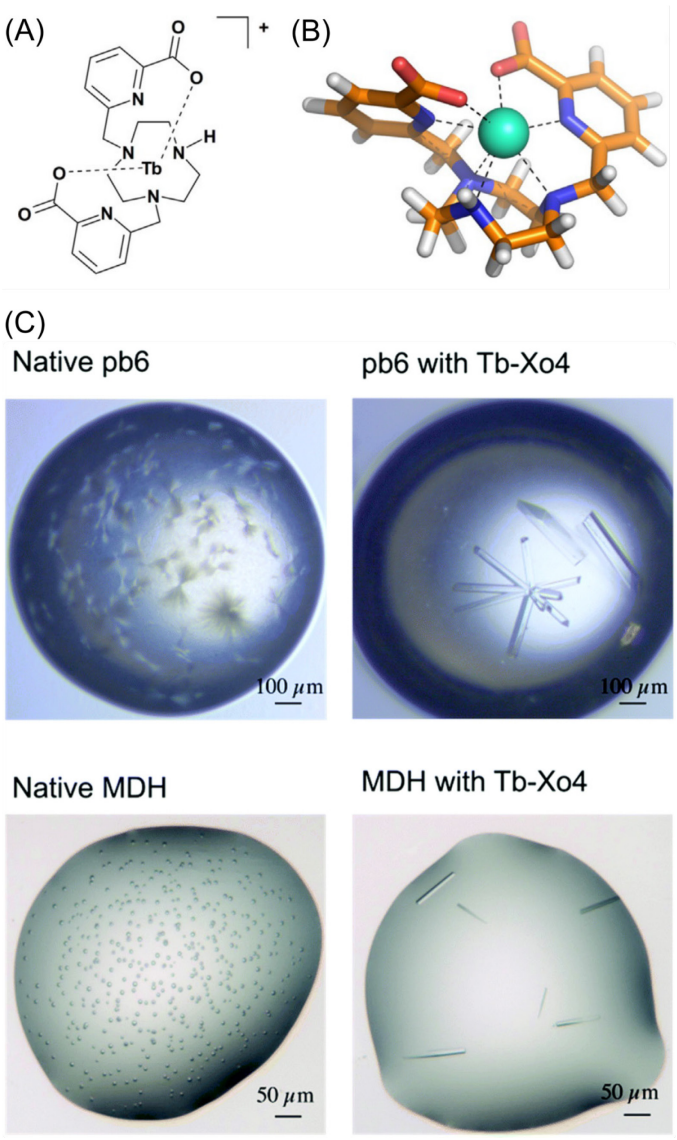

Figure 2-1 : The nucleant Tb-Xo4 and its effect on crystallization. A) Chemical structure of Tb-Xo4. B) 3D representation of Tb-Xo4. C) Comparison of crystal size and habit under strictly similar conditions for the two proteins of unknown structures pb6 (protein of the T5 phage tail) and MDH (malate dehydrogenase), in the absence and in the presence of 10 mM of Tb-Xo4 (adapted from Engilberge *et al.*, 2017, 2018).

As illustrated in **Figure 2-1** Tb-Xo4 is a small molecule used as an additive. It can be stored as a powder and dissolved with the macromolecule solution prior to crystallization assays. The nucleating property of this complex was shown for several target proteins: Tb-Xo4 can increase the crystal quality when conditions are already known and help finding new conditions, as illustrated for pb6 and MDH (**Figure 2-1**). In Engilberge *et al*., 2017, the authors even determined the crystallization diagram of

hen egg white lysozyme (HEWL) in the absence and in the presence of Tb-Xo4 and demonstrated a clear effect of the molecule on crystal formation at low concentrations of both protein and crystallizing agent.

2.1.2 Crystallization in unconventional environments

The Grashof number N_G allows to estimate the balance between convection and diffusion in a defined environment by measuring the ratio between buoyancy driven convection (due to two liquids/elements of different density) and diffusion. The aim of a variety of methods involving unconventional environments is to reduce this value (Carter and Sweet 1997). The underlying idea is to reduce the Grashof number N_G in order to reduce convection in the crystallization environment and associated crystal growth defects. The smaller this value, the higher the influence of diffusion to drive particle transport in the solution. As presented in section 1.4, during crystal growth macromolecules surrounding the crystal will attach to its surface, thus creating a gradient of macromolecule concentration in the neighboring solution. In a conventional environment (a liquid vapor diffusion drop for instance), uncontrolled convective movements will take place due to the concentration (and density) differences. If a convection-free environment can be reached (for example in a capillary or in a microfluidic channel of small section, typically < 100 µm), the only force driving particles' movement inside the solution will be diffusion. Reduction or absence of convection was shown to enhance crystal quality by minimizing crystal defects (Lorber et al. 1999).

The Grashof number is defined as following:

$$N_G = g \times \rho(\delta\rho/\delta c) \times \Delta c \times d^3 \times \mu^{-2}$$

where g is the gravity value, ρ the density of the fluid, $\delta\rho/\delta c$ the density gradient in the solution due to the concentration differences, Δc the difference in concentration for example around a growing crystal, d the smallest dimension of the system (i.e. the crystallization chamber) and μ the viscosity of the medium (Carter and Sweet 1997)).

To reduce the value of N_G, several parameters can be tuned: g, $(\delta\rho/\delta c)$, d and μ. Modifying the density gradient is difficult in practice and is not of major impact. The

gravity value can be modified by performing micro- or zero-gravity experiments (Ng et al. 2002). This can reduce the N_G value by a factor of 10^4 to 10^6. Increase of the viscosity in the solution, which is to the second power in the equation, can be performed by addition of viscous compounds into the solution, such as low concentrations of agarose (García-Ruiz et al. 2001), polyethylene glycol (PEG) or dextran (unpublished work from Bernard Lorber). But this is limited by the maximum viscosity that can be pipetted and correspond to about 10 times the viscosity of water, thus maximally reducing the N_G value by a factor of 100. In contrast, the smallest dimension of the system is a very interesting parameter, as it appears to the third power in the equation and is relatively easy to modify. The reduction in the volume of droplets (a few µL to 100 nL), and thus their diameter (from 2.7 mm for a 5 µL drop to 0.8 mm for a 100 nL drop), by the development of pipetting robots in the past decades already reduced this parameter. But in vapor diffusion assays, evaporation of the solution at the surface also induces convection. The use of capillaries or a microfluidic device further reduces the size of the crystallization chamber, down to 100 µm and below, and thus reducing the N_G value by a factor of 10^3 compared to 100 nL droplets. Agarose gel can also be added to the solution, its fiber network forming even smaller pores and reducing the N_G value by a factor of 10^5 (Gavira and García-Ruiz 2002). Another advantage of capillaries, microfluidic devices and agarose gel is to avoid sedimentation, which would induce movements in the solution and generate stacks of intertwined crystals.

2.1.3 Seeding techniques

Seeding is a common practice in material science to grow large crystals. The rationality behind seeding is to by-pass the nucleation energetic barrier by providing nuclei or small crystals into a mother liquor which is already supersaturated, but in the metastable zone of the phase diagram (i.e. a zone not favorable to spontaneous nucleation). The first method used in biological crystallization was the transfer of macro-crystals, which was followed by the use of animal hairs to transfer small pieces of crystal from one drop to another to favor crystallization. The principle was to rub a hair over a crystal, thus removing small crystal parts and storing them on hair asperities and transferring them to a new drop. A drawback of this technique was that it was time

consuming when setting up hundreds of drops manually, in order to perform screening for instance. The situation was improved using pipetting robots which led to the development of MMS.

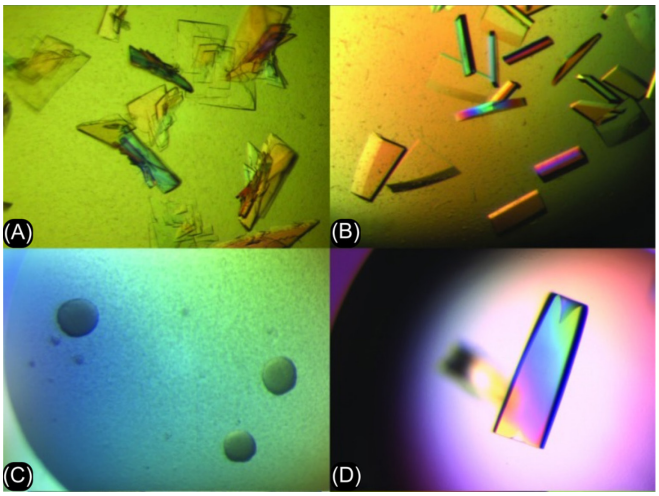

Figure 2-2 : Illustration of crystal morphology improvement by MMS. A) Crystals of serine protease grown in 30% (w/v) PEG 3350, 0.1 M Tris-HCl pH 8.5 used to prepare seed stock. B) Optimized crystals of serine protease grown in 30% (w/v) PEG 3350, 0.2 M magnesium chloride, 0.1 M Tris–HCl pH 8.5 after MMS with the crystals from A). C) These small, unpromising crystalline aggregates of a serine protease complexed with a natural product inhibitor were grown in 20% (w/v) PEG 10 000, 0.1 M Tris–HCl pH 8.5 and used to make a seed stock. D) Optimized crystals of the same complex after MMS with the seed stock from the original conditions. The final conditions were 25% (w/v) PEG 3350, 0.2 M lithium sulfate, 0.1 M HEPES pH 7.5 (adapted from D'Arcy *et al*., 2014).

MMS is based on the systematic introduction of small crystal pieces, or even nuclei, in a crystallization screen. Crystals, even of poor quality (in diffraction limit and/or morphology) are crushed by means of beads or a pipet tip to produce what is called a seed stock. This resulting suspension can be used in different dilutions in a screening assay. This method was shown to increase the number of hits obtained during screening and to improve crystal quality (D'Arcy et al. 2007, 2014). It can indeed be used to improve quality of existing crystals, find new crystallization conditions and identify new crystal forms of the same macromolecule (as illustrated in **Figure 2-2**) or even to crystallize structurally-related proteins. This latter procedure is called cross-

seeding. Although it presents a lower success rate compared to regular MMS, it may be used when no crystallization conditions were found by screening but crystals of an homologous protein are available. The power of MMS is to enable the exploration of the metastable zone of the phase diagram (not only the nucleation zone) by providing nuclei or small crystals into crystallization assays. Hence, all conditions that are already supersaturated, even if they would stay clear for a while without seed, may be activated by seeding and yield crystals.

2.2 Methods to detect nucleation and crystal growth

2.2.1 DLS and DDLS

Dynamic light scattering is a method to study the diffusion of macromolecules or assemblies in solution. It is based on the relation between the diffusion coefficient on one side, and the viscosity of the solution and the hydrodynamic radius of the objects on the other side. The setup consist in a laser, a detector and a correlator. It principle is illustrated in **Figure 2-3**:

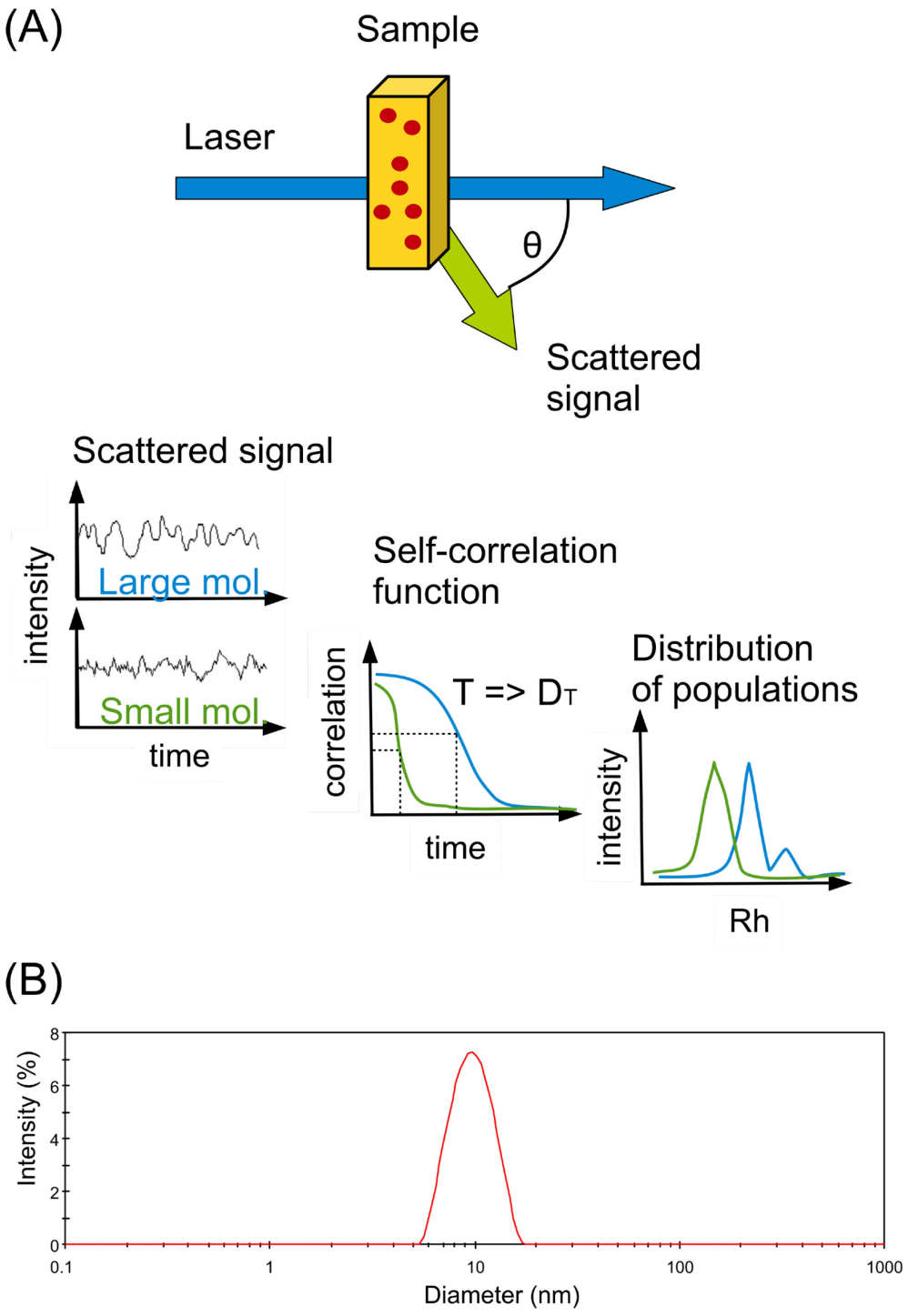

Figure 2-3 : Principle of DLS and example of analysis. A) A laser is shone on the sample and the scattered light is collected by a detector at a defined angle θ (adapted from Claude Sauter). The signal is processed by a correlator to extract a characteristic time (t), which is related to the translational diffusion coefficient (D_T) of the molecule. The hydrodynamic radius of the latter can be estimated using the Stockes-Einstein relation: $rh=kT/6\pi\mu D_T$. B) Typical output of a DLS measurement for a monodisperse sample. The distribution of particle diameter in nm is plotted as a function of the percent of total intensity of scattered signal (on the X-axis).

The intensity of the scattered signal directly depends on the velocity (represented by the diffusion coefficient) of a particle in solution. Knowing this information, as well as the viscosity of the solution, enables an estimation of the hydrodynamic radius of the particles. In addition, DLS indicates whether the sample contains one (monomodal) or several populations (multimodal distribution, which is generally a sign of instability and aggregation) and whether these populations are homogeneous in size (monodisperse). **Figure 2-3** (B) show an example of monomodal and monodisperse sample, which is a prerequisite for crystallization assays.

DLS began in the early 90's to be a method of choice to evaluate macromolecular interactions and detect formation of aggregates or assemblies in solution (Mikol et al. 1990). Thus, this technique was used as a diagnostic tool for the search of solvent conditions and crystallizing agents in which crystallization can occur, such as for lysozyme (Skouri et al. 1991) in the laboratory of Richard Giegé. However DLS later lost interest of the community for study of nucleation and crystal growth. It was rather used for sample quality control (characterization of the sample homogeneity) and for interaction studies thanks to its practical qualities: it is non-invasive, non-destructive, provides fast, precise and reproducible quality check and requires only a minimum amount of sample (typically 2-20 µl; reviewed in Stetefeld *et al.*, 2016). It was recently used again in crystallography analysis to study nucleation and crystal growth (Petsev and Vekilov 2000), in particular with its implementation in the Xtal Controller presented later in this thesis (Meyer et al. 2012; Schubert et al. 2017; Baitan et al. 2018). Due to the increasing relevance of growing and characterizing micro- and nanocrystals for free electron laser (XFEL) studies, modified versions of DLS have also been developed. For example depolarized dynamic light scattering (DDLS) can distinguish nanocrystals from amorphous precipitate in a more reliable way (Schubert et al. 2015). This method is based on the differences in optical properties between ordered and disordered assemblies and allows to distinguish them but is still technically difficult.

2.2.2 TFL

Detection by visual observation of crystals with white light in a crystallization assay is not always obvious. Crystals can be missed because they are hidden behind precipitate or by non-optimal placement in the droplet or close to the surface. In addition, distinction between salt and macromolecule crystals can lead to false positive and negative. A method to overcome these difficulties is the use of UV-illumination, but this is limited by the intrinsic fluorescence of tryptophan residues, the crystal packing as well as the materials used which need to be UV-transparent (Meyer et al. 2015). The TFL method introduced here leads to a much brighter fluorescent signal and is not limited by the protein sequence, folding or materials, as the excitation wavelength is in the visible spectrum (Pusey et al. 2008, 2015). It is based on covalently labeling on surface lysines of proteins with carboxyrhodamine-succinimidyl ester (**Figure 2-4**).

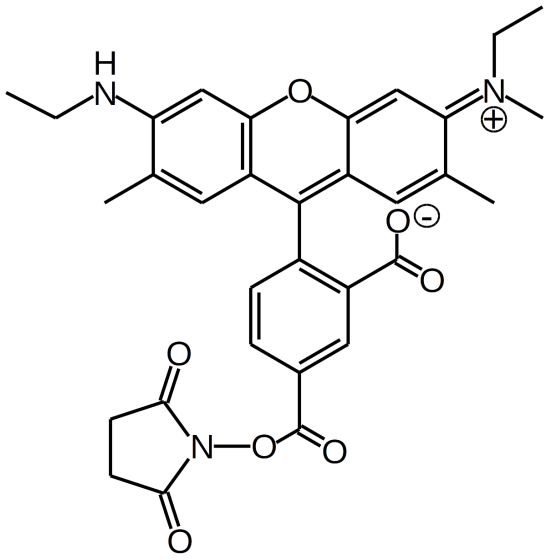

Figure 2-4 : Chemical drawing of carboxyrhodamine-succinimidyl ester

For this method, part of the protein solution is labeled in a one-step reaction and then mixed with the unlabeled stock solution. The use of a tiny percentage of labeled protein (less than 1% in total) is enough for bright detection (**Figure 2-5**) and was shown not to perturbate crystal growth nor diffraction (Pusey et al. 2015). The drops are illuminated with green light at 520 nm and observed after a low-pass filter at 550 nm.

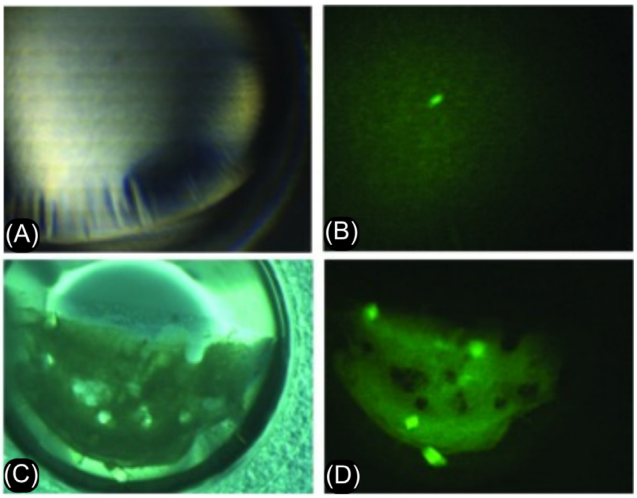

2.3 The Xtal Controller

Recently a new instrument called Xtal Controller 900 was developed by the groups of Profs Christian Betzel (University of Hamburg) and Rolf Hilgenfeld (University of Lübeck) and the company Xtal-Concepts GmbH in Hamburg as a rational technology for the study and the preparation of biological molecule crystals (Garcia-Caballero et al. 2011; Meyer et al. 2012). This instrument allows to manipulate a crystallization drop of a few µL by playing on the concentrations of macromolecule and crystallizing agent (thanks to microinjectors), while following the evolution of the system directly by DLS (detection of aggregation or nucleation events, formation of nanocrystals) and video-microscopy (monitoring of crystal growth), all in a temperature-controlled and humidity-controlled enclosure (**Figure 2-6**).

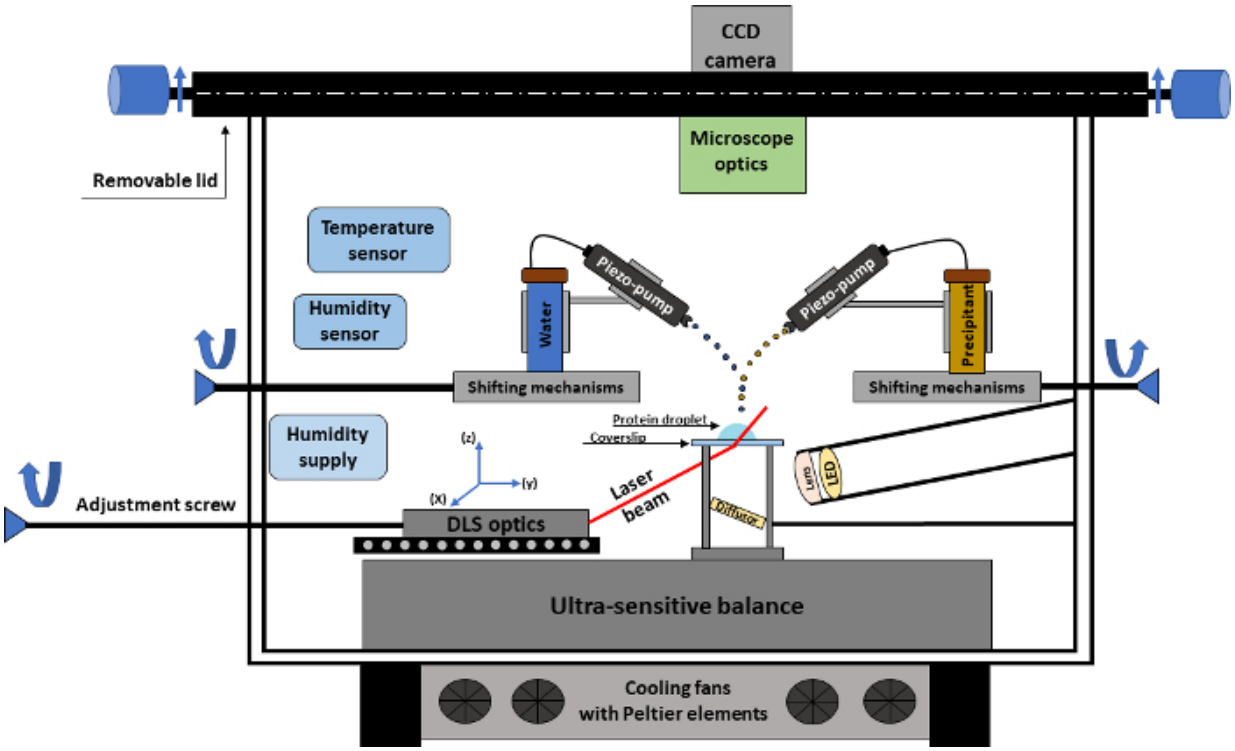

Figure 2-6 : Schematic representation of the Xtal-controller experimental chamber with all its technical parts (adapted from Baitan *et al*., 2018).

The crystallization droplet is deposited on a coverslip, which sits on the ultra-sensitive balance. This balance is the center of the instrument, allowing precise determination of concentration changes by measuring weight changes of the droplet. The use of microinjectors with reservoirs containing water and the crystallizing agent allows the experimenter to precisely control volumes and concentrations in the droplet. Measuring at the same time the evolution of assemblies by DLS and using a camera couple to a microscope enables to investigate the droplet during all stages of crystallization (Baitan et al. 2018). This instrument as well as its use will be described in more details later in this thesis.

3 Biological questions

The biological part of this thesis was focused on enzymes involved in the maturation or aminoacylation of transfer ribonucleic acids (tRNAs) and of their complexes. Two aspects were studied: i) the structural characterization of a psychrophilic CCA adding-enzyme and ii) the biochemical characterization of inhibitors targeting aspartyl-tRNA synthetases, such as the one from the multi-resistant pathogen *Pseudomonas aeruginosa*.

3.1 Transfer RNAs

tRNAs are essential adaptor molecules present in every kingdom of life and are the most abundant non-coding RNAs in cells (reviewed in Kirchner & Ignatova, 2015). They are in charge of decoding the genetic information contained in the messenger RNA to translate it into peptides and proteins. Their structure is very characteristic and important for their function.

Figure 3-1 : 3D representation of $tRNA^{Asp}$ from Escherichia coli without CCA in conformation for binding to the aspartyl-tRNA synthetase. The different arms are colored individually: acceptor arm in orange, anticodon arm in blue, variable region in white, D arm in green and T arm in magenta (PDB entry 1EFW) (Briand et al. 2000).

tRNAs exhibit a 2D cloverleaf structure, which fold into a characteristic L-shape in 3D (**Figure 3-1**). Their length varies between 73 and 96 nucleotides and five regions compose a tRNA. The acceptor stem, where aminoacylation will occur (orange), the anticodon hairpin (blue) which will decode the codon on the messenger RNA, a variable region (white) varying in length and the D (green) and T (magenta) arms.

To fulfill their role, tRNAs are going through a long maturation process and are associated with a high diversity of partners.

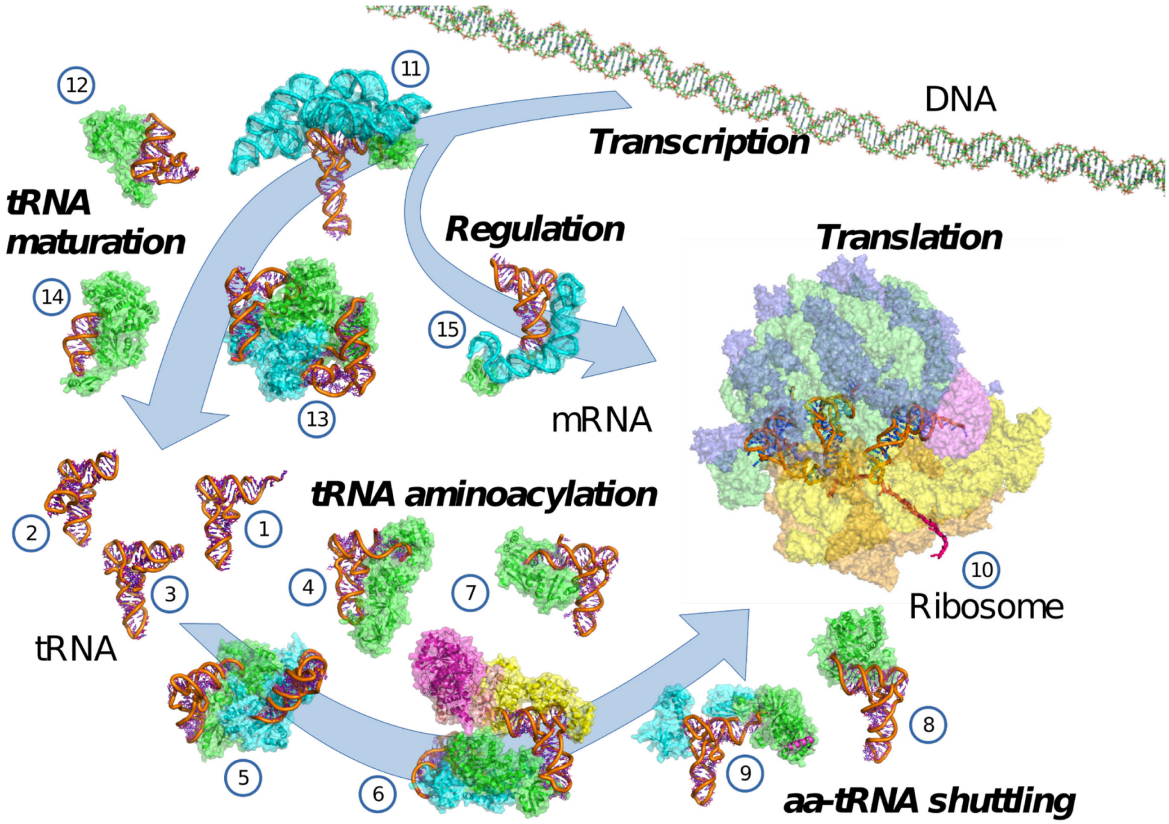

Figure 3-2 : Structural gallery of tRNAs and their cellular partners (Fernández-Millán et al. 2016).

Figure 3-2 presents a gallery of tRNAs and partners with their respective structures, showing the diversity of existing interactions. Several key steps are represented, starting from tRNA maturation by the ribonucleic RNase P at the 5'-end (11), the ribonuclease Z at the 3'-end (12) and the CCA-adding enzyme for addition at the 3'-end (14), up to translation by the bacterial ribosome bound to EF-Tu:tRNA (10) (Schmeing et al. 2009; Reiter et al. 2010; Pellegrini et al. 2012; Tomita et al. 2004). In the middle are illustrated the aminoacylation of tRNAs by several enzymes, or even complexes, such as a monomeric glutaminyl-tRNA synthetase (4), a dimeric aspartyl-tRNA synthetase (5) or the transamidosome (6) (Rould et al. 1989; Ruff et al. 1991; Blaise et al. 2010).

3.2 CCA-adding enzymes

tRNA nucleotidyltransferases, among which can be found CCA-adding enzymes, include enzymes involved in the posttranscriptional maturation of tRNAs by polymerizing nucleotides at their 3' end. They belong to the polymerase β superfamily, which share the amino acid signature hG[GS]x(9,13)Dh[DE]h (x represents any amino acid, h represents a hydrophobic amino acid) (Holm and Sander 1995), and class II of this superfamily. Poly(A) polymerase, terminal uridylyl transferase, terminal deoxynucleotidyltransferase and tRNA nucleotidyltransferase form a subgroup inside the polymerase β superfamily which are able to add nucleotides at the end of DNA or RNA sequences without any nucleic acid template (reviewed in Betat *et al.*, 2010).

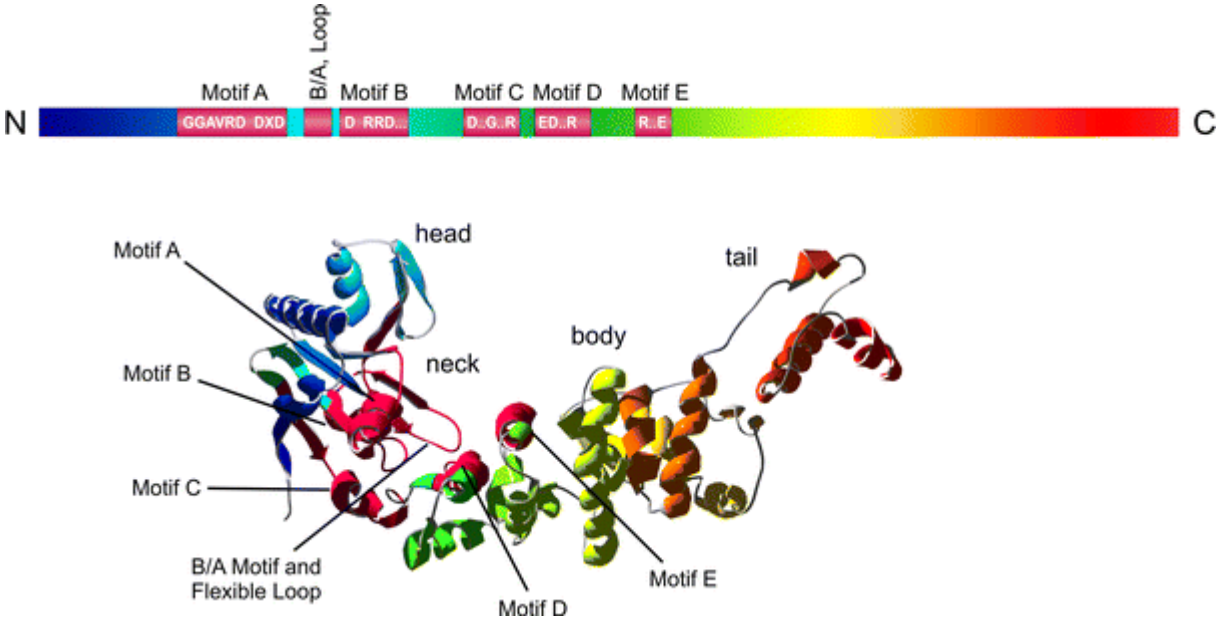

CCA-adding enzymes are tRNA nucleotidyltransferases able to add two cytosines and one adenine and maintaining this specific C-C-A sequence. The overall structure of class II CCA-adding enzymes exhibit a typical seahorse-like shape and is principally made of α-helices (**Figure 3-3**). The only beta sheet is in the head domain.

The enzyme can be divided into four domains: head, neck, body and tail; the catalytic center is located in a cleft formed by the head and neck domains, while body and tail domains recognize the tRNA. The motif A is the signature motif of all nucleotidyltransferases with two metal binding carboxylates DxD (x is any amino acid); Motif B is responsible for the discrimination between NTPs and dNTPs; Motifs C and E have no specific function assigned; Motif D is the single nucleotide-binding pocket specific for CTP and ATP (Tomita *et al.*, 2004; Augustin *et al.*, 2003; Li *et al.*, 2002; Toh *et al.*, 2009; reviewed in Betat *et al.*, 2010).

The polymerization activity of CCA-adding enzymes is performed without any DNA or RNA template, but is controlled by a set of highly conserved amino acid residues in addition to movements in the binding pocket (Tomita et al. 2006). A single CCA-adding enzyme must be able to adapt to all tRNAs in the cell, which requires a tightly controlled flexibility. Among others, the maturation of tRNAs by CCA-adding enzymes plays a key role in the faithful expression of the genetic code by its specificity and efficiency. This 3'-CCA sequence is necessary for further processing and roles of the tRNAs: (i) it is indeed the aminoacylation site for the aminoacyl-tRNA synthetases as the cognate amino acid is fused to the ribose moiety of the terminal A residue (Sprinzl, 1979), (ii) is required for positioning in the ribosome to ensure correct peptide-bond formation during translation (Green and Noller, 1997), and (iii) is involved in translation termination when the nascent peptide is released from the ribosome (Simonovic and Steitz, 2008). During specificity switch between cytosine triphosphate (CTP) and adenosine triphosphate (ATP) during the polymerization process, not only amino acids near the catalytic center are subjected to movement, but also a global motion of the enzyme was observed (Tomita et al. 2006).

3.3 Cold adaptation strategies

Organisms living at low temperature needed to find adaptation strategies to still be able to perform enzymatic activities. Several strategies have been described and psychrophilic organisms usually combine them, meaning that cold adaptation does not rely on a single modification. Among others, an increased mobility of surface loops induced by the mutation of key residues (Åqvist 2017) and the destabilization of catalytic complexes to reduce their activation energy (Khrapunov et al. 2017) were

observed. In general proteins of psychrophilic origin display common features, enhancing their structural flexibility (reviewed in De Maayer *et al.*, 2014). Intriguingly, the defined and controlled flexibility of CCA-adding enzymes does not seem to be compatible with an enhanced structural flexibility, associated with cold adaptation. This is why the structural study of the CCA-adding enzyme from *Planococcus halocryophilus*, a bacterium thriving in the Arctic permafrost (Mykytczuk et al. 2012) was initiated during this thesis. Cold adaptation is further developed in chapter III.

3.4 Aminoacyl-tRNA synthetases

Aminoacyl-tRNA synthetases (aaRSs) are essential enzymes that catalyze the covalent attachment of amino acids to their cognate tRNA. The aminoacylation reaction is a two-step process. The first step consists of the activation of the amino acid by an adenosine triphosphate with release of inorganic pyrophosphate (PPi), to form the aminoacyl-adenylate. This step occurs in presence of Mg2+ and is mostly tRNA independent, excepted for a limited set of aaRSs (ArgRs, GluRS, GlnRs; Schimmel & Söll, 1979). The second step corresponds to a nucleophilic attack by the 2' or 3' hydroxyl of the ribose on the terminal adenylate in position 76 of tRNAs to form the aminoacyl-tRNA with the release of adenosine monophosphate (AMP) (**Figure 3-4**).

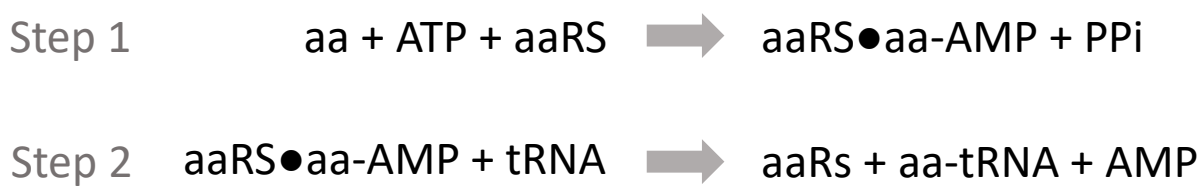

Synthetases are classified into two classes (class I and class II) and several subclasses (**Figure 3-5**) according to their structural organization.

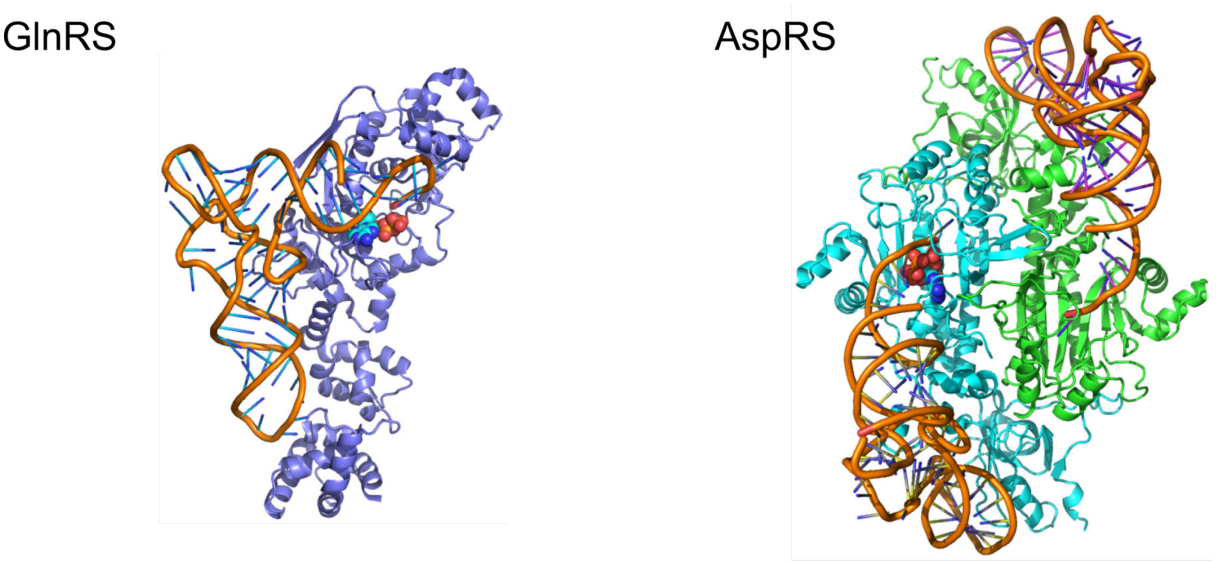

class I			class II		
Ia	Ib	Ic	IIa	IIb	IIc
ValRS (α)	TyrRS (α2)	GluRS (α)	SerRS (α2)	*AspRS (α2)*	PheRS (α2β2)
IleRS (α)	TrpRS (α2)	*GlnRS (α)*	ThrRS (α2)	LysRS (α2)	AlaRS (α4)
LeuRS (α)		ArgRS (α)	ProRS (α2)	AsnRS (α2)	GlyRS (α2β2)
MetRS (α)			HisRS (α2)		
CysRS (α)					

Figure 3-5 : Classification of aminoacyl-tRNA synthetases. The characteristic structural organization of each class is illustrated by the crystal structure of one member of the class in complex with its cognate tRNA, with the monomeric class I glutaminyl-tRNA synthetase (GlnRS) and the dimeric class II aspartyl-tRNA synthetase (AspRS). The table shows the partition of aaRSs in classes and subclasses (Eriani *et al.*, 1990) and corresponding oligomerization states, as observed in bacteria (adapted from Claude Sauter).

The classes possess very distinct structural and functional properties. Class I synthetases esterify the amino acid on the 2'-OH of the terminal adenosine of the tRNA, and bind the minor groove of the accepting arm. Their structure is organized around a domain consisting of a parallel beta sheet, surrounded by alpha helixes called Rossmann fold. They are essentially monomeric, with a few dimeric forms (α or α2). Class II aminoacyl-tRNA synthetases esterify the amino acid on the 3'-OH of the terminal adenosine of the tRNA, bind the major groove of its accepting arm and present a dimeric or tetrameric oligomerization state (Eriani et al. 1990) with a catalytic core build around an anti-parallel beta sheet.

3.5 Targeting synthetases from multi-resistant pathogens

The 27th of February 2017, the World Health Organization (WHO) described antibiotic resistance of pathogens as one of the biggest threats to human health and called for a general effort of the scientific community in the discovery of new antibiotics (WHO, Tacconelli & Magrini, 2017). In accordance, they published a list of bacteria species or families for which new antibiotics are urgently needed, as they are developing resistance to known antibiotics, and classified them into three distinct categories of priority: critical / high / medium (**Table 3-1**) with new resistances recently observed.

Table 3-1 : Published priority list by the World Health Organization

Priority	Bacteria	Resistance
Critical	*Pseudomonas aeruginosa*	Carbapenem-resistant
	Acinetobacter baumannii	Carbapenem-resistant
	Enterobacteriaceae	Carbapenem-resistant
High	*Enterococcus faecium*	Vancomycin-resistant
	Staphylococcus aureus	Methicillin-resistant and vancomycin-intermediate resistant
	Helicobacter pylori	Clarithromycin-resistant
	Campylobacter spp	Fluoroquinolone-resistant
	Salmonellae	Fluoroquinolone-resistant
	Neisseria gonorrhoeae	Cephalosporin-resistant, fluoroquinolone-resistant
Medium	*Streptococcus pneumoniae*	Penicillin-non-susceptible
	Haemophilus influenzae	Ampicillin-resistant
	Shigella spp.	Fluoroquinolone-resistant

Among the “critical” category can be found the species *Pseudomonas aeruginosa*. This Gram-negative bacterium is an opportunistic pathogen, thus mostly affecting immunocompromised patients. It is responsible for hospital-acquired infections such as generalized inflammations and sepsis, which can be lethal when the colonization occurs in the lungs, kidneys or urinary tract.

Carbapenem, against which *P. aeruginosa* developed a resistance, are molecules in the family of the β-lactams, which are targeting penicillin binding proteins of Gram-positive and Gram-negative bacteria (reviewed in Papp-Wallace *et al.*, 2011). They are unique in this family, as in some cases they are also inhibitors of β-lactamases and are described as “last-line agents” or “antibiotics of last resort” in our antimicrobial armamentarium. The first carbapenem compound, thienamycin, used as model for subsequent developments, was discovered in 1976 and today, only around 42 years later, resistance against this family is widespread (**Table 3-1** and WHO reports).

In the perspective of developing new active compounds, aaRSs are well recognized targets because these enzymes are essential to cell life. Chapter V will discuss the search of inhibitors targeting bacterial aspartyl-tRNA synthetases and drug design approaches.

3.6 Serial crystallography at room-temperature

At the beginning of bio-crystallography, a complete data set was collected on one or several large crystals (hundreds of µm in size) at room-temperature (RT). Later, due to the increase in synchrotron X-ray beam brilliance, cryo-cooling of crystals was developed to reduce radiation damages. These damages are inherent of the use of X-rays, increase with the brilliance, induce a reduction of the diffraction properties of a crystal and accumulate in time (reviewed in Garman, 2010). Very recently in the field, thanks to the emergence of X-ray Free Electron Lasers (XFELs), a revival of room-temperature and multi-crystal data collection is observed. These installations are very limited in term of numbers. As today, only five XFEL facilities are accessible around the world: LCLS in the USA, SACLA in Japan, European XFEL in Germany, PAL-XFEL in South Korea and SwissFEL in Switzerland. They allow the new approach called SFX for serial femtosecond crystallography which is based on the diffraction-before-destruction principle and avoid radiation damage (Schlichting 2015). Due to limited number of XFEL installations, the collection system and strategy was recently adapted to synchrotrons and described as SMX for serial millisecond crystallography (Weinert et al. 2017) in opposition to SFX. In practice, a suspension containing nano- or microcrystals is produced and passed under X-ray radiation. Crystals hit by the XFEL

beam will produce one diffraction pattern before destruction. Therefore, collecting a complete dataset requires a high amount of crystals and diffraction patterns (reviewed in Johansson *et al.*, 2017). This collection strategy pushed the development of new software to treat up to hundreds of thousands diffraction patterns produced by XFEL. Among others is ccCluster (Santoni et al. 2017) which was used in this thesis to analyze, compare and combine partial datasets collected in the microfluidic chips. The production and quality control of microcrystal suspensions for XFEL experiments is another challenge. One of the device developed to overcome it is the Xtal Controller, which is described in chapter IV. An additional advantage of the ultra-fast beam pulses is the development of what is called “molecular movies”. It consists in the collection of diffraction data corresponding to molecular snapshots along a reaction process. Thanks to the beam characteristics of XFELs and the mix-on-demand technology, fusion of these snapshot enables to study in more details protein dynamics and enzyme catalysis (Nango et al. 2016; Suga et al. 2017).

Serial RT analysis performed with XFEL or at synchrotron facilities is a new trend in crystallography. It enables studies without cryo-cooling and with no radiation damages in case of XFEL.

4 Thesis goal

This thesis had two main aspects as indicated in its title “Application of new crystallization approaches and serial crystallography to the structural study of enzyme:tRNA complexes”, which where to i) carry out the structural and functional characterization of biologically relevant molecules and ii) develop and implement new crystallography methods. These tasks were performed simultaneously and associated to facilitate the structural studies performed during my PhD work.

4.1 Biological target molecules

Because of their essential nature and their substrate specificity, aaRS are prime targets for drug design. Part of this work has been the biochemical study and structural characterization of the binding mode of two families of AspRS inhibitors that specifically bind L-aspartate (see Chapter V). The first is represented by a natural antibiotic produced by some strains of *E. coli* to block the AspRS catalytic site of competing strains (collaboration with Professor Sylvie Rebuffat of the Musée National d'Histoire Naturelle, Paris); the second is a series of chemically synthesized peptides that were selected against the AspRS of the opportunistic human pathogen *P. aeruginosa* (collaboration with Professor Hiroaki Suga of the University of Tokyo).

This work was also part of a French-German cooperation programme PROCOPE with the team of Professor Mario Mörl (University of Leipzig) on the structural study of CCA-adding enzymes of different organisms, including extremophiles. This cooperation led to the crystal structure of the enzyme *Planococcus halocryophilus*, a psychrophilic bacterium, capable of living at very low temperatures (see Chapter III).

4.2 New methods in crystallography

The research team turned to an innovative and more rational technology for the preparation of biological molecule crystals called Xtal Controller 900 (Xtal-Concepts GmbH, Hamburg). This work explored the possibilities offered by this technology for the study of crystallogenesis and better control of crystal production for exploitation in structural biology (see Chapter IV). This led us to investigate the effect of different crystallizing agents on different protein models, but also of a new nucleant (mentioned in section 2.1.1), a lanthanide complex called Tb-Xo4 that facilitates the nucleation and growth of biological crystals (collaboration with Eric Girard from IBS, Grenoble). These experiments are based on proteins of biological interest, including a CCA-adding enzyme and proteins provided by our collaborators.

The psychrophilic CCA-adding enzyme has also been used as a guinea pig for the development of crystallization methods and strategies, with the objective of further improving the quality of the structural data available. Following my participation in an international crystallization school[2], two methods were introduced in the laboratory that have proven their effectiveness: trace fluorescent labelling (mentioned in section 2.2.2) that facilitates the identification of crystals during initial screening, as well as microseed matrix screening (mentioned in section 2.1.3) to increase the number of crystallization conditions. A new concept of microfluidic chips developed in the team was also used to determine the structure of several macromolecules at room temperature using the serial crystallography approach (see Chapter II)

[2] « Advanced methods in Macromolecular Crystallization VII » organized by the FEBS society in 2016 at Nové Hrady, Czech Republic.

II. ChipX3: a new microfluidic crystallization device

En dépit de nombreux progrès en matière de criblage, l'exploration de combinaisons de solvants possible et du diagramme de phases pour identifier les conditions produisant des cristaux de qualité suffisante en diffraction, ceci à partir d'une quantité limitée de macromolecules reste longue et couteuse, et constitue un goulot d'étranglement des études cristallographiques. Ce processus implique généralement un échantillonnage par essai et erreur de l'espace chimique et physique en examinant des centaines de cocktails différents composés de tampons à différents pH, de divers agents de cristallisation et différentes températures pour trouver au moins un solvant approprié et des conditions de sursaturation propices à la croissance cristalline. La miniaturisation des essais de cristallisation dans des microplaques et l'automatisation de la procédure de criblage ont rendu cette tâche considérablement plus efficace, permettant de mener à bien un projet avec seulement quelques milligrammes d'échantillon pur.

Dans ce premier chapitre de résultats de ma thèse, axé sur un développement méthodologique, le système de cristallisation en puce microfluidique est décrit avec tous les avantages qui vont avec (voir section 2.1.2), est décrit à travers deux articles en préparation. Premièrement en section 5 l'article « Crystallization and structural determination of an enzyme : substrate complex by serial crystallography in a user-friendly and versatile microfluidic chip » préparé pour JoVE (Journal of Visualized Experiments) avec la vidéo associée, qui décrit le protocole de chargement d'une puce ChipX3 et la collecte in situ à température ambiante. Deuxièmement l'article « A simple and versatile microfluidic device for efficient biomacromolecule crystallization and structural analysis by serial crystallography » en section 6 qui présente une collection de cristaux obtenus dans les puces avec utilisation de méthodes avancées de cristallogenèse (voir section 2) et les stratégies d'analyse sous rayonnement synchrotron ainsi que les jeux de données et les structures associées.

5 Crystallization and structural determination of an enzyme:substrate complex by serial crystallography in a user-friendly and versatile microfluidic chip (in preparation for JoVE)

Link to the video:

https://seafile.unistra.fr/d/d9ecd3ed40674ffb9b37/

Manuscript for Journal of Visualized Experiments (JoVE)

Crystallization and structural determination of an enzyme:substrate complex by serial crystallography in a user-friendly and versatile microfluidic chip

Raphaël de Wijn[1], Vincent Olieric[2], Oliver Hennig[3], Caroline Paulus[1], Nicola Thome[1], Bernard Lorber[1], Heike Betat[3], Mario Mörl[3], Claude Sauter[1]

[1]Architecture et Réactivité de l'ARN, UPR 9002, CNRS, Institut de Biologie Moléculaire et Cellulaire, Université de Strasbourg, Strasbourg, France
[2]Paul Scherrer Institute, Swiss Light Source, X06DA *beamline*, Villigen, Switzerland
[3]Biochemistry and Molecular Biology, Institute for Biochemistry, Leipzig University, Leipzig, Germany

Corresponding Author: Claude Sauter
Email: c.sauter@ibmc-cnrs.unistra.fr
Tel: +33 388 417 102

KEYWORDS: crystallization, serial crystallography, 3D structure, counter-diffusion, ChipX, microfluidics, CCA-adding enzyme, soaking, seeding

SUMMARY: A versatile microfluidic device is described that enables the crystallization of an enzyme using the counter-diffusion method, the introduction of a substrate in the crystals by soaking, and the 3D structure determination of the enzyme:substrate complex by a serial analysis of crystals inside the chip at room temperature.

ABSTRACT: The preparation of well diffracting crystals and their handling before their X-ray analysis are two critical steps of biocrystallographic studies. We describe a versatile microfluidic chip that enables the production of crystals by counter-diffusion. The convection-free environment provided by the microfluidic channels is ideal for crystal growth and useful to diffuse a substrate into the active site of the crystalline enzyme. Here we applied this approach to the CCA-adding enzyme of the psychrophilic bacterium *Planococcus halocryophilus* in the presented example. After crystallization and substrate diffusion/soaking, the crystal structure of the enzyme:substrate complex was determined at room temperature by serial crystallography and the analysis of multiple crystals directly inside the chip. The whole procedure preserves the genuine diffraction properties of the samples because it requires no crystal handling.

Manuscript for Journal of Visualized Experiments (JoVE)

INTRODUCTION: Crystallography is a method to decipher the 3D architecture of biological macromolecules. The latter is important to understand how an enzyme selects and processes its substrates. The determination of a crystal structure requires the crystallization of the target macromolecule and the conditioning of the crystals for their analysis by X-ray diffraction[1]. Both crystal preparation and handling are crucial but delicate steps that can affect crystal quality and diffraction properties, and, thus, the resolution – i.e. the accuracy – of the resulting 3D structure. To facilitate the preparation of high quality crystals and eliminate unnecessary handling to preserve their diffraction properties, we designed a user-friendly and versatile microfluidic device called ChipX[2].

In this video, we demonstrate how to load the protein solution into ChipX channels using conventional laboratory material to prepare crystals by counter-diffusion. This crystallization method provides an efficient screening of supersaturation and of potential nucleation conditions along the microfluidic channels containing the enzyme solution due to the concentration gradient generated by the diffusion of the crystallizing agent[3,4].

The chip setup is simple, it uses only standard laboratory pipets and does not require any costly equipment. When crystals have grown in ChipX, ligands of the enzyme can be introduced by diffusion. Diffraction data are then collected at room temperature on a series of crystals contained in the channels of the chip using a synchrotron X-ray source. The structural study described here led to the determination of structures of a tRNA maturation enzyme, a CCA-adding enzyme, in its apo form and in complex with an analogue of CTP substrate introduced by soaking. The comparison of the two 3D images obtained by serial crystallography reveals local conformational changes related to the binding of the ligand in conditions that are more physiological than those used in cryo-crystallography. The protocol described in this video is generally applicable to any biomolecule, be it a protein, a nucleic acid or a multi-component complex.

PROTOCOL:

1. Setting up crystallization assays in ChipX

NOTE: a description of the chip is given in **Figure 1**. Solutions containing the crystallant (or crystallizing agent) used to trigger crystallization may be of commercial origin or prepared by the experimenter.

1.1. Loading the biomolecule sample

1. Pipet 5-6 µl of enzyme solutions using standard 10 µl pipet and tip.
2. Introduce the tip vertically in the sample inlet and inject the solution until the eight channels are filled up to their opposite end (entry of the crystallant reservoir)
3. Inject 1 µl of paraffin oil in the sample inlet in order to disconnect the channels from each others.
4. Recover the extra solution in the crystallant reservoir at the extremity of the channel.
5. Seal the sample inlet with a piece of tape.

1.2. Loading the crystallization solutions

1. Pipet 5 µl of crystallization solution using standard 10 µl pipet and tip. If initial

crystallization conditions were obtained by vapor diffusion, the crystallant concentration should be increased by a factor of 1.5 – 2. Solutions can be different in every reservoir (in the presented case, 1 M diammonium hydrogen phosphate, 100 mM sodium acetate, pH 4.5 was used throughout).

2. Orient the pipet tip towards the entry of the channel in the funnel shaped part of the reservoir to avoid the formation of an air bubble upon solution deposition. It would prevent the contact between the two solutions and crystallant diffusion into the channel.
3. Inject the crystallant solution into the reservoir.
4. Seal the reservoirs with a piece of tape.
5. Incubate the chip under controlled temperature.

2. Protein labeling with carboxyrhodamine for fluorescence detection

NOTE: this step is optional. It must be performed prior to sample loading to facilitate the detection of crystals in the chip using fluorescence. The detailed method of trace fluorescent labeling was described by Pusey and coworkers[5]. All steps are carried out at room temperature.

1. Dissolve 5 mg of carboxyrhodamine ester powder in 1 ml anhydrous dimethyl-formamide, split the solution in 0.6 µL aliquots to be stored at -20°C.
2. Prepare a 1 M Na-borate pH 8.75 stock solution.
3. Dilute the stock to prepare the reaction buffer at 0.05 M Na-borate pH 8.75.
4. Rinse a Zeba spin desalting column (7K MWCO, 0.5 ml) with 800 µl of reaction buffer.
5. Centrifuge the column for 1 min at 1400 x g, remove the filtrate.
6. Repeat this operation twice (steps 4-5) to wash the column.
7. Dilute the protein 2-4 times in its buffer.
8. Deposit 80 µl of diluted protein on the column.
9. Centrifuge the column for 1 min at 1400 x g.
10. Recover the flow-through, and mix it with 0.6 µl aliquot of carboxyrhodamine solution.
11. Incubate 5 min at room temperature.
12. Meanwhile, rinse the column 3 x with the protein buffer, centrifuge the column for 1 min at 1400 x g and discard the filtrate.
13. Deposit the reaction solution on the column.
14. Centrifuge the column for 1 min at 1400 x g and recover the flow-through (i.e. labeled solution).
15. Supplement the stock solution with 0.1-1 % (w/w) of labeled protein.
16. Setup your crystallization assays as described.
17. Check for the presence of protein crystals in your assays by exciting the fluorescent probe with a 520 nm wavelength light source.

3. Crystal observation

1. ChipX device may be handled without special care, even with crystals inside, except if the temperature needs to be controlled.
2. Use any binocular or microscope to check the outcome of crystallization assays in ChipX. Its footprint has the standard dimensions of microscope slides and is compatible with any system and slide holder.

Manuscript for Journal of Visualized Experiments (JoVE)

3. Check the content of microfluidic channels starting from the reservoir where the crystallant concentration is the highest to the sample inlet where the crystallant concentration is the lowest. The ChipX material is transparent to visible light, compatible with the use of polarizers, as well as with UV illumination for protein crystal identification by intrinsic tryptophane fluorescence[6].
4. Record crystal positions using the labels embossed along the channels or mark crystal locations with a permanent marker by drawing color dots next to them on the chip surface.

4. Crystal soaking with ligands

NOTE: this procedure is optional. It is used to introduce ligands, enzyme substrates or heavy atoms into the crystals and should be carried out at least 24-48 h before X-ray analysis to allow the compound diffusion along the channels and into the crystals.

1. Gently remove the sealing tape from the reservoirs.
2. Add up to 5 µl of ligand solution in one or several reservoirs using a 10 µl micropipet (in the example, 3 µl of 10 mM cytidine-5'-[(α,β)-methyleno] triphosphate (CMPcPP) solution was added to achieve a final concentration of 3.75 mM). CMPcPP (Cat. No NU-438, Jena Bioscience) is a non-hydrolizable analog of CTP, a natural substrate of the enzyme.
3. Seal the reservoirs with a piece of tape.
4. Incubate the chip under controlled temperature for 24-48 h to allow ligand diffusion along the channels of the chip.

5. Crystal analysis by serial crystallography

NOTE: this part of the protocol needs to be adapted depending on the beamline setup and the diffraction properties of the crystals. Only general indications are given for the crystallographic analysis based on experiments performed at XDA06 beamline (SLS, Villigen, Switzerland).

ChipX mounting on beamline goniometer

NOTE: The file for 3D printing ChipX holder is provided as supplemental material.

1. Turn off the cryo-jet of the beamline (NB: the analysis is carried out at room temperature).
2. Mount the ChipX on a dedicated holder with the channel containing the crystals to be analyzed positioned at the center of the holder.
3. Attach the holder to the goniometer.

Data collection

1. Orient the thickest layer (top layer) of ChipX towards the direct beam and the thinnest face behind the crystal to minimize the attenuation of the diffracted signal.
2. To avoid collision of ChipX with the surrounding material (beamstop, collimator), restrict goniometers movements in the range -30° / +30° (0° corresponding to the channels being perpendicular to the X-ray beam).
3. Find crystals position with the help of the labels embossed along the channels.
4. Select a crystal position.

Manuscript for Journal of Visualized Experiments (JoVE)

5. Center the crystal either by standard low dose grid/raster screening or 1-click procedure (the video shows an example of grid screening).
6. Collect diffraction data within the range -30° / +30°.
7. Restart the procedure at steps 4-6 on another crystal in the same channel after translation of the chip.
8. Manually realign another ChipX channel at the center of the holder and carry on data collection on crystals present in this channel.
9. Use standard crystallographic packages and procedures to process and merge the data.

REPRESENTATIVE RESULTS:

The microfluidic chip described here was designed to enable easy setup of crystallization assays and crystal analysis at room temperature. The procedure described above and in the video was applied in the frame of the structural characterization of the CCA-adding enzyme from *Planococcus halocryophilus.* This enzyme belongs to an essential polymerase family that catalyses the sequential addition of the 3' CCA sequence on tRNAs using CTP and ATP [7,8].

The chip was first used to prepare crystals of the enzyme for structural analysis by the method of counter-diffusion. To this end, the enzyme solution was loaded in the eight microfluidic channels (crystallization chambers) by a single injection in the sample inlet of the chip (see **Figure 1).** This step is performed manually with a standard 10 µL micropipet. Crystallization solutions are then deposited in the reservoirs at the other extremity of the channels. The loading procedure is straightforward and does not take longer than five minutes (**Figure 2**). The crystallant then diffuses into the channels, creates a gradient of concentration and supersaturation, and triggers crystal nucleation and growth. Bipyramidal crystals of CCA-adding enzyme appear along the channels after a few days of incubation at 20°C (**Figure 3**). The optional fluorescent labeling[5] of the protein greatly facilitates the identification of protein crystals and their discrimination from salt crystals (**Figure 4**).

We exploited the diffusive environment in chip channels to deliver a substrate to the enzyme that builds up the crystals. In the present case, CMPcPP, a CTP analog, was added to the reservoir solutions at a final concentration of 3.75 mM (**Figure 5**). This addition was performed two days before the crystallographic analysis to allow CMPcPP to reach and occupy the catalytic site of the enzyme, as later confirmed by the crystal structure (see below).

We manufactured a chip holder (**Figure 6**) in polylactic acid using a 3D printer (Ultimaker 2 extended+). The holder enables chip mounting on goniometers using standard magnetic heads. Hence the chip can be easily positioned and translated in the X-ray beam to bring the crystals in diffraction position. The data collection strategy needs to be adapted depending on the beamline characteristics and on the crystal properties. In case of the CCA-adding enzyme, 30° of rotation were collected with images of 0.1° and 0.1 s exposure on each crystal. Full dataset were reconstituted by merging data from 5 crystals (Table 1). Crystal structures were derived by molecular replacement using standard crystallographic packages and procedures for data processing[9] and refinement[10]. The comparison of the structures of the enzyme and of its complex with CMPcPP reveals the local conformational adaptation that accompanies substrate binding in the active site of the CCA-adding enzyme (**Figure 7**).

Manuscript for Journal of Visualized Experiments (JoVE)

FIGURE AND TABLE:

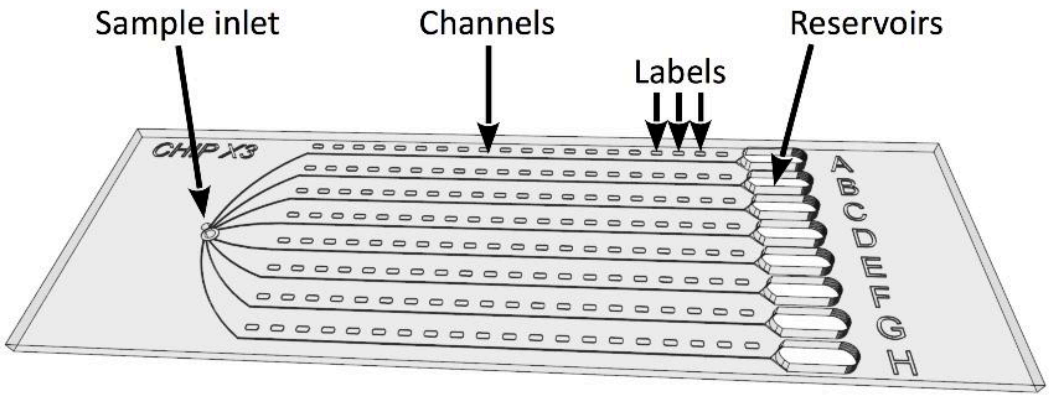

Figure 1: ChipX design. The chips consists of a top layer made of COC (thickness: 1 mm) in which eight microfluidic channels and reservoirs are imprinted. The whole is sealed by a layer of COC (thickness: 0.1 mm). All channels are connected to a single inlet for simultaneous sample injection, on one side, and to individual reservoirs in which crystallization solutions are deposited, on the opposite side. The channels, which constitute the actual crystallization chambers of the chip are 4 cm long and have a cross section of 80 µm x 80 µm. Labels embossed along the channels facilitate crystal positioning under the microscope and the preparation of a sample list for data collection. ChipX has the size of a standard microscope slide (7.5 cm x 2.5 cm).

Manuscript for Journal of Visualized Experiments (JoVE)

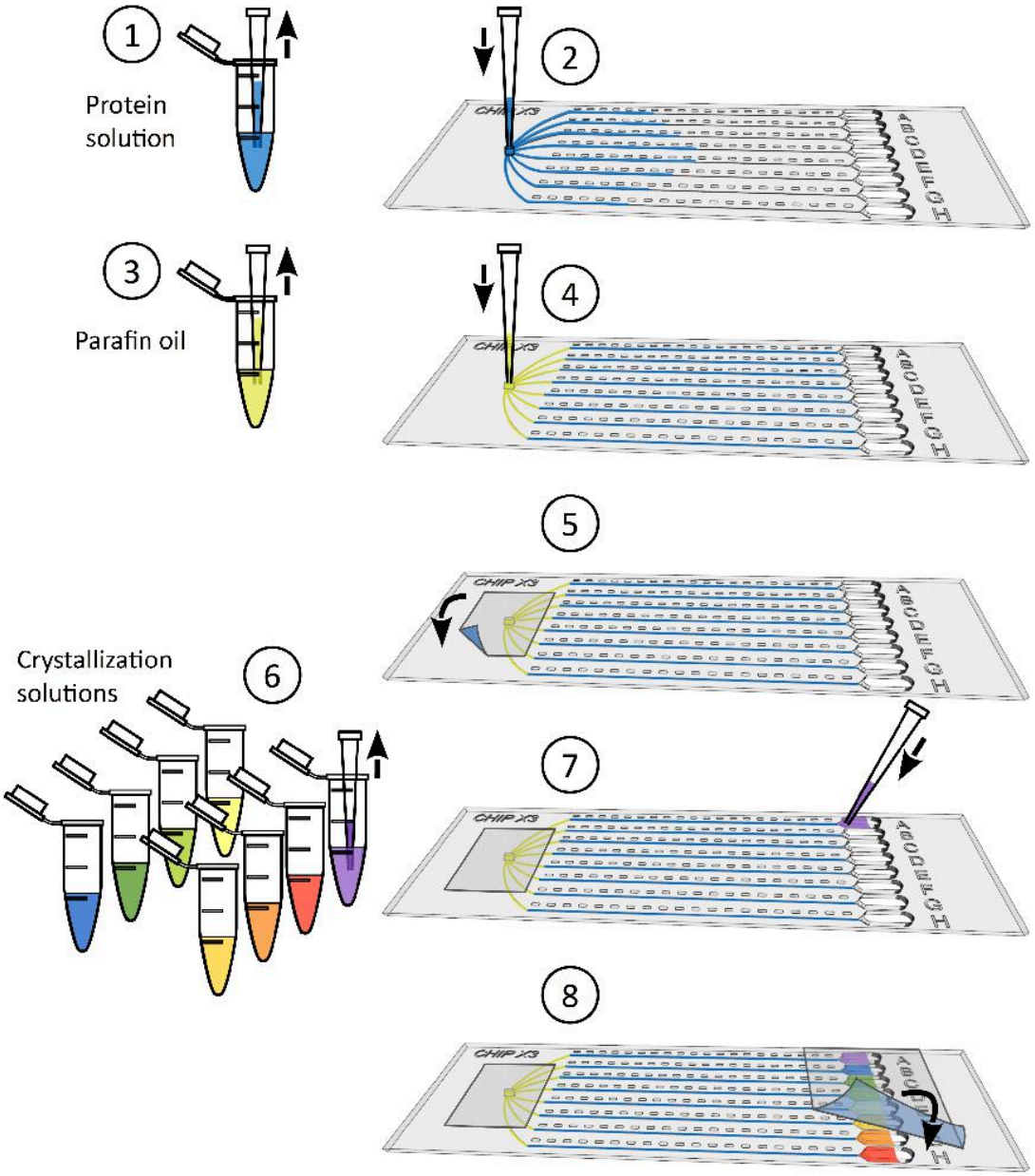

Figure 2: Setting up crystallization assays in ChipX. 1) Deposit 5-6 µl of enzyme solutions using standard 10 µl pipet and tip. 2) Introduce the tip vertically in the sample inlet and inject the solution in the eight channels. 3) Pipet 1 µl of paraffin oil. 4) Introduce the tip vertically in the sample inlet and inject the oil in order to disconnect the channels from each others. 5) Seal the inlet with a piece of tape. 6) Pipet 5 µl of crystallization solution using standard 10 µl pipet and tip. Solutions can be different in every reservoir (p.ex. from a screening kit). 7) Orient the pipet tip towards the entry of the channel in the funnel shaped part of the reservoir (to avoid the formation of an air bubble upon solution deposition) and inject the crystallant solution in the reservoir. 8) Seal the reservoirs with a piece of tape and incubate the chip at controlled temperature.

Manuscript for Journal of Visualized Experiments (JoVE)

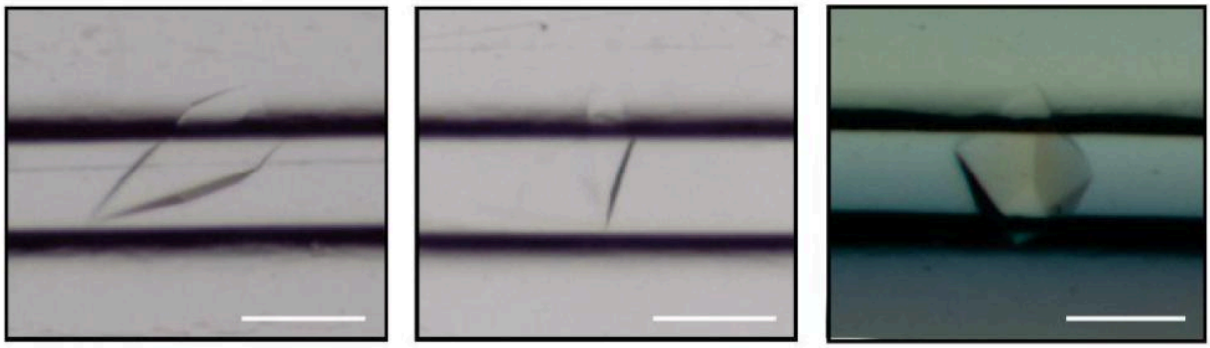

Figure 3: Crystals of CCA-adding enzyme grown by counter-diffusion in the microfluidic channels of ChipX. Scale bar is 0.1 mm.

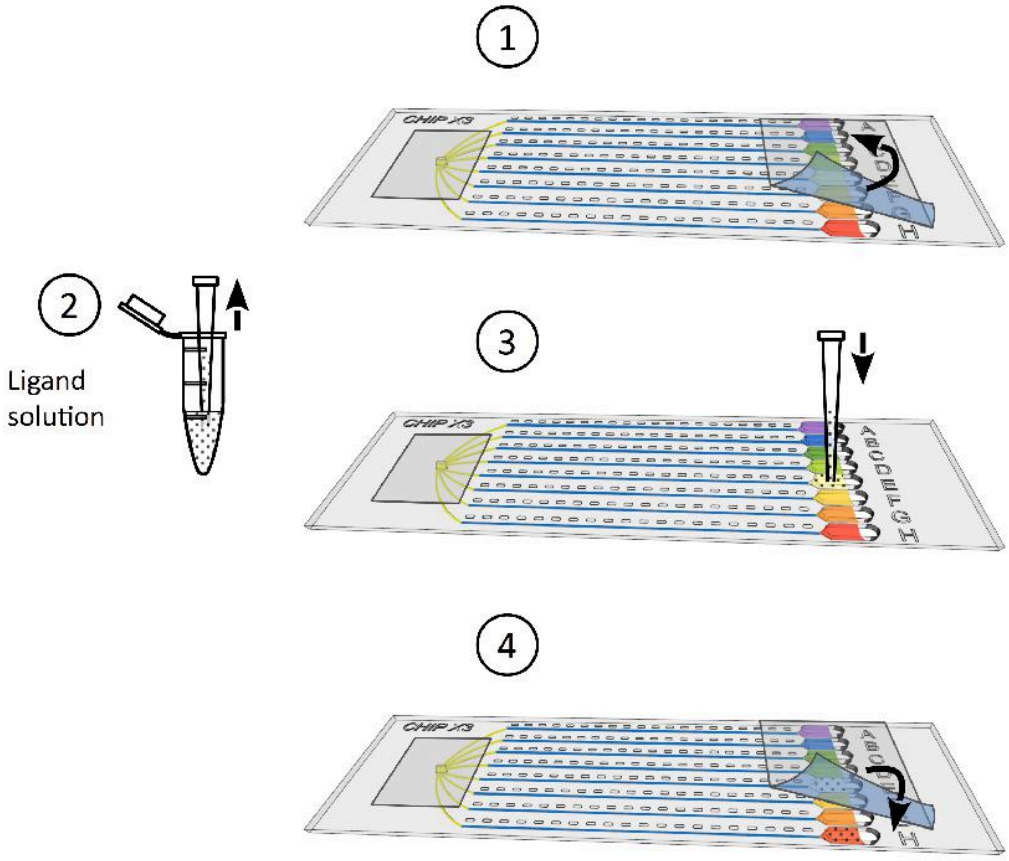

Figure 4: Crystal soaking procedure. 1) Gently remove the tape from the reservoirs. 2) Deposit up to 5 µl of ligand solution using a 10 µl micropipet. 3) Add the ligand to one or several reservoirs. 4) Seal again the reservoirs with a piece of tape and incubate the chip under controlled temperature for 24-48 h before data collection.

Manuscript for Journal of Visualized Experiments (JoVE)

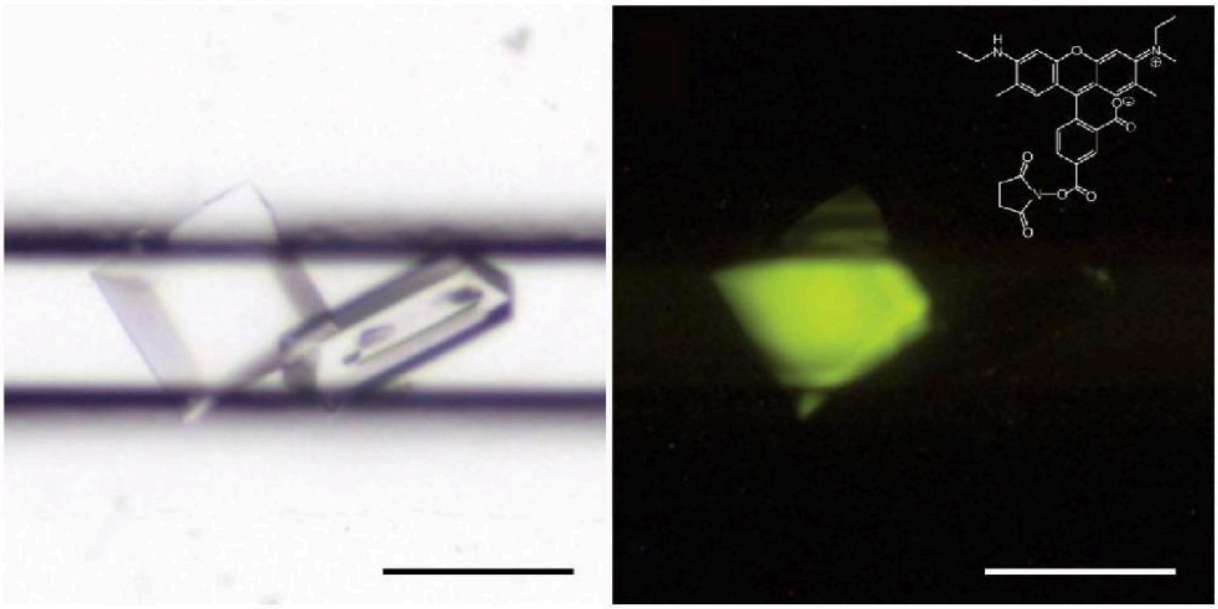

Figure 5: Trace fluorescent labeling discriminates protein (left) from salt (right) crystals. The CCA-adding enzyme solution contained 0.4 % (w/w) of protein labeled with carboxyrhodamine. On the right, crystals are illuminated with a 520 nm wavelength light source (XtalLight-100C source from Xtal Concepts, Hamburg) and the image is taken with a low pass filter at 550 nm (LP550); (inset) structure of carboxyrhodamine-succinimidyl ester.

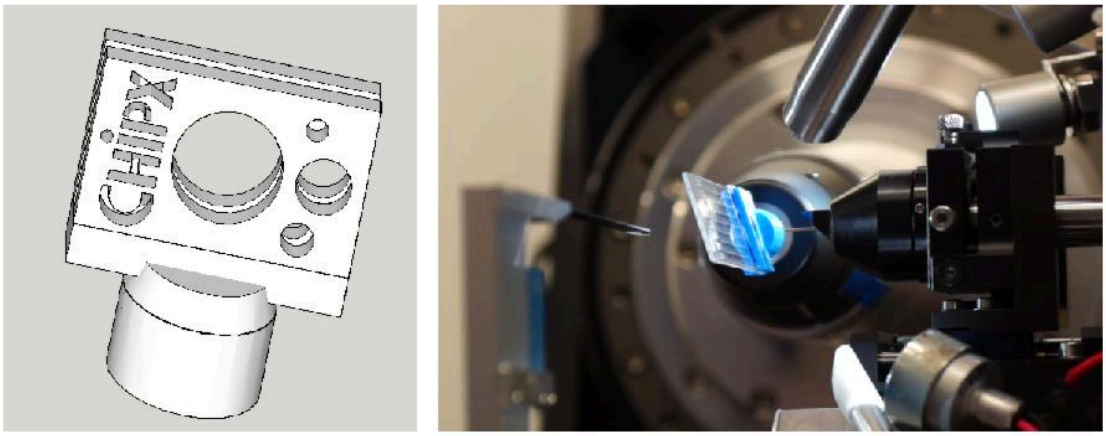

Figure 6: (Left) Drawing of the ChipX holder and (Right) ChipX mounted on the goniometer of beamline X06DA at SLS (Villigen, Switzerland) for serial crystal analysis.

Manuscript for Journal of Visualized Experiments (JoVE)

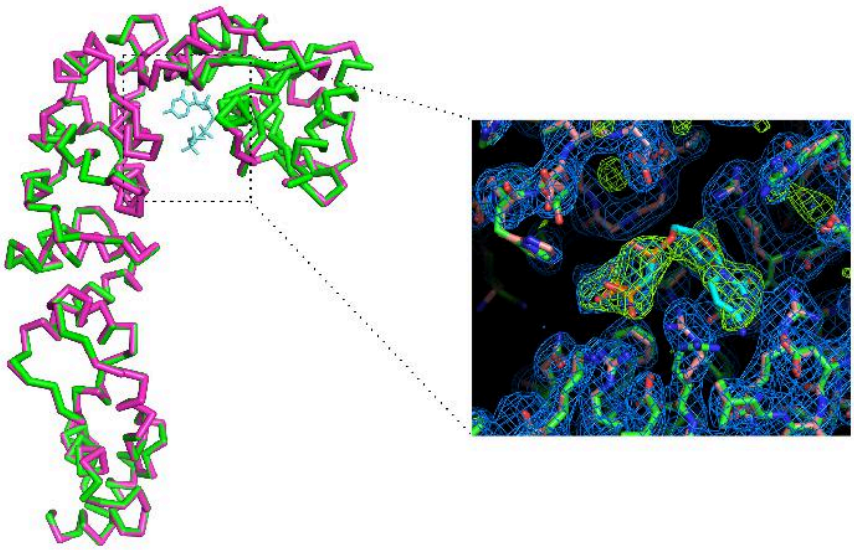

Figure 7: Comparison of CCA-adding enzyme active site in the apo form (in blue) and in the complex with CTP (in orange). Although the overall conformation of the enzyme is not affected, the binding of the CMPcPP ligand is accompanied by a slight reorganization of side chains in the active site. The 2*Fo-Fc* electron density map (in blue) is contoured at 1.2 sigma. The difference electron density map contoured at 4 sigma (in green) confirms the presence of the ligand in the active site.

Manuscript for Journal of Visualized Experiments (JoVE)

Table 1: Data collection and refinement statistics

Sample	CCA-adding enzyme	CCA-adding enzyme + CMPcPP
Crystal analysis		
X-ray beamline	SLS – XDA06	SLS – X10SA
Wavelength (Å)	1.000	1.000
Temperature (K)	293	293
Detector	Pilatus 2M-F	Pilatus 6M
Crystal-detector distance (mm)	300	400
Crystals collected	6	14
Crystals selected	5	5
Rotation range per image (°)	0.1	0.2
Exposure time per image (s)	0.1	0.1
No. of images selected	1000	540
Total rotation range (°)	100	108
Space group	$P4_32_12$	$P4_32_12$
a, *c* (Å)	71.5, 293.8	71.4, 293.6
Mean mosaicity (°)	0.04	0.04
Resolution range (Å)	46 – 2.54 (2.6 – 2.54)	48 – 2.3 (2.4 – 2.3)
Total No. of reflections	176105 (9374)	232642 (32937)
No. of unique reflections	23922 (1598)	34862 (4066)
Completeness (%)	90.6 (84.6)	99.5 (100.0)
Redundancy	7.5 (6.0)	6.7 (8.1)
$\langle I/\sigma(I) \rangle$	8.1 (1.3)	6.9 (0.7)
*R*meas (%)	18.6 (126.0)	18.0 (231.2)
CC1/2 (%)	98.7 (55.0)	98.7 (46.9)
Overall *B* factor from Wilson plot (Å 2)	57.4	60.6
Crystallographic refinement		
No. of reflections, working set / test set	23583 / 1180	34840 / 3405
Final Rcryst (%) / R_{free} (%)	18.8 / 21.4	20.0 / 22.9
No. of non-H atoms: overall / protein / ligand / solvent	2998 / 2989 / 0 / 9	3057 / 2989 / 29 / 10
R.m.s. deviations for bonds (Å) / angles (°)	0.009 / 1.23	0.010 / 1.22
Average *B* factors ($Å^2$): overall / protein / ligand / solvent	60.1 / 60.1 / 0 / 52.7	62.5 / 62.6 / 60.1 / 55.5
Ramachandran plot: most favoured (%) / allowed (%)	98.1 / 1.9	97.2 / 2.8
PDB id	6IBP	6Q52

Manuscript for Journal of Visualized Experiments (JoVE)

DISCUSSION:

Current protocols in biocrystallography involve the preparation of crystals using methods such as vapor diffusion or batch[11,12], and their transfer into a microloop for cryo-cooling[13,14] before performing the diffraction analysis in a nitrogen jet at cryogenic conditions. In contrast, while cryo-cooling is not possible in ChipX, the protocol described in the video provides a fully integrated pipeline for the determination of crystal structures at room temperature, i.e. in more physiological conditions. The main advantages of the protocol are the following:

- the crystals are produced in a convection-free environment (microfluidic channels) which is very favorable to the growth of high quality crystals,
- the counter-diffusion method implemented in ChipX is very efficient at screening the supersaturation landscape and at finding nucleation and growth conditions,
- crystals are never directly handled, but are analyzed in situ, inside the chip, which preserves their genuine diffraction properties,
- the diffraction analysis is performed on a series of crystals distributed along the chip channels with low dose exposure to minimize radiation damage, and a full dataset is assembled by merging partial data from the series.
- the standard footprint and simple design of ChipX will allow in the future a complete automation of *in situ* data collection using synchrotron or XFEL facilities.

All steps of the protocol are carried out in ChipX. From the experimenter point-of-view, chip setup is simple and easy to perform with standard pipets and does not require any extra equipment. The tree-like channel connection at the sample inlet minimizes dead volumes in the system, which is important when working with samples that are difficult to purify or that are only available in limited quantity. The volume actually required for individual counter-diffusion assays is less than 300 nl in ChipX.

In conclusion, the lab-on-a-chip approach implemented in ChipX simplifies and efficiently miniaturizes the process of crystallization by counter-diffusion and crystal structure determination, allowing to go from the sample to its 3D structure in a single device. It is widely applicable and offers a user-friendly, cost-effective solution for routine serial biocrystallography investigations at room temperature.

ACKNOWLEDGMENTS:

The authors acknowledge the Swiss Light Source (Villigen, Switzerland) for beamtime allocation to the project on beamlines X10SA (PXII) and X06DA (PXIII). This work was supported by the French Centre National de la Recherche Scientifique (CNRS), the University of Strasbourg, the LabEx consortium "NetRNA" (ANR-10-LABX-0036_NETRNA), a Ph.D funding to R.dW from the Excellence initiative (IdEx) of the University of Strasbourg in the frame of the French National Program "Investissements d'Avenir", the Deutsche Forschungsgemeinschaft (grant no. Mo 634/10-1). The authors benefitted from the PROCOPE Hubert Curien cooperation program (French Ministry of Foreign Affair and Deutscher Akademischer Austauschdienst).

DISCLOSURES:

The authors have nothing to disclose.

Manuscript for Journal of Visualized Experiments (JoVE)

REFERENCES:

(1) Giegé, R.; Sauter, C. Biocrystallography: Past, Present, Future. *HFSP J.* **2010**, *4* (3–4), 109–121.

(2) Pinker, F.; Brun, M.; Morin, P.; Deman, A.-L.; Chateaux, J.-F.; Oliéric, V.; Stirnimann, C.; Lorber, B.; Terrier, N.; Ferrigno, R.; et al. ChipX: A Novel Microfluidic Chip for Counter-Diffusion Crystallization of Biomolecules and in Situ Crystal Analysis at Room Temperature. *Cryst. Growth Des.* **2013**, *13* (8), 3333–3340.

(3) García-Ruiz, J. M.; Otálora, F.; Novella, M. L.; Gavira, J. A.; Sauter, C.; Vidal, O. A Supersaturation Wave of Protein Crystallization. *J. Cryst. Growth* **2001**, *232* (1–4), 149–155.

(4) Otálora, F.; Gavira, J. A.; Ng, J. D.; García-Ruiz, J. M. Counterdiffusion Methods Applied to Protein Crystallization. *Prog. Biophys. Mol. Biol.* **2009**, *101* (1–3), 26–37.

(5) Pusey, M.; Barcena, J.; Morris, M.; Singhal, A.; Yuan, Q.; Ng, J. Trace Fluorescent Labeling for Protein Crystallization. *Acta Crystallogr. Sect. F Struct. Biol. Commun.* **2015**, *71* (7), 806–814.

(6) Meyer, A.; Betzel, C.; Pusey, M. Latest Methods of Fluorescence-Based Protein Crystal Identification. *Acta Crystallogr. Sect. F Struct. Biol. Commun.* **2015**, *71* (2), 121–131.

(7) Betat, H.; Rammelt, C.; Mörl, M. tRNA Nucleotidyltransferases: Ancient Catalysts with an Unusual Mechanism of Polymerization. *Cell. Mol. Life Sci.* **2010**, *67* (9), 1447–1463.

(8) Ernst, F. G. M.; Erber, L.; Sammler, J.; Jühling, F.; Betat, H.; Mörl, M. Cold Adaptation of tRNA Nucleotidyltransferases: A Tradeoff in Activity, Stability and Fidelity. *RNA Biol.* **2018**, *15* (1), 144–155.

(9) Kabsch, W. XDS. *Acta Crystallogr. D Biol. Crystallogr.* **2010**, *66* (Pt 2), 125–132.

(10) Adams, P. D.; Afonine, P. V.; Bunkóczi, G.; Chen, V. B.; Davis, I. W.; Echols, N.; Headd, J. J.; Hung, L.-W.; Kapral, G. J.; Grosse-Kunstleve, R. W.; et al. PHENIX: A Comprehensive Python-Based System for Macromolecular Structure Solution. *Acta Crystallogr. D Biol. Crystallogr.* **2010**, *66* (Pt 2), 213–221.

(11) Dessau, M. A.; Modis, Y. Protein Crystallization for X-Ray Crystallography. *J. Vis. Exp.* **2011**, No. 47.

(12) Sauter, C.; Lorber, B.; McPherson, A.; Giegé, Richard. Crystallization - General Methods. In *In International Tables of Crystallography, Vol. F, Crystallography of Biological Macromolecules (2nd edition), E. Arnold, D.M. Himmel & M.G. Rossmann (eds)*; John Wiley and Sons: Chichester, 2012; pp 99–120.

(13) Garman, E. "Cool" Crystals: Macromolecular Cryocrystallography and Radiation Damage. *Curr. Opin. Struct. Biol.* **2003**, *13* (5), 545–551.

(14) Li, D.; Boland, C.; Aragao, D.; Walsh, K.; Caffrey, M. Harvesting and Cryo-Cooling Crystals of Membrane Proteins Grown in Lipidic Mesophases for Structure Determination by Macromolecular Crystallography. *J. Vis. Exp.* **2012**, No. 67.

6 A simple and versatile microfluidic device for efficient biomacromolecule crystallization and structural analysis by serial crystallography (in preparation for IUCrJ)

A simple and versatile microfluidic device for efficient biomacromolecule crystallization and structural analysis by serial crystallography

Raphaël de Wijn[1], Oliver Hennig[2], Jennifer Roche[3], Sylvain Engilberge[4], Kevin Rollet[1], Pablo Fernandez-Millan[1], Karl Brillet[1], Heike Betat[2], Mario Mörl[2], Alain Roussel[3], Eric Girard[4], Christoph Mueller-Dieckmann[5], Gavin C. Fox[6], Vincent Oliéric[7], José-Antonio Gavira[8], Bernard Lorber[1], Claude Sauter[1]

[1]*Architecture et Réactivité de l'ARN, UPR 9002, CNRS, Institut de Biologie Moléculaire et Cellulaire (IBMC), Université de Strasbourg, 15 rue René Descartes, 67084 Strasbourg, France*

[2]*Institute for Biochemistry, Leipzig University, Bruederstr. 34, 04103 Leipzig, Germany*

[3]*Architecture et Fonction des Macromolécules Biologiques, UMR 7257 CNRS-Aix Marseille University, 163 avenue de Luminy, 13288 Marseille, France*

[4]*Univ. Grenoble Alpes, CEA, CNRS, IBS, 38000 Grenoble, France*

[5]*Structural Biology, European Synchrotron Radiation Facility, 6 Rue Jules Horowitz, Grenoble, 38043, France*

[6]*Synchrotron SOLEIL, PROXIMA 2A beamline, L'Orme des Merisiers Saint-Aubin, 91192 Gif-sur-Yvette, France*

[7]*Paul Scherrer Institute, Swiss Light Source, Forschungsstrasse 111, 5232 Villigen PSI, Switzerland*

[8]*Laboratorio de Estudios Cristalográficos, IACT, CSIC-Universidad de Granada, Av. Las Palmeras, 4, Armilla, 18100 Granada, Spain*

Synopsis An innovative microfluidic design is described for simple biomacromolecule crystallization by counter-diffusion allowing semi-automated structural analysis by serial crystallography at room temperature. ChipX3 functionalities are demonstrated using case studies leading to high resolution structures of four proteins and one RNA.

Abstract - Determining optimal conditions to produce well diffracting crystals is a key step of every biocrystallography project. We describe a microfluidic device that enables the production of crystals by counter-diffusion and their direct on-chip analysis by serial crystallography at room temperature. Nine "non-model" and diverse biomacromolecules, including seven soluble proteins, a membrane protein and a RNA duplex, were crystallized and treated on chip with a variety of standard techniques including micro-seeding, crystal soaking with ligands and crystal detection by fluorescence. Furthermore, the crystal structures of four proteins and one RNA were determined based on serial data collected on four synchrotron beamlines, demonstrating the general applicability of this multipurpose chip concept.

Keywords: macromolecule; crystallization; counter-diffusion; microfluidics; seeding; ligand soaking; trace fluorescent labelling; serial crystallography; room temperature

1. Introduction

Crystallography plays a central role in contemporary biology because it enables the visualization of the 3D architecture of biological macromolecules, which provides insights at the atomic scale into their cellular functions and partnerships (Giegé & Sauter, 2010; Jaskolski *et al.*, 2014). Over the past two decades, the advent of structural genomics and associated high throughput (HTP) technologies (Vincentelli *et al.*, 2003; Pusey *et al.*, 2005), together with the dramatic improvements in experimental setups and computational environment at synchrotron facilities (Terwilliger *et al.*, 2009; Owen *et al.*, 2016), have revolutionized the field and led to a torrent of new crystal structures. This productivity boost is clear from the number of structures deposited in the Protein Databank (PDB), which will exceed 150.000 entries by the end of 2018.

In spite of such advances, the time consuming and costly mapping of reagents and phase space to identify conditions yielding diffraction quality crystals from a limited amount of macromolecule remains a bottleneck of crystallographic studies (McPherson & Gavira, 2013; Luft *et al.*, 2014; Giegé, 2017). This process generally involves a trial-and-error sampling of chemical and physical space by screening hundreds of different cocktails composed of buffers at different pHs, various crystallants – salts, alcohols and polymers – and temperature to find at least one appropriate solvent and the right supersaturation conditions. The miniaturization of crystallization assays in microplates with drop volumes of 0.1-1 µL (typically containing 1-10 µg of macromolecule) and the automation of the screening procedure have made this task considerably more efficient, making it possible to successfully conduct a project with only a few milligrams of pure sample (Sauter *et al.*, 2012).

With the introduction of the first microfluidic systems dedicated to HTP screening 15 years ago, the sample volume required for a single experiment was reduced by another order of magnitude, down to a few nanoliters (Hansen *et al.*, 2002; Zheng *et al.*, 2003). Indeed, microfluidics was immediately regarded as a major breakthrough, especially for biochemists dealing with samples difficult to purify in large quantities, such as macromolecules from higher eukaryotes, large biological assemblies, or membrane proteins (Hansen & Quake, 2003; van der Woerd *et al.*, 2003). However, despite their potential, microfluidic technologies have not yet been massively adopted by the global community for crystal growth, as illustrated by the limited number of PDB entries (only about 25 as of October 2018) specifically citing the use of microfluidic systems. This can be partly explained by the cost of these microsystems and their associated equipments, but also by the difficulty to successfully extract fragile crystals from the chips, or the requirement to reproduce them using conventional crystallization methods before they can be subjected to a crystallographic analysis.

To expand the functionality and attractiveness of microchips beyond crystallization and HTP screening, several teams have explored the possibility of analyzing crystals directly in their microfluidic environment (Yadav *et al.*, 2005; Ng *et al.*, 2008; Sauter *et al.*, 2007; Dhouib *et al.*, 2009; Emamzadah *et al.*, 2009; Hansen *et al.*, 2006; Stojanoff *et al.*, 2011). Various geometries and materials have been tested and led to promising results in terms of data collection, anomalous phasing or time-resolved applications (Pinker *et al.*, 2013; Khvostichenko *et al.*, 2014; Perry *et al.*, 2013, 2014). The difficulty of cryopreserving crystals, to protect them from radiation damage inside chips – due to the wide flat surfaces of the device causing vapor condensation and ice formation in the cryojet – was first perceived as an obstacle. However, the recent revival of multi-

crystal data collection techniques at room temperature by the X-ray Free Electron Laser (X-FEL) community has changed the paradigm and popularized serial crystallography (Chapman *et al.*, 2011; Stellato *et al.*, 2014; Ayyer *et al.*, 2015). In this context, microfluidic systems provide promising solutions to prepare, handle and analyze crystals, both at synchrotron beamlines and at X-FEL (Heymann *et al.*, 2014; Sui *et al.*, 2016).

In this report, we describe a versatile and low-cost microfluidic chip for crystal production and characterization. This chip was initially designed to miniaturize and facilitate the identification of crystal growth conditions using the counter-diffusion method and its efficient self-optimizing process (Dhouib *et al.*, 2009; Pinker *et al.*, 2013). With the latest version of the chip design, ChipX3, we demonstrate that crystals can i) be easily produced in the chip by seeding, ii) soaked *in situ* with ligands or iii) visualized by fluorescence imaging. In addition, the chip provides a stable platform for crystal storage, handling, shipment and *in situ* analysis by serial crystallography. We illustrate a range of applications for ChipX3 by the crystallization of seven soluble proteins, a membrane protein and an RNA duplex, as well as the structure determination of five "non-model" macromolecules at room temperature with data collected on four beamlines at three different synchrotron sites. This lab-on-a-chip approach simplifies and efficiently miniaturizes the crystallographic structure determination process, from the sample to its 3D structure, in a single device. It offers a user-friendly, cost-effective solution for routine biocrystallographic investigations at room temperature.

2. Material and methods

2.1. Biomacromolecules, biochemicals and chemicals

Recombinant proteins used in this work include Protease 1 from *Pyrococcus horikhoshii* (PhP1), a Llama nanobody PorM_02 (Nb02), a lipase from *Thermomyces lanuginosus* (Lip, provided by Macrocystal Oy, Finland), the CCA-adding enzyme from psychrophilic bacterium *Planococcus halocryophilus* (CCA), TonB dependent heme/hemoglobin Outer Membrane Transporter (OMT) ShuA from pathogen *Shigella dysenteriae* (OMT ShuA), the human mitochondrial aspartyl-tRNA synthetase (hmDRS) and the aspartyl-tRNA synthetase 1 from bacterium *Thermus thermophilus* (ttDRS), which were purified as previously described (Engilberge *et al.*, 2018; Duhoo *et al.*, 2017; Ernst *et al.*, 2018; Brillet *et al.*, 2009; Sauter *et al.*, 2015; Zhu *et al.*, 2001). Horse hemoglobin was purchased from Sigma. A nine base pair RNA duplex $[r(CGUGAUCG)dC]_2$ was prepared as described (Masquida *et al.*, 1999). Stock concentrations and storage buffers are indicated in **Table 1**.

To facilitate the detection of CCA crystals by trace fluorescent labeling (TFL – Pusey *et al.,* 2015), the protein was fluorescently labeled with carboxyrhodamine-succinimidyl ester (Invitrogen, catalog No. C6157) as described by de Wijn *et al.* (2018). The labeled protein solution was stored at 277 K and mixed with the protein stock solution just before preparing crystallization assays as a fraction corresponding to less than 0.5 % of the total protein stock. This solution will be referred to as "CCA-TFL".

The non-hydrolizable analog of cytidyl tri-phosphate (CTP) soaked in CCA crystals, cytidine-5'-[(α,β)-methyleno] triphosphate (CMPcPP, Cat. No NU-438) was purchased from Jena Bioscience (Germany). The lanthanide complex Terbium-Xo4 (commercial name Crystallophore) used to crystallize PhP1 was synthesized as described (Engilberge *et al.*, 2017).

2.2. ChipX3 manufacturing

ChipX3 devices were designed at IBMC (Strasbourg, France) in collaboration with Synchrotron SOLEIL (Saint-Aubin, France) and manufactured by MicroLIQUID (Arraste, Spain). The fluidic layer (thickness 1 mm) was produced in cyclic olefin copolymer (COC; TOPAS® 5013F-04) by injection molding. Channels and reservoirs were sealed by a second layer of COC (thickness 100 µm). The bonding process was carried out at 398 K and a pressure of 5 bar. The straight section of microfluidic channels is 4 cm long with a cross-section of 80 µm x 80 µm for a volume of 260 nL. The reservoir at their extremity has a volume of 10 µL (**Figure 1**).

2.3. Sample loading and crystallization

Crystallization experiments in the ChipX3 were set up in three steps with a conventional 10 µL micropipet (Gilson) and regular tips (StarLab). First, 4 to 6 µL of macromolecule solution were injected in the sample inlet connecting all channels, to fill the entire arborescence up to the reservoirs. Second, 1 µL of paraffin oil (Fluka) was injected into the sample inlet to isolate the channels from each others and the inlet was sealed with CrystalClear tape (Hampton Research) to prevent evaporation and solution movements. The third and last step consisted in filling the reservoirs with 5 µL of crystallization solutions before sealing them with CrystalClear tape. Solutions used to setup the chips are listed in **Table 1**. All experiments were incubated at 293 K, except the RNA duplex which was crystallized at 310 K.

2.4. Crystallization by seeding

The condition producing the best CCA crystals (de Wijn *et al.*, 2018) was found using the microseed matrix screening (MMS) method described by D'Arcy *et al.*, (2007, 2014). Small crystals grown by hanging drop with a reservoir containing 1 M diammonium hydrogen phosphate, 100 mM sodium acetate, pH 4.5 (condition E8 from commercial screen JCSG++ from Jena Biosciences) were recovered, vigorously resuspended, vortexed and diluted in 50 uL of the same crystallant solution. This suspension was stored at 277 K and is referred to as "seed stock". Protein crystallization solutions were prepared by mixing 6 µL enzyme (5.5 mg/mL), 1.5 µL of seed stock (either original or diluted solution) and 1 µL of CCA-TFL. Crystallization of ttDRS enzyme in the ChipX3 was also performed using seeds. The "seed stock" suspension was prepared as described for the CCA enzyme, by crushing crystals grown by vapor diffusion in hanging drops with a reservoir containing 7% (m/v) PEG800 and 10 mM $MgCl_2$. ttDRS crystallization solutions were prepared as a mix containing 6.5 µL enzyme (19 mg/mL) and 1.5 µL of seed stock, either original or diluted solution.

2.5. Crystal soaking with substrate

To soak CCA crystals grown in the ChipX3, the tape covering the reservoirs was removed and 3 µL of 10 mM CMPcPP solution were added in selected reservoirs (final concentration of 3.75 mM) before sealing them again. This step was performed a week before data collection to ensure a good diffusion along the microfluidic channels and in an attempt to maximize site occupancy in the crystals.

2.6. X-ray data collection and analysis

Diffraction data were collected either: i) on beamline PXII (Fuchs *et al.*, 2014) equipped with a Pilatus 6M detector and PXIII (Bingel-Erlenmeyer *et al.*, 2011) equipped with a MarCCD or a Pilatus 2M-F detector at the Swiss Light Source (SLS, Villigen, Switzerland), ii) on beamline Proxima-2-A (Duran *et al.*, 2013) equipped with an Eiger X 9M detector at SOLEIL (Saint-Aubin, France), or iii) on beamline ID30B (McCarthy *et al.*, 2018) equipped with a Pilatus3 6M detector at the ESRF (Grenoble, France). All diffraction data were collected at room temperature (T = 293-298 K) on crystals inside the ChipX3 without any prior treatment, owing to the reduced scattering background of the chip (Pinker *et al.*, 2013). In most cases a dedicated 3D-printed holder mounted on a standard goniometer (see **Figure 5** and **Figure S2**) was used for data collections.

To collect the widest possible rotation angle for each crystal in ChipX3, the channel containing the crystal was aligned relative to the rotation axis of the goniometer. Crystal alignment was performed either by standard low dose grid screening at SLS and SOLEIL, or by a 1-click procedure at ESRF, as described (McCarthy *et al.*, 2018). To avoid collisions with the surrounding equipment (beamstop, collimator), we typically collected 30° rotations per collection between positions -30° and +30° (0° corresponding to the channels being perpendicular to the X-ray beam). Two collection strategies were used to obtain complete data: one consisted in merging several partial datasets (sweeps) from the same crystal (one orientation and a wide rotation range), or merging several datasets from different crystals (several orientations and a smaller rotation range per crystal). **Table 2** gives details about each data collection and processing.

Partial datasets were individually processed with XDS (Kabsch, 2010). When their number did not exceed 10, they were manually merged with XSCALE to find the best combination and determine the appropriate resolution range. In the case of PhP1 enzyme, the program ccCluster (Santoni *et al.*, 2017) was used to determine the best partial datasets to merge among the 35 available. For all remaining steps, the PHENIX package was used (Adams *et al.*, 2010). Phases were determined by molecular replacement using the following structures: PDB entries 1MIV for CCA, 5LMW for NB02, 1G2I for PhP1, 4GWL for Lip and 485D for the RNA. The latter crystals (space group H3) presented a translational pseudo-symmetry due to the intrinsic symmetry of the duplex and a merohedral twin (twin fraction 0.21-0.39). Hence, the structure was refinement using the twin law “h,-k-h,-l”. The structure of the psychrophilic CCA-adding enzyme was determined in its apo form and in complex with CMPcPP by letting the substrate analogue diffuse in the channels and into the crystals. Two conformations were modelled for the tri-phosphate moiety of CMPcPP according to the observed difference density. All structures were built and refined with COOT and PHENIX, respectively (Emsley & Cowtan, 2004; Adams *et al.*, 2010).

3. Results and discussion

3.1. ChipX3 design and setup

ChipX3 was designed to perform counter-diffusion (CD) experiments and take advantage of convection-free conditions (a prerequisite of CD) in channels of small cross-section (width: 80 µm, depth: 80 µm) to enable the creation of crystallant concentration gradients by pure diffusion (**Figure 1A**). The channels with a

length of 4 cm allow a broad screening of supersaturation states as does conventional CD in microcapillaries (García-Ruiz *et al.*, 2001; Otálora *et al.*, 2009).

The geometry of the sample inlet was adapted to fit standard P2/P10 micropipet tips for chip loading using standard laboratory material. No extra equipment (such as a pump) is required. The standard micropipet is used to inject the solution into the fluidic system. The branching channel configuration (**Figure 1B**) allows simultaneous loading of the eight channels in a single manipulation, thus limiting the loading time and solution dead volumes. Note that in the case of membrane protein samples containing a detergent (like ShuA in this work), solutions enter and fill the channels spontaneously due to capillary action and the native wettability of the COC material. Labels embossed along the channels facilitate crystal location and grid mapping at synchrotron beamlines (**Figure 1C**).

Once the channels are filled with the macromolecule solution and the inlet closed with tape, the crystallant solutions are deposited in the reservoirs (**Figure 1D**). Their funnel-like shape has been optimized to facilitate the contact between the crystallization and macromolecule solutions and to avoid trapping air bubbles, which could prevent the diffusion process. One microliter of low-gelling temperature agarose solution at 1% (w/v) can optionally be deposited in the funnel prior to the crystallization cocktail to constitute a physical buffer at the entry of the channels that stabilizes the diffusion interface.

The loading procedure of ChipX3 is fast and straightforward. Setting up a chip with eight different conditions takes less than five minutes even for untrained experimenters, as attested by numerous assays performed in the five laboratories involved in this work and by the many participants of crystallization workshops (FEBS courses 2014-2018 in Nové Hrady, Czech Republic; International School of Biological Crystallization, ISBC 2015-2017 in Granada, Spain).

3.2. Crystallization in ChipX3

After prototyping phase of small batches made by hot embossing (Pinker *et al.*, 2013), a 3D mold was machined with the new ChipX3 specifications to produce a larger batch by injection molding. This enabled the validation of the concept on real cases, beyond classical model proteins such as lysozyme or thaumatin. We report here on eight proteins of different sizes and sources (from bacteria to human), and a RNA oligomer (**Table 1**) crystallized in ChipX3. Crystallization conditions were modified from those initially used in vapor diffusion or batch crystallization by increasing the concentration of the crystallant by a factor of 1.5 – 2. Representative examples ranging from small microcrystals to large crystals filling a portion of the channel are shown in **Figure 2**. Typical counter-diffusion patterns can be observed along the concentration gradient, with microcrystalline material close to the reservoirs where supersaturation is maximal, and larger crystals towards the other extremity of the channels (see **Figure S1**).

Crystals appeared after a few hours or days, and could be visualized under polarized light. To facilitate detection of small crystals, we exploited different fluorescence approaches such as the classical UV excitation (Meyer *et al.*, 2015), the fluorescent lanthanide compound Tb-Xo4 developed by Engilberge *et al.* (2017) and trace fluorescent labeling (TFL) developed by Pusey *et al.* (2015). All three approaches were compatible with ChipX3, but Tb-Xo4 molecule and TFL gave a much brighter signal (**Figure 3**). Fluorescence has the

advantage of rapidly localize samples in the channels and may be used in the future to automate and speed up serial analysis.

3.3. Advanced crystallogenesis strategies

In addition to providing an efficient screening of supersaturation conditions, the CD process has other practical benefits, including the possibility to diffuse anomalous scatterers into pre-grown crystals for phasing, or cryoprotecting with compounds such as glycerol (Gavira *et al.*, 2002; Ng *et al.*, 2003). In a previous study, we demonstrated the feasibility of on-chip SAD phasing at room temperature with crystals soaked by CD with a lanthanide complex (Pinker *et al.*, 2013). Along the same lines, CMPcPP, a non-hydrolizable analog of CTP, which is a substrate of CCA-adding enzymes, was added to the reservoirs once CCA crystals had grown and one week before the synchrotron session. The resulting X-ray structures confirmed that the crystals were derivatized by smooth diffusion without any sign of damage (**Figure 4** and **Figure 6**).

Microseeding can also be used together with CD crystallization (Bergfors, 2003; Gavira *et al.*, 2011) to bypass the nucleation step and promote rapid crystal growth. Hence, CCA and ttDRS crystals were grown by a combination of CD and seeding. Microseeds were added to the protein solution just before it was injected into the chips and the first crystals appeared in the channels after a few days. Seeding proved to be an effective way to trigger a fast and abundant crystal production, which is particularly interesting for a serial analysis.

We also used a new nucleant called crystallophore or Xo4 (Engilberge *et al.*, 2018) in the case of the protein PhP1, for which the crystallization condition (**Table 1**) was determined only in the presence of this Terbium complex. Tb-Xo4 was added to the protein solution before filling the channels. It triggered the nucleation and the growth of large PhP1 crystals, which completely filled the available volume. An added value with macromolecules crystallizing in the presence of Xo4 is the strong luminescence when illuminated by UV light (see **Figure 3**).

3.4. Crystal analysis inside ChipX3

The ChipX3 was designed for *in situ* characterization. Its overall thickness was optimized to give a good compromise between material rigidity and X-ray absorption / scattering (Pinker *et al.*, 2013). During data collection, the chip is oriented with its thickest layer facing the direct beam and the thinnest face behind the crystal to minimize the attenuation of the diffraction signal (**Figure 5**). Labels embossed along the channels enable easy localization of crystals before analysis, in view to a future automation of the procedure on synchrotron beamlines. The chip can also be positioned in the beam using a plate gripper as illustrated in **Figure S3**. To avoid intervention from beamline staff to mount/unmounts the gripper, we developed a light chip holder that can be directly attached to a standard goniometer. This chip holder is manufactured by 3D printing (**Figures 5, S2**) and integrates a standard metal base (B5, SPINE style, Mitegen) that is in contact with the goniometer magnet. The holder can be used with any flat device of microscope slide dimensions on synchrotron beamlines and lab-based instruments. The 3D description file for printing this device is provided as **supplementary material**.

To illustrate the general applicability of on-chip serial crystallography at room temperature we present the results of structure determination in the 1.5-2.5 Å resolution range of one RNA and four proteins (**Table 2, Figures 5 & 6**). This includes a new structure of a psychrophilic CCA-adding enzyme in its apo form and in complex with a substrate introduced in the crystals by diffusion. The data collections were carried out on series of crystals and their parameters were adapted to crystal size and sensitivity to radiation damage. Final crystal structures were obtained either from a single large crystal and two wedges (Nb02) or from combining partial datasets from several individuals crystals (RNA, Lip, CCA, PhP1). In the latter case, the use of ccCluster considerably facilitated the choice of partial datasets to be merged.

Note that performing *in situ* analysis – i.e. without direct handling of the crystals – is a guarantee that their genuine diffraction properties have been preserved. Comparative tests on thaumatin or lipase crystals in ChipX3 sent by regular postal mail or carried to the synchrotron by experimenter did not show significant differences (result not shown), indicating that the chip is a stable and robust container for crystal storage and transport.

The high sensitivity and low background of the latest hybrid pixel detectors (HPDs) over CCD detectors (Pinker *et al.*, 2013), and the very short analysis time (seconds) of the largest wedge of reciprocal space from single crystals are crucial to outrun radiation damage for room temperature data collection. The analysis in shutter-less mode also limits systematic errors in crystal orientation and, thus, improves the data quality. For example, the highest apparent mosaicity of RNA crystals (see **Table 2**) that were analyzed at an early stage of this work with a MarCCD detector is a direct symptom of data collection strategies used before the advent of HPDs. In the future, the wide spread integration of HPD technology at synchrotron sites and on lab-based X-ray sources will undoubtedly facilitate the development of serial crystallography.

4. Conclusion

Microfluidics has demonstrated its value in terms of miniaturization for macromolecular crystallization experiments and HTP screening. With ChipX3 we propose a versatile tool that integrates all steps of a crystallographic study on a single device with the size of a microscope slide. The same chip serves to produce crystals by counter-diffusion (including seeding techniques), to soak them with ligands (for substrate catalysis, ligand screening in fragment-based drug-design, or phasing purposes), and to perform their diffraction analysis by *in situ* serial crystallography. The latter step carried out on-chip at room temperature, does no longer require any crystal handling, neither fishing, nor mounting or cryo-cooling. This guarantees the preservation of the intrinsic crystals quality, the chip being a safe means of sample storage and transportation. ChipX3 is easy to use with standard laboratory equipment for sample loading and crystal observation, making it cost-effective with minimal training or expertise required. We show with several case studies the general applicability of this lab-on-chip concept. Sample fluorescent labeling, as exemplified in this work, may be exploited to detect and center individual crystals in the X-ray beam and perform their characterization fully automatically. Such microfluidic devices show great promise in the future, in combination of serial analysis pipelines developed at advanced X-ray sources (XFEL, synchrotrons), for routine structure determination at temperatures close to physiological conditions (Martin-Garcia *et al.*, 2016; Johansson *et al.*, 2017).

Aknowledgements The authors thank the following synchrotron facilities and associated scientists for beamtime allocation to the project and assistance during data collection: beamlines X06DA (PXIII) and X10SA (PXII) at the Swiss Light Source (Villigen, Switzerland), PROXIMA 2A at SOLEIL synchrotron (Saint-Aubin, France), A. McCarthy for support on ID30B at the European Synchrotron Radiation Facility (Grenoble, France). They also acknowledge F. Riobé, O. Maury from Laboratoire de Chimie at ENS-Lyon and Polyvalan (Lyon, France) for providing Tb-Xo4, V. Vanel and the team of the Shadok fablab (Strasbourg, France) for assistance with 3D printers, as well as the participants and organizers of crystallization schools at Nové Hrady in Czech Republic (FEBS courses 2014-2018) and at Granada in Spain (ISBC 2013-2015) for their active participation in operational tests of ChipX3 and their technical feedback.

Funding information This work was supported by the Mission Ressources Compétences Technologiques (MRCT to C.S. and G.C.F.) of French Centre National de la Recherche Scientifique (CNRS), the University of Strasbourg, the LabEx consortia "MitoCross" (ANR-11-LABX-0057_MITOCROSS to C.S. and B.L.), "NetRNA" (ANR-10-LABX-0036_NETRNA to C.S. and B.L.), the French ANR agency (program Ln23 ANR-13-BS07-0007-01 to S.E. and E.G.), a Ph.D funding to R.dW from the Excellence initiative (IdEx) of the University of Strasbourg in the frame of the French National Program "Investissements d'Avenir", the Deutsche Forschungsgemeinschaft (grant no. Mo 634/10-1 to M.M. and H.B.). The authors benefitted from the PROCOPE Hubert Curien cooperation program (French Ministry of Foreign Affair and DAAD to C.S. and M.M.).

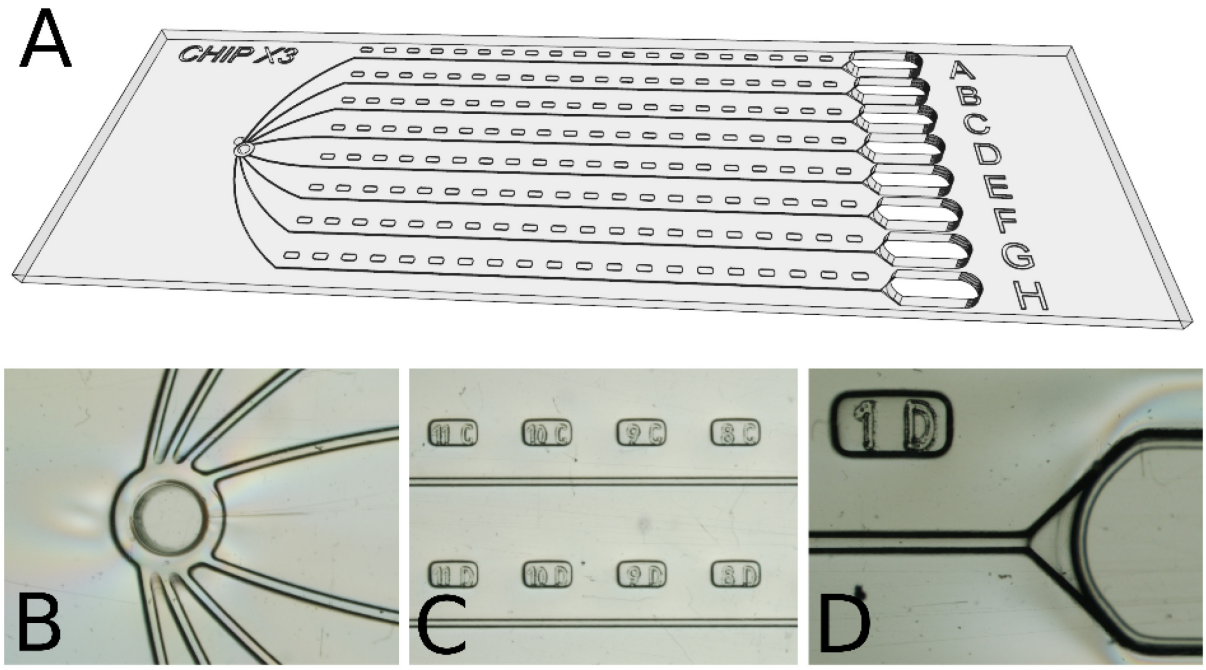

Figure 1 ChipX3 setup. (A) Schematic view of the chip, which has the dimension of a microscope slide (75 mm x 25 mm) and eight channels with a straight segment of 4 cm and a cross-section of 80 µm x 80 µm. Close-up views of (B) the inlet for the biomacromolecule solution, (C) channels and labels, (D) end of channel and crystallant reservoir.

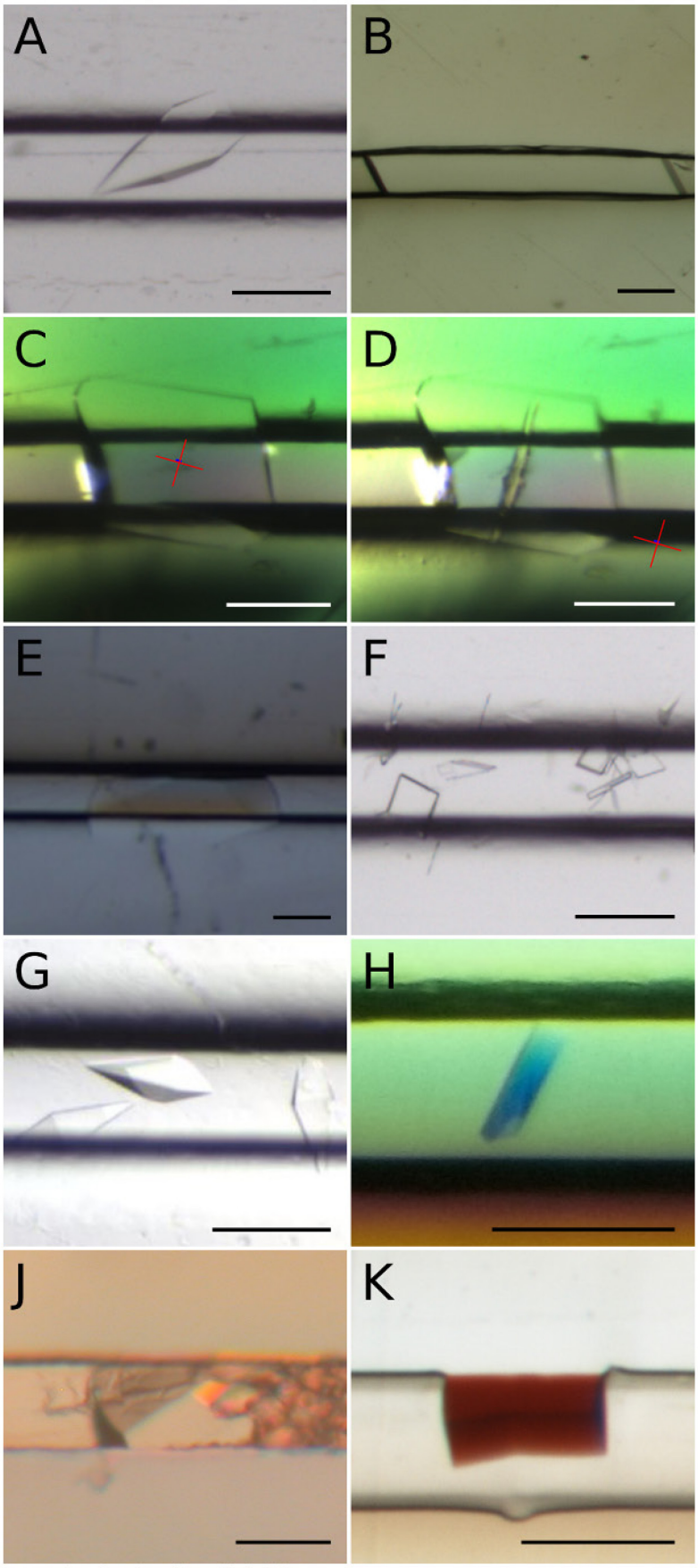

Figure 2 Examples of crystals obtained in ChipX3. Crystals were grown as described in **Table 1**. (A) CCA enzyme, (B) PhP1, (C) Nb02 before and (D) after data collection with X-ray beam footprint, (E) Lipase, (F) ttDRS, (G) hmDRS, (H) ShuA, (J) oligo RNA duplex, (K) hemoglobin. Scale bar = 0.1 mm. The panel was prepared with ImageJ (version 1.48k; Schneider *et al.*, 2012) and the FigureJ addon (version 1.10b; Mutterer and Zinck, 2013), as well as figures 3, 4, 5 and 6.

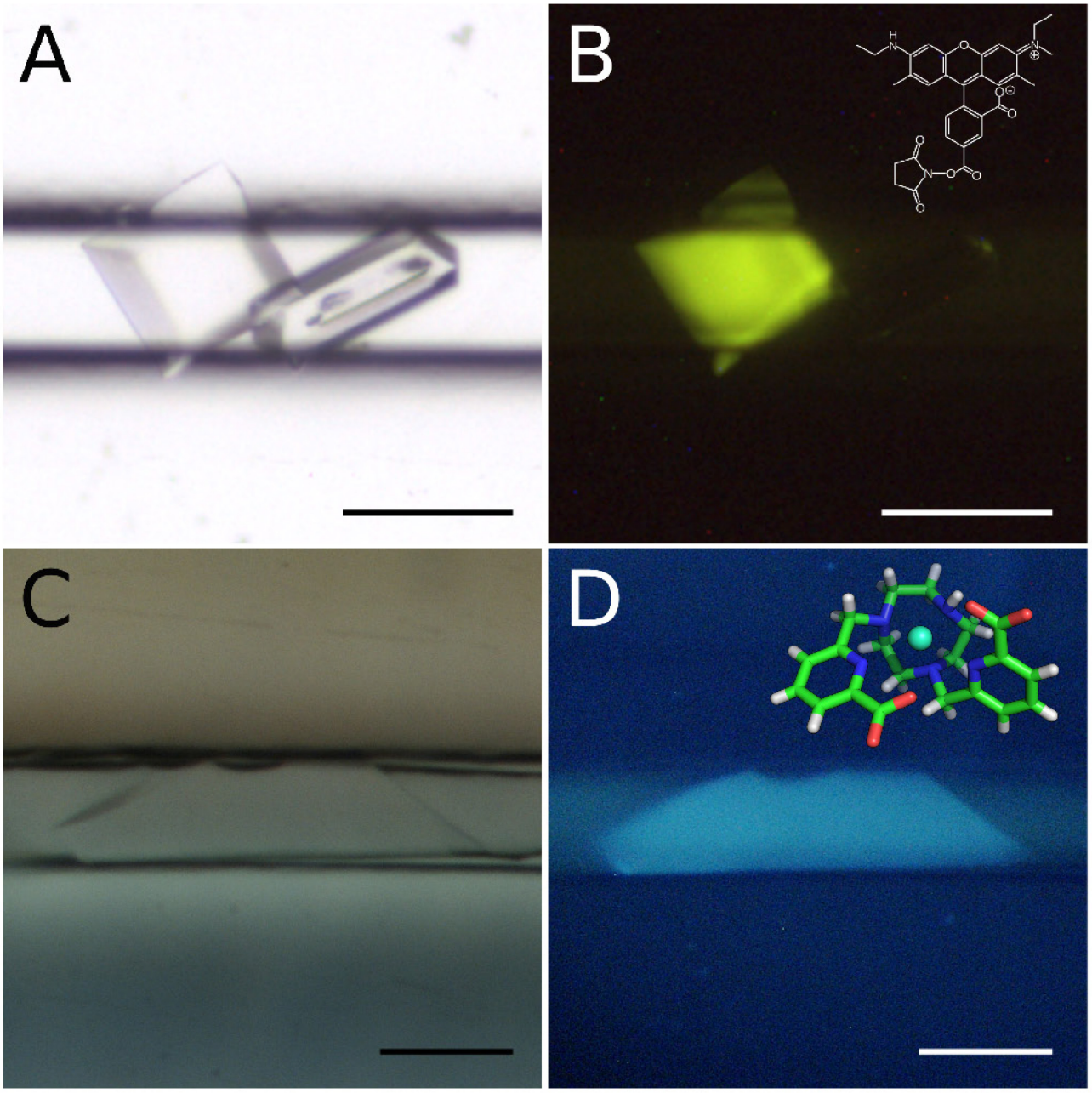

Figure 3 Crystal detection in ChipX3 by fluorescence. (A) and (B) CCA crystals grown as described in **Table 1** with 0.6% CCA-TFL; (C) and (D) PhP1 crystals grown as described in Table 1 with 10 mM Tb-Xo4. (A) and (C) Crystals illuminated with white light. (B) Crystal illuminated with a 520 nm light source and image taken with a low pass filter at 550 nm (LP550), (inset) structure of carboxyrhodamine-succinimidyl ester. (D) Crystal illuminated with a 280-380 nm UV source, (inset) structure of Tb-Xo4. Scale bar = 0.1mm.

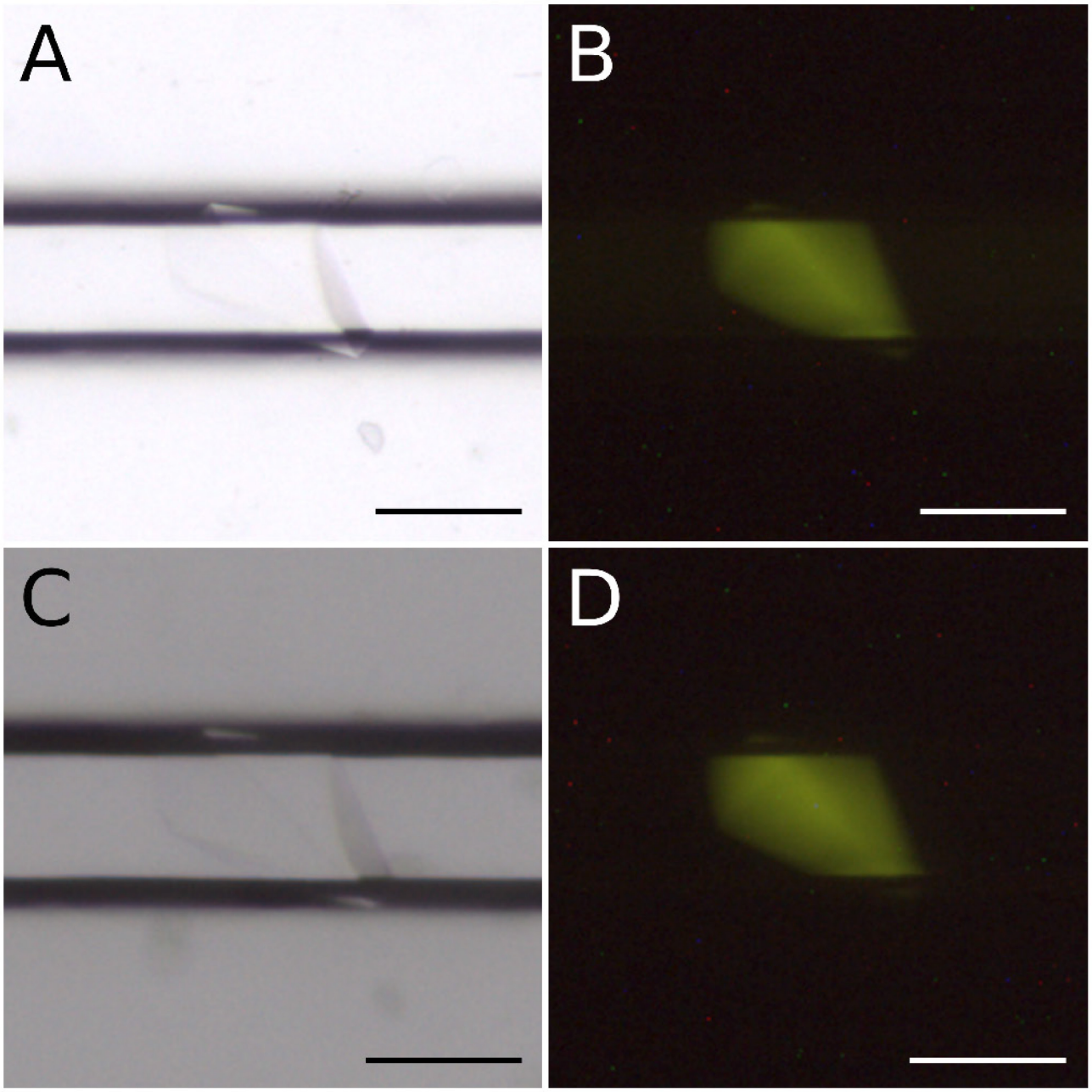

Figure 4 Crystals before and after soaking in ChipX3. Images of CCA crystals grown as described in **Table 1** with 0.6% CCA-TFL. (A) and (B) before soaking. (C) and (D) image taken six days after soaking with CMPcPP at a final concentration of 3.75 mM. (A) and (C) White light illumination. (B) and (D) images taken with a 520 nm light source and a low pass filter at 550 nm (LP550). Scale bar = 0.1 mm

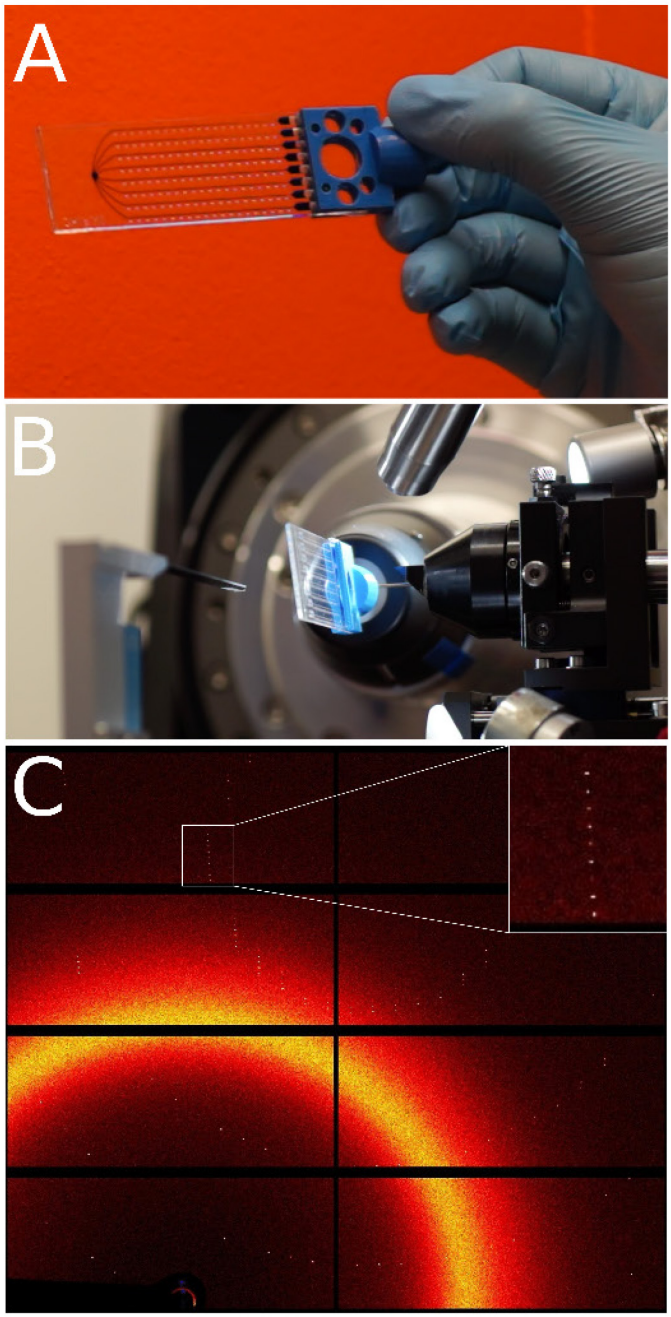

Figure 5 Diffraction analysis in ChipX3. (A) ChipX3 on its holder (B) ChipX3 on beamline PXIII at the SLS synchrotron (C) Example of diffraction pattern of the CCA adding-enzyme in ChipX3 at room temperature (exposure 0.1 s, rotation 0.2°). (inset) the close-up view illustrates the sharpness of Bragg peaks (low mosaic spread).

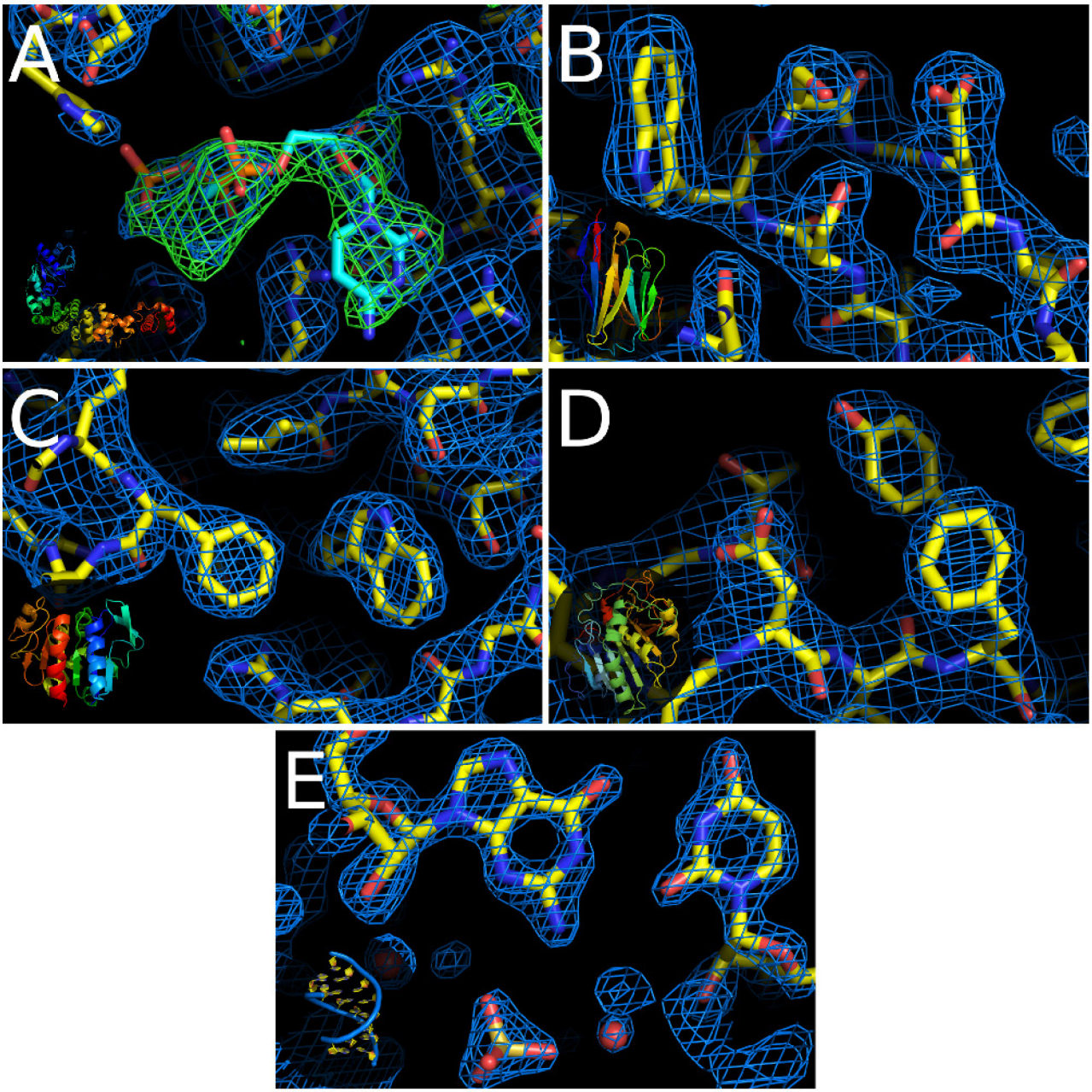

Figure 6 Electron density maps and structures of target macromolecules. (A) CCA-adding enzyme with the positive density from the ligand, (B) nanobody, (C) protease 1, (D) lipase, (E) RNA duplex. (insets) Schematic representation of the whole macromolecules. The figure was prepared using PyMOL (v1.8.6, Schrödinger) with 2Fo-Fc electron density maps (in blue) contoured at 1.2 sigma, difference map (in green) contoured at 4 sigma.

Table 1: Biomolecules and crystallization conditions

	Biological source	Nb. of residues / Mol. mass (kDa)	Biomolecule concentration	Biomolecule buffer solution	Crystallant solution
CCA-adding enzyme	*Planococcus halocryophilus*	420 / 48.5	5.5 mg/mL	50 mM Tris-HCl pH 7.5, 200 mM NaCl, 5 mM MgCl2	30% (m/v) PEG3350, 200 mM ammonium chloride pH 6.6
Nanobody 02	Llama	129 / 14.5	13.8 mg/mL	10 mM HEPES NaOH pH 7.25, 150 mM NaCl	20% (m/v) PEG3000, 0.1 M trisodium citrate pH 5.5
Protease 1	*Pyrococcus horikhoshii*	6x166 / 111.6	7.4 mg/mL	20 mM Tris-HCl pH 7.5, 10 mM Xo4	3.4 M malonate pH 7.5
Lipase	*Thermomyces lanuginosus*	269 / 29.3	30 mg/mL	25 mM HEPES-NaOH pH 7.5	0.3 M Na/K Phosphate, 50 mM NaAc pH 4.5
Aspartyl-tRNA synthetase 1	*Thermus thermophilus*	2x580 / 132	19 mg/mL	50 mM Tris-HCl pH 7.2, 1 mM EDTA, 1 mM DTT	10% (m/v) PEG8000
Mitochondrial aspartyl-tRNA synthetase	*Homo sapiens*	2x630 / 140	30 mg/mL	50 mM HEPES NaOH pH 7.5, 150 mM NaCl, 10% glycerol, 1 mM DTT	100 mM Tris-HCL pH 7.0, 40% (m/v) PEG3350, 0.2 M NaSCN
OMT ShuA	*Shigella dysenteriae*	632 / 69.5	20 mg/mL	10 mM Tris-HCL pH 8.0, 1.4% β-D-glucopyranoside	0.1 M sodium acetate, 20% (m/v) PEG400, 15% (m/v) PEG4000, 10% (m/v) PEG8000 pH 5.0
RNA duplex	Synthetic	2x9 / 5.8	10 mg/mL	10 mM Na-cacodylate pH 6.0, 5 mM MgCl2	2.6 M ammonium sulfate, 50 mM Na-cacodylate pH 6.0, 5 mM MgSO4, 1 mM spermine
Hemoglobin	*Equus caballus*	574 / 62	20 mg/mL	50 mM K-phosphate pH 7.5	3.3 M ammonium sulfate, 50 mM K-phosphate pH 7.5

Table 2: Data collection and refinement statistics

	CCA-adding enzyme	CCA-adding enzyme + CMPcPP	Nanobody 02	Protease I	Lipase	RNA duplex
X-ray beamline	SLS - PXIII	SLS - PXII	SOLEIL – Proxima 2-A	SLS - PXIII	ESRF – ID30B	SLS - PXIII
Wavelength (Å)	1.000	1.000	0.826	1.240	0.976	0.826
Temperature (K)	293	293	293	293	293	293
Detector	Pilatus 2M-F	Pilatus 6M	Eiger	Pilatus 2M-F	Pilatus3 6M	MarCCD
Crystal-detector distance (mm)	300	400	154	150/200	502	200
Crystals collected	6	14	9	1/11	14	3
Crystals selected	5	5	1	8	2	3
Rotation range per image (°)	0.1	0.2	0.1	0.2	0.1	2-3
No. of images selected	1000	540	500	1300	600	80
Total rotation range (°)	100	108	50	260	60	155
Exposure time per image (s)	0.1	0.1	0.1	0.1	0.02	1-2
Space group	P4(3)2(1)2	P4(3)2(1)2	P4(3)2(1)2	P4(1)2(1)2	P6(1)	R3
a, *c* (Å)	71.5, 293.8	71.4, 293.6	66.7, 91.8	125.6, 133.9	142.6, 80.7	40.0, 69.1
Solvent content (%)	68.3	67.8	65.0	74.0	68.6	54.7
Mean mosaicity (°)	0.0405	0.0358	0.0675	0.042	0.03	0.11-0.21
Resolution range (Å)	46 – 2.54 (2.6 – 2.54)	48 – 2.3 (2.4 – 2.3)	50 – 2.1 (2.18 – 2.1)	50 – 2.15 (2.21 – 2.15)	49.06 – 2.50 (2.60 – 2.50)	23 – 1.55 (1.59 – 1.55)
Total No. of reflections	176105 (9374)	232642 (32937)	45307 (4574)	1095436 (85346)	102820 (11312)	21681 (605)
No. of unique reflections	23922 (1598)	34862 (4066)	12281 (1196)	57690 (4522)	31982 (3668)	5485 (304)
Completeness (%)	90.6 (84.6)	99.5 (100.0)	97.2 (98.3)	98.5 (99.6)	98.5 (98.9)	91.5 (69.7)
Redundancy	7.5 (6.0)	6.7 (8.1)	3.7 (3.8)	19.0 (18.9)	3.2 (3.1)	3.9 (2.0)
$\langle I/\sigma(I)\rangle$	8.1 (1.3)	6.9 (0.7)	11.3 (1.8)	12.0 (1.4)	6.3 (0.8)	6.1 (1.8)
*R*meas (%)	18.9 (126.0)	18.0 (231.2)	7.5 (84.7)	17.4 (206.4)	8.6 (86.8)	17.9 (45.6)
CC1/2 (%)	98.7 (55.0)	98.7 (46.9)	99.7 (73.5)	99.7 (69.4)	99.4 (49.4)	98.8 (75.5)
Overall *B* factor from Wilson plot (Å 2)	57.4	60.6	45.2	50.8	63.3	23.6
No. of reflections, working set / test set	23583 / 1180	34840 / 3405	11053 / 1228	57659 / 5758	31516 / 1573	5484 / 382
Final Rcryst (%) / R_{free} (%)	18.8 / 21.4	20.0 / 22.9	16.9 / 21.1	16.2 / 18.4	17.2 / 19.9	19.2 / 22.3
No. of non-H atoms	2998	3057	970	4017	4314	390
Protein / ion / ligand / solvent	2989 / 0 / 0 / 9	2989 / 0 / 29 / 10	947 / 0 / 0 / 23	3921 / 0 / 0 / 96	4404 / 2 / 35 /47	342 / 5 / 0 / 43
R.m.s. deviations						
Bonds (Å)	0.009	0.010	0.008	0.012	0.004	0.004
Angles (°)	1.23	1.22	0.897	1.43	1.08	0.680
Average *B* factors (Å^2)	60.1	62.6	53.8	57.1	83.8	17.8
Macromolecule	60.1	60.1	53.8	57.1	82.9	17.6
Solvent	52.7	55.5	50.9	56.1	62.6	15.1
Ramachandran plot						
Most favoured (%)	98.1	97.2	95.8	98.4	96.6	/
Allowed (%)	1.9	2.8	4.2	1.6	3.2	/
PDB id	6IBP	6Q52	6GZP	6Q3T	6HW1	6IBQ

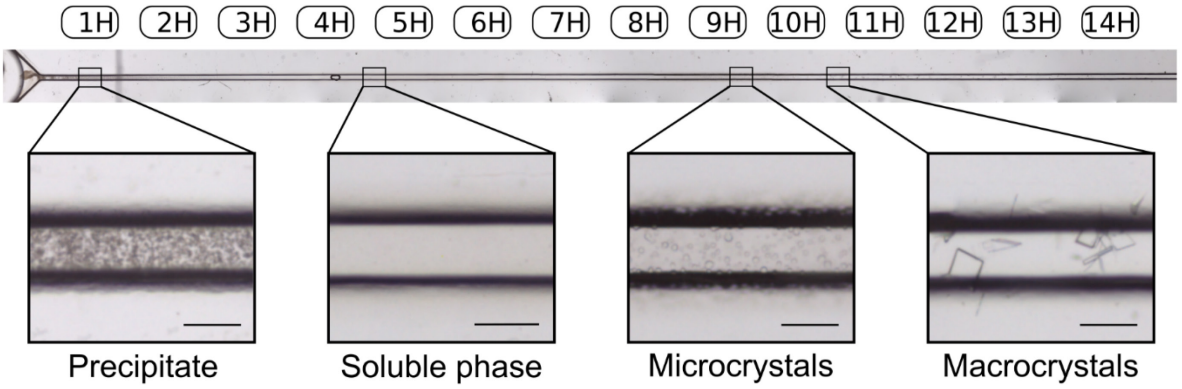

Supplementary figure S1: Crystallization of ttDRS by counter-diffusion in ChipX3. Labels printed along the capillaries are represented on top. The displayed linear segment of the channel measures 3 cm. Scale bars = 0.1 mm.

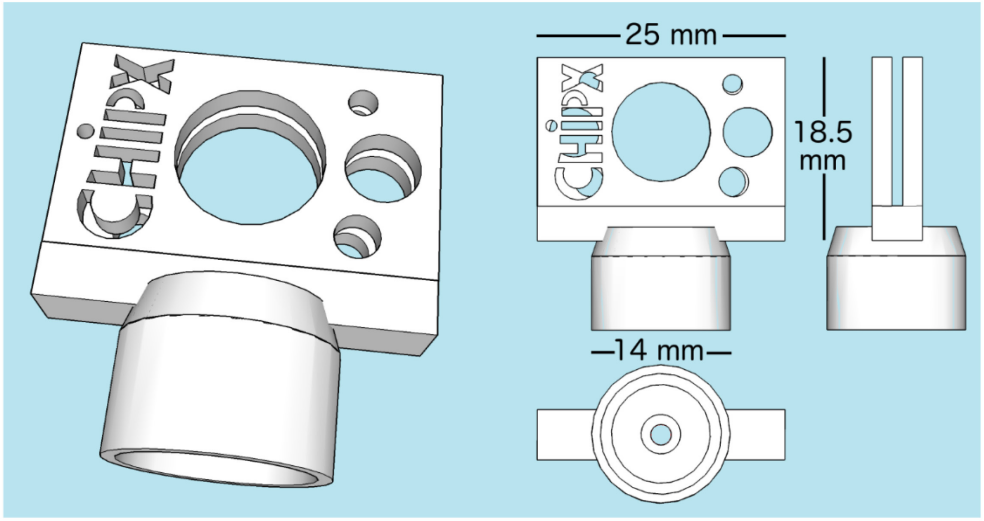

Supplementary figure S2: Perspective view and projections of the ChipX3 holder. It was printed using an Ultimaker 2 extended+ printer and a polylactic acid (PLA) filament. After printing, a standard metal base (B5 SPINE style, Mitegen) was glued at the bottom of the holder for coupling with magnetic goniometer heads.

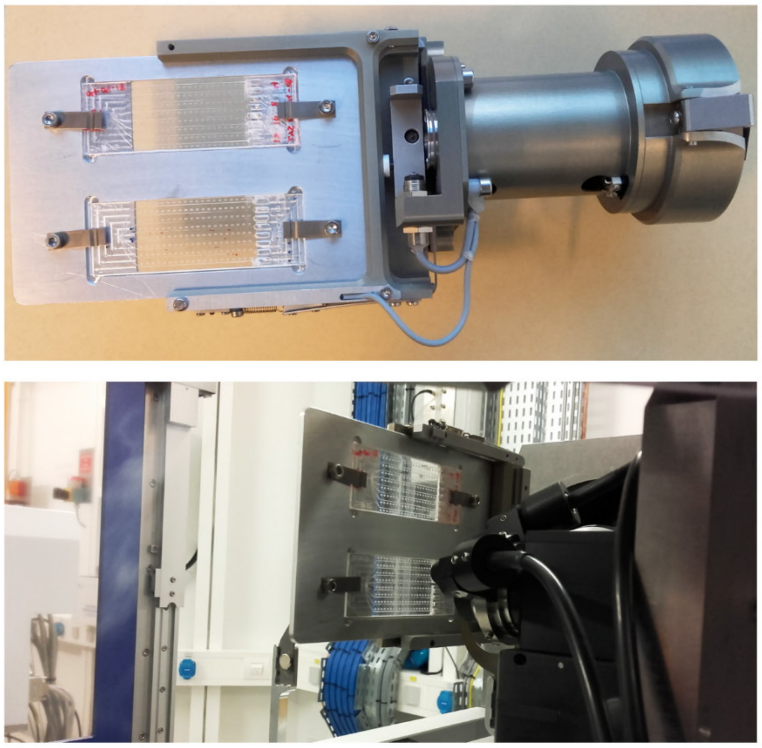

Supplementary figure S3: **ChipX3 on ID30B beamline (ESRF, Grenoble)**. (Top) An aluminium holder for two chips with the same footprint as a crystallisation microplate is maintained by a plate gripper designed for *in situ* screening. (Bottom) Plate and gripper mounted on the MD2S diffractometer of ID30B beamline (McCarthy *et al.,* 2018).

References

Adams, P. D., Afonine, P. V., Bunkóczi, G., Chen, V. B., Davis, I. W., Echols, N., Headd, J. J., Hung, L.-W., Kapral, G. J., Grosse-Kunstleve, R. W., McCoy, A. J., Moriarty, N. W., Oeffner, R., Read, R. J., Richardson, D. C., Richardson, J. S., Terwilliger, T. C. & Zwart, P. H. (2010). *Acta Crystallogr. D Biol. Crystallogr.* **66**, 213–221.

Ayyer, K., Geloni, G., Kocharyan, V., Saldin, E., Serkez, S., Yefanov, O. & Zagorodnov, I. (2015). *Struct. Dyn.* **2**, 041702.

Bergfors, T. (2003). *J. Struct. Biol.* **142**, 66–76.

Bingel-Erlenmeyer, R., Olieric, V., Grimshaw, J. P. A., Gabadinho, J., Wang, X., Ebner, S. G., Isenegger, A., Schneider, R., Schneider, J., Glettig, W., Pradervand, C., Panepucci, E. H., Tomizaki, T., Wang, M. & Schulze-Briese, C. (2011). Cryst. Growth Des. 11, 916–923.

Brillet, K., Meksem, A., Thompson, A. & Cobessi, D. (2009). *Acta Crystallogr. F Struct. Biol. Cryst. Commun.* **65**, 402–405.

Chapman, H. N., Fromme, P., Barty, A., White, T. A., Kirian, R. A., Aquila, A., Hunter, M. S., Schulz, J., DePonte, D. P., Weierstall, U., Doak, R. B., Maia, F. R. N. C., Martin, A. V., Schlichting, I., Lomb, L., Coppola, N., Shoeman, R. L., Epp, S. W., Hartmann, R., Rolles, D., Rudenko, A., Foucar, L., Kimmel, N., Weidenspointner, G., Holl, P., Liang, M., Barthelmess, M., Caleman, C., Boutet, S., Bogan, M. J., Krzywinski, J., Bostedt, C., Bajt, S., Gumprecht, L., Rudek, B., Erk, B., Schmidt, C., Hömke, A., Reich, C., Pietschner, D., Strüder, L., Hauser, G., Gorke, H., Ullrich, J., Herrmann, S., Schaller, G., Schopper, F., Soltau, H., Kühnel, K.-U., Messerschmidt, M., Bozek, J. D., Hau-Riege, S. P., Frank, M., Hampton, C. Y., Sierra, R. G., Starodub, D., Williams, G. J., Hajdu, J., Timneanu, N., Seibert, M. M., Andreasson, J., Rocker, A., Jönsson, O., Svenda, M., Stern, S., Nass, K., Andritschke, R., Schröter, C.-D., Krasniqi, F., Bott, M., Schmidt, K. E., Wang, X., Grotjohann, I., Holton, J. M., Barends, T. R. M., Neutze, R., Marchesini, S., Fromme, R., Schorb, S., Rupp, D., Adolph, M., Gorkhover, T., Andersson, I., Hirsemann, H., Potdevin, G., Graafsma, H., Nilsson, B. & Spence, J. C. H. (2011). *Nature*. **470**, 73–77.

de Wijn, R., Hennig, O., Ernst, F. G. M., Lorber, B., Betat, H., Mörl, M. & Sauter, C. (2018). *Acta Crystallogr. F Struct. Biol. Cryst. Commun.* **74**, 747–753.

D'Arcy, A., Bergfors, T.,Cowan-Jacob, S. W., Marsh, M. (2014). *Acta Crystallogr. F Struct. Biol. Cryst. Commun.* **70**, 1117-1126.

D'Arcy, A., Villard, F. & Marsh, M. (2007). *Acta Crystallogr. D Biol. Crystallogr.* **63**, 550–554.

Dhouib, K., Khan Malek, C., Pfleging, W., Gauthier-Manuel, B., Duffait, R., Thuillier, G., Ferrigno, R., Jacquamet, L., Ohana, J., Ferrer, J.-L., Théobald-Dietrich, A., Giegé, R., Lorber, B. & Sauter, C. (2009). *Lab Chip.* **9**, 1412–1421.

Duhoo, Y., Roche, J., Trinh, T. T. N., Desmyter, A., Gaubert, A., Kellenberger, C., Cambillau, C., Roussel, A. & Leone, P. (2017). *Acta Crystallogr. F Struct. Biol. Cryst. Commun.* **73**, 286–293.

Duran, D., Couster, S. L., Desjardins, K., Delmotte, A., Fox, G., Meijers, R., Moreno, T., Savko, M. & Shepard, W. (2013). *Journal of Physics.* 425, 012005.

Emamzadah, S., Petty, T. J., De Almeida, V., Nishimura, T., Joly, J., Ferrer, J. L. & Halazonetis, T. D. (2009). *Acta Crystallogr. D Biol. Crystallogr.* **65**, 913–920.

Emsley, P. & Cowtan, K. (2004). *Acta Crystallogr. D Biol. Crystallogr.* **60**, 2126–2132.

Engilberge, S., Riobé, F., Di Pietro, S., Lassalle, L., Coquelle, N., Arnaud, C.-A., Pitrat, D., Mulatier, J.-C., Madern, D., Breyton, C., Maury, O. & Girard, E. (2017). *Chem. Sci.* **8**, 5909–5917.

Engilberge, S., Riobé, F., Wagner, T., Pietro, S. D., Breyton, C., Franzetti, B., Shima, S., Girard, E., Dumont, E. & Maury, O. (2018). *Chem. Eur. J.* **24**, 9739–9746.

Ernst, F. G. M., Erber, L., Sammler, J., Jühling, F., Betat, H. & Mörl, M. (2018). *RNA Biol.* **15**, 144–155.

Fuchs, M. R., Pradervand, C., Thominet, V., Schneider, R., Panepucci, E., Grunder, M., Gabadinho, J., Dworkowski, F. S. N., Tomizaki, T., Schneider, J., Mayer, A., Curtin, A., Olieric, V., Frommherz, U., Kotrle, G., Welte, J., Wang, X., Maag, S., Schulze-Briesec, C. and Wanga, M. (2014). *Journal of Synchrotron Radiation.* **21**, 340-351.

García-Ruiz, J. M., Otálora, F., Novella, M. L., Gavira, J. A., Sauter, C. & Vidal, O. (2001). *J. Cryst. Growth.* **232**, 149–155.

Gavira, J. A., Hernandez-Hernandez, M. A., Gonzalez-Ramirez, L. A., Briggs, R. A., Kolek, S. A. & Shaw Stewart, P. D. (2011). *Cryst. Growth Des.* **11**, 2122–2126.

Gavira, J. A., Toh, D., Lopéz-Jaramillo, J., García-Ruíz, J. M. & Ng, J. D. (2002). *Acta Crystallogr. D Biol. Crystallogr.* **58**, 1147–1154.

Giegé, R. (2017). *IUCrJ.* **4**, 340–349.

Giegé, R. & Sauter, C. (2010). *HFSP J.* **4**, 109–121.

Hansen, C. L., Classen, S., Berger, J. M. & Quake, S. R. (2006). *J. Am. Chem. Soc.* **128**, 3142–3143.

Hansen, C. L., Skordalakes, E., Berger, J. M. & Quake, S. R. (2002). *Proc. Natl. Acad. Sci. U. S. A.* **99**, 16531–16536.

Hansen, C. & Quake, S. R. (2003). *Curr. Opin. Struct. Biol.* **13**, 538–544.

Heymann, M., Opthalage, A., Wierman, J. L., Akella, S., Szebenyi, D. M. E., Gruner, S. M. & Fraden, S. (2014). *IUCrJ.* **1**, 349–360.

Jaskolski, M., Dauter, Z. & Wlodawer, A. (2014). *FEBS J.* **281**, 3985–4009.

Johansson, L. C., Stauch, B., Ishchenko, A. & Cherezov, V. (2017). *Trends Biochem. Sci.* **42**, 749–762.

Kabsch, W. (2010). *Acta Crystallogr. D Biol. Crystallogr.* **66**, 125–132.

Khvostichenko, D. S., Schieferstein, J. M., Pawate, A. S., Laible, P. D. & Kenis, P. J. A. (2014). *Cryst. Growth Des.* **14**, 4886–4890.

Luft, J. R., Newman, J. & Snell, E. H. (2014). *Acta Crystallogr. F. Struct. Biol. Cryst. Commun.* **70**, 835–853.

Martin-Garcia, J. M., Conrad, C. E., Coe, J., Roy-Chowdhury, S. & Fromme, P. (2016). *Arch. Biochem. Biophys.* **602**, 32–47.

Masquida, B., Sauter, C. & Westhof, E. (1999). *RNA*. **5**, 1384–1395.

McCarthy, A. A., Barrett, R., Beteva, A., Caserotto, H., Dobias, F., Felisaz, F., Giraud, T., Guijarro, M., Janocha, R., Khadrouche, A., Lentini, M., Leonard, G. A., Lopez Marrero, M., Malbet-Monaco, S., McSweeney, S., Nurizzo, D., Papp, G., Rossi, C., Sinoir, J., Sorez, C., Surr, J., Svensson, O., Zander, U., Cipriani, F., Theveneau, P. & Mueller-Dieckmann, C. (2018). *Journal of Synchrotron Radiation*. **25**, 1249–1260.

McPherson, A. & Gavira, J. A. (2013). *Acta Crystallogr. Sect. F Struct. Biol. Cryst. Commun.* **70**, 2–20.

Meyer, A., Betzel, C. & Pusey, M. (2015). *Acta Crystallogr. F Struct. Biol. Cryst. Commun.* **71**, 121–131.

Mutterer, J. & Zinck, E. (2013). *Journal of Microscopy*. **252**, 89-91.

Ng, J. D., Clark, P. J., Stevens, R. C. & Kuhn, P. (2008). *Acta Crystallogr. D Biol. Crystallogr.* **64**, 189–197.

Ng, J. D., Gavira, J. A. & García-Ruíz, J. M. (2003). *J. Struct. Biol.* **142**, 218–231.

Otálora, F., Gavira, J. A., Ng, J. D. & García-Ruiz, J. M. (2009). *Prog. Biophys. Mol. Biol.* **101**, 26–37.

Owen, R. L., Juanhuix, J. & Fuchs, M. (2016). *Archives of Biochemistry and Biophysics*. **602**, 21–31.

Perry, S. L., Guha, S., Pawate, A. S., Bhaskarla, A., Agarwal, V., Nair, S. K. & Kenis, P. J. A. (2013). *Lab Chip*. **13**, 3183.

Perry, S. L., Guha, S., Pawate, A. S., Henning, R., Kosheleva, I., Srajer, V., Kenis, P. J. A. & Ren, Z. (2014). *J. Appl. Crystallogr.* **47**, 1975–1982.

Pinker, F., Brun, M., Morin, P., Deman, A.-L., Chateaux, J.-F., Oliéric, V., Stirnimann, C., Lorber, B., Terrier, N., Ferrigno, R. & Sauter, C. (2013). *Cryst. Growth Des.* **13**, 3333–3340.

Pusey, M., Barcena, J., Morris, M., Singhal, A., Yuan, Q. & Ng, J. (2015). *Acta Crystallogr. Sect. F Struct. Biol. Cryst. Commun.* **71**, 806–814.

Pusey, M. L., Liu, Z.-J., Tempel, W., Praissman, J., Lin, D., Wang, B.-C., Gavira, J. A. & Ng, J. D. (2005). *Prog. Biophys. Mol. Biol.* **88**, 359–386.

Santoni, G., Zander, U., Mueller-Dieckmann, C., Leonard, G. & Popov, A. (2017). *J. Appl. Crystallogr.* **50**, 1844–1851.

Sauter, C., Dhouib, K. & Lorber, B. (2007). *Cryst. Growth Des.* **7**, 2247–2250.

Sauter, C., Lorber, B., Gaudry, A., Karim, L., Schwenzer, H., Wien, F., Roblin, P., Florentz, C. & Sissler, M. (2015). *Sci. Rep.* **5**, 17332.

Sauter, C., Lorber, B., McPherson, A. & Giegé, Richard (2012). *In International Tables of Crystallography, Vol. F, Crystallography of Biological Macromolecules (2nd Edition), E. Arnold, D.M. Himmel & M.G. Rossmann (Eds)*, Vol. pp. 99–120. Chichester: John Wiley and Sons.

Schneider, C., Rasband, W., Eliceiri, K. (2012). *Nature Methods*. **9**, 671-675.

Stellato, F., Oberthür, D., Liang, M., Bean, R., Gati, C., Yefanov, O., Barty, A., Burkhardt, A., Fischer, P., Galli, L., Kirian, R. A., Meyer, J., Panneerselvam, S., Yoon, C. H., Chervinskii, F., Speller, E., White, T. A., Betzel, C., Meents, A. & Chapman, H. N. (2014). *IUCrJ*. **1**, 204–2012.

Stojanoff, V., Jakoncic, J., Oren, D. A., Nagarajan, V., Poulsen, J.-C. N., Adams-Cioaba, M. A., Bergfors, T. & Sommer, M. O. A. (2011). *Acta Crystallogr. F Struct. Biol. Cryst. Commun.* **67**, 971–975.

Sui, S., Wang, Y., Kolewe, K. W., Srajer, V., Henning, R., Schiffman, J. D., Dimitrakopoulos, C. & Perry, S. L. (2016). *Lab Chip*.

Terwilliger, T. C., Stuart, D. & Yokoyama, S. (2009). *Annual Review of Biophysics*. **38**, 371–383.

Vincentelli, R., Bignon, C., Gruez, A., Canaan, S., Sulzenbacher, G., Tegoni, M., Campanacci, V. & Cambillau, C. (2003). *Acc. Chem. Res.* **36**, 165–172.

van der Woerd, M., Ferree, D. & Pusey, M. (2003). *J. Struct. Biol.* **142**, 180–187.

Yadav, M. K., Gerdts, C. J., Sanishvili, R., Smith, W. W., Roach, L. S., Ismagilov, R. F., Kuhn, P. & Stevens, R. C. (2005). *J. Appl. Crystallogr.* **38**, 900–905.

Zheng, B., Roach, L. S. & Ismagilov, R. F. (2003). *J. Am. Chem. Soc.* **125**, 11170–11171.

Zhu, D. W., Lorber, B., Sauter, C., Ng, J. D., Bénas, P., Le Grimellec, C. & Giegé, R. (2001). *Acta Crystallogr. D Biol. Crystallogr.* **57**, 552–558.

III. Structural and functional study of a psychrophilic CCA-adding enzyme

Dans ce second chapitre sont présentés deux articles qui concernent l'étude structurale et biochimique de l'ARNt nucléotidyltransférase de l'organisme *Planococcus halocryophilus* (*Pha*CCA), une bactérie vivant dans le permafrost arctique.

Le premier article « Combining crystallogenesis methods to produce diffraction quality crystals of a psychrophilic tRNA-maturation enzyme » publié dans Acta crystallographica Section F décrit la stratégie de cristallogenèse employée pour définir rapidement et efficacement les conditions de croissance de cristaux de *Pha*CCA diffractant à haute résolution ouvrant la voie à la détermination de la structure de l'enzyme en question.

La recherche des conditions de cristallisation d'une nouvelle biomolécule prend souvent beaucoup de temps et d'échantillons. Cette étape critique consiste généralement en l'examen de milliers de conditions de solvants. Cependant, il a été démontré que le fait d'élargir l'ensemble des essais de cristallisation au-delà de quelques centaines n'augmente pas de façon significative le nombre de conditions utiles. Au lieu de cela, l'utilisation d'approches alternatives qui fournissent un meilleur échantillonnage des conditions de sursaturation, facilitent directement la nucléation ou la détection des résultats positifs peut améliorer considérablement l'efficacité du processus de criblage (voir section 2). Dans ce travail axé sur les enzymes de maturation de l'ARNt, nous avons combiné le criblage conventionnel avec des méthodes de cristallogenèse plus avancées mais faciles à mettre en œuvre, pour accélérer la définition de conditions de cristallisation d'une nouvelle enzyme qui ajoute deux nucléotides cytosine et un nucléotide adénine à l'extrémité 3' de l'ARNt, représentant le site universellement conservé d'aminoacylation des ARNt par les aminoacyl-ARNt transférases.

Le second article encore en préparation est intitulé « CCA-addition in the cold : Structural and biochemical characterization of the enzyme from *Planococcus halocryophilus* » et se concentre sur les caractéristiques de l'adaptation au froid de l'enzyme *Pha*CCA. Celui-ci présente les résultats biologiques obtenus en partie grâce à l'utilisation de méthodes avancées de cristallisation employées lors de cette thèse.

Plusieurs études comparatives entre les enzymes thermophiles et psychrophiles ont montré qu'il n'existait pas de stratégie universelle d'adaptation au froid. Au contraire, chaque enzyme semble utiliser des adaptations différentes. Dans la plupart des cas, ces adaptations aboutissent à une augmentation générale de la flexibilité de l'enzyme. Les CCA-adding enzymes sont des ARN polymérases hautement spécifiques qui ajoutent et maintiennent cette séquence en 3' des ARNt. Pour une incorporation adéquate et efficace, des réaménagements structuraux sont nécessaires. Toutefois, pour les enzymes de cette famille qui sont adaptées au froid, il existe une contradiction entre une flexibilité étroitement contrôlée nécessaire à la spécificité de polymérisation et une flexibilité accrue en lien avec l'adaptation au froid. Des éléments de réponses seront apportés par la comparaison de l'enzyme psychrophile et de ses homologues thermophile/mésophile.

7 Combining crystallogenesis methods to produce diffraction quality crystals of a psychrophilic tRNA-maturation enzyme (article in press in Acta Cryst. section F)

electronic reprint

STRUCTURAL BIOLOGY
COMMUNICATIONS

ISSN: 2053-230X
journals.iucr.org/f

Combining crystallogenesis methods to produce diffraction-quality crystals of a psychrophilic tRNA-maturation enzyme

Raphaël de Wijn, Oliver Hennig, Felix G. M. Ernst, Bernard Lorber, Heike Betat, Mario Mörl and Claude Sauter

Acta Cryst. (2018). F**74**, 747–753

STRUCTURAL BIOLOGY COMMUNICATIONS

ISSN 2053-230X

Combining crystallogenesis methods to produce diffraction-quality crystals of a psychrophilic tRNA-maturation enzyme

Raphaël de Wijn,[a] Oliver Hennig,[b] Felix G. M. Ernst,[b] Bernard Lorber,[a] Heike Betat,[b] Mario Mörl[b] and Claude Sauter[a]*

[a]Architecture et Réactivité de l'ARN, UPR 9002, Université de Strasbourg, IBMC, CNRS, 15 Rue R. Descartes, 67084 Strasbourg, France, and [b]Institute for Biochemistry, Leipzig University, Brüderstrasse 34, 04103 Leipzig, Germany. *Correspondence e-mail: c.sauter@ibmc-cnrs.unistra.fr

Received 31 August 2018
Accepted 16 October 2018

Edited by R. Sankaranarayanan, Centre for Cellular and Molecular Biology, Hyderabad, India

Keywords: microseeding; counter-diffusion; trace fluorescent labeling; optimization; crystallogenesis; tRNA maturation; CCA-adding enzyme; *Planococcus halocryophilus*.

The determination of conditions for the reproducible growth of well diffracting crystals is a critical step in every biocrystallographic study. On the occasion of a new structural biology project, several advanced crystallogenesis approaches were tested in order to increase the success rate of crystallization. These methods included screening by microseed matrix screening, optimization by counter-diffusion and crystal detection by trace fluorescent labeling, and are easily accessible to any laboratory. Their combination proved to be particularly efficient in the case of the target, a 48 kDa CCA-adding enzyme from the psychrophilic bacterium *Planococcus halocryophilus*. A workflow summarizes the overall strategy, which led to the production of crystals that diffracted to better than 2 Å resolution and may be of general interest for a variety of applications.

1. Introduction

The search for crystallization conditions for a new biomolecule is often sample-consuming and time-consuming. This critical step generally consists of a trial-and-error process and the screening of thousands of solvent conditions. However, it has been shown that expanding the set of crystallization trials beyond a few hundred does not significantly increase the number of useful hits (Newman *et al.*, 2005; Newman, 2011). Instead, using alternative approaches that provide a better sampling of the supersaturation landscape, such as counter-diffusion (CD; Otálora *et al.*, 2009), that facilitate nucleation, such as microseeding (Bergfors, 2003; D'Arcy *et al.*, 2007; D'Arcy *et al.*, 2014), or that help to detect positive results, such as trace fluorescent labeling (TFL; Pusey *et al.*, 2015), may dramatically improve the output of the screening process. In this work focused on tRNA-maturation enzymes, we combined conventional screening with more advanced although easy-to-implement crystallogenesis methods to accelerate the definition of crystallization conditions for a new CCA-adding enzyme.

CCA-adding enzymes are ubiquitous nucleotidyltransferases that are involved in the post-transcriptional maturation of transfer RNAs (tRNAs) and belong to the polymerase β superfamily (Betat *et al.*, 2010). They add two cytosine nucleotides and one adenine nucleotide at the 3′ end of tRNA to synthesize and maintain this specific CCA sequence, which represents a highly conserved site for tRNA aminoacylation

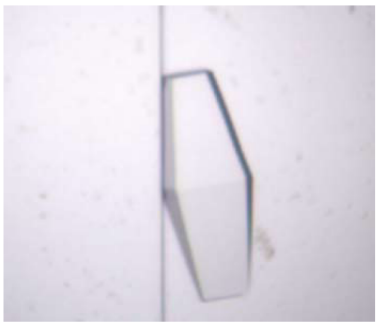

Table 1
Macromolecule-production information.

Source organism	*P. halocryophilus*
Expression vector	pET-30 Ek/LIC
Expression host	*E. coli* BL21 (DE3)
Complete amino-acid sequence of the construct†	MHHHHHHSSGLVPRGSGMKETAAAKFER QHMDSPDLGTDDDDKMNTAIKVIHTL KAAGFEAYIVGGAVRDLLLGKTPHDV DVASSALPQQVKVLFDRTVDTGIDHG TVLVLLDGEGIEVTTFRTESSYSDNR RPDSVEFVLSLEEDLRRRDFTINAMA MTEDLKIIDPFGGKEDLKNKVIRAVG DPDERFEEDALRMLRAIRFSGQLDFI IDMKTLLSIRRHARLIRFIAVERLKS EIDKIFVNPSMQKSMAYLKDSVLTRF LPVGGLFEVDWITYHTDGNPTYGWLY LLHQQKRQFTDIKDYRFSNEEKRLIE KSLELTALNTWDQWTFYKYTLKQLEM ASRVTGKKKDLAAIKRQLPIQSRSEL AVDGWDLIEWSGAKSGPWLKVWIEKI ERLIVYGILKNDKELIKDWFEDEYHS HT
No. of amino acids	420
Molecular mass (Da)	48423
Abs 0.1%‡ at 280 nm (M^{-1} cm^{-1})	1.36

† The purification tag, including 6×His, is underlined. ‡ Equal to a 1 g l^{-1} solution.

by cognate aminoacyl-tRNA synthetases. This polymerization activity is performed without any DNA or RNA template, but is exclusively controlled by a set of highly conserved amino-acid residues and specific movements in the single nucleotide-binding pocket (Li *et al.*, 2002; Neuenfeldt *et al.*, 2008; Ernst *et al.*, 2015). During the switch between cytosine triphosphate (CTP) and adenosine triphosphate (ATP) specificity, motion affects not only the amino acids near the catalytic center, but also the global structure and organization of the enzyme (Tomita *et al.*, 2006). The present work was initiated to examine the situation in psychrophilic organisms that thrive in the cold and produce proteins with enhanced structural flexibility (De Maayer *et al.*, 2014). Therefore, unlike their thermophilic homologs, which are known to be rigid and stable, psychrophilic enzymes constitute more challenging targets for crystallization (Bae & Phillips, 2004). To study the cold-adaptation of CCA-adding enzymes, we selected the protein from *Planococcus halocryophilus* (*Pha*CCA), a bacterium that lives in the Arctic permafrost (Mykytczuk *et al.*, 2012). In this article, we describe the crystallogenesis strategy which enabled us to rapidly and efficiently define growth conditions for crystals that diffracted to high resolution, paving the way for the structure determination of a psychrophilic CCA-adding enzyme.

2. Materials and methods

2.1. Macromolecule production and fluorescent labeling

The CCA-adding enzyme from *P. halocryophilus* (*Pha*CCA) was produced as described by Ernst *et al.* (2018). Briefly, it was overproduced in *Escherichia coli* BL21 (DE3) cca:cam cells lacking the endogenous CCA-adding enzyme. Gene expression was induced with IPTG and *Pha*CCA was purified by affinity chromatography and size-exclusion chromatography (SEC) using HisTrap FF and Superdex 75 columns (GE Healthcare), respectively. After SEC, fractions containing the enzyme were pooled and concentrated using a 3 ml Slide-A-Lyzer cassette (3.5 kDa molecular-weight cutoff; Thermo Fisher Scientific) embedded in PEG 20 000 (Roth) to a final concentration of 4 to 5 mg ml^{-1} (depending on the batch). The purified enzyme was stored at 277 K in 50 m*M* Tris–HCl pH 7.5, 200 m*M* NaCl, 5 m*M* $MgCl_2$. Its homogeneity at 293 K was verified by SEC using a Bio SEC-3 150 column (Agilent) on an Agilent 1200 ChemStation HPLC system and by dynamic light scattering (DLS) using a Zetasizer Nano ZS instrument (Malvern) and a 20 µl quartz cuvette (Fig. 1). The protein concentration was determined using a NanoDrop ND-1000 spectrophotometer. Macromolecule-production information is summarized in Table 1.

In order to facilitate the detection of protein crystals, *Pha*CCA was fluorescently labeled with carboxyrhodamine succinimidyl ester (Invitrogen; catalog No. C6157). Protein labeling was performed with 80 µl of enzyme solution at 5 mg ml^{-1} (close to the maximum solubility in the storage buffer). The labeled solution was not mixed back with the protein stock solution but kept separately at 277 K. It will be referred to as *Pha*CCA-TFL. Other steps of the TFL were as described by Pusey *et al.* (2015).

2.2. Crystallization

2.2.1. Initial screening by vapor diffusion. All experiments were performed at 293 K. Prior to crystallization assays, *Pha*CCA was ultracentrifuged at 105 000*g* and 277 K for 1 h in a Sorvall Discovery M150 SE ultracentrifuge (Hitachi). Initial screens, microseed matrix screening and further optimizations were carried out by vapor diffusion using a Mosquito Crystal pipetting robot (TTP Labtech, UK) and 96-well sitting-drop plates (CrystalQuick plate, three round subwells; Greiner Bio-One). Initial screens were performed using the commercial kits Index (Hampton Research) and JBScreen JCSG++ (Jena Bioscience). Drops were prepared by mixing 300 or 150 nl *Pha*CCA at 4.5 mg ml^{-1} in storage buffer with 150 nl of the kit solution and were equilibrated against 50 µl reservoir solution. Duplicates were stored at either 277 or 293 K.

2.2.2. Optimization by counter-diffusion (CD). Initial hits obtained in ammonium sulfate were optimized using a CD kit (Triana Science & Technologies, Spain) consisting of six solutions of this salt at a pH ranging from 4 to 9. Capillaries (length 50 mm, inner diameter 0.2 mm) were filled with protein solution, sealed at one extremity with plasticine and plunged into Granada Crystallization Box-Dominos (GCB-D; Triana Science & Technologies) containing individual kit solutions. CD experiments were performed at 293 K. The section of the capillary containing the largest crystals was cut, sealed with plasticine, mounted on a standard goniometer base and cryocooled in liquid nitrogen.

2.2.3. Seed-stock preparation. To perform microseed matrix screening (MMS; D'Arcy *et al.*, 2007, 2014), small crystals grown by counter-diffusion (see above) with a solution consisting of 3 *M* ammonium sulfate, 0.1 *M* sodium acetate

pH 5 were recovered from the capillaries, crushed with Seed Beads (Hampton Research), vortexed and diluted in 50 µl of the same crystallant solution. This suspension was stored at 277 K and is referred to as the 'seed stock'.

2.2.4. Microseed matrix screening and optimization by vapor diffusion. For easy crystal detection in subsequent experiments, 22.5 µl *Pha*CCA at 5 mg ml^{-1} was added to 0.5 µl *Pha*CCA-TFL at 1.3 mg ml^{-1} (corresponding to a 0.6% contamination with TFL protein) and 7.5 µl seed-stock solution just before dispensing with the Mosquito robot. MMS was performed with JBScreen JCSG++ at 293 K by mixing 200 nl macromolecule solution (native and TFL enzyme plus seeds) with 140 nl crystallant solution. For further optimization, plates were set up with drops with the same mixing ratio against a reservoir containing 50 µl of the selected conditions (Table 2). Crystallization drops were observed with a Zeiss Scope A1 (Explora Nova) and TFL was revealed under illumination provided by an XtalLight 100C (Xtal Concepts).

2.3. Data collection and processing

Prior to cryocooling, the crystals grown by vapor diffusion were soaked in cryoprotectant solutions. For crystals grown in conditions A8 and B12 (see Table 2) containing PEG 3350, the crystallant concentration was increased to 25%(*m*/*v*); for those in condition E8 20%(*m*/*v*) glycerol was added to the condition. Crystals were soaked for 30 s in their respective cryoprotectant solution, fished out with cryomounts (MiTeGen) and plunged into liquid nitrogen. Crystals grown by CD were directly cryocooled inside the capillaries. Diffraction data were collected on beamline X06DA at the Swiss Light Source, Villigen, Switzerland or on the PROXIMA-1 beamline at Synchrotron SOLEIL, Saint-Aubin, France, which were equipped with PILATUS 2M and 6M detectors, respectively. All data sets were processed with *XDS* (Kabsch, 2010) and data-collection statistics are summarized in Table 3. Molecular replacement (MR) was performed with *Phaser* and the *PHENIX* package (McCoy *et al.*, 2007; Adams *et al.*, 2010) using data collected from a crystal grown by CD in capillaries and PDB entry 1miv (Li *et al.*, 2002; sequence identity 38%), corresponding to the CCA-adding enzyme from *Geobacillus stearothermophilus*, as a search model.

3. Results and discussion

The CCA-adding enzyme from *P. halocryophilus* overproduced in *E. coli* was purified by two chromatographic steps. Quality control of the purified protein by analytical SEC and DLS confirmed its homogeneity, monodispersity and stability in solution, with a single population with a mean diameter of 9.2 nm and a polydispersity index of 0.08% (Fig. 1). The initial crystallization performed with two commercial kits, both at 277 and 293 K, and *Pha*CCA at 4.5 mg ml^{-1} yielded small crystals in seven conditions (A4, A9, C6, B5 and C11 from Index and E2 and H2 from JBScreen JCSG++) at 293 K using a 2:1 ratio of protein:crystallant solution (Fig. 2, top). Three of these hits yielded crystals that produced diffraction patterns with reflections to between 5 and 10 Å resolution. Ammonium sulfate was a common feature of five of the hits and of two of the diffracting crystals. This encouraged us to carry out optimization assays by CD with this crystallant at various pH values. This crystallization method samples the supersaturation space through the creation of extended concentration gradients by diffusion of the crystallant inside

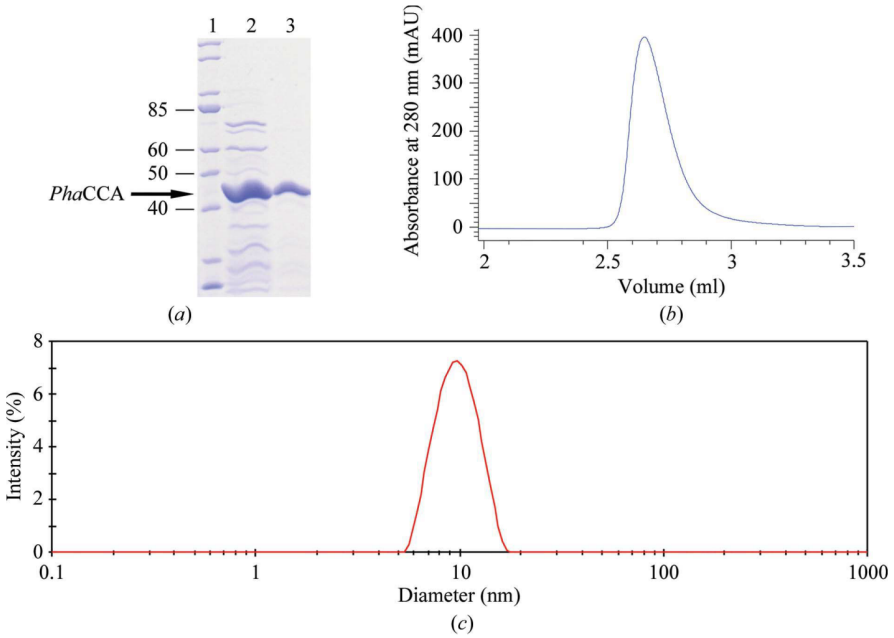

Figure 1
Quality control of *Pha*CCA prior to crystallization. (*a*) Denaturing SDS–PAGE gel showing the purity of the sample at different steps of the purification process. Lane 1, molecular-mass ladder (labeled in kDa); lane 2, after elution from the HisTrap column; lane 3, after elution from the SEC column. The sample homogeneity was assessed by analytical SEC (*b*) and DLS (*c*).

Table 2
Crystallization conditions for *Pha*CCA.

Method	Counter-diffusion	Vapor diffusion
Container	Glass capillary in GCB-Domino	CrystalQuick plate
Temperature (K)	293	293
Protein concentration (mg ml^{-1})	4.5	5
Composition of protein buffer solution	50 m*M* Tris–HCl pH 7.5, 200 m*M* NaCl, 5 m*M* $MgCl_2$	50 m*M* Tris–HCl pH 7.5, 200 m*M* NaCl, 5 m*M* $MgCl_2$
Composition of crystallant solution	3 *M* ammonium sulfate, 100 m*M* sodium acetate pH 5	A8: 20%(*m*/*v*) PEG 3350, 200 m*M* lithium sulfate pH 6.6 B12: 20%(*m*/*v*) PEG 3350, 200 m*M* potassium citrate pH 8.3 E8: 100 m*M* sodium acetate, 1 *M* diammonium hydrogen phosphate pH 4.5
Volume of sample	1.5 µl	200 nl
Volume of reservoir	1 ml	50 µl

Table 3
Data collection and processing.

Values in parentheses are for the outer shell.

		Vapor diffusion		
Crystal source	Counter-diffusion	Condition A8	Condition B12	Condition E8
Diffraction source	X06DA, SLS	PROXIMA-1, SOLEIL	PROXIMA-1, SOLEIL	PROXIMA-1, SOLEIL
Wavelength (Å)	1.000	0.978	0.978	0.978
Temperature (K)	100	100	100	100
Detector	PILATUS 2M	PILATUS 6M	PILATUS 6M	PILATUS 6M
Crystal-to-detector distance (mm)	350	320	320	320
Rotation range per image (°)	0.2	0.1	0.1	0.1
Total rotation range (°)	360	180	180	180
Exposure time per image (s)	0.2	0.1	0.1	0.1
Space group	$P4_32_12$	$P4_32_12$	$P4_32_12$	$P4_32_12$
a, *b*, *c* (Å)	70.0, 70.0, 292.5	69.7, 69.7, 290.9	69.8, 69.8, 291.6	69.4, 69.4, 290.9
α, β, γ (°)	90, 90, 90	90, 90, 90	90, 90, 90	90, 90, 90
Mosaicity (°)	0.19	0.06	0.07	0.04
Resolution range (Å)	50–2.70 (2.87–2.70)	50–1.85 (1.96–1.85)	50–2.09 (2.22–2.09)	50–1.80 (1.91–1.80)
Total No. of reflections	481011 (78334)	812446 (127833)	467767 (71156)	890444 (139573)
No. of unique reflections	19869 (3210)	62686 (9806)	43652 (6782)	68555 (10787)
Completeness (%)	94.4 (97.9)	99.8 (98.7)	99.7 (98.2)	99.9 (99.3)
Multiplicity	24.2 (24.4)	13.0 (13.0)	10.7 (10.5)	13.0 (12.9)
$\langle I/\sigma(I)\rangle$†	13.9 (1.7)	18.1 (0.9)	12.0 (0.75)	19.5 (0.7)
R_{meas}‡ (%)	29.5 (217.8)	9.2 (223.2)	12.4 (264.7)	7.4 (264.8)
$CC_{1/2}$† (%)	99.7 (65.2)	100 (51.0)	99.9 (49.6)	100 (59.0)
Overall *B* factor from Wilson plot (Å^2)	55.9	43.6	56.0	44.8
Solvent content (%)	66.7	66.6	66.7	66.6

† Data with low $I/\sigma(I)$ in the outer shell (<2.0) were included based on the $CC_{1/2}$ criterion (correlation between two random halves of the data set of >50%) as proposed by Karplus & Diederichs (2012). ‡ Redundancy-independent $R_{meas} = \sum_{hkl}\{N(hkl)/[N(hkl)-1]\}^{1/2}\sum_i |I_i(hkl) - \langle I(hkl)\rangle|/\sum_{hkl}\sum_i I_i(hkl)$, where $N(hkl)$ is the data multiplicity.

capillaries. Crystals with a round-shaped habit were observed after two weeks at pH values from 4 to 8, except at pH 5 where they grew as well faceted bipyramids (Fig. 2). X-ray analysis of one of these crystals led to a first data set to 2.7 Å resolution (first column in Table 3). This tetragonal crystal form was characterized by an elongated unit cell ($a = b = 70$, $c = 290$ Å), a single protein molecule in the asymmetric unit and a high solvent content (67%). A clear molecular-replacement solution was found in space group $P4_32_12$ with *Phaser* (LLG score of 158) using a polyalanine version of the *G. stearothermophilus* enzyme (PDB entry 1miv) as a starting model.

To increase the diffraction limit of the crystals and/or find new crystallization conditions, MMS was performed using crushed crystals extracted from CD capillaries. A single screen of 96 conditions (JBScreen JCSG++, Jena Bioscience) was set up with and without seeds. The use of MMS drastically increased the number of hits obtained by vapor diffusion: a total of 34 hits were obtained after 4 d with seeds, compared with a single hit after several months without seeds (Fig. 2). The latter condition (H2 from JBScreen JCSG++) was also found by MMS and in the initial screening. It cannot be excluded that the ammonium sulfate present in the seed stock had a positive effect on the screening result. However, a seed stock prepared from one of the new conditions (E8 from JBScreen JCSG++), which did not contain this salt, was found to be equally effective in optimization, suggesting that the effect was at least partially owing to the microcrystals.

Fluorescent protein labeling with carboxyrhodamine succinimidyl ester facilitated discrimination between protein and salt crystals (owing to the high salt concentration in the seed stock, MMS generated many salt crystals). Although the protein contains nine tryptophan residues, TFL led to a much brighter fluorescent signal than intrisic tryptophan fluorescence under UV light. It did not perturb crystallization and provided a clear identification of the *Pha*CCA crystals, as presented in Fig. 3. Nucleation is generally the limiting event

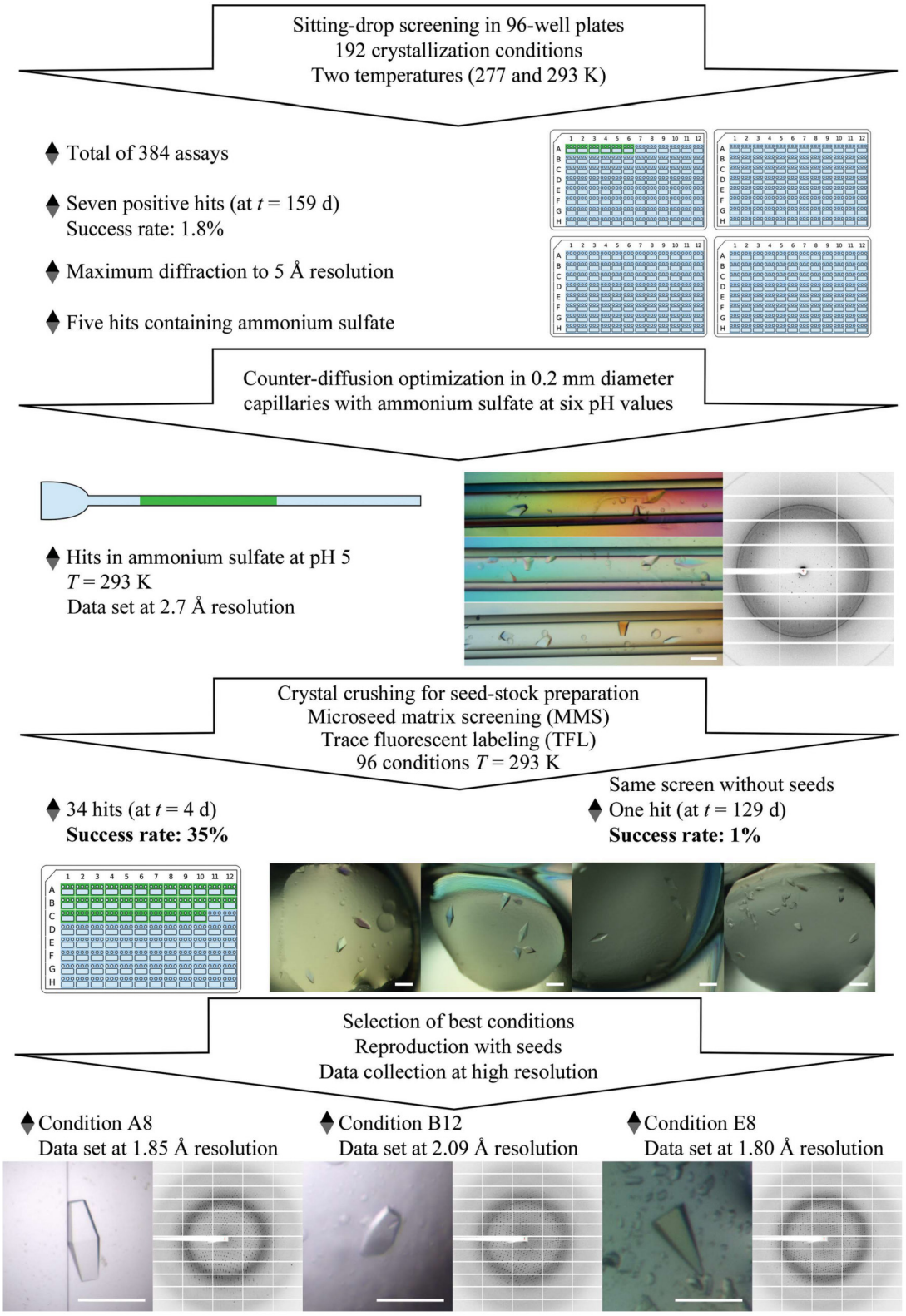

Figure 2
Workflow of the crystallogenesis strategy for *Pha*CCA. The color photograph in the center displays bipyramidal crystals that grewn in three contiguous regions of a CD capillary. The other photographs in color show crystals grown in drops equilibrated by vapor diffusion. The scale bars on the crystal micrographs are 0.2 mm in length.

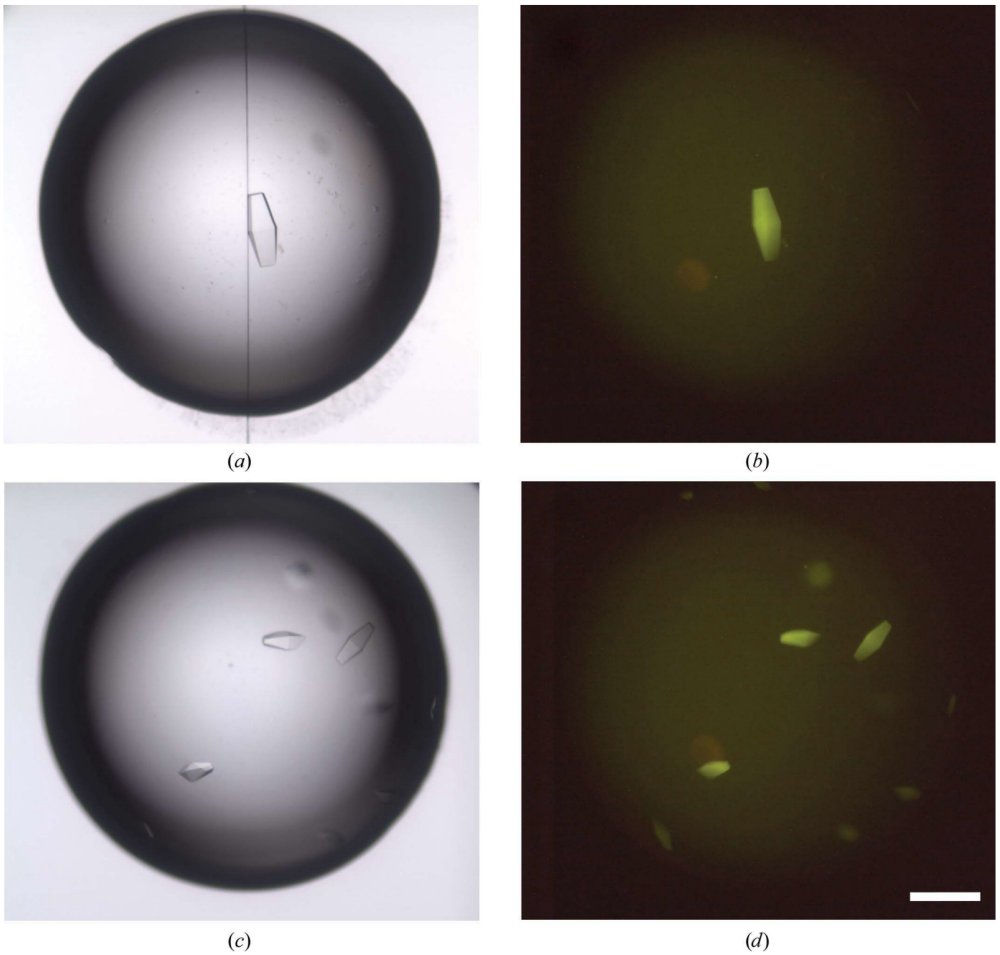

Figure 3
Detection of *Pha*CCA crystals by TFL. Crystals were grown in sitting drops from a sample containing 0.6% labeled protein mixed with a solution consisting of 100 m*M* sodium acetate, 1 *M* diammonium hydrogen phosphate pH 4.5 (the scale bar is 0.2 mm in length). The images in (*a*) and (*c*) were obtained with white-light illumination. The images in (*b*) and (*d*) were obtained with a 520 nm light source and a low-pass filter at 550 nm (LP550).

in crystal growth, and the high success rate of MMS in this study was accompanied by a drastic decrease in the time required for crystal production. Consequently, seeding was systematically used in the following optimization experiments.

Out of the 34 hits obtained in the presence of seeds, several could be reproduced. The three best hits are displayed in Fig. 2. They corresponded to JBScreen JCSG++ conditions A8, B12 and E8 (Table 2) and yielded crystals that diffracted to 1.85, 2.09 and 1.80 Å resolution, respectively (Table 3). They all belonged to the same tetragonal space group and showed comparable unit-cell parameters. Refinement of the respective crystal structures is in progress and a complete analysis of the corresponding structures at high resolution will be published elsewhere.

To conclude, this work illustrates the usefulness of combining various crystallogenesis methods to efficiently define and optimize multiple crystallization conditions, and to ensure the production of well diffracting crystals. The availability of various growth conditions for *Pha*CCA crystals will also be an advantage for future soaking experiments with substrates (CTP, ATP and small RNAs).

Acknowledgements

The authors acknowledge the assistance of Guillaume Bec (IBMC–CNRS) from the UPR 9002 crystallization platform, as well as the following synchrotron facilities and associated scientists for beamtime provision for the project and assistance during data collection: the X06DA beamline at the Swiss Light Source, Villigen, Switzerland and PROXIMA-1 at the SOLEIL synchrotron, Saint-Aubin, France. They are grateful to the organizers and speakers of the Sixth FEBS Advanced Course on Macromolecular Crystallization (Czech Republic, June 2016), especially Terese Bergfors, Allan D'Arcy and Marc Pusey, for their advice regarding seeding and TFL methods.

Funding information

Funding for this research was provided by: LabEx NetRNA (grant No. ANR-10-LABX-0036_NETRNA); Labex Mito-Cross (grant No. ANR-11-LABX-0057_MITOCROSS); Ministère des Affaires Etrangères–Deutscher Akademischer Austauschdienst (grant No. 35317YM/57207407 PROCOPE

Hubert Curien 2016); Centre National de la Recherche Scientifique; Deutsche Forschungsgemeinschaft (grant No. MO 634/8-1); Université de Strasbourg (IDEX PhD grant).

References

Adams, P. D., Afonine, P. V., Bunkóczi, G., Chen, V. B., Davis, I. W., Echols, N., Headd, J. J., Hung, L.-W., Kapral, G. J., Grosse-Kunstleve, R. W., McCoy, A. J., Moriarty, N. W., Oeffner, R., Read, R. J., Richardson, D. C., Richardson, J. S., Terwilliger, T. C. & Zwart, P. H. (2010). *Acta Cryst.* D**66**, 213–221.

Bae, E. & Phillips, G. N. Jr (2004). *J. Biol. Chem.* **279**, 28202–28208.

Bergfors, T. (2003). *J. Struct. Biol.* **142**, 66–76.

Betat, H., Rammelt, C. & Mörl, M. (2010). *Cell. Mol. Life Sci.* **67**, 1447–1463.

D'Arcy, A., Bergfors, T., Cowan-Jacob, S. W. & Marsh, M. (2014). *Acta Cryst.* F**70**, 1117–1126.

D'Arcy, A., Villard, F. & Marsh, M. (2007). *Acta Cryst.* D**63**, 550–554.

De Maayer, P., Anderson, D., Cary, C. & Cowan, D. A. (2014). *EMBO Rep.* **15**, 508–517.

Ernst, F. G. M., Erber, L., Sammler, J., Jühling, F., Betat, H. & Mörl, M. (2018). *RNA Biol.* **15**, 144–155.

Ernst, F. G. M., Rickert, C., Bluschke, A., Betat, H., Steinhoff, H. J. & Mörl, M. (2015). *RNA Biol.* **12**, 435–446.

Kabsch, W. (2010). *Acta Cryst.* D**66**, 125–132.

Karplus, P. A. & Diederichs, K. (2012). *Science*, **336**, 1030–1033.

Li, F., Xiong, Y., Wang, J., Cho, H. D., Tomita, K., Weiner, A. M. & Steitz, T. A. (2002). *Cell*, **111**, 815–824.

McCoy, A. J., Grosse-Kunstleve, R. W., Adams, P. D., Winn, M. D., Storoni, L. C. & Read, R. J. (2007). *J. Appl. Cryst.* **40**, 658–674.

Mykytczuk, N. C. S., Wilhelm, R. C. & Whyte, L. G. (2012). *Int. J. Syst. Evol. Microbiol.* **62**, 1937–1944.

Neuenfeldt, A., Just, A., Betat, H. & Mörl, M. (2008). *Proc. Natl Acad. Sci. USA*, **105**, 7953–7958.

Newman, J. (2011). *Methods*, **55**, 73–80.

Newman, J., Egan, D., Walter, T. S., Meged, R., Berry, I., Ben Jelloul, M., Sussman, J. L., Stuart, D. I. & Perrakis, A. (2005). *Acta Cryst.* D**61**, 1426–1431.

Otálora, F., Gavira, J. A., Ng, J. D. & García-Ruiz, J. M. (2009). *Prog. Biophys. Mol. Biol.* **101**, 26–37.

Pusey, M., Barcena, J., Morris, M., Singhal, A., Yuan, Q. & Ng, J. (2015). *Acta Cryst.* F**71**, 806–814.

Tomita, K., Ishitani, R., Fukai, S. & Nureki, O. (2006). *Nature (London)*, **443**, 956–960.

8 CCA addition in the cold: Structural and biochemical characterization of the enzyme from *Planococcus halocryophilus* (article in preparation)

This section presents an article in preparation entitled: “CCA addition in the cold: Structural and biochemical characterization of the enzyme from *Planococcus halocryophilus”.* It provides the crystallographic characterization and biochemical analysis of the *Pha*CCA enzyme performed with our collaborators from the group of Prof. Mario Mörl in Leipzig.

8.1 Introduction

A variety of organisms are exposed to temperatures below 5°C and are described as psychrophilic. Because of their living conditions, their enzymes have to be cold adapted.

8.1.1 Examples for adaptation strategies

Several comparative studies between thermophilic and psychrophilic enzymes have shown that there is no universal strategy for cold-adaptation. Rather, each enzyme seems to use different adaptations to acquire enough flexibility to be active in cold environments. In most cases these adaptations lead to a reduction of non-covalent stabilizing interactions, for instance via reduced hydrophobic cores, less charged surfaces, increased surface hydrophobicity, weaker interdomain interactions, less disulfide bridges, hydrogen bonds, or electrostatic interactions, increased number and size of loops and changes in amino acid composition leading to lower arginine/lysine ratio, lower amount of proline residues and higher frequency of glycine residues (Feller and Gerday 2003; Siddiqui et al. 2002; Siddiqui and Cavicchioli 2006; Struvay and Feller 2012; Yang et al. 2015; Sarmiento et al. 2015; Dick et al. 2016; Kovacic et al. 2016; Siddiqui et al. 2013). Recently, additional work on structural

strategies of cold adapted enzymes were published, showing that global conformational changes of the protein, rather than structural changes close to the active site, enhances the efficiency of substrate binding to the catalytic site, thus reducing activation energy and increasing substrate turnover rates (Hashim et al. 2018; Khrapunov et al. 2017; Lee et al. 2017; Sočan et al. 2018).

8.1.2 Special case of RNA polymerases: need for controlled flexibility

CCA-adding enzymes are highly specific RNA polymerases that add and maintain the sequence (C-C-A) at tRNA 3‘-ends (Sprinzl and Cramer 1979; Deutscher 1990; Hoffmeier et al. 2010). These enzymes are not only vital in organisms that do not encode the CCA-triplet in their tRNA genes, but are equally important in organisms with encoded CCA ends for tRNA repair and quality control (Wellner et al. 2018). For proper and efficient CCA incorporation considerable structural rearrangements are required (Tomita et al. 2004; Ernst et al. 2015). However, for cold-adapted CCA-adding enzymes there is a discrepancy between the need of a tightly controlled flexibility during polymerization and an increased flexibility as a strategy for cold-adaptation.

8.1.3 Recent work on psychrophilic CCA-adding enzymes

In a recent study published by Ernst and coworkers in 2018 focused on *Exiguobacterium sibiricum* CCA-adding enzyme (*Esi*CCA), data from chimeric enzymes between psychrophilic *Esi*CCA and thermophilic enzyme from *Geobacillus stearothermophilus* revealed that both N- and C-terminal parts (corresponding to the catalytic core and the tRNA binding domain, respectively) are equally important for cold-adaptation. Whereas both parental enzymes exhibit the typical temperature dependent activities, both the chimeric enzymes are truly cold-adapted although they carry only a psychrophilic N- or C-terminal part.

It was also shown that the CCA-adding enzyme from *Planococcus halocrophilus* (*Pha*CCA), a bacterium from the Arctic permafrost which grows at -15°C, is strongly cold-adapted and catalyzes CCA-addition down to 0°C in vitro (Ernst et al. 2018).

Here, we provide a structural analysis of how this psychrophilic RNA polymerase (*Pha*CCA) is adapted to very low temperatures.

8.2 Results

8.2.1 Functional analysis

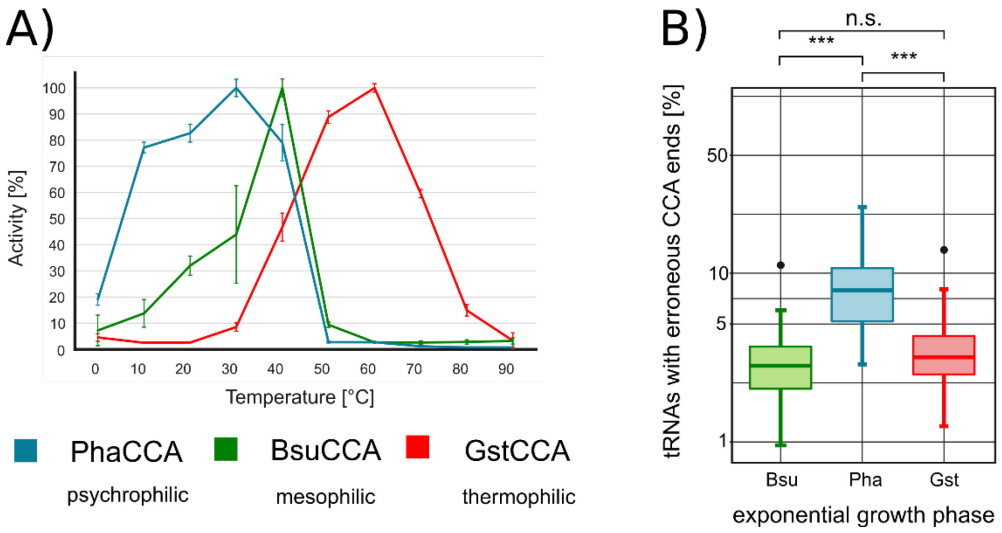

Figure 8-1 : Stability and fidelity from *Pha*CCA, *Bsu*CCA and *Gst*CCA, adapted from Ernst *et al*. 2018. A) *In vitro* activity assays at different temperatures. B) *In vivo* fidelity measurements.

Figure 8-1 recapitulates the observations in Ernst *et al*, 2018. One can see in panel A results of activity assays performed at several temperatures with *Pha*, *Bsu* and *Gst*CCA enzymes, which are psychrophilic, mesophilic and thermophilic respectively. *Pha*CCA is the only enzyme presenting more than 70% activity at 10°C and even 20% at 0°C, nicely illustrating its cold adaptation. On panel B, *in vivo* fidelity quantitative measurements were performed and significantly showed that *Pha*CCA is adding nucleotides to tRNAs with an increased error rate compared to the other ones.

8.2.2 Structural analysis of *Pha*CCA

The *Pha*CCA enzyme was crystallized in its apo-form and soaked with CTP. Experimental phases were determined by sulfur SAD-phasing using a PRIgo goniometer (Waltersperger et al. 2015) and collected as described in Weinert *et al.*, 2015. Structural data and refinement statistics are presented in **Table 8-1**.

Crystals were produced by combining advanced crystallogenesis methods as described previously (article in section 7, de Wijn *et al.*, 2018), and led to X-ray analysis of crystals from the *Pha*CCA apo-form and in complex with CTP. Incorporation of CTP was performed by soaking the crystals 30 s in a drop containing the crystallization solution with 20% (m/v) glycerol as cryoprotectant and 5 mM CTP. Diffraction data were collected on crystals grown by vapor diffusion with microseeds in condition E8 from JCSG++ commercial screen (Jena Bioscience) containing 100 mM sodium acetate, 1 M di-ammonium hydrogen phosphate, pH 4.5. SAD dataset was collected on beamline PXIII at the Swiss Light Source (Villigen, Switzerland).

Table 8-1 : Structural data and refinement statistics

	*Pha*CCA SAD phasing	*Pha*CCA Apo-form	*Pha*CCA with CTP
X-ray beamline	SLS - PXIII	SOLEIL – PROXIMA-1	SOLEIL – PROXIMA-1
Wavelength (Å)	2.067	0.979	0.979
Temperature (K)	100	100	100
Detector	Pilatus 2M-F	Pilatus 6M	Pilatus 6M
Crystal-detector distance (mm)	120	320	296
Oscillation (° / s)	0.2 / 0.1	0.1 / 0.1	0.1 / 0.1
No. of images	7 x 1800	1800	1677
Space group	$P4_32_12$	$P4_32_12$	$P4_32_12$
a, b, *c* (Å)	69.7, 69.7, 290.7	69.4, 69.4, 290.9	70.3, 70.3, 291.5
α, β, γ (°)	90, 90, 90	90, 90, 90	90, 90, 90
Mosaicity (°)	0.07	0.04	0.05
Resolution range (Å)	50 – 2.25 (2.35 - 2.25)	50 – 1.8 (1.91 – 1.8)	50 – 1.85 (1.96 – 1.85)
Total No. of reflections	5015162 (223140)	890444 (139573)	776857 (123819)
No. of unique reflections	64194 (7615)	68555 (10787)	63935 (10060)
Completeness (%)	99.0 (96.3)	99.9 (99.3)	99.8 (99.2)
Redundancy	78.1 (29.3)	13.0 (12.9)	12.2 (12.3)
$\langle I/\sigma(I)\rangle$	30.8 (1.11)	19.5 (0.66)	22.11 (0.95)
*R*meas (%)	17.0 (278.4)	7.4 (264.8)	6.9 (239.4)
CC1/2 (%)	99.9 (51.8)	100 (59)	100 (45.1)
Overall *B* factor from Wilson plot (Å 2)	36.2	44.8	45.0
No. of reflections, working set / test set	34091 / 1813	64991 / 3420	60676 / 3195
Final Rcryst (%) / R_{free} (%)	22.8 / 27.0	24.4 / 26.7	19.8 / 22.4
No. of non-H atoms	2967	2989	3422
R.m.s. deviations			
Bonds (Å)	0.009	0.008	0.008
Angles (°)	1.07	1.01	1.07
Average *B* factors (Å^2)	43.7	41.6	40.9
Protein	43.7	41.6	40.1
Water	/	/	47.6
Ramachandran plot			
Most favoured (%)	97.0	99.0	98.0
Allowed (%)	2.7	0.7	1.7
Rotamer outliers (%)	0.9	0.6	0.6

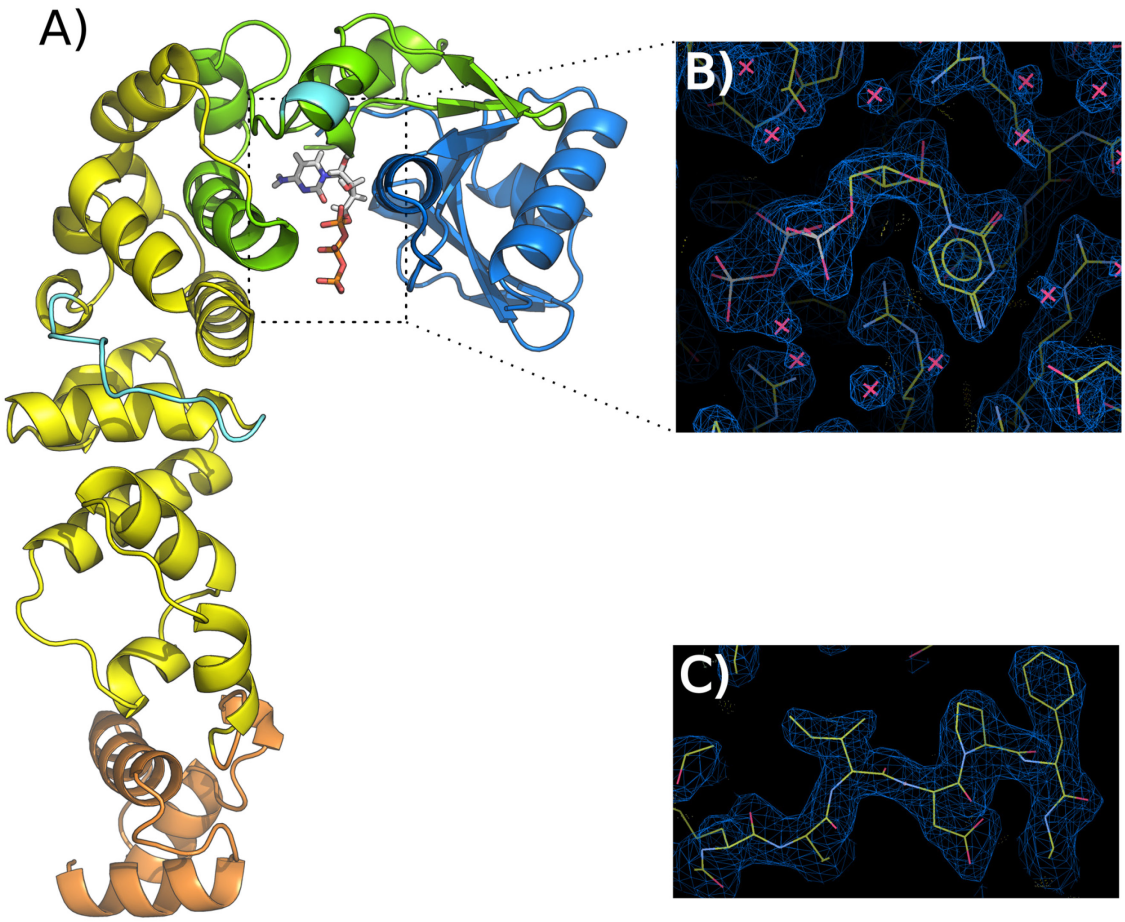

Figure 8-2 : Overall structure of *Pha*CCA. A) Cartoon representation of the enzyme with the typical seahorse-like shape with bound CTP substrate. Domains are represented in different colors: blue for head, green for neck, yellow for body and orange for tail. B) Electron density map of the catalytic site with CTP. C) Electron density map from the sulfur SAD-phasing. Maps are contoured at 1.2 sigma.

The *Pha*CCA crystal structure was determined by sulfur SAD phasing. A snapshot of the experimental map at 2.1 Å is presented panel C. The complex with CTP was obtained at 1.85 Å resolution and is presented in mode cartoon **Figure 8-2** panel A. The electron density map of the CTP is well defined (panel B).

Table 8-2 : Alpha-helix contents in CCA-adding enzyme structures from different bacteria. Calculations of percentages were performed using the DSSP web-server.

Structure	*Pha*CCA Apo-form	*Gst*CCA 1MIV	3H3A	4WC2
Source	*Planococcus halocryophilus*	*Geobacillus stearothermophilus*	*Thermotoga maritima*	*Aquifes aeolicus*
Living temp.	Psychrophilic	Thermophilic	Hyperthermo.	Thermophilic
Total helices (%)	49	50	52	56
Helices in body domain (%)	57	62	65	69

To determine variations in the helix content of different structures (our apo-form and a selection of other structures from the PDB) we used the web-server DSSP (Touw et al. 2015). It uses pdb files to determine their content in secondary structure elements as summarized in **Table 8-2**. Percentages indicated in this table were normalized to the number of amino acids in the protein or in the indicated domain, without taking purification tags into account. If we only consider the whole enzyme, only marginal differences can be observed between *Pha* and *Gst*CCA. But taking a closer look at the body domains, which are less conserved and thus more susceptible to exhibit adaptations, a reduction of 5% in the helices content is observed in *Pha*CCA with respects to other enzymes.

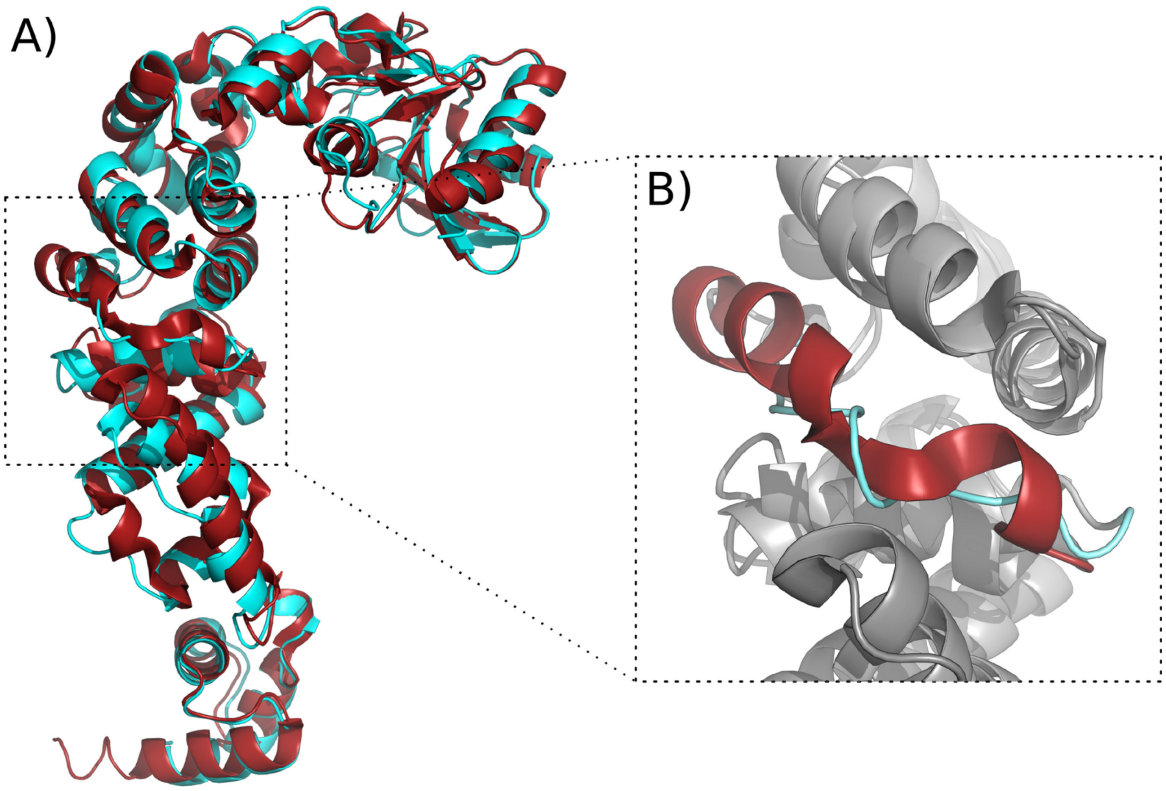

Figure 8-3 : Comparison of *Pha* (red) and *Gst*CCA (blue) enzyme structures. A) Structural alignment and B) close-up view of a region of the body domain, highlighting significant secondary structure differences.

Pha and *Gst* enzymes can be superimposed with an RMSD of 1.4 Å (calculated with PYMOL, **Figure 8-3** panel A). Head and neck domains exhibit very few differences, whereas a loss of α-helices in the body domain of the *Pha*CCA can be observed (as presented in **Table 8.2**). One instance is illustrated in panel B from amino acids 227 to 237, highlighted in blue. This reduced content of α-helices is a hallmark of psychrophilic enzymes (as mentioned above). This kind of adaptation may arise in this C-terminal domain which is generally less conserved and thus more tolerant to variations, in contrast to the N-terminus which is highly conserved because it is involved in catalysis.

8.3 Discussion

Several studies showed that psychrophilic adaptation can be reached without any amino acid substitution in the active site (Struvay and Feller 2012). Very often, a cumulative effect of different changes outside the catalytic core leads to cold-adaptation and even single substitutions of individual residues can have long-range effects on the general stability of the enzyme (Fitter 2005; Siddiqui and Cavicchioli 2006; Struvay and Feller 2012; Kovacic et al. 2016). For example, in adenylate kinase, a single methionine replacement (from the thermophilic homolog) to threonine (in the cold-adapted homolog) is sufficient to generate the required flexibility of the psychrophilic enzyme (Bae and Phillips 2004). In addition, in comparative studies of α-amylases of different Bacillales it was shown that an exchange of individual residues can increase or decrease the enzyme's overall thermostability (Fitter 2005).

A number of studies have raised the question whether cold-adapted proteins achieve flexibility throughout their whole structure (global flexibility) or whether they have distinct regions of local flexibility (Siddiqui and Cavicchioli 2006). The cold-adapted *Pha* CCA-adding enzymes uses a global flexibility in the tRNA-binding C-terminus, indicated by a reduction of α-helix content.

It was already shown for cold-adapted CCA-adding enzymes from *Planococcus halocryophilus* and *Exiguobacterium sibiricum* that their adaptation comes with a tradeoff in activity, stability and fidelity (Ernst et al. 2018), but as presented here this adaptation is not occurring in the nucleotide binding pocket. As it occurs in tRNA-binding C-terminus, it could be related to mistakes in tRNA binding.

8.4 Conclusion

The remarkable cold adaptation of *Pha*CCA seems to be linked to an increased overall flexibility and a lower thermal stability of the enzyme provided by the loss of secondary structure elements. Hence compared to the thermophilic CCA-adding enzyme from *Geobacillus stearothermophilus*, the structure of the *Pha*CCA enzyme shows a reduced content of alpha-helices in its body domain.

However, the price to be paid for such a cold-adaptation of *Pha*CCA is not only a thermal destabilization, but, importantly, a significant reduction in polymerization fidelity.

IV. Crystallization study with the Xtal Controller

Ce troisième chapitre a pour but de présenter l'instrument Xtal Controller ainsi qu'une sélection d'expériences qu'il a permis de réaliser. Ces travaux s'inscrivent dans le développement de nouvelles approches de cristallogenèse appliquées à des systèmes protéiques présentant un intérêt biologique pour le laboratoire.

En dépit des progrès récents sur les techniques de croissance cristalline, la recherche de cristaux ou encore les méthodes de diagnostic, la détermination de conditions de cristallisation et leur optimisation reste très empirique. Les méthodes classiques ne permettent pas un contrôle direct de la nucléation ni de la croissance. Le concept du Xtal Controller 900 (XC900) a pour objectif de combler ce manque.

Comme présenté en section 2.3, cet instrument permet un contrôle précis des paramètres physico-chimiques autour et à l'intérieur d'une goutte de cristallisation : température, humidité, concentrations des macromolécules et de l'agent cristallisant. La modification des concentrations est rendue possible par la présence de deux pompes reliées à un réservoir contenant soit de l'eau, soit l'agent cristallisant. Le XC900 rend également possible le suivi en temps réel de l'évolution de la goutte par l'utilisation d'une caméra couplée à un microscope, ainsi que d'un appareil de DLS.

9 Introduction to the Xtal Controller system

Despite recent advances in crystal growth, crystal detection and diagnostic methods (DLS), research and optimization of crystallization conditions remains empirical. We do not control nucleation or growth in the classical methods (sections 1 and 2).

Experiments in microgravity in space started in the late 80's (Vergara et al. 2005) helped the development and rationalization of crystallization practices but the community was still lacking an instrument that brings a complete control and follow-up of a crystallization experiment. It was in this context that the concept that led to the Xtal Controller germinated (Garcia-Caballero et al. 2011). The instrument provides the follow-up by DLS and camera and a means of action by the piezo-pumps. It was built in the lab of Prof. Christian Betzel (University of Hamburg) then developed and marketed by Xtal Concept. Our team is the first lab to have acquired this technology at the beginning of my thesis, which allowed me to use it and establish experimental protocols.

This instrument was initially conceived for a purpose of crystal growth in difficult cases: when no usable crystals where available or in case of sensitive systems (which were either remaining clear or precipitating) with aim to control and slow down the system. New applications were also more recently envisaged: development of protocol for preparation of nanocrystals suitable for XFEL analysis with use of the DLS or more recently, the study of nucleating agent addition to determine the effect on kinetics of nucleation and growth.

Figure 9-1 presents some important features of the instrument and pictures. A more detailed schematic representation is given section 2.3.

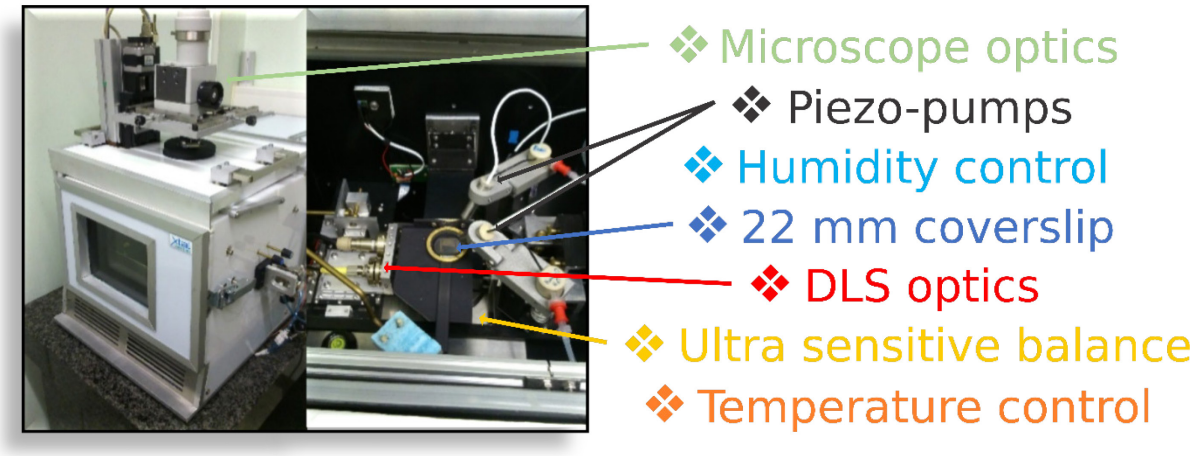

Figure 9-1 : Pictures of the Xtal Controller in our laboratory with view of the experimental chamber. Some important elements are indicated on the right with their localization.

As described before, this instrument allows a precise control of several conditions inside a crystallization droplet: temperature, humidity, macromolecule and crystallization agent concentrations. It enables to follow a desired path inside the phase diagram (**Figure 9-2**). Movements are made possible thanks to the controlled use of the different pumps and of evaporation.

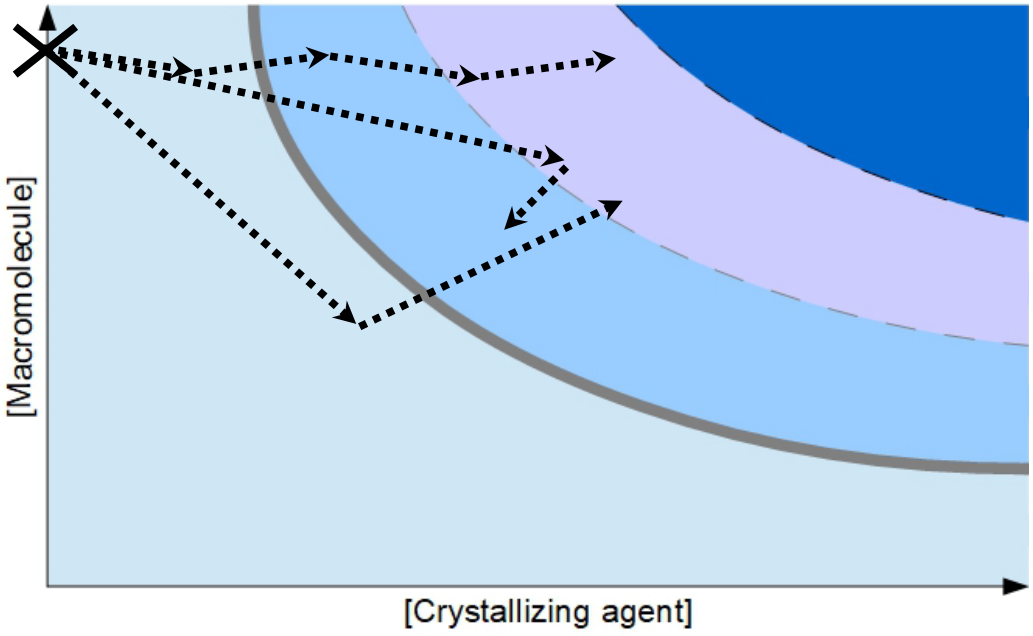

Two articles were recently published involving the use of the Xtal Controller (Schubert et al. 2017; Baitan et al. 2018). Schubert *et al,* 2017 describes some observations by electron microscopy of populations detected by DLS in the instrument for model proteins. The second one published in JoVE presents an experimental protocol to grow crystals in the instrument. No publication is available yet on applications that do not concern model proteins or standard experiment.

10 Setting up an experiment

The following protocol for the Xtal Controller 900 was written in collaboration with Daniela Baitan PhD candidate in the Xtal Concepts startup and in the group of Prof. Christian Betzel. The same steps were followed for all experiments, except when mentioned. The graphical user interface (GUI) is split in three windows (**Figure 10-1**): the camera window on the right, the curve panel at the bottom and the main control window with all experimental subdirectories accessible on the left.

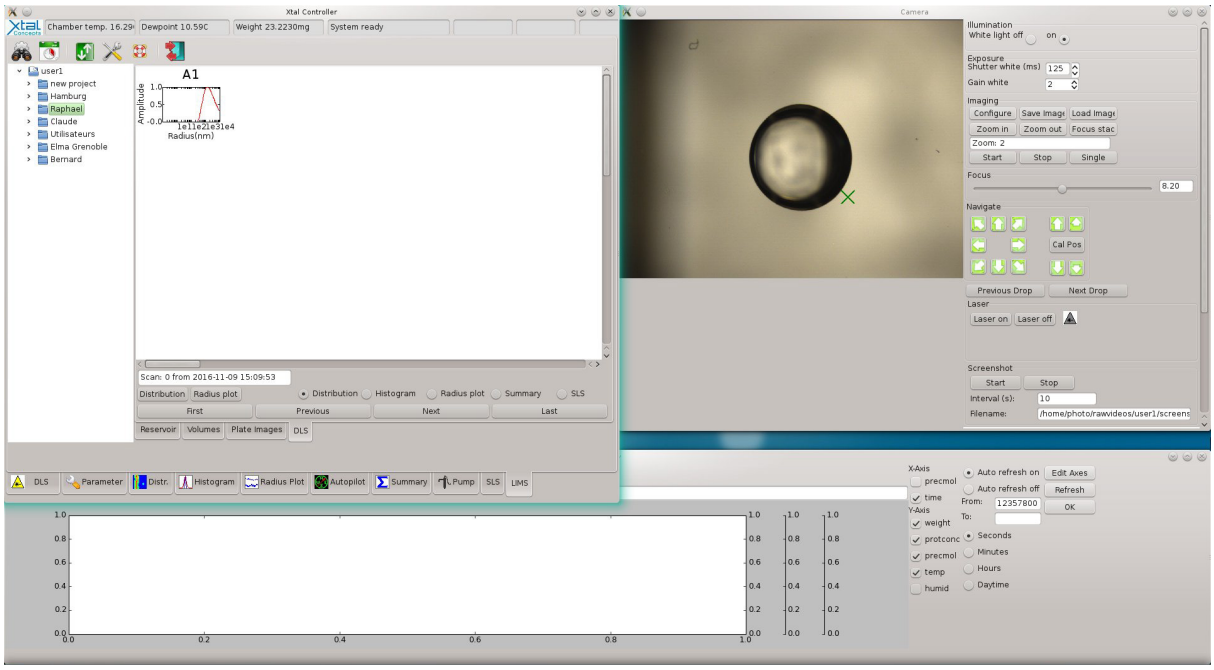

Figure 10-1 : Screenshot of the complete Xtal Controller GUI.

10.1 Launching the software

- in a Terminal console go to the pms directory (cd /pms)
- start the program (python main.py). This will automatically launch the software and the connection to the instrument.

10.2 Creating a new project

- Go to LIMS panel (**Figure 10-2**)

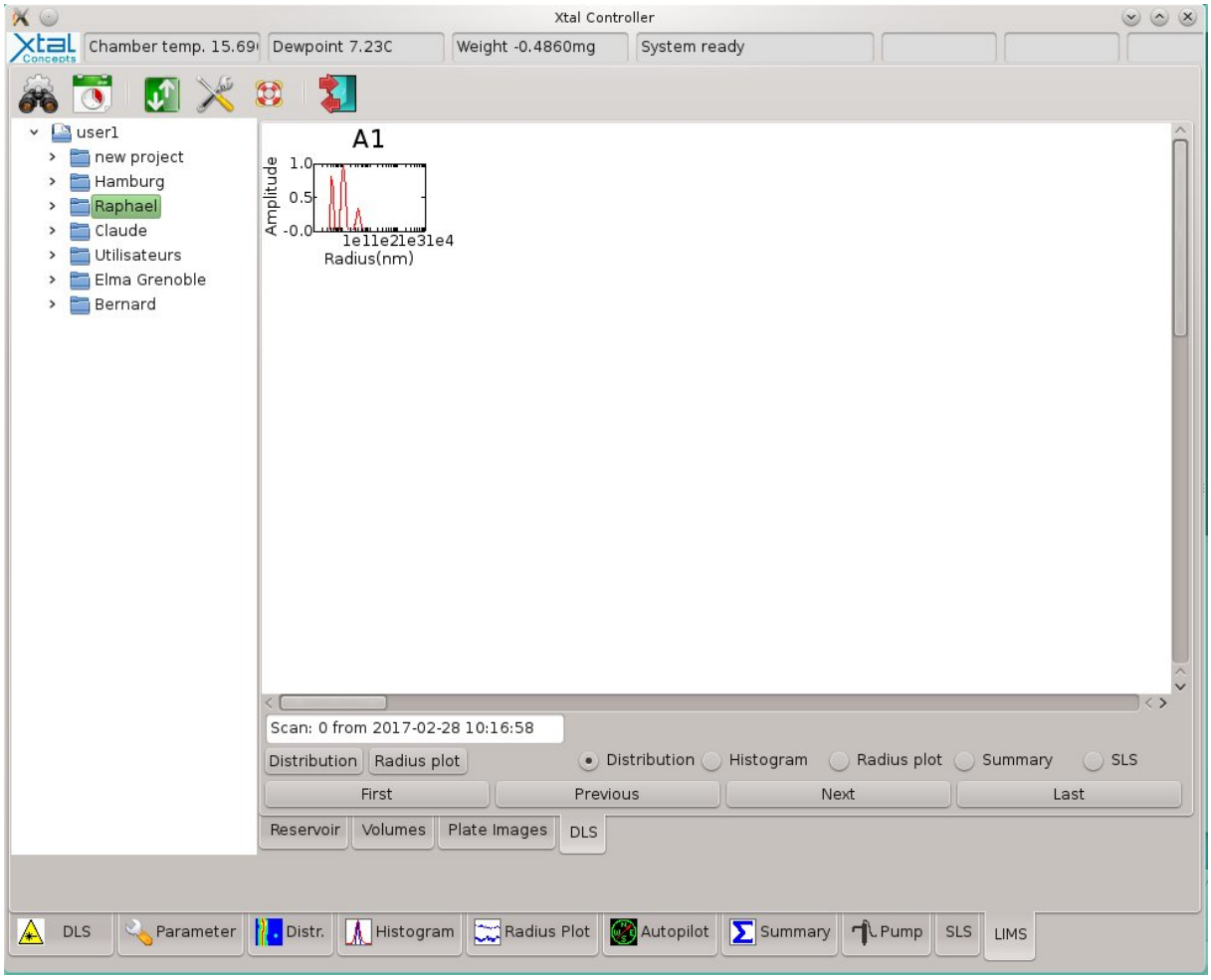

Figure 10-2 : Screenshot of the “LIMS” panel.

- Right click on the user folder / Add / Project name and Project description
- Right click on the project that has just been created and create new experiment. This will create a new folder which will further contain the desired tests for your sample.
- Right click on the experiment folder / Add / Plate name to enter a new drop experiment and give it a name. Also a short description of the conditions and of the sample can be added in “Plate description”. Follow the window protocol for your experiment. Only letters should be used for the description of the protein/precipitant or other substances and only numbers (e.g. 10 or 10.5) for concentrations.

Press the green box with the two arrows to start your experiment. You will be asked to introduce your experiment. Click on the new created experiment and validate by clicking “Insert”.

IMPORTANT: directly start a first DLS measurement to set t=0 for DLS.

10.3 Experimental Setup

10.3.1 Temperature and humidity

- Go to “Parameter” (**Figure 10-3**) and set up the temperature in the “Temperature (C)” and the humidity in the “Dewpoint (C)”. Note that the Dewpoint value cannot exceed the temperature value. Two equal values will mean 100% humidity in the chamber.

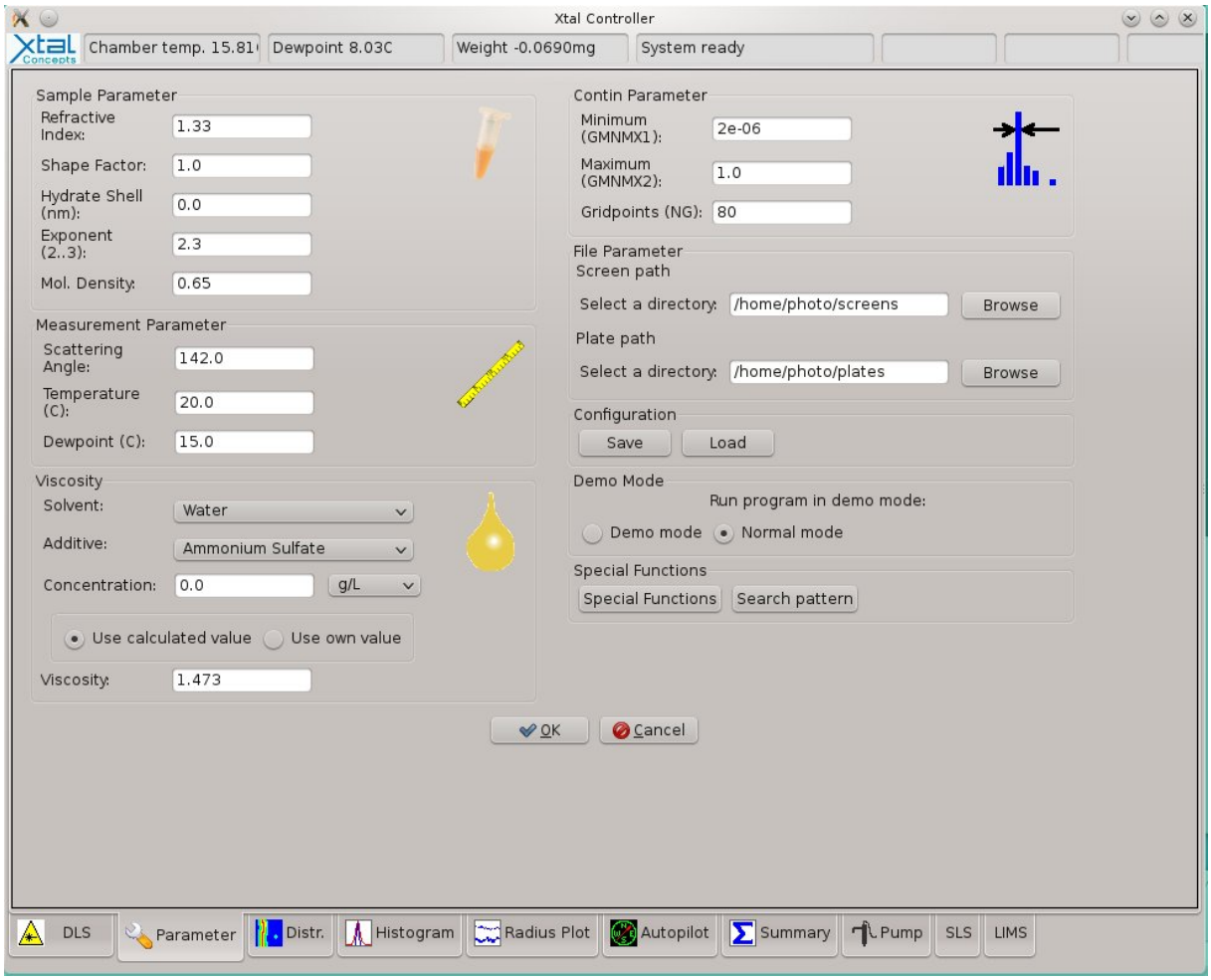

Figure 10-3 : Screenshot of “Parameter” panel.

- Open the lid and the door of the experimental chamber
- Load the cover slip by using the pallet/ passe partout (the passe partout is at the right position when you feel a smooth click)

10.3.2 Pumps and protein drop

- Go to “PUMP” (**Figure 10-4**) to define the initial setup.

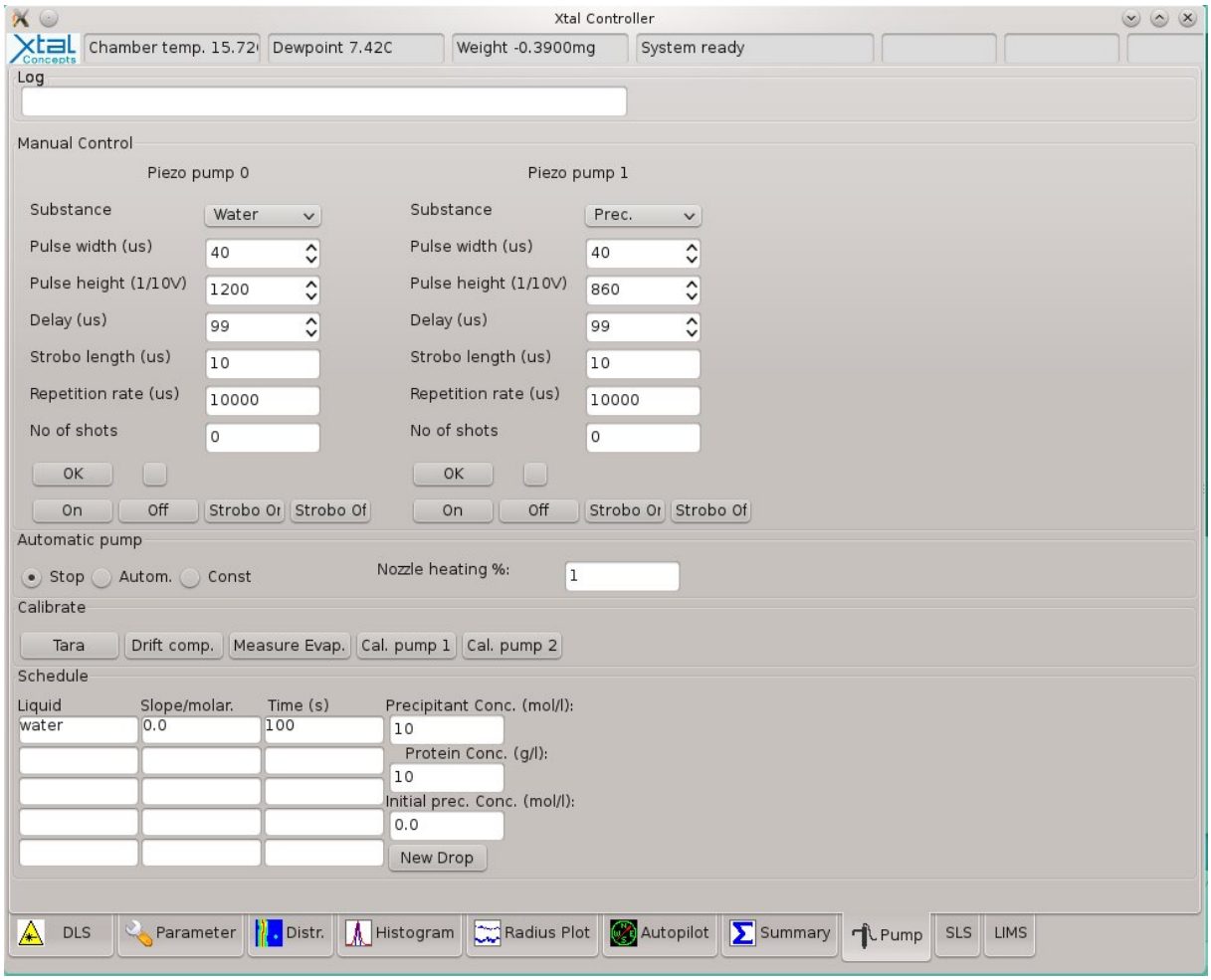

Figure 10-4 : Screenshot of the “Pump” panel.

- Piezo Pump 0 injects water and Piezo Pump 1 the precipitant (crystallant) solution. When using high viscosity solutions, first set the nozzle heating power to the desired percentage. No detailed viscosity assays were performed to determine the upper limit but as an example 5 % (m/v) is close to the concentration limit manageable by the pump for PEG 3350.
- Test each pump individually. Click “OK” for a few drops or “On” for a continuous jet shooting.
- Align manually the two pumps in such a way that they shoot at the same position on the cover slip. This can be done by using the two screws (blue for water, grey for precipitant) on the right-hand side of the instrument.
- After alignment, the cover slip can be exchanged with a clean one for setting up the protein drop.

- After the new cover slip has been placed in, press “TARA”. Then, press “OK” or “On” for the water pump. This will generate a drop indicating the position to deposit the protein drop.
- After depositing the protein drop close the lid and the door.
- Press on “Const” (to ensure constant weight by injecting water to compensate for drop evaporation) and then on “New drop” (to declare the record of a new experiment).
- Check in the top-left white window that the values are correct and the precipitant molarity “mol” of the drop is set to zero. From this time on, the protein is setup in a constant mode where the drop weight is kept constant.

10.3.3 Experimental schedule

In the schedule table, precipitant addition, evaporation/concentration of the droplet as well as a constant weight mode for the droplet can be planned.
Table description:

“Liquid” column
- For water write “water”
- For precipitant write “prec”

“Slope/molar.” column
- For water addition (dilution/constant mode) the value introduced represents the percentage of drop weight that will be added/evaporated.
E.g.: “water 0.4” indicates that water will be added to extend the drop weight by 40% whereas “water -0.4” that the drop will be evaporated until the weight is down by 40%.
- For precipitant addition, the value introduced represents the precipitant molarity which will be added to the sample drop. The value introduced cannot exceed the initial concentration of precipitant.

“Time (s)” column
- Enter the time planned for each step in seconds.

NB: At the beginning of each experimental schedule, set a line for the automatic adjustment of the weight in a constant mode. This should be:

water 0.0 100

To start the experimental schedule, press “Autom.”

10.3.4 DLS measurements

When the drop is ready, check the position of the DLS laser in the droplet. It should not be too close to the drop limit (where the light path through the mother liquor is minimal).

- Go to the camera window (**Figure 10-5**)

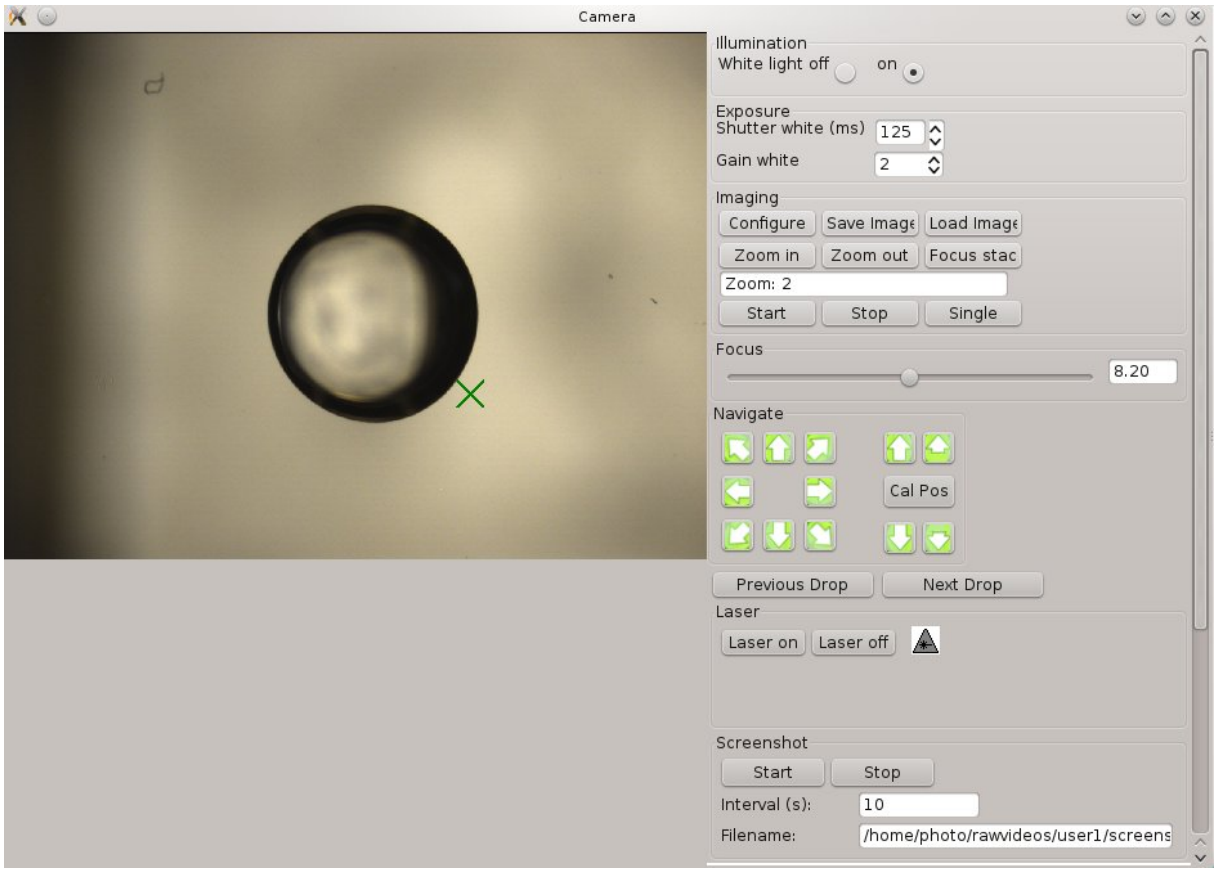

Figure 10-5 : Screenshot of the camera panel.

- Make sure the “illumination/white light” is switched on.
- Activate the laser by clicking “Laser on”.

- The laser position can be adjusted manually by using the two screws on the left-hand side of the device. They will coordinate the laser X and Y position.
- To check the DLS position, go to “DLS” (**Figure 10-6**) and press “START”. This will run a first DLS measurement. If the auto-correlation function and/or the Count rate do not have a good signal, readjust the laser position. If the signal is not good enough, press “STOP” before the measurement ends. This will prevent it from being recorded. (In this case, each measurement takes 60 seconds).

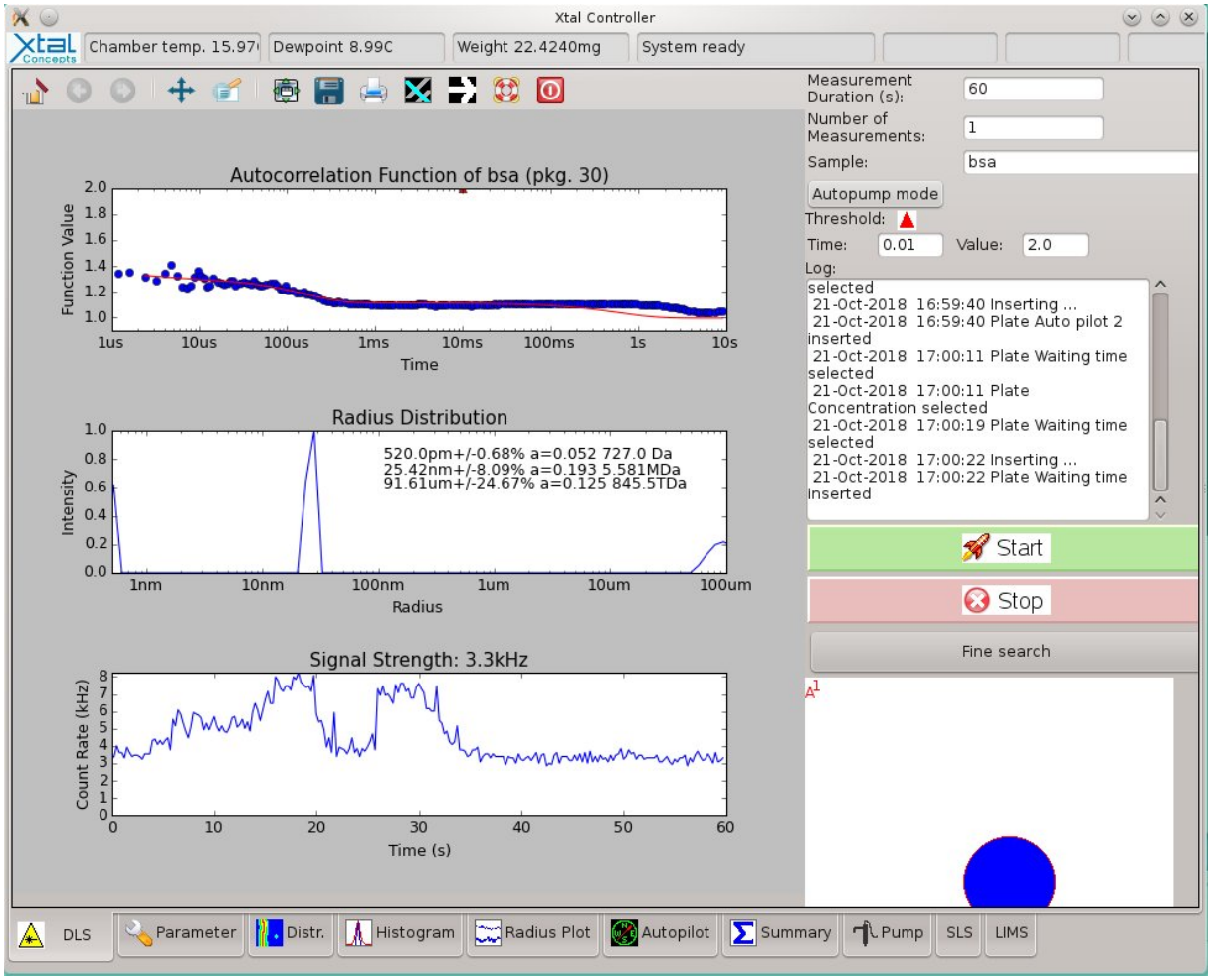

Figure 10-6 : Screenshot of the “DLS” window of a test experiment.

10.3.5 To setup a series of DLS measurements and/or of images

- Go to Autopilot (**Figure 10-7**)

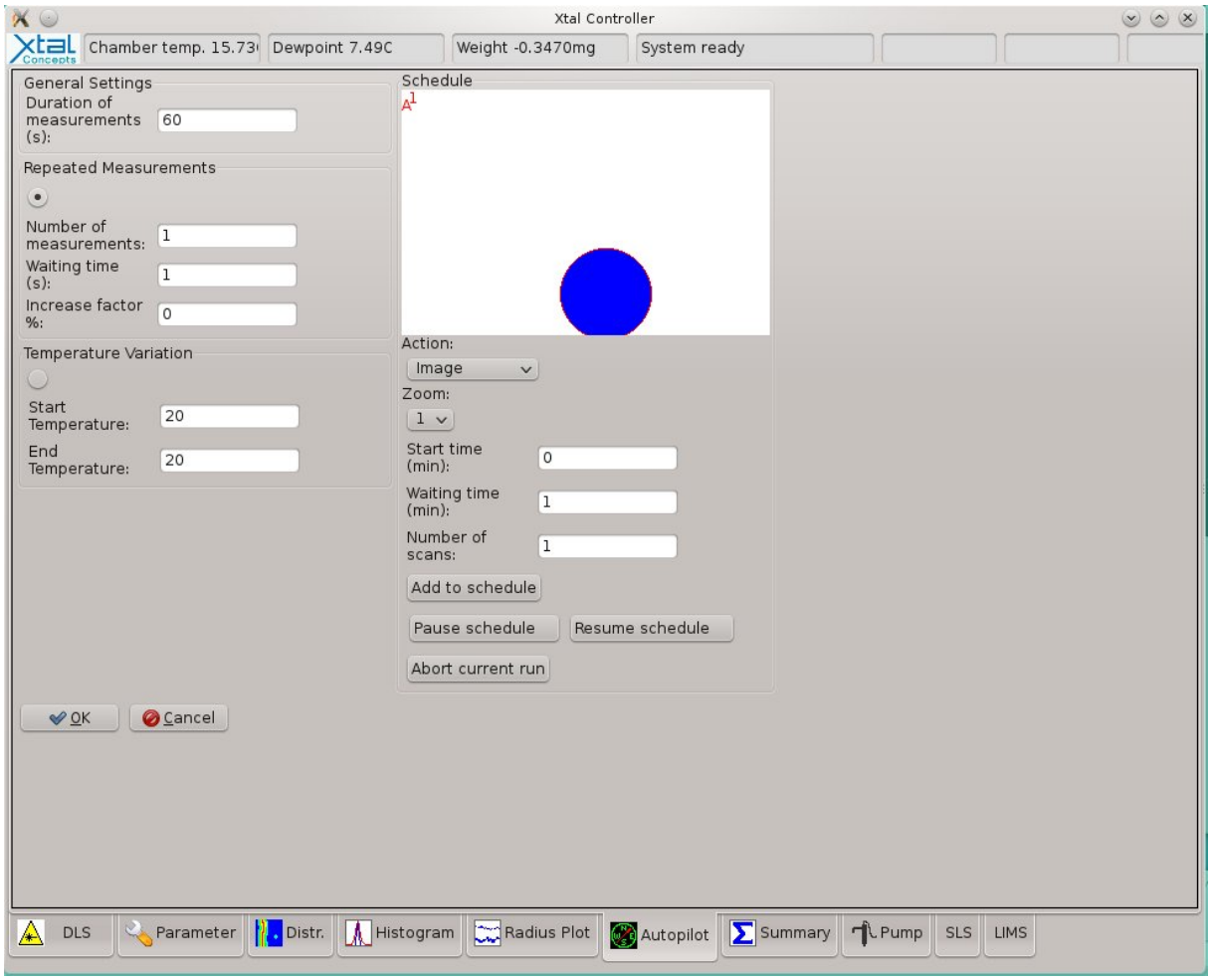

Figure 10-7 : Screenshot of the “Autopilot” window

-In the “Action” box, choose the type of action you want to schedule (DLS/Image/Calib).
*The “Calib” action is not intended to be scheduled on a regular basis. This should only be used at times, when the balance is showing a drifting or when strange jumps occur in the curves.
- After selecting the action, fill in the next boxes.
“Start time (min)” - this represents the time when the action starts. “0” means that the action will start as soon as one presses “Add to schedule”.
“Waiting time (min)” - is the time period between two actions.
“Number of scans” - is the total number of action planned during the experiment.

To activate the schedule, press “Add to schedule”. This will also show you a summary of the number of scans and the time period for it.
To check the schedule, go to LIMS panel and click on the second icon from the top “Schedule”.

To remove the schedule actions press right click on the table and continue.

To check the status of the experiment, check the DLS measurements or the images that are being recorded. This is done in “LIMS” with a single click on the experiment file. At the bottom of the window, there are buttons to access DLS measurements and Plate Images.

10.4 Stopping an experiment

When an experiment is finished and the cover slip has to be removed, make sure at first that the “experimental schedule” in “PUMP” is stopped by pressing the “Stop” button. Then the cover slip can be removed.
In the case where DLS measurements images are still scheduled after the experiment finished, go to the “Schedule” and remove all remaining entries.

During the experiment, results of measurements can be monitored live following the parameter curves (including concentrations extrapolated from the weight record), as well as DLS heat map and size distribution plot indicating the evolution of particle populations in the drop (**Figure 10-8**).

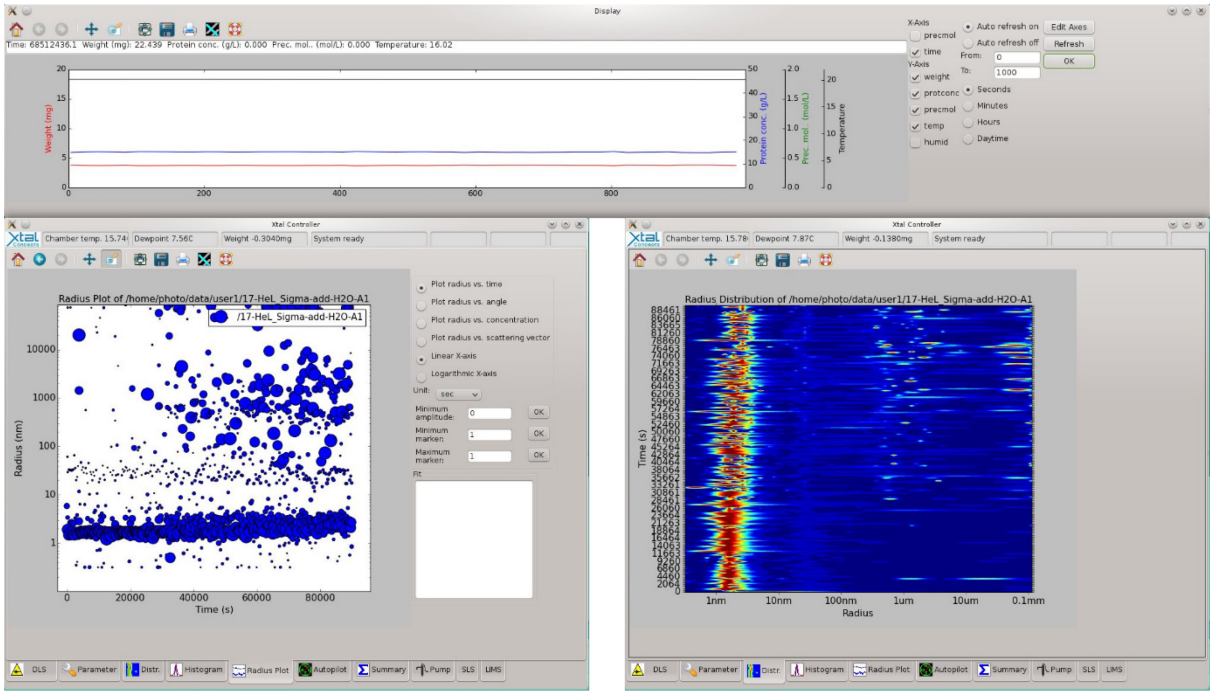

Figure 10-8 : Monitoring drop evolution through parameter curves (top), particle radius plot (bottom left) and heat map (bottom right). Curves are presented with different colors: red for the weight, blue for the protein concentration, green for precipitant (crystallant) solution and black for the temperature. X and Y-axes of the radius plot represents the time (in s) and the radius (in nm), respectively. Sizes of the dots are proportional to the scattering signal intensity. In the heat map, the axes are exchanged: X-axis corresponds to the radius and Y-axis to the time. Intensities of measurements are illustrated by colors from blue to red.

11 Results

Different types of experiments were performed with the Xtal Controller on various protein targets. A selection is presented in this chapter, illustrating what can be performed with the instrument.

11.1 Presentation of a precipitation case

Before interpreting crystallization events with the help of the DLS, a precipitation case with it characteristic pattern is presented (**Figure 11-1**). In this case, precipitation was induced on purpose by a rapid and concomitant increase of the *Pha*CCA enzyme and crystallizing agent (100 mM sodium acetate, 1 M di-ammonium hydrogen phosphate, pH 4.5, as described in chapter III) concentrations. Precipitation is characterized in the DLS profile by a burst in the particle size (radius) and the complete disappearance of the monomeric fraction with a radius size below 10 nm. Accordingly, a strong dark precipitate can be observed with the camera (right picture).

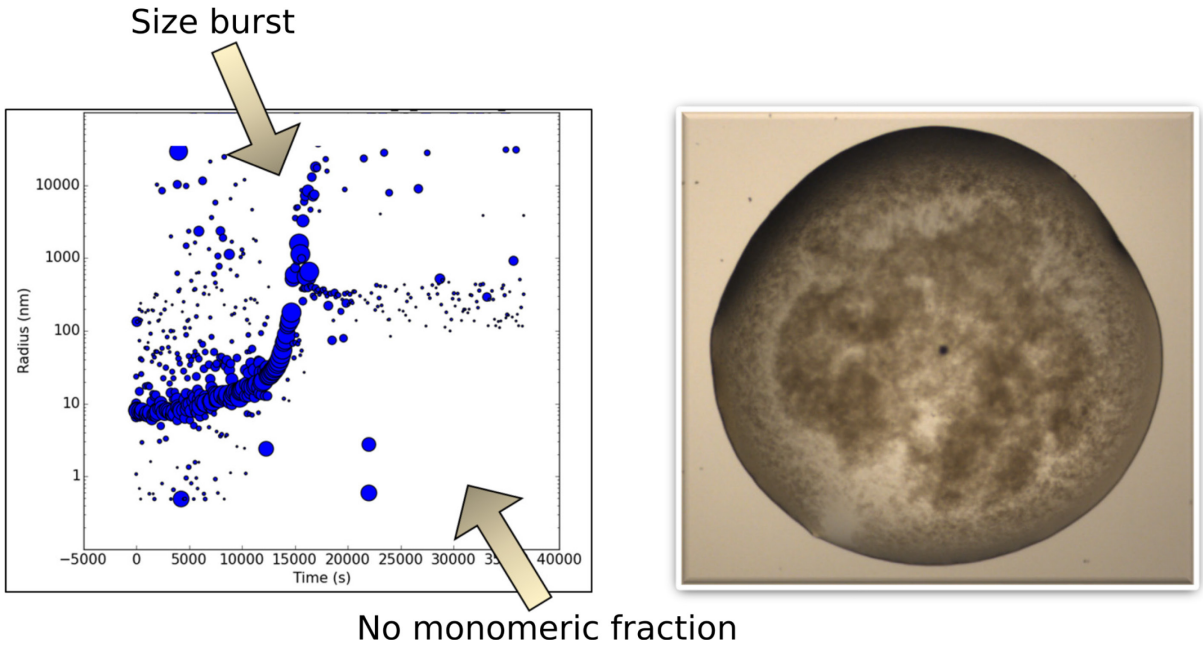

11.2 Crystallization of the CCA-adding enzyme from *P. halocryophilus*

A controlled crystallization protocol of the *Pha*CCA enzyme was established in the Xtal Controller, followed by crystals analysis at the ESRF. The same crystallizing agent as presented in section 11.1 was used and the protein was at 5 mg/mL at the beginning of the experiment. A complete experimental procedure with results is illustrated in **Figure 11-2** from schedule, curve profiles, DLS plots, drop pictures, to diffraction patterns and resulting electron density map.

The DLS profile is very different compared to the one in the precipitation case: the monomeric fraction remains present and a population between 1000 and 2000 nm appears and remains stable. According to its size, this population corresponds to micro- or nano-crystals. To define them more precisely, an electron microscopy analysis of this population should be performed. Interestingly, this population is observed by DLS immediately after the start of crystallizing agent injection, but crystals become visible at the edge of the droplet after more than 24 hours and further addition of crystallizing agent. After completing the Xtal Controller experiment, the coverslip was transferred to a Limbro plate over a reservoir containing the same salt concentrations as the droplet to maintain it on an equilibrium. After five months only a slight increase in the crystals size was observed. One of these crystals was prepared for diffraction and cryocooled at 100 K as presented in chapter III. Diffraction at the ESRF (Grenoble) on beamline BM30A allowed collection of a complete dataset at 1.85 Å (illustrated in the bottom panel).

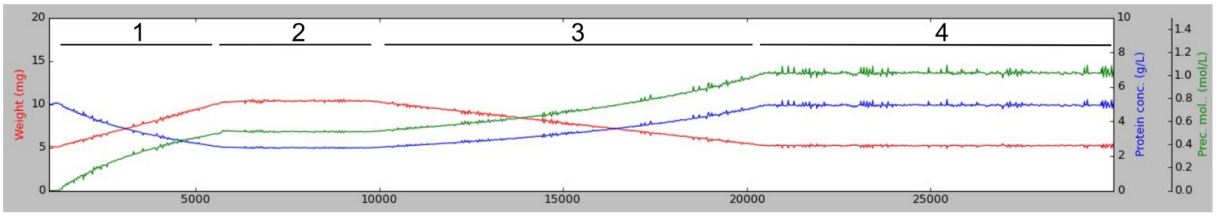

Live monitoring by DLS and optical microscopy

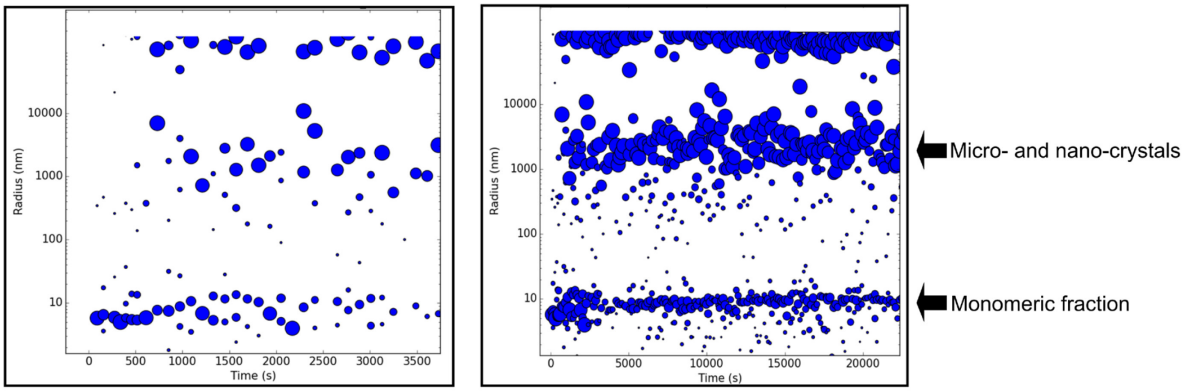

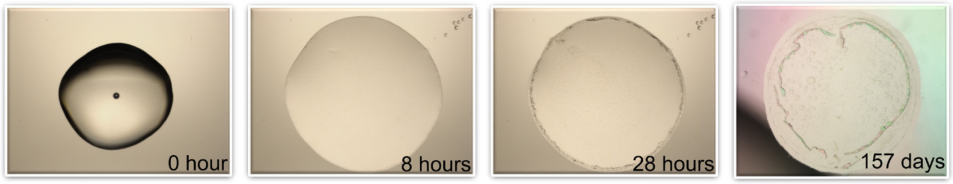

X-ray diffraction

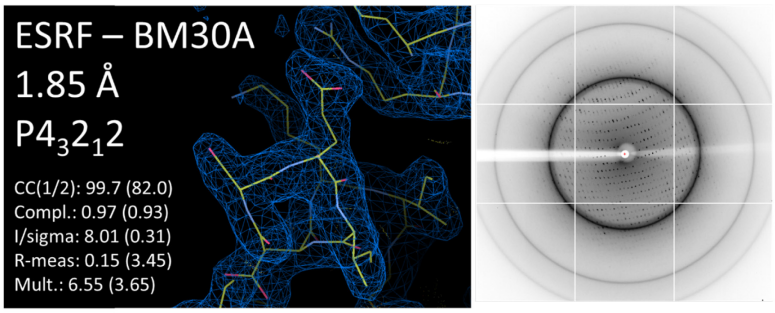

11.3 Tracking of the effect of Tb-Xo4 on nucleation and crystal growth

I used the instrument to test the effect of Tb-Xo4 nucleant provided by our collaborators (Eric Girard and Sylvain Engilberge, CEA Grenoble) on nucleation and crystal growth. In this section, a selection of experiments carried out on several target proteins are presented.

11.3.1 Hen egg white lysozyme in water

Our collaborators published a study showing a spectacular effect of Tb-Xo4 on the phase diagram of commercial hen egg white lysozyme crystallized in the presence of NaCl (Engilberge *et al*., 2017). In addition, they also observed that lysozyme can be crystallized in water containing 10 mM Tb-Xo4 without any other salt (unpublished results). In this context, we decided to follow the effect of the addition of Tb-Xo4 to lysozyme only solubilized in water. For this, we developed a specific experimental protocol. It consists in a manual addition of 1 µL of 100 mM Tb-Xo4 to a 10 µL lysozyme droplet (by the means of an Hamilton syringe) to a final concentration of 10 mM of nucleating agent, while the Xtal Controller is running in constant mode. This mode implies that the instrument will keep the weight stable to a beforehand defined value by shooting water to compensate for evaporation. The addition of 1 µL to the droplet induces a punctual and sharp weight increase. The instrument will then stop shooting water until evaporation brings the weight back to the target value. Tb-Xo4 was added after an incubation time was introduced in the protocol to check the stability of lysozyme in water. To assess if manual addition of solution was not disturbing the solution and inducing some pattern in the droplets, we performed a control experiment by adding 1 µL water. An experiment and the corresponding control following this protocol are presented **Figure 11-3**.

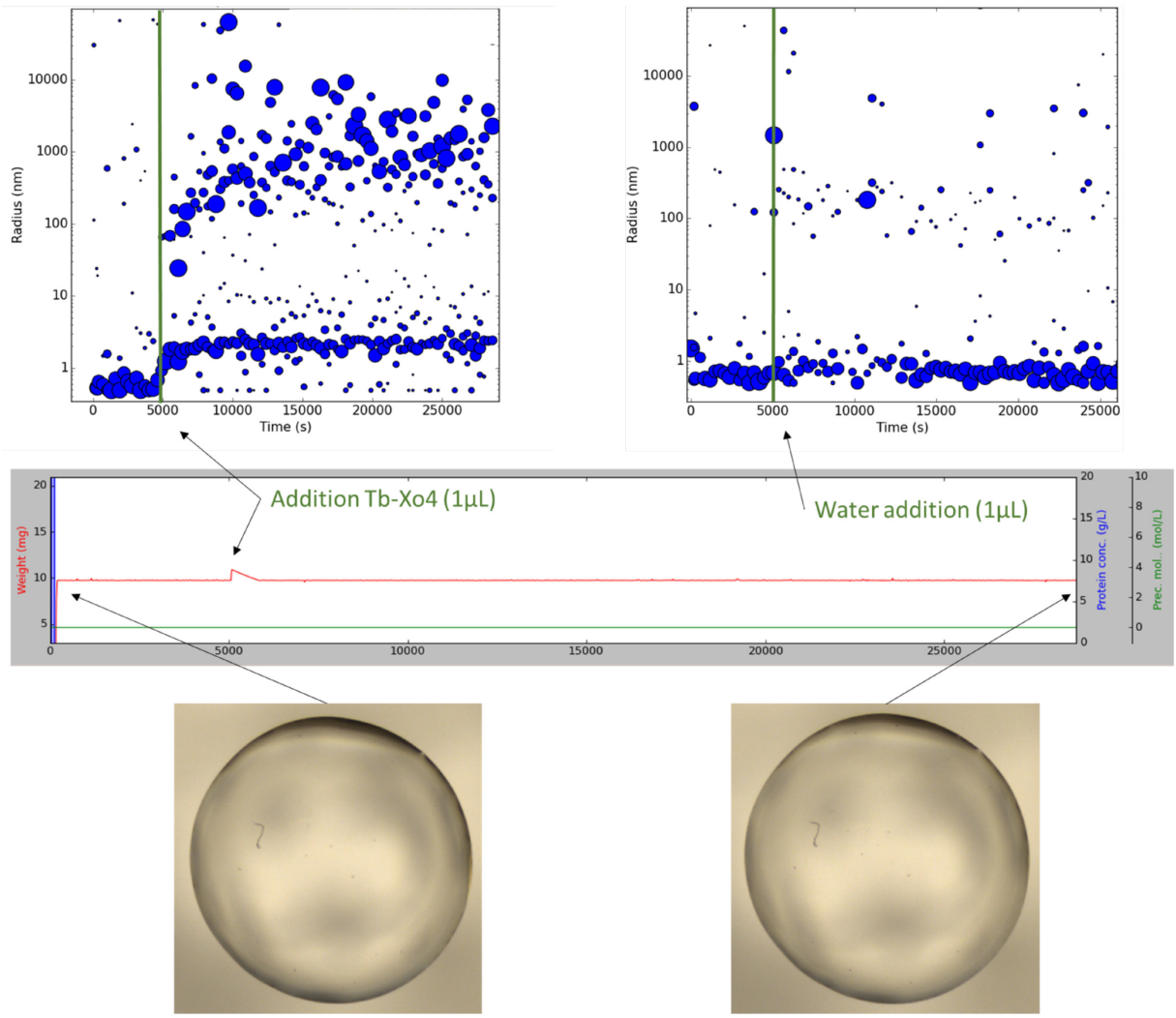

Figure 11-3 : Monitoring Tb-Xo4 addition to a lysozyme solution in water and corresponding control experiment with water addition. Top panels present the DLS profiles, green bars indicating manual addition of Tb-Xo4 or water. Bottom panels present pictures from the droplet taken at the beginning and the end of the experiment.

Experiments were performed with lysozyme in water at 20 mg/mL and no crystallizing agent. Addition of Tb-Xo4 to the droplet is easily observable on the weight curve as well as the time needed for the system to come back to its initial weight. In the DLS profile, addition of Tb-Xo4 is also clearly visible as it is characterized by two responses: increase of the monomeric population size (such as in Schubert *et al.*, 2017) and appearance of particles with a size about 1000 nm. These effects are not induced in the control (top right panel). Interestingly, these particles are not yet visible

with the camera, the droplet remains clear even at the end of the experiment (bottom panels).

This study clearly presents a direct nucleation effect of the crystallophore Tb-Xo4 addition on lysozyme in water, without added buffer and crystallizing agent. To conclude this study, droplets should be analyzed before and after addition of Tb-Xo4 by electron microscopy to confirm the formation of nanocrystals.

11.3.2 Protease 1

A second protein model, protease 1 from *Pyrococcus horikhoshii*, was used to study the effect of Tb-Xo4 with the Xtal Controller. Our collaborators were able to crystallize this protein in 2.9 to 3.2 sodium malonate at pH 5 in the absence or presence of Tb-Xo4 (Engilberge *et al*., 2017 and unpublished results). For this model, the same experimental protocol as described in section 11.3.1 was applied, with addition of 3.4 M sodium malonate pH 5 as crystallizing agent after an incubation period, as addition of Tb-Xo4 alone was not inducing a visible effect. Protease 1 was used at 7.6 mg/mL in Tris-HCl pH 8. A control experiment with water is presented **Figure 11-4**, and that with Tb-Xo4 **Figure 11-5**.

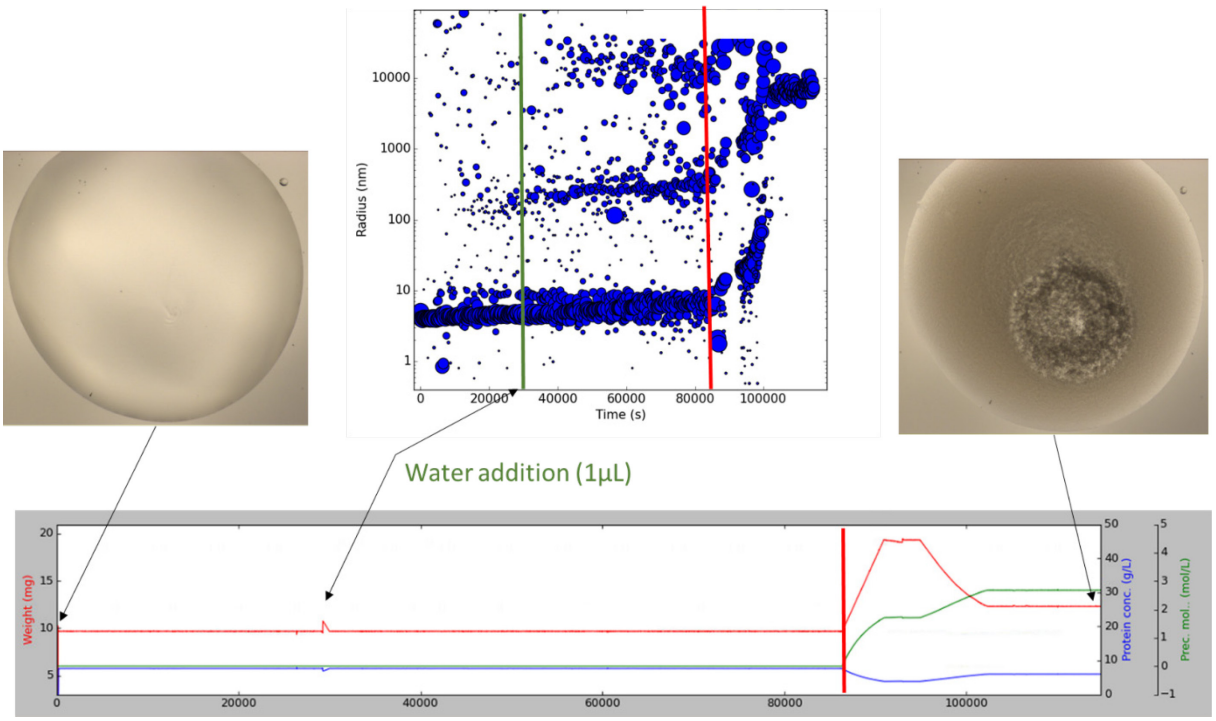
Radius (nm)
Time (s)
Water addition (1µL)
Weight (mg)
Protein conc. (g/L)
Prec. mol.. (mol/L)

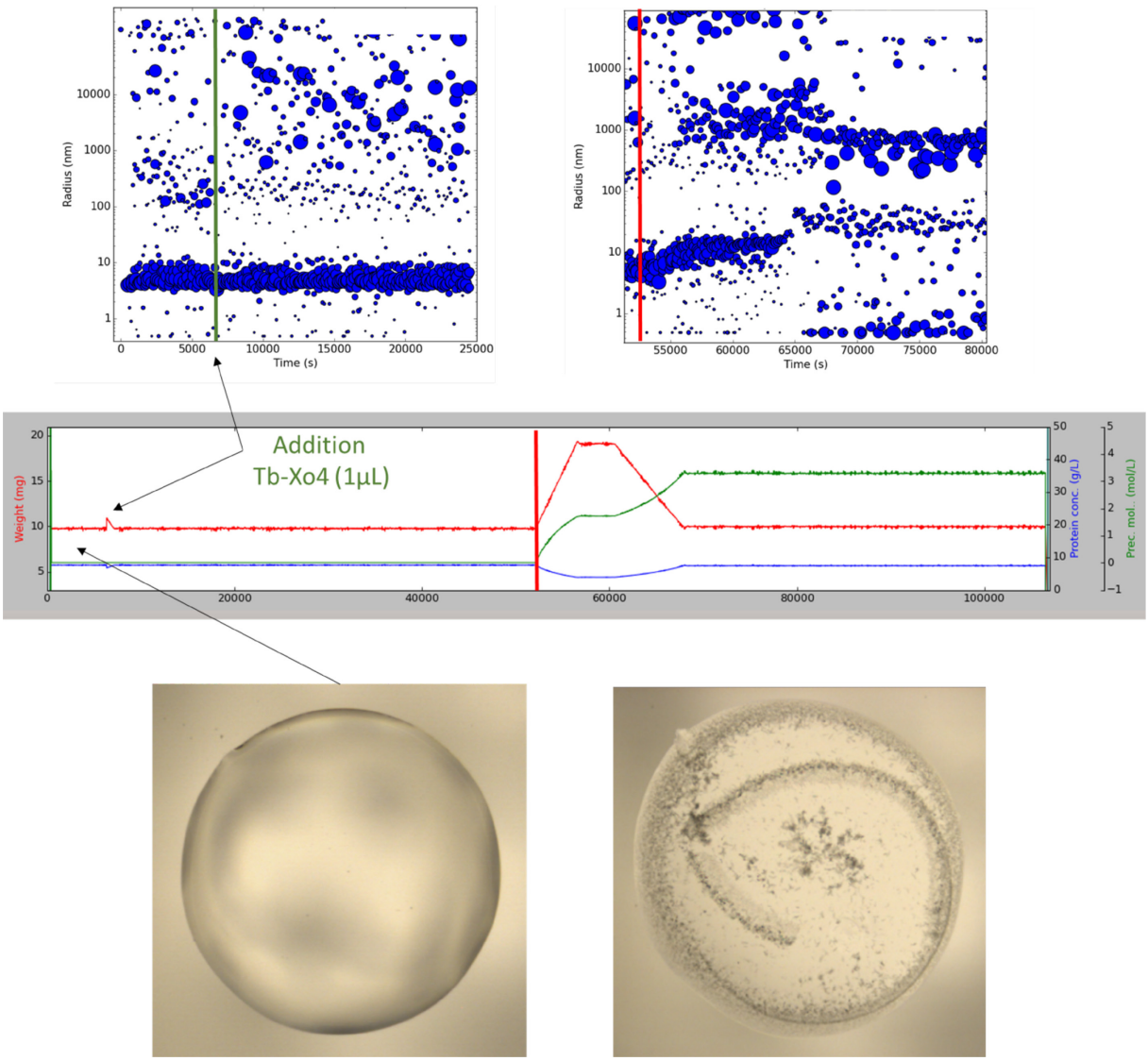

The reaction of protease 1 to the addition of Tb-Xo4 seems different compared to lysozyme. No direct and strong effect was observed immediately after its addition, but a secondary addition of crystallizing agent was necessary after an incubation time, to detect the influence of the nucleant. In the control experiment without Tb-Xo4 with water addition, a precipitation like effect (as described in section 11.1) is observed just after addition of the crystallizing agent and the droplet was precipitated at the end of the experiment. This is probably due to a destabilization of the protein by too rapid

addition of sodium malonate. In the presence of Tb-Xo4, the behavior is different. As described in section 11.2, the monomeric fraction increased in size and a stable population around 1000 nm appeared. This led to crystals as illustrated in the bottom panel of **Figure 11-5**.

In the case of protease 1, addition of Tb-Xo4 seems to stabilize a defined population after addition of sodium malonate and avoids a disordered association leading to precipitation, but does not present a direct effect after addition. As for the lysozyme study, the visualization of the particles with electron microscopy could be relevant to characterize their nature. Further experiments could be performed:

1. Use the protein at a lower concentration to accentuate the difference between situations with and without Tb-Xo4.
2. In the opposite direction, increase protein concentration to test if there is a threshold beyond which a direct effect of Tb-Xo4 can be observed.
3. Our collaborators identified several binding sites of Tb-Xo4 on protease 1 and designed mutants of interacting residues (unpublished results), which could be interesting to confirm the effect of Tb-Xo4.
4. This system seems very sensible to crystallizing agent addition, so it is an interesting model for kinetic experiments, where sodium malonate could be added very slowly to the droplet to detect a potential induction threshold.

In conclusion, this series of experiments allowed us to get insights into early nucleation and growth events for different systems. It illustrates the power of using *in situ* DLS for monitoring in real time the evolution of particle populations in a crystallization drop. In addition, it was extremely useful to finalize the implementation of the technology in the laboratory, test the possibilities offered by the Xtal Controller and develop new protocols.

V. Drug design targeting aspartyl-tRNA synthetases

Ce dernier chapitre est axé sur l'étude de deux familles d'inhibiteurs de l'AspRS. La communauté scientifique a constamment besoin d'innovation dans le développement d'antibiotiques pour faire face à l'apparition rapide de résistances bactériennes par évolution et transfert horizontal de gènes, tel que présenté à la section 3.5. Dans ce contexte, les méthodes de conception de nouvelles molécules présentent une importance stratégique de santé publique. Les aaRS étant des enzymes essentielles, l'inhibition de l'une d'entre elles entraine l'arrêt de la synthèse des protéines, ce qui a un effet létal. Ces enzymes sont donc des cibles intéressantes pour le développement d'antibiotiques dans la lutte contre les bactéries et autres microorganismes.

La première famille est composée de peptides macrocycliques contenant des acides aminés non conventionnels. Le design de ces peptides repose sur le système RaPID (Random nonstandard Peptide Integrated Discovery). Six peptides ont été sélectionné par cette procédure dans le but de tester leur effet inhibiteur ainsi que leur potentiel pouvoir d'agent co-cristallisant de l'AspRS de *Pseudomonas aeruginosa*. La seconde famille est un inhibiteur naturel, la microcine C, un analogue de l'intermédiaire réactionnel naturel qu'est l'aspartyl adenylate, découvert dans la famille des Enterobacteriaceae et qui empêche la croissance d'organismes concurrents.

12 Macrocyclic peptides against the AspRS from *Pseudomonas aeruginosa*

12.1 Introduction to the RaPID system

The scientific community is in constant need of innovation to combat bacterial resistance development through evolution and gene transfer, as presented in section 3.5. In this context, methods for design of new molecules, drugs, are gaining importance. Inhibition of aaRSs causes protein synthesis to stop, which has a lethal effect. These enzymes are therefore attracting targets for antibiotics development in the fight against bacteria and other microorganisms.

One method to find new active molecules is the Random non-standard Peptide Integrated Discovery (RaPID) developed by the team of Prof. Hiroaki Suga in Tokyo, Japan (**Figure 12-1**, reviewed recently by Passioura & Suga, 2017). The aim of this process is to find, within partially randomized libraries, macrocyclic peptides containing unconventional amino acids that are able to specifically bind a target. These peptides are then tested for their potential inhibition capacities on the same target.

The central element of this procedure is the Flexible *in vitro* Translation (FIT) system and genetic code reprogramming (Goto et al. 2011). This translation system is based on the fact that the genetic code not only relies on the specificity codon:anticodon carried out by the mRNA:tRNA recognition, but also on the specific aminoacylation of tRNAs with their cognate amino acid by the corresponding aminoacyl-tRNA synthetase. Thus, one can reprogram the genetic code without interfering with the codon:anticodon recognition by changing the amino acid carried by tRNAs. This presents the advantage, over modification of the codon:anticodon recognition, that the reprogramming is not limited to STOP or rare codons. This was made easier in 2001 by the invention of a first ribozyme prototype, called flexizyme (Fx), able to aminoacylate tRNAs (Saito and Suga 2001). Hiroaki Suga and his team later enhanced the system and developed a set of three flexizymes, called dFx, eFx and aFx virtually able to perform aminoacylation with any unconventional amino acid (Murakami et al. 2006; Niwa et al. 2009). The FIT is a reconstituted bacterial translation

system containing all factors necessary for translation including all aminoacyl-tRNA synthetases, excepted the one associated to the reprogramed tRNA. This specific tRNA will be associated to a flexizyme for aminoacylation.

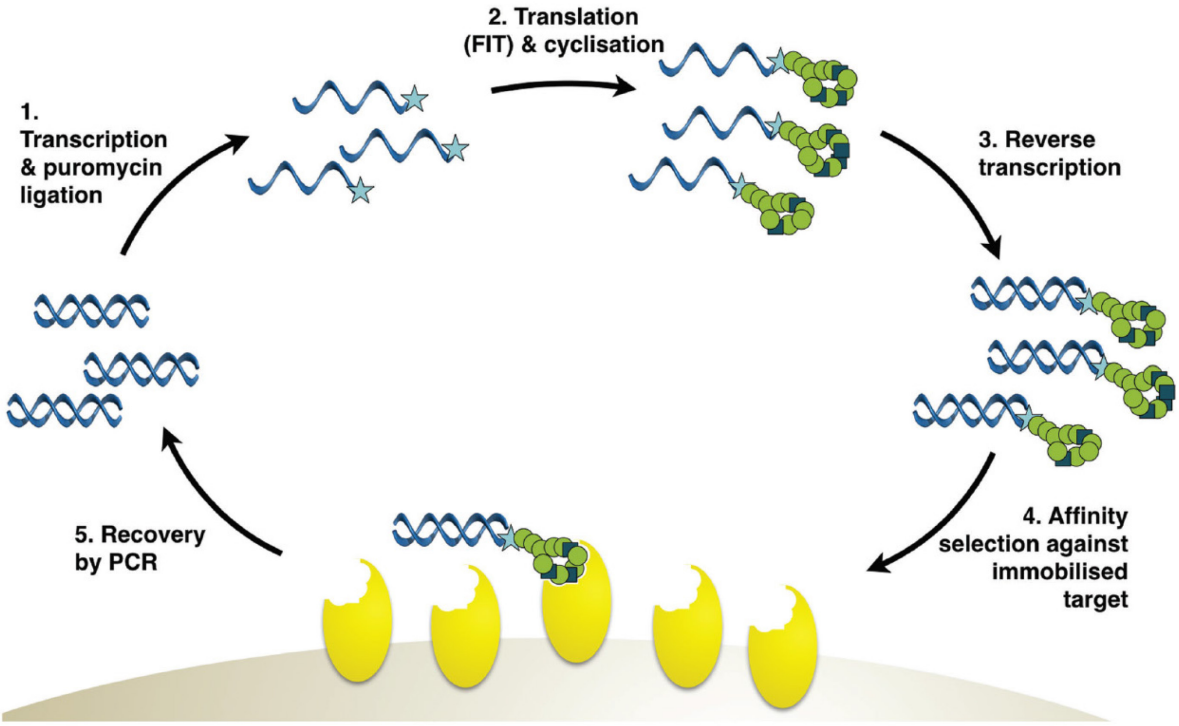

As illustrated in **Figure 12-1**, the first step of the RaPID selection process consists in the transcription of a partially randomized mRNA library and attachment of a puromycin linker to their 3'-end. These mRNA are then transcribed in a FIT system (allowing incorporation of unconventional amino acids) and peptides are cyclized (step 2). The puromycin linker allows the mRNA to be covalently attached to the peptide chain and causes the end of synthesis by the ribosome. Following comes a reverse transcription (step 3) and the affinity selection of peptides against immobilized targets (step 4). Finally the DNA sequence of the selected peptides are recovered by PCR amplification (step 5). This cycle is repeated several times until specificity is reached and enough enrichment is obtained to sequence the DNA. Macrocyclic peptides were chosen as potential drugs because they present several advantages. They have the potential to combine characteristics of small molecules (rapid degradation in the organism and relatively easy synthesis) and of bigger biomolecules, as antibodies and

hormones (specificity and interactions with macromolecules). Example of success stories of the use of the RaPID system concern the inhibitors of the Akt2 human kinase (Hayashi et al. 2012) or the inhibitors and cocrystallization ligands of a MATE family transporter (Hipolito et al. 2013; Tanaka et al. 2013). We decided to apply the RaPID selection to find binders and potential inhibitors of the aspartyl-tRNA synthetase (AspRS) of *P. aeruginosa*, a pathogen rapidly developing resistances.

12.2 Macrocyclic peptides

P. aeruginosa possesses just one non-discriminating aspartyl-tRNA synthetase, able to aminoacylate $tRNA^{Asp}$ and $tRNA^{Asn}$ (Bernard et al. 2006). The latter is loaded with L-Asp which is then converted in L-Asn by an amidotransferase to compensate for the absence of AsnRS in the bacterium.

The protein batch used to perform RaPID selection was purified by the team of Prof. Jacques Lapointe in Québec (Canada). The selection process was performed during my internship in the lab of Hiroaki Suga (Tokyo, Japan) in summer 2014, under the supervision of Toby Passioura. Toby finalized the last selection round, purified the peptides, performed surface plasmon resonance (SPR) analysis and sent them to Strasbourg for inhibition and cocrystallization assays. For all further assays, the protein was produced and purified in our team. I established the purification protocol, performed cocrystallization assays and first aminoacylation tests to determine potential inhibition and the reaction conditions. Complementary inhibition analyses were realized in collaboration with Joëlle Rhudinger-Thirion from our team.

12.2.1 Synthesis

The library was designed with the following characteristics: a first AUG codon reprogrammed with an initiator tRNA *N*-(2-chloroacetyl)-(L or D)-tyrosine (L or D amino acid according to the name of the peptide), followed by a random region of 7 to 15 NNK codons (where N represents any of the four bases and K represents either U or G) and terminated by a sequence coding the CGSGSGS peptide. Results of the selection are listed in **Table 12-1**.

Table 12-1 : Listing of selected peptides, with their name, sequence and mass over charge (m/z) for mass spectrometry identification. In the sequences, highlighted in yellow are the randomized sequences, in blue the terminal non-variable sequences and in green the unconventional amino acids.

Name	Sequence	m/z
D2	YQRSTRLLBYWCGSGSGS	1750.00
D4	YKVWSLIRRRLVVCGSGSGS	1830.05
L1	YWIAWLASHRLLIIHNCGSGSGS	2358.17
L2	YKVWSLIRRRLVVCGSGSGS	1830.05
L3	YLVVBBTPBHFTVSRKCGSGSGS	2148.11
L4	YBFYLVQSWKLLFLSCGSGSGS	2172.08

The first Y coding for *N*-(2-chloroacetyl)-(L or D)-tyrosine and the first cysteine of the non-variable sequence at the 3'-end are used for the macrocyclization reaction and the glycine-serine triple repeat is necessary for binding of puromycin (highlighted in blue in **Table 12-1**). Amino acid B corresponds to the unconventional amino acid biphenylalanine, encoded by the CAU codon (highlighted in green). Peptides were selected against the *Pa*-AspRS enzyme after biotinylation and binding on metal beads carrying streptavidin, following the procedure established in Suga's team and described in several articles, such as Hayashi *et al.*, 2012, Hipolito *et al.*, 2013 and in section 12.1.

After selection, SPR analysis with the *Pa*-AspRS and peptides was carried out to determine their binding affinity (except L1 which was unsuccessful due to its probable binding to the matrix). Results are presented in **Figure 12-2**.

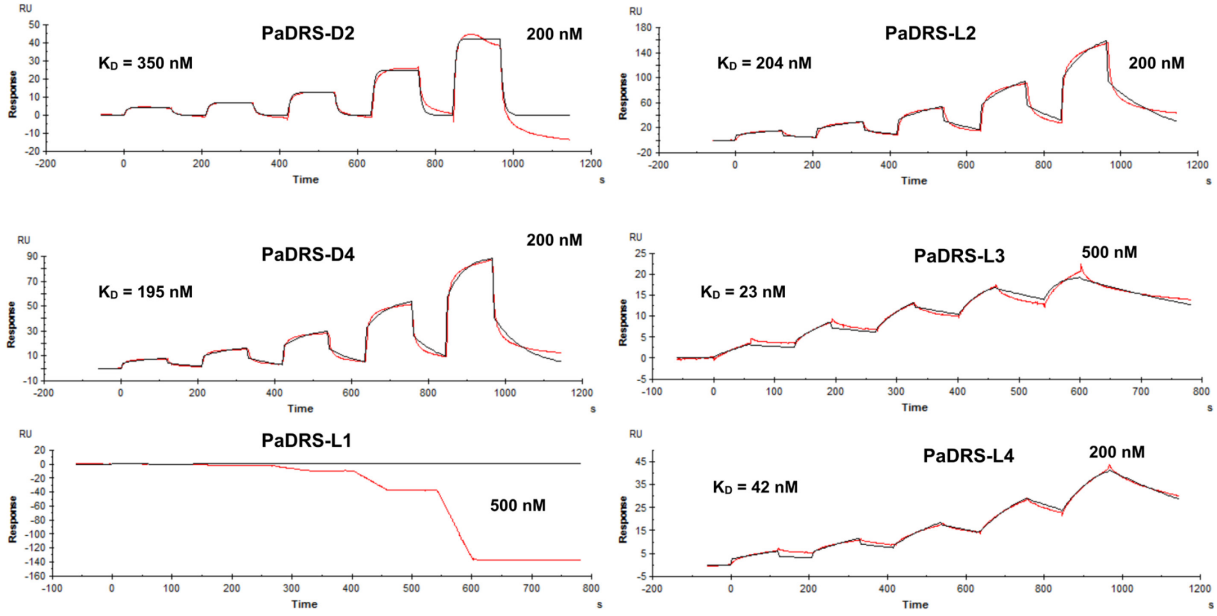

For the five peptides tested, the K_D value ranges from 23 to 350 nM, with L3 exhibiting the best affinity.

12.2.2 Inhibition assays

To determine a potential inhibitory effect of the selected macrocyclic peptides towards *Pa*-AspRS enzymatic activity, aminoacylation assays in the absence and in the presence of the peptides were performed following the procedure schematically described in **Figure 12-3** (for more details refer to Bonnefond *et al.*, 2005).

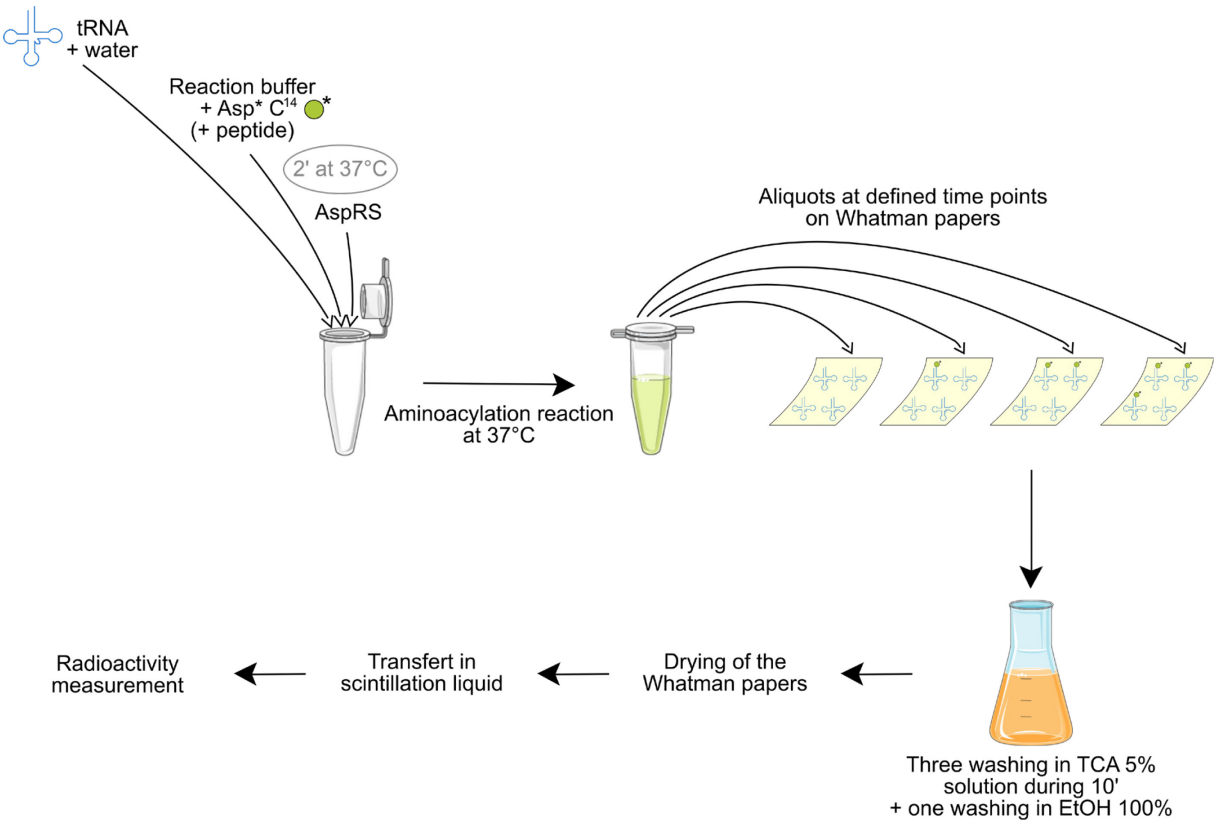

The following molecules were used for aminoacylation assays: AspRS from *Pseudomonas aeruginosa* (*Pa*-AspRS), *Escherichia coli* (*Ec*-AspRS), *Homo sapiens* (*Hs*-AspRS) and $tRNA^{Asp}$ from *Escherichia coli* (*Ec*-$tRNA^{Asp}$) as well as transcripts from *Homo sapiens* (*Hs*-$tRNA^{Asp}$). Several couples AspRS:tRNA from different species were tested, with and without peptides. The first test was performed with the couple

Pa-AspRS:*Ec*-tRNA^{Asp} and all peptides. According to the results, the peptides showing an inhibitory effect were tested on the couples *Ec*-AspRS:*Ec*-tRNA^{Asp} and *Hs*-AspRS:*Hs*-tRNA^{Asp} to assess their specificity. During all aminoacylation tests, concentrations of every elements were kept constant except that of macrocyclic peptides. 1.2 µM tRNA, 1 µM AspRS and 32 µM Asp* C^{14} were used, peptides were varied from 0.4 to 40 µM. Results with the couple *Pa*-AspRS:*Ec*-tRNA^{Asp} are presented in **Figure 12-4**, with the other couples in **Figure 12-5**.

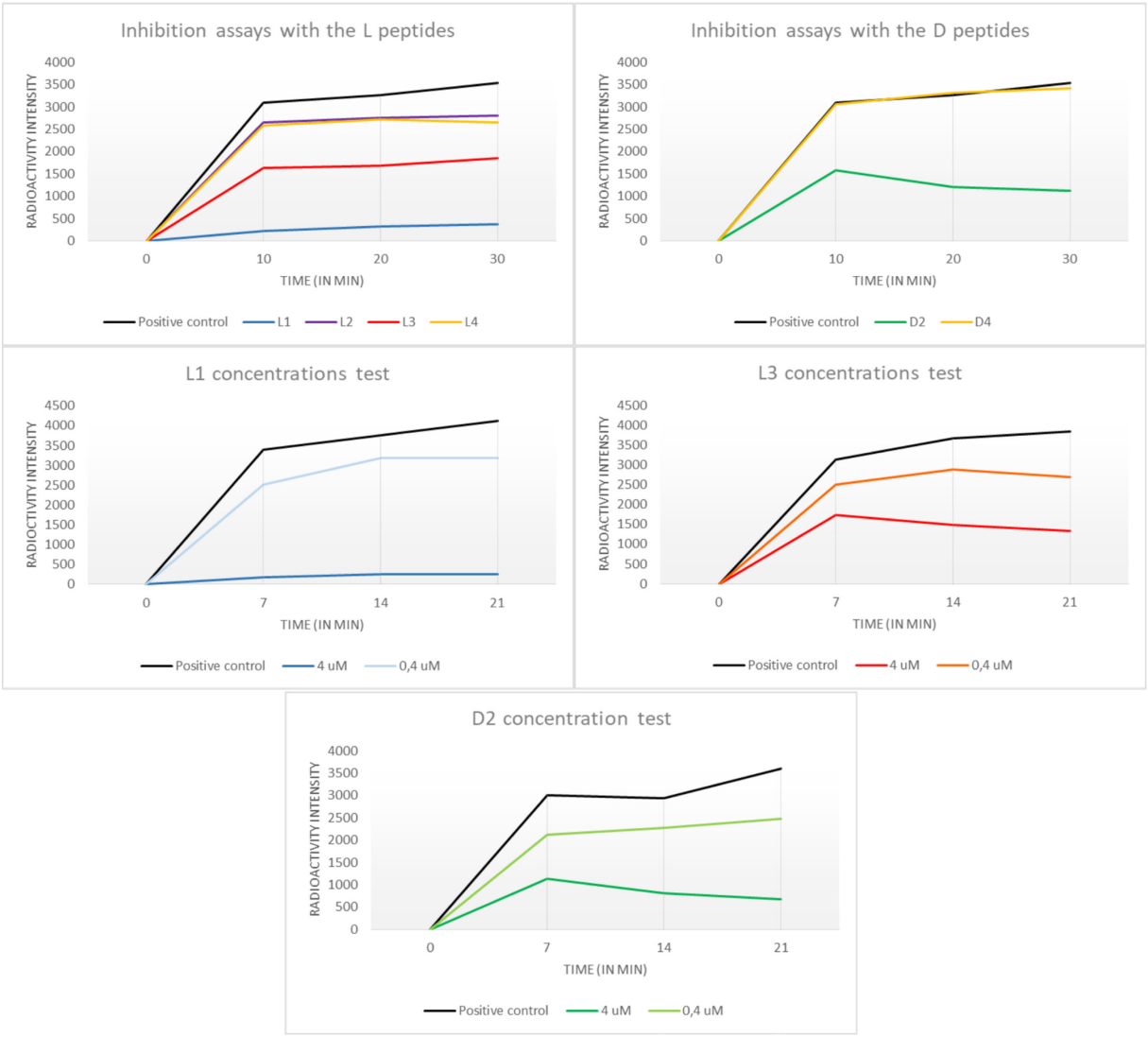

Figure 12-4 : Aminoacylation assays performed with the couple *Pa*-AspRS:*Ec*-tRNA^{Asp}. Aliquots of the reaction mixture were taken out after 0/10/20/30 or 0/7/14/21 minutes, as indicated in each plot. Peptides were at 40 µM in the top two assays and at indicated concentrations in others.

The first two plots present aminoacylation assays performed with all peptides at high concentration (40 µM). This allowed to determine that peptides L1, L3 and D2 present an interesting effect, they reduced *Pa*-AspRS activity to respectively 10, 50 and 40 percents. All further experiments were then performed with these peptides. The second step was to determine the minimal concentration at which they still showed an effect on aminoacylation efficiency (see three last plots from **Figure 12-4**). At 4 µM the same effect as at 40 µM was observed, but at 0.4 µM the effect was drastically reduced. Presented plots illustrate one assay but they were reproduced several times to determine K_M and k_{cat} values of the aminoacylation with and without peptides. Corresponding values are presented in **Table 12-2**.

Table 12-2 : Summary of inhibition assays with peptides L1, L3 and D2.

	Pa-AspRS:*Ec*-tRNA^{Asp}			
	Nativ	+ L1 at 2 µM	+ L3 at 2 µM	+ D2 at 2 µM
Mean K_M	0.3 µM	1.5 µM	1.6 µM	3.5 µM
Mean k_{cat}	30 min-1	22 min-1	32 min-1	33 min-1
Number of independent assays	2	6	3	4
Conclusion	/	Increased K_M (5x), slightly reduced k_{cat} (1.3x)	Increased K_M (>5x), unchanged k_{cat}	Increased K_M (>10x), unchanged k_{cat}
Inhibitor type	/	Competitive	Competitive	Competitive

For comparison, the KM value published for the couple *Ec*-AspRS:*Ec*-tRNA^{Asp} is 0.33 µM (Hasegawa et al. 1989), similar to what was measured for the couple *Pa*-AspRS:*Ec*-tRNA^{Asp} without peptide. All peptides induce an increase K_M value and a slight or no effect on the k_{cat}, indicating that they decrease the affinity of tRNA for AspRS but do not affect the speed of the reaction, which is characteristic of competitive inhibitors.

Following, assays were performed to assess peptides specificity by testing the *E.coli* and Human enzymes (**Figure 12-5**).

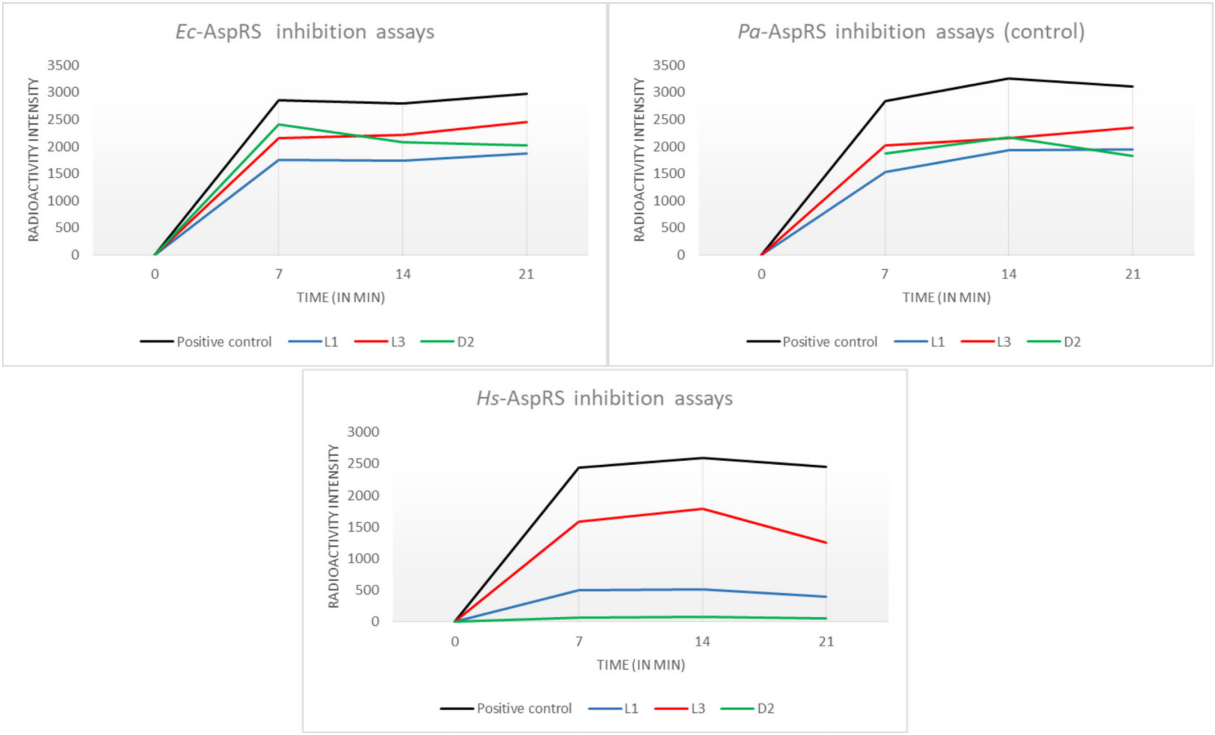

Figure 12-5 : Aminoacylation assays performed with the couples *Ec*-AspRS:*Ec*-tRNA^{Asp}, *Pa*-AspRS:*Ec*-tRNA^{Asp} and *Hs*-AspRS:*Hs*-tRNA^{Asp}. Aliquots of the reaction mixture were taken out after 0/7/14/21 minutes. Peptides were used at 0.8 µM for *Ec*-AspRS and *Pa*-AspRS assays, at 40 µM for *Hs*-AspRS.

For the first specificity assay, we wanted to test another bacterial AspRS and we choose the one from *E. coli*. *Ec*-AspRS and *Pa*-AspRS aminoacylation assays were performed once at the same time. The designed peptides also presented a slight effect on *Ec*-AspRS activity, thus we tried the human enzyme, which shares a lower sequence similarity with the *P. aeruginosa* enzyme. For the human enzyme, peptide concentration was increased to 40 µM, as for the first test with the *P. aeruginosa* enzyme. Results are presented in the bottom graph of **Figure 12-5** and show that the designed peptides are not specific, they also inhibit the human enzyme. Therefore, it is likely that their biding site is close, if not directly in the catalytic site (whose sequence has been conserved during evolution), which would explain both their competitive

nature and the fact that they hardly distinguish the three AspRSs. In an attempt to confirm this hypothesis, I tried to co-crystallize the peptides with AspRS.

12.2.3 Co-crystallization assays

In the literature, the macrocyclic peptides designed with the RaPID selection process were also shown to be good cocrystallization partners, allowing easier crystallization (Hipolito et al. 2013; Tanaka et al. 2013) through the conformational stabilization of their target. In this optic, several cocrystallization assays from *Pa*-AspRS with inhibitory peptides L1, L3 and D2 were performed using the commercial screens JCSG++ from Jena Bioscience and Index from Hampton Research. The *Pa*-AspRS was used at 11 mg/mL in a ratio 1:1 with the peptides. Drops were prepared by mixing 150 and 100 nL of enzyme:peptide and crystallant volumes respectively, over a reservoir containing 60 µL with the help of a Mosquito Crystal pipetting robot (TTP Labtech, UK). One unique crystal, in form of a sea urchin, was observed with the protein alone in JCSG++ condition F10 (0.5% w/v Jeffamine ED-2001, 100 mM HEPES-NaOH and 1.1 M sodium malonat at pH 7.0) and presented diffraction spots up to 8 Å, but I never succeeded to reproduce it and crystal amount was not enough to perform microseeding. Tb-Xo4 was also even used as nucleant in screening assays but without success.

13 Microcin C

13.1 Introduction to known AspRS inhibitors

Recently, several compounds targeting aaRSs of *P. aeruginosa* were discovered by screening of synthetic library, as BT_03F04 and BT_04B09 against the GluRS (Hu et al. 2015) or BT02A02 and BT02C05 against the AspRS (Corona et al. 2018). They are described as non-competitors inhibitors with respect of amino acids or tRNAs, exhibit specificity to the pathogen but a very moderate effect on *P. aeruginosa* cultures.

General competitive inhibitors of AspRS, such as non-hydrolysable substrates analogs, have also been described. **Figure 13-1** presents two of the most efficient inhibitors (Asp-AMS and Asp-ol-AMP) (Bernier et al. 2005), as well as the natural reaction intermediate, Asp-AMP and microcin C (McC) which is an inhibitor discovered in Enterobacteriaceae family. McC is produced by some strains to inhibit growth of surrounding competitors (Metlitskaya et al. 2006). In opposition to those presented before, these inhibitors are efficient on cultures but are both active on bacterial and human AspRSs.

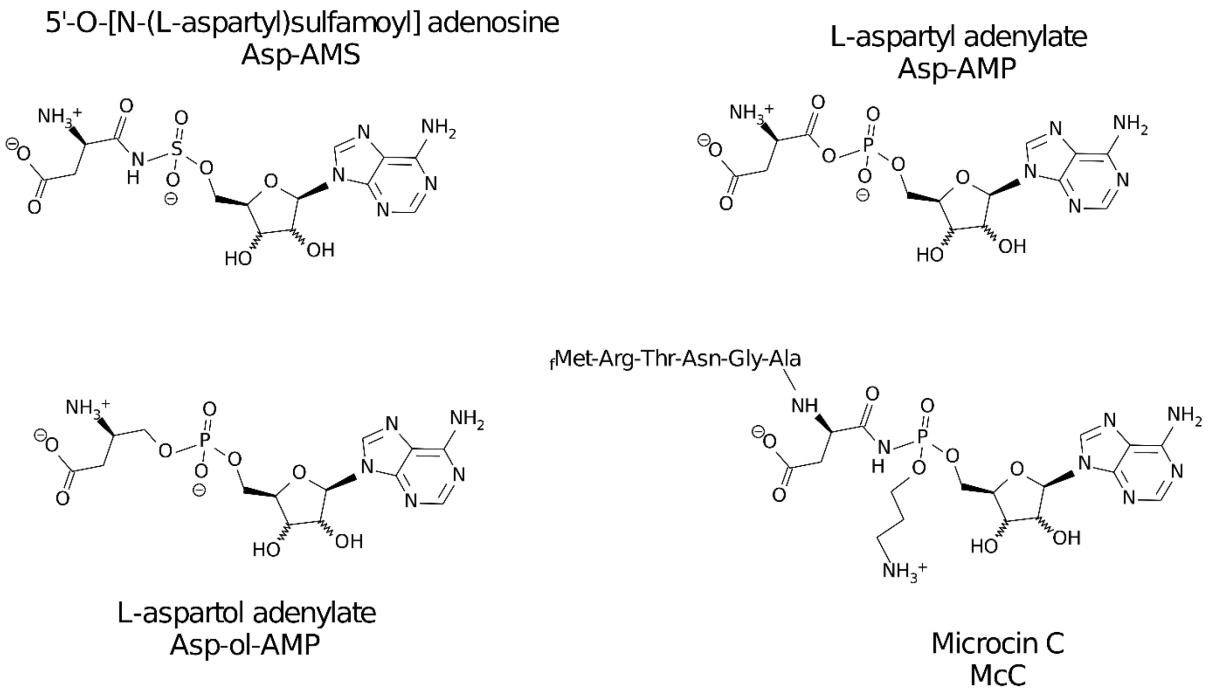

Figure 13-1 : Chemical drawing of L-aspartyl adenylate, the reaction intermediate of tRNA aspartylation, and three non-hydrolysable analogs: 5'-O-[N-(L-aspartyl)sulfamoyl] adenosine (Asp-AMS), L-aspartol adenylate (Asp-ol-AMP) and the natural antibiotics microcin C (McC) (adapted from Claude Sauter).

McC is very similar to Asp-AMP but possesses an amid instead of an acid anhydride linkage between the aspartyl and the AMP moities, which stabilizes the junction and make it non-hydrolysable. McC also has a peptide attached to the NH_2 function of aspartyl that allows it to penetrate target organisms through a membrane transporter. This peptide is cleaved after entry into sensitive cells by an aminopeptidase, allowing it to perform its activity as a non-hydrolyzable inhibitory analog (Severinov and Nair 2012). It has also an AMP part modified by a propylamine arm on the phosphate (Metlitskaya et al. 2009). The position of this arm and its function have never yet been precisely defined. This difference is the most notable with current synthetic AspRS inhibitors, Asp-AMS and Asp-ol-AMP. The mature form of McC without the small peptide is called McC*. McC has been further studied and modified, for example to allow inhibition of other synthetases, such as LeuRS and GluRS by changing the aspartate residue (Van De Vijver et al. 2009) or to modify cellular import as well as the entry process itself by altering the attached peptide sequence and length

(Bantysh et al. 2015). These inhibitors are not specific to bacteria and are therefore difficult to use as antibiotics as they may interact with enzymes in patients.

At the beginning of my thesis, several datasets from *Ec*-AspRS soaked with McC* were already available. The McC* was provided by our collaborators from Paris (Prof. Sylvie Rebuffat, Musée National d'Histoire Naturelle). I performed data treatment and the best one is presented in section 13.2. In section 13.3, assays to collect data from the AspRS from *Thermus thermophilus* (*Tt*-AspRS) in complex with McC* are described.

13.2 McC* in *Ec*-AspRS

Ec-AspRS crystals were grown by vapor diffusion in 16% (m/v) PEG 6000, 1.6 M NaCl and 100 mM Bis-Tris pH 7.0 with the protein at 20 mg/mL. The table summarizing statistics is presented below (**Table 13-1**).

In this crystal form of the *Ec*-AspRS, three monomers are present in the asymmetric unit. McC* was only visible in one catalytic site when soaked 15 min in a drop with 2.5 mM McC*. Its position is well defined in the density map excepted for the propylamine arm. Still, it was positioned on one side of the phosphate due to steric clashes on the other side (**Figure 13-2**) but even the first carbon of the arm is not visible in the density. Two reasons could explain this fact:

i) this arm is highly flexible and not involved in stable interactions, even in the catalytic pocket.

ii) this arm was partially or totally degraded and is not present in the crystal. Following our results, our collaborators tested the molecule by mass spectrometry and concluded that their purified solution of McC* is composed of a mixture, with and without the propylamine arm. So we cannot conclude about this arm with the data we possess in *Ec*-AspRS.

Table 13-1 : Data collection and refinement statistics

	Ec-AspRS soaked 15 min with 2.5 mM McC*
X-ray beamline	SLS - PXIII
Wavelength (Å)	1.000
Temperature (K)	100
Detector	Pilatus 2M
Crystal-detector distance (mm)	300
Oscillation (° / s)	0.3 / 0.5
No. of images	2400
Space group	C2
a, b, *c* (Å)	118, 162, 132
α, β, γ (°)	90, 110, 90
Mosaicity (°)	0.13
Resolution range (Å)	30 – 2.24 (2.38 - 2.34)
Total No. of reflections	1467900 (207231)
No. of unique reflections	109063 (16710)
Completeness (%)	98.2 (90.6)
Redundancy	13.5 (12.4)
$\langle I/\sigma(I)\rangle$	30.6 (3.5)
*R*meas (%)	6.5 (81.3)
CC1/2 (%)	100 (87.6)
Overall *B* factor from Wilson plot (Å 2)	51.4
No. of reflections, working set / test set	103604 / 5451
Final Rcryst (%) / R_{free} (%)	18.06 / 22.76
No. of non-H atoms	14621
R.m.s. deviations	
Bonds (Å)	0.006
Angles (°)	0.935
Ramachandran plot	
Most favoured (%)	96.03
Allowed (%)	3.57
Rotamer outliers (%)	2.31

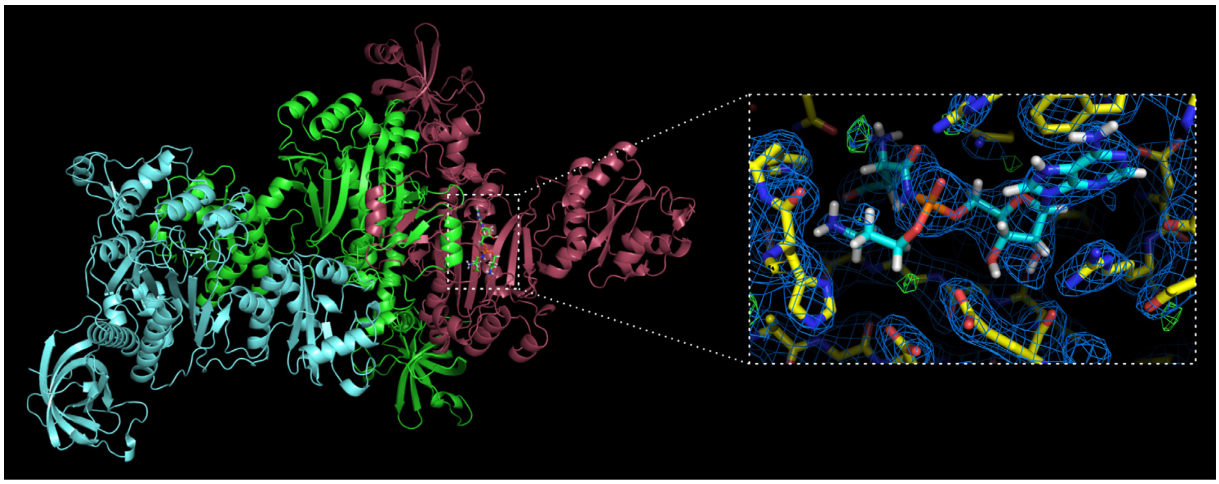

13.3 Crystallization of *Tt*-AspRS

Due to the difficulty to produce good diffracting *Ec*-AspRS crystals, the model system to study McC* was switched to *Thermus thermophilus* AspRS (*Tt*-AspRS). *Thermus* possesses two distinct AspRSs, we choose to use AspRS-1 which is very similar to the *E. coli* enzyme (Becker et al. 1997; Ng et al. 2002). The expression and purification protocol was adapted from Poterszman *et al.*, 1993 and Becker *et al.*, 1997. Briefly, gene expression was induced with IPTG at 37°C in *Escherichia coli* (Rosetta 2). Thanks to the thermostability of the *Thermus* enzyme, a first purification step could be performed by flocculating *E. coli* proteins by heating the cell extract 30 min at 70°C. This step was followed by ion-exchanged chromatography (DEAE) and size-exclusion chromatography (SEC), using Sephacel (BioRad) and Superdex 200 columns (GE Healthcare), respectively. The protein was finally concentrated using Amicon 50K (MILLIPORE) to the desired concentration and stored in 50 mM Tris-HCl, pH 7.5, 1 mM DTT and 1 mM EDTA.

Several crystallization assays were performed with the purified enzyme, screening with the commercial kits JCSG++ from Jena Bioscience and Index from Hampton Research and optimization with already known conditions in sodium formate or ammonium sulfate and PEG 8000 (Zhu et al. 2001). As illustrated in **Figure 13-3**, crystals were obtained in absence and presence of agarose gel, but the maximum diffraction limit observed was only 2.8 Å, while we expected a resolution beyond 2 Å. Hence, another step of crystal quality optimization will be necessary before concluding this structural study of the binding of McC* and the orientation of its propylamine arm in AspRS catalytic site.

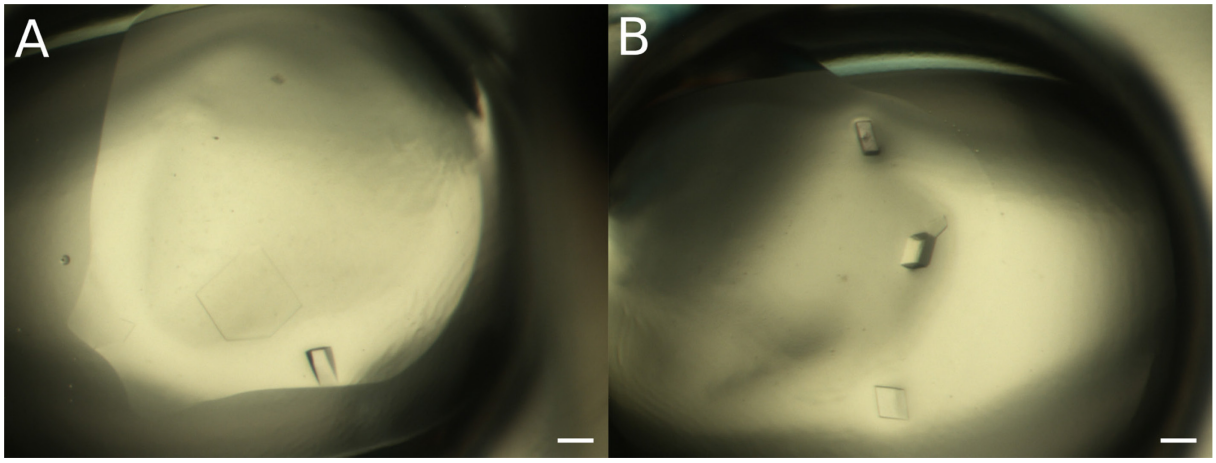

VI. Conclusions and perspectives

This thesis entitled “Application of new crystallization approaches and serial crystallography to the structural study of enzyme/tRNA complexes” was focused on two aspects, the first oriented towards crystallography and crystallogenesis and the second towards biologically relevant enzyme/tRNA complexes. The ChipX3 microfluidic device (developed by Claude Sauter) and the Xtal Controller 900 (developed by Xtal Concept, Hamburg, Germany) were used to assess their efficiency in several cases. Other methods that were available more broadly, such as trace fluorescent labeling (TFL, developed by Marc Pusey) and microseed matrix screening (MMS, developed by Allan D’Arcy) and the use of the crystallophore Tb-Xo4 (developed by Eric Girard and Sylvain Engilberge) were implemented in the standard screening process of our team. All these devices, instruments and methods were used to study new macromolecules and ligands, including among others the CCA-adding enzyme from the psychrophilic bacterium *P. halocryophilus* (in collaboration with Prof. Mario Mörl), as well as several aspartyl-tRNA synthetases interacting with two family of inhibitors, the natural inhibitor microcin C (in collaboration with Prof. Sylvie Rebuffat) and macrocyclic peptides containing unconventional amino acids (in collaboration with Prof. Hiroaki Suga).

14 Biological aspects

Aminoacyl-tRNA synthetases

Aminoacyl-tRNA synthetases are essential enzymes involved in the first stages of protein synthesis. They are responsible for the transfer of amino acids, in the form of amino acid adenylate, to the 3'end of their cognate tRNA. My work led to the development of a purification protocol for *Thermus thermophilus* and *Pseudomonas aeruginosa* AspRSs, to ensure their quality and quantity, for crystallization assays and biochemical studies. Due to their highly essential and specific activity, these enzymes are potential good targets for drug design. Part of this thesis consisted in the characterization of two different types of inhibitors. The first one was microcin C (McC), a natural inhibitor produced by some *E. coli* strains to inhibit their surrounding competitors. This molecule is very similar to the natural aspartyl-adenylate natural substrate, the only differences consist in a nitrogen instead of an oxygen between the aspartyl and the adenylate to make it non-hydrolyzable and a propylamine arm on the phosphate. My structural study of the role of this arm in making McC specific for bacterial enzymes, was not conclusive with the *E. coli* AspRS. Further analysis of this inhibitor in complex with the *T. thermophilus* AspRS, an enzyme that is more stable and easy to handle, should help to improve the resolution of the complex and bring a clear answer to this question. The second family consists of macrocyclic peptides containing non-conventional amino acids. I selected six of them with the RaPID procedure for their binding properties to the AspRS of the pathogen *P. aeruginosa* and performed their characterization. Enzymatic tests indicated that three of the six selected peptides have an interesting inhibitory effect. Therefore I conducted a more detailed kinetic study of these inhibitors to find out that they are competitive inhibitors. Test with the *E. coli* and human enzymes revealed that these peptides are non-specific and thus would need further improvement to be used as drugs. I also tested them as co-crystallizing compound without obtaining crystals that would allow to solve the complex structure at high resolution. This enzyme has been resisting to crystallization since several years in our team and will require additional effort in the future to eventually determine its structure in the presence of peptidic inhibitors.

CCA-adding enzymes

CCA-adding enzymes are other essential actors of tRNA life cycle, involved in the addition and the maintenance of the CCA sequence at the 3' end of tRNAs. I included the enzyme from the psychrophilic bacterium *P. halocryophilus* in my set of model macromolecules for method development. This work led me to solve the crystallographic structure of the apo-enzyme and of the complex with the CTP substrate. These structures have been elucidated at high resolution (1.8 - 2 Å) in several chemical environments and by different crystallographic methods (molecular replacement and sulfur-SAD, at room or cryo-temperatures). The tests for co-crystallization or soaking of the enzyme crystals with the ATP substrate have not been successful, which suggests that the latter does not bind alone but most probably requires the prior presence of tRNA. In addition, the study of the different structures at 100 K compared to the available structures in the PDB of other bacterial organisms highlighted several cold adaptation features: the catalytic core in the N-terminus part does not show strong adaptation, compared to the C-terminus, which is responsible for tRNA binding and presents a significantly reduced α-helices content. It would be very interesting now to continue this project by solving the structure of the *Pha*CCA in complex with a tRNA or a mini helices (corresponding to the acceptor arm of a tRNA) at different stages of the CCA addition process. This could be performed by the study of static structures or by serial crystallography and the determination of the "molecular movie" by the use of XFEL radiation, thanks to sample preparation performed with the Xtal Controller (see below). Finally, another CCA-adding enzyme purified by our collaborators in Leipzig could be interesting to study. They discovered and managed to purify the enzyme from *Romanomermis culicivorax*, which is able to process the world smallest functional tRNAs, lacking the D- and T-arms (Wende et al. 2014; Jühling et al. 2018). The structure of this enzyme and the way it interacts with these peculiar tRNAs has never been described. Crystallization of the apo-form and of the complexes are in progress.

15 Crystallization and crystallographic aspects

Several goals were achieved during this thesis in term of development and implementation of new crystallization approaches and serial crystallography.

TFL, MMS and ChipX3

First, TFL and MMS were implemented in the laboratory with the *Pha*CCA project, following my participation in a FEBS course[3], and led to several crystal structures at high resolution (de Wijn et al. 2018). These methods, which proved to be powerful and easy-to-use are now used in routine for other projects in our team.

In addition, my work allowed to further demonstrate the advantages of the microfluidic ChipX3. Inside these chips, counter-diffusion crystallization experiments can be performed, allowing to screen a large panel of crystallizing agent concentrations in a convection-free environment. A previous study in our team presented a previous version of the chips with room-temperature (RT) data-collection on model proteins, as well as experimental phase determination using an ytterbium derivative (Pinker et al. 2013). I was able to go further by demonstrating the compatibility of the device with microseeding, illustrating the easy detection of protein crystal by UV (with Tb-Xo4) and green light (after TFL), and carrying out serial crystallography RT data collection of “non-model” macromolecules. RT analysis are gaining popularity in our field, firstly by the success of recent structures obtained under XFEL radiation, but also more using conventional synchrotron radiation and this approach can be made easier by the ChipX3. In a study described in 2011 (Fraser et al. 2011) on a set of 30 proteins, they showed that in crystal cryo-cooled to 100 K more than 35% of amino acids side chains presented alternate conformations, thus advocating for analysis at RT, i.e. in more physiological conditions. The two articles presented in chapter II should help popularize these chips and the method of counter-diffusion in the community of crystallographers.

[3] « Advanced methods in Macromolecular Crystallization VII » organized by the FEBS society in 2016 at Nové Hrady, Czech Republic.

Xtal Controller

The Xtal Controller was acquired by the team shortly before the beginning of my thesis. It allows to control and follow-up a crystallization experiment in a closed chamber with an ultra-sensitive balance, two piezo-pump injectors, DLS and a camera. The initial purpose was the crystallization of difficult and/or sensitive cases, but more applications were recently imagined: the preparation of micro- and/or nanocrystalline samples for XFEL experiments, as well as the study of nucleation events and early crystal growth. My work allowed to define a precise experimental protocol for the use of this instrument and to test it for several purposes. As a result, the *Pha*CCA enzyme was crystallized and a dataset was collected at 1.85 Å. The instrument was also used to study the effect of Tb-Xo4 on nucleation and crystal growth of lysozyme and protease 1 from *P. horikhoshii*, leading to the observation of different types of behaviors.

To precisely link a DLS profile obtained in the instrument to specific structures (nuclei, nanocrystals, microcrystals…), I performed preliminary tests to determine how to prepare a grid by negative staining to visualize these particles by transmission electron microcopy (TEM). The first assays were successful with fragmented *Pha*CCA crystals and are illustrated **Figure 15-1**. This observation of crystalline structures inside a solution are a prerequisite for the attribution of XFEL beamtime. Preparing samples for such kind of experiments is one of the future goals to achieve with support of the Xtal Controller. XFEL facilities, growing in number around the world, already proved their efficiency for high quality room-temperature data collection and time resolved crystallography, or production of molecular movies (Nango et al. 2016; Suga et al. 2017; Johansson et al. 2017). To conclude, a scheme of the sample preparation for a mix-and-diffuse experiment at a XFEL installation is presented **Figure 15-1**. Crystals grown in the Xtal Controller could also be used for electron diffraction experiments, as this method is growing in terms of capacities (Clabbers et al. 2017, 2018).

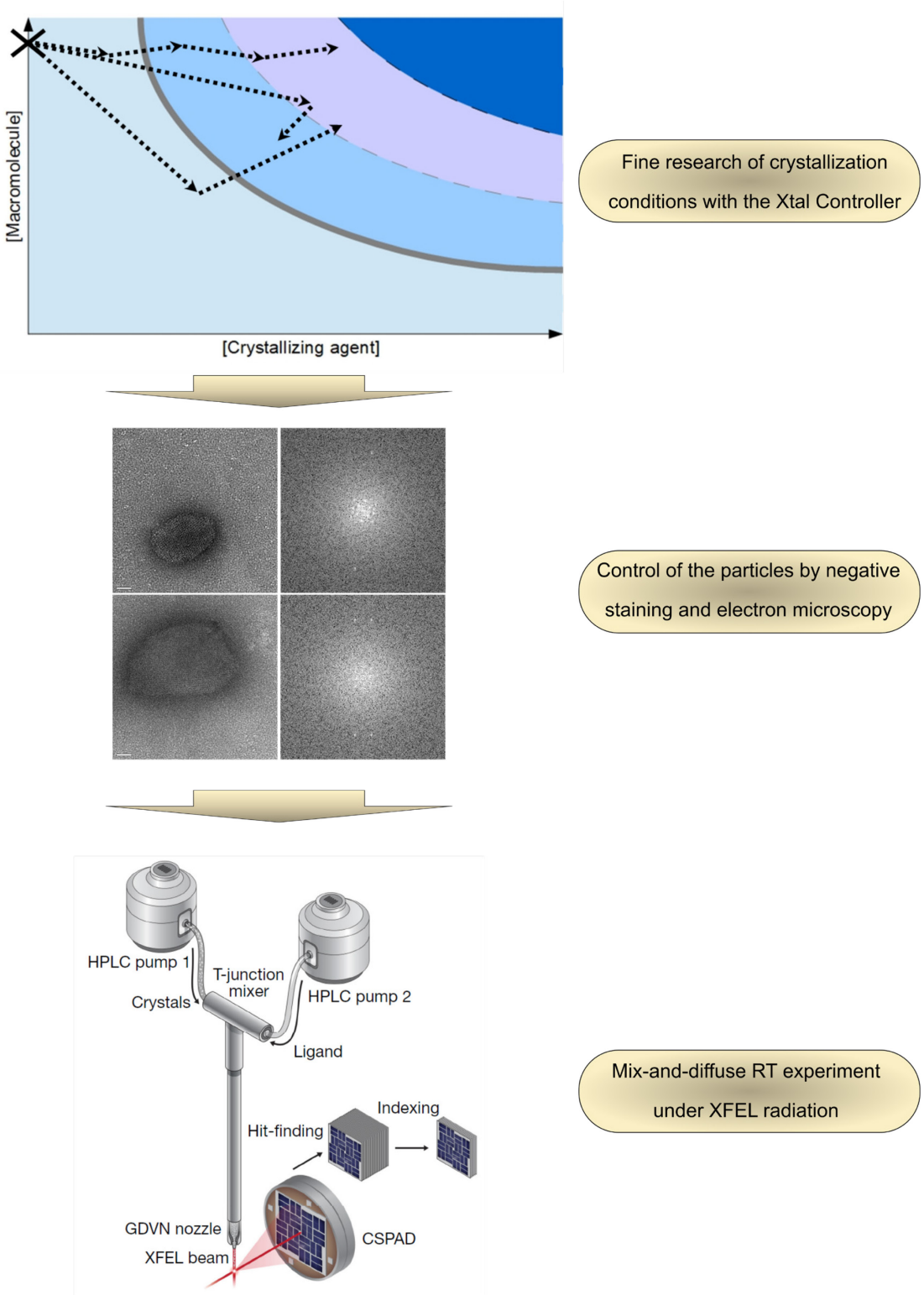

Figure 15-1 : Schematic representation of an experimental protocol based on the Xtal Controller and electron microscopy to prepare a sample for time-resolved RT experiment under XFEL radiation. The middle panel corresponds to fragments of *Pha*CCA crystals observed by TEM after negative staining (scale bars = 50 µm) and the corresponding reciprocal lattices obtained by Fourier transform. Bottom panel is adapted from Stagno *et al.*, 2017.

VII. Bibliographie

Adams PD, Afonine P V, Bunkóczi G, Chen VB, Davis IW, Echols N, Headd JJ, Hung L-W, Kapral GJ, Grosse-Kunstleve RW, et al. 2010. PHENIX: a comprehensive Python-based system for macromolecular structure solution. *Acta Crystallogr D Biol Crystallogr* **66**: 213–21.

Åqvist J. 2017. Cold Adaptation of Triosephosphate Isomerase. *Biochemistry* **56**: 4169–4176.

Asherie N. 2004. Protein crystallization and phase diagrams. *Methods* **34**: 266–272.

Augustin MA, Reichert AS, Betat H, Huber R, Mörl M, Steegborn C. 2003. Crystal structure of the human CCA-adding enzyme: Insights into template-independent polymerization. *J Mol Biol* **328**: 985–994.

Bae E, Phillips GN. 2004. Structures and analysis of highly homologous psychrophilic, mesophilic, and thermophilic adenylate kinases. *J Biol Chem* **279**: 28202–8.

Baitan D, Schubert R, Meyer A, Dierks K, Perbandt M, Betzel C. 2018. Growing Protein Crystals with Distinct Dimensions Using Automated Crystallization Coupled with In Situ Dynamic Light Scattering. *J Vis Exp*.

Bantysh O, Serebryakova M, Zukher I, Kulikovsky A, Tsibulskaya D, Dubiley S, Severinov K. 2015. Enzymatic Synthesis and Functional Characterization of Bioactive Microcin C-Like Compounds with Altered Peptide Sequence and Length. *J Bacteriol* **197**: 3133–3141.

Becker HD, Reinbolt J, Kreutzer R, Giege R, Kern D. 1997. Existence of two distinct aspartyl-tRNA synthetases in Thermus thermophilus. Structural and biochemical properties of the two enzymes. *Biochemistry* **36**: 8785–8797.

BERNAL JD, CROWFOOT D. 1934. X-Ray Photographs of Crystalline Pepsin. *Nature* **133**: 794–795.

Bernard D, Akochy P, Beaulieu D, Lapointe J, Roy PH. 2006. Two residues in the anticodon recognition domain of the aspartyl-tRNA synthetase from Pseudomonas aeruginosa are individually implicated in the recognition of tRNAAsn. *J Bacteriol* **188**: 269–74.

Bernier S, Akochy P-M, Lapointe J, Chênevert R. 2005. Synthesis and aminoacyl-tRNA synthetase inhibitory activity of aspartyl adenylate analogs. *Bioorg Med Chem* **13**: 69–75.

Betat H, Rammelt C, Mörl M. 2010. TRNA nucleotidyltransferases: Ancient catalysts

with an unusual mechanism of polymerization. *Cell Mol Life Sci* **67**: 1447–1463.

Blaise M, Bailly M, Frechin M, Behrens MA, Fischer F, Oliveira CLP, Becker HD, Pedersen JS, Thirup S, Kern D. 2010. Crystal structure of a transfer-ribonucleoprotein particle that promotes asparagine formation. *EMBO J* **29**: 3118–29.

Bonnefond L, Fender A, Rudinger-Thirion J, Giegé R, Florentz C, Sissler M. 2005. Toward the full set of human mitochondrial aminoacyl-tRNA synthetases: Characterization of AspRS and TyrRS. *Biochemistry* **44**: 4805–4816.

Briand C, Poterszman A, Eiler S, Webster G, Thierry JC, Moras D. 2000. An intermediate step in the recognition of tRNA(Asp) by aspartyl-tRNA synthetase. *J Mol Biol* **299**: 1051–1060.

Carter CW, Sweet RM. 1997. *Macromolecular crystallography*. Academic Press.

Chernov AA. 1997. Crystals built of biological macromolecules. *Phys Rep* **288**: 61–75.

Clabbers MTB, Gruene T, Parkhurst JM, Abrahams JP, Waterman DG. 2018. Electron diffraction data processing with DIALS. *Acta Crystallogr Sect D, Struct Biol* **74**: 506–518.

Clabbers MTB, van Genderen E, Wan W, Wiegers EL, Gruene T, Abrahams JP. 2017. Protein structure determination by electron diffraction using a single three-dimensional nanocrystal. *Acta Crystallogr Sect D, Struct Biol* **73**: 738–748.

Corona A, Palmer SO, Zamacona R, Mendez B, Dean FB, Bullard JM. 2018. Discovery and Characterization of Chemical Compounds That Inhibit the Function of Aspartyl-tRNA Synthetase from Pseudomonas aeruginosa. *SLAS Discov Adv life Sci R D* **23**: 294–301.

D'Arcy A, Bergfors T, Cowan-Jacob SW, Marsh M. 2014. Microseed matrix screening for optimization in protein crystallization: What have we learned? *Acta Crystallogr Sect Struct Biol Commun* **70**: 1117–1126.

D'Arcy A, Villard F, Marsh M, IUCr. 2007. An automated microseed matrix-screening method for protein crystallization. *Acta Crystallogr Sect D Biol Crystallogr* **63**: 550–554.

De Maayer P, Anderson D, Cary C, Cowan DA. 2014. Some like it cold: Understanding the survival strategies of psychrophiles. *EMBO Rep* **15**: 508–517.

de Wijn R, Hennig O, Ernst FGM, Lorber B, Betat H, Mörl M, Sauter C. 2018. Combining crystallogenesis methods to produce diffraction-quality crystals of a

psychrophilic tRNA-maturation enzyme. *Acta Crystallogr Sect FStructural Biol Commun* **F74**: 747–753.

Deutscher MP. 1990. Ribonucleases, tRNA nucleotidyltransferase, and the 3' processing of tRNA. *Prog Nucleic Acid Res Mol Biol* **39**: 209–40.

Dick M, Weiergräber OH, Classen T, Bisterfeld C, Bramski J, Gohlke H, Pietruszka J. 2016. Trading off stability against activity in extremophilic aldolases. *Sci Rep* **6**: 17908.

Ducruix A, Giegé R. 1992. Crystallization of Nucleic Acid And Proteins. *Oxford Univ Press* **17**: 255–288.

Engilberge S, Riobé F, Di Pietro S, Lassalle L, Coquelle N, Arnaud CA, Pitrat D, Mulatier JC, Madern D, Breyton C, et al. 2017. Crystallophore: A versatile lanthanide complex for protein crystallography combining nucleating effects, phasing properties, and luminescence. *Chem Sci* **8**: 5909–5917.

Engilberge S, Riobé F, Wagner T, Di Pietro S, Breyton C, Franzetti B, Shima S, Girard E, Dumont E, Maury O. 2018. Unveiling the Binding Modes of the Crystallophore, a Terbium-based Nucleating and Phasing Molecular Agent for Protein Crystallography. *Chem - A Eur J* **24**: 9739–9746.

Eriani G, Delarue M, Poch O, Gangloff J, Moras D. 1990. Partition of tRNA synthetases into two classes based on mutually exclusive sets of sequence motifs. *Nature* **347**: 203–206.

Ernst FGM, Erber L, Sammler J, Jühling F, Betat H, Mörl M. 2018. Cold adaptation of tRNA nucleotidyltransferases: A tradeoff in activity, stability and fidelity. *RNA Biol* **15**: 144–155.

Ernst FGM, Rickert C, Bluschke A, Betat H, Steinhoff HJ, Mör M. 2015. Domain movements during CCA-addition: A new function for motif C in the catalytic core of the human tRNA nucleotidyltransferases. *RNA Biol* **12**: 435–446.

Feller G, Gerday C. 2003. Psychrophilic enzymes: Hot topics in cold adaptation. *Nat Rev Microbiol* **1**: 200–208.

Fernández-Millán P, Schelcher C, Chihade J, Masquida B, Giegé P, Sauter C. 2016. Transfer RNA: From pioneering crystallographic studies to contemporary tRNA biology. *Arch Biochem Biophys* **602**: 95–105.

Fitter J. 2005. Structural and dynamical features contributing to thermostability in α-amylases. *Cell Mol Life Sci* **62**: 1925–1937.

Fraser JS, van den Bedem H, Samelson AJ, Lang PT, Holton JM, Echols N, Alber T. 2011. Accessing protein conformational ensembles using room-temperature X-ray crystallography. *Proc Natl Acad Sci* **108**: 16247–16252.

Garcia-Caballero A, Gavira JA, Pineda-Molina E, Chayen NE, Govada L, Khurshid S, Saridakis E, Boudjemline A, Swann MJ, Shaw Stewart P, et al. 2011. Optimization of protein crystallization: The opticryst project. *Cryst Growth Des* **11**: 2112–2121.

García-Ruiz JM. 2003. Counterdiffusion Methods for Macromolecular Crystallization. *Methods Enzymol* **368**: 130–154.

García-Ruiz J., Novella M., Moreno R, Gavira J. 2001. Agarose as crystallization media for proteins: I: Transport processes. *J Cryst Growth* **232**: 165–172.

Garman EF. 2010. Radiation damage in macromolecular crystallography: what is it and why should we care? *Acta Crystallogr D Biol Crystallogr* **66**: 339–51.

Gavira JA, García-Ruiz JM. 2002. Agarose as crystallisation media for proteins II: Trapping of gel fibres into the crystals. *Acta Crystallogr Sect D Biol Crystallogr* **58**: 1653–1656.

Giegé R, Dock a. C, Kern D, Lorber B, Thierry JC, Moras D. 1986. The role of purification in the crystallization of proteins and nucleic acids. *J Cryst Growth* **76**: 554–561.

Goto Y, Katoh T, Suga H. 2011. Flexizymes for genetic code reprogramming. *Nat Protoc* **6**: 779–790.

Hasegawa T, Himeno H, Ishikura H, Shimizu M. 1989. Discriminator base of tRNAAsp is involved in amino acid acceptor activity. *Biochem Biophys Res Commun* **163**: 1534–1538.

Hashim NHF, Mahadi NM, Illias RM, Feroz SR, Abu Bakar FD, Murad AMA. 2018. Biochemical and structural characterization of a novel cold-active esterase-like protein from the psychrophilic yeast Glaciozyma antarctica. *Extremophiles* **22**: 607–616.

Hayashi Y, Morimoto J, Suga H. 2012. *In Vitro* Selection of Anti-Akt2 Thioether-Macrocyclic Peptides Leading to Isoform-Selective Inhibitors. *ACS Chem Biol* **7**: 607–613.

Hipolito C, Tanaka Y, Katoh T, Nureki O, Suga H, Hipolito CJ, Tanaka Y, Katoh T, Nureki O, Suga H. 2013. A Macrocyclic Peptide that Serves as a Cocrystallization Ligand and Inhibits the Function of a MATE Family Transporter. *Molecules* **18**:

10514–10530.

Hirano Y, Takeda K, Miki K. 2016. Charge-density analysis of an iron-sulfur protein at an ultra-high resolution of 0.48 Å. *Nature* **534**: 281–284.

Hoffmeier A, Betat H, Bluschke A, Günther R, Junghanns S, Hofmann H-J, Mörl M. 2010. Unusual evolution of a catalytic core element in CCA-adding enzymes. *Nucleic Acids Res* **38**: 4436–47.

Holm L, Sander C. 1995. DNA polymerase β belongs to an ancient nucleotidyltransferase superfamily. *Trends Biochem Sci* **20**: 345–347.

Hu Y, Guerrero E, Keniry M, Manrrique J, Bullard JM. 2015. Identification of Chemical Compounds That Inhibit the Function of Glutamyl-tRNA Synthetase from Pseudomonas aeruginosa. *J Biomol Screen* **20**: 1160–70.

Irwin MJ, Nyborg J, Reid BR, Blow DM. 1976. The crystal structure of the Tyrosyl-transfer RNA Synthetase at 2.7 A resolution. *J Mol Biol* 577–586.

Johansson LC, Stauch B, Ishchenko A, Cherezov V. 2017. A Bright Future for Serial Femtosecond Crystallography with XFELs. *Trends Biochem Sci* **42**: 749–762.

Jühling T, Duchardt-Ferner E, Bonin S, Wöhnert J, Pütz J, Florentz C, Betat H, Sauter C, Mörl M. 2018. Small but large enough: structural properties of armless mitochondrial tRNAs from the nematode Romanomermis culicivorax. *Nucleic Acids Res* **46**: 9170–9180.

Kabsch W. 2010. XDS. *Acta Crystallogr D Biol Crystallogr* **66**: 125–32.

Kendrew JC, Bodo G, Dintzis HM, Parrish RG, Wyckoff H, Phillips DC. 1958. A three-dimensional model of the myoglobin molecule obtained by x-ray analysis. *Nature* **181**: 662–666.

Khrapunov S, Chang E, Callender RH. 2017. Thermodynamic and Structural Adaptation Differences between the Mesophilic and Psychrophilic Lactate Dehydrogenases. *Biochemistry* **56**: 3587–3595.

Kim SH, Quigley G, Suddath FL, McPherson A, Sneden D, Kim JJ, Weinzierl J, Rich A. 1973. Three-dimensional structure of yeast phenylalanine transfer RNA: Folding of the polypeptide chain. *Science (80-)* **179**: 285–288.

Kirchner S, Ignatova Z. 2015. Emerging roles of tRNA in adaptive translation, signalling dynamics and disease. *Nat Rev Genet* **16**: 98–112.

Kovacic F, Mandrysch A, Poojari C, Strodel B, Jaeger K-E. 2016. Structural features determining thermal adaptation of esterases. *Protein Eng Des Sel* **29**: 65–76.

Lee JH, Choi JM, Kim HJ. 2017. Crystal structure of 5-enolpyruvylshikimate-3-phosphate synthase from a psychrophilic bacterium, Colwellia psychrerythraea 34H. *Biochem Biophys Res Commun* **492**: 500–506.

Li F, Xiong Y, Wang J, Cho HDD, Tomita K, Weiner AM, Steitz TA. 2002. Crystal structures of the Bacillus stearothermophilus CCA-adding enzyme and its complexes with ATP or CTP. *Cell* **111**: 815–824.

Lorber B, Sauter C, Robert MC, Capelle B, Giegé R, IUCr. 1999. Crystallization within agarose gel in microgravity improves the quality of thaumatin crystals. *Acta Crystallogr Sect D Biol Crystallogr* **55**: 1491–1494.

Lorber B, Sauter C, Théobald-Dietrich A, Moreno A, Schellenberger P, Robert MC, Capelle B, Sanglier S, Potier N, Giegé R. 2009. Crystal growth of proteins, nucleic acids, and viruses in gels. *Prog Biophys Mol Biol* **101**: 13–25.

McPherson A. 2009. *Introduction to Macromolecular Crystallography*. John Wiley & Sons, Inc., Hoboken, NJ, USA

McPherson A, Kuznetsov YG. 2014. Mechanisms, kinetics, impurities and defects: Consequences in macromolecular crystallization. *Acta Crystallogr Sect FStructural Biol Commun* **70**: 384–403.

McPherson A, Kuznetsov YG, Malkin A, Plomp M. 2003. Macromolecular crystal growth as revealed by atomic force microscopy. *J Struct Biol* **142**: 32–46.

McPherson A, Malkin AJ, Kuznetsov YG, Plomp M. 2001. Atomic force microscopy applications in macromolecular crystallography. *Acta Crystallogr Sect D Biol Crystallogr* **57**: 1053–1060.

Metlitskaya A, Kazakov T, Kommer A, Pavlova O, Praetorius-Ibba M, Ibba M, Krasheninnikov I, Kolb V, Khmel I, Severinov K. 2006. Aspartyl-tRNA synthetase is the target of peptide nucleotide antibiotic microcin C. *J Biol Chem* **281**: 18033–18042.

Metlitskaya A, Kazakov T, Vondenhoff GH, Novikova M, Shashkov A, Zatsepin T, Semenova E, Zaitseva N, Ramensky V, Van Aerschot A, et al. 2009. Maturation of the translation inhibitor microcin C. *J Bacteriol* **191**: 2380–7.

Meyer A, Betzel C, Pusey M. 2015. Latest methods of fluorescence-based protein crystal identification. *Acta Crystallogr Sect F, Struct Biol Commun* **71**: 121–31.

Meyer A, Dierks K, Hilterhaus D, Klupsch T, Mühlig P, Kleesiek J, Schöpflin R, Einspahr H, Hilgenfeld R, Betzel C. 2012. Single-drop optimization of protein

crystallization. *Acta Crystallogr Sect F Struct Biol Cryst Commun* **68**: 994–998.

Mikol V, Hirsch E, Giegé R. 1990. Diagnostic of precipitant for biomacromolecule crystallization by quasi-elastic light-scattering. *J Mol Biol* **213**: 187–195.

Murakami H, Ohta A, Ashigai H, Suga H. 2006. A highly flexible tRNA acylation method for non-natural polypeptide synthesis. *Nat Methods* **3**: 357–359.

Mykytczuk NCS, Wilhelm RC, Whyte LG. 2012. Planococcus halocryophilus sp. nov., an extreme sub-zero species from high arctic permafrost. *Int J Syst Evol Microbiol* **62**: 1937–1944.

Nango E, Royant A, Kubo M, Nakane T, Wickstrand C, Kimura T, Tanaka T, Tono K, Song C, Tanaka R, et al. 2016. A three-dimensional movie of structural changes in bacteriorhodopsin. *Science* **354**: 1552–1557.

Newman J. 2011. One plate, two plates, a thousand plates. How crystallisation changes with large numbers of samples. *Methods* **55**: 73–80.

Newman J, Egan D, Walter TS, Meged R, Berry I, Ben Jelloul M, Sussman JL, Stuart DI, Perrakis A. 2005. Towards rationalization of crystallization screening for small- to medium-sized academic laboratories: the PACT/JCSG+ strategy. *Acta Crystallogr Sect D Biol Crystallogr* **61**: 1426–1431.

Ng JD, Sauter C, Lorber B, Kirkland N, Arnez J, Giegé R. 2002. Comparative analysis of space-grown and earth-grown crystals of an aminoacyl-tRNA synthetase: space-grown crystals are more useful for structural determination. *Acta Crystallogr Sect D* 87–100.

Niwa N, Yamagishi Y, Murakami H, Suga H. 2009. A flexizyme that selectively charges amino acids activated by a water-friendly leaving group. *Bioorg Med Chem Lett* **19**: 3892–3894.

Olga Gliko †, Nikolaus Neumaier ‡, Weichun Pan †, Ilka Haase ‡, Markus Fischer ‡, Adelbert Bacher ‡, Sevil Weinkauf ‡ and, Peter G. Vekilov* †. 2005. A Metastable Prerequisite for the Growth of Lumazine Synthase Crystals.

Otálora F, Gavira JA, Ng JD, García-Ruiz JM. 2009. Counterdiffusion methods applied to protein crystallization. *Prog Biophys Mol Biol* **101**: 26–37.

Papp-Wallace KM, Endimiani A, Taracila MA, Bonomo RA. 2011. Carbapenems: Past, present, and future. *Antimicrob Agents Chemother* **55**: 4943–4960.

Passioura T, Suga H. 2017. A RaPID way to discover nonstandard macrocyclic peptide modulators of drug targets. *Chem Commun* **53**: 1931–1940.

Pellegrini O, Li de la Sierra-Gallay I, Piton J, Gilet L, Condon C. 2012. Activation of tRNA Maturation by Downstream Uracil Residues in B. subtilis. *Structure* **20**: 1769–1777.

Perutz MF, Rossmann MG, Cullis AF, Muirhead H, Will G, North ACT. 1960. Structure of Hæmoglobin: A three-dimensional fourier synthesis at 5.5-. resolution, obtained by X-ray analysis. *Nature* **185**: 416–422.

Petsev DN, Vekilov PG. 2000. Evidence for Non-DLVO Hydration Interactions in Solutions of the Protein Apoferritin. *Phys Rev Lett* **84**: 1339–1342.

Pinker F, Brun M, Morin P, Deman AL, Chateaux JF, Oli??ric V, Stirnimann C, Lorber B, Terrier N, Ferrigno R, et al. 2013. ChipX: A novel microfluidic chip for counter-diffusion crystallization of biomolecules and in situ crystal analysis at room temperature. *Cryst Growth Des* **13**: 3333–3340.

Poterszman A, Plateau P, Moras D, Blanquet S, Mazauric MH, Kreutzer R, Kern D. 1993. Sequence, overproduction and crystallization of aspartyl-tRNA synthetase from Thermus thermophilus. Implications for the structure of prokaryotic aspartyl-tRNA synthetases. *FEBS Lett* **325**: 183–186.

Pusey M, Barcena J, Morris M, Singhal A, Yuan Q, Ng J. 2015. Trace fluorescent labeling for protein crystallization. *Acta Crystallogr Sect Struct Biol Commun* **71**: 806–814.

Pusey M, Forsythe E, Achari A. 2008. Fluorescence Approaches to Growing Macromolecule Crystals. pp. 377–385, Humana Press

Raynal B, Lenormand P, Baron B, Hoos S, England P. 2014. Quality assessment and optimization of purified protein samples: why and how? *Microb Cell Fact* **13**: 180.

Reiter NJ, Osterman A, Torres-Larios A, Swinger KK, Pan T, Mondragón A. 2010. Structure of a bacterial ribonuclease P holoenzyme in complex with tRNA. *Nature* **468**: 784–789.

Robertus JD, Ladner JE, Finch JT, Rhodes D, Brown RS, Clark BFC, Klug A. 1974. Structure of yeast phenylalanine tRNA at 3 Å resolution. *Nature* **250**: 546–551.

Rould MA, Perona JJ, Söll D, Steitz TA. 1989. Structure of E. coli glutaminyl-tRNA synthetase complexed with tRNA(Gln) and ATP at 2.8 A resolution. *Science* **246**: 1135–42.

Ruff M, Krishnaswamy S, Boeglin M, Poterszman A, Mitschler A, Podjarny A, Rees B, Thierry JC, Moras D. 1991. Class II aminoacyl transfer RNA synthetases: crystal

structure of yeast aspartyl-tRNA synthetase complexed with tRNA(Asp). *Science* **252**: 1682–9.

Saito H, Suga H. 2001. A Ribozyme Exclusively Aminoacylates the 3‘-Hydroxyl Group of the tRNA Terminal Adenosine. *J Am Chem Soc* **123**: 7178–7179.

Santoni G, Zander U, Mueller-Dieckmann C, Leonard G, Popov A. 2017. Hierarchical clustering for multiple-crystal macromolecular crystallography experiments: The ccCluster program. *J Appl Crystallogr* **50**: 1844–1851.

Sarmiento F, Peralta R, Blamey JM. 2015. Cold and Hot Extremozymes: Industrial Relevance and Current Trends. *Front Bioeng Biotechnol* **3**: 148.

Sauter A, Roosen-Runge F, Zhang F, Lotze G, Jacobs RMJ, Schreiber F. 2015. Real-Time Observation of Nonclassical Protein Crystallization Kinetics. *J Am Chem Soc* **137**: 1485–1491.

Sauter C, Dhouib K, Lorber B. 2007. From Macrofluidics to Microfluidics for the Crystallization of Biological Macromolecules †. *Cryst Growth Des* **7**: 2247–2250.

Sauter C, Lorber B, McPherson A, Giegé R. 2001. International Tables for Crystallography. *Int Tables Crystallogr*.

Schimmel PR, Söll D. 1979. Aminoacyl-tRNA Synthetases: General Features and Recognition of Transfer RNAs. *Annu Rev Biochem* **48**: 601–648.

Schlichting I. 2015. Serial femtosecond crystallography: the first five years. *IUCrJ* **2**: 246–55.

Schmeing TM, Voorhees RM, Kelley AC, Gao Y-G, Murphy F V, Weir JR, Ramakrishnan V. 2009. The crystal structure of the ribosome bound to EF-Tu and aminoacyl-tRNA. *Science* **326**: 688–694.

Schmidt A, Teeter M, Weckert E, Lamzin VS. 2011. Crystal structure of small protein crambin at 0.48 Å resolution. *Acta Crystallogr Sect F Struct Biol Cryst Commun* **67**: 424–428.

Schubert R, Meyer A, Baitan D, Dierks K, Perbandt M, Betzel C. 2017. Real-Time Observation of Protein Dense Liquid Cluster Evolution during Nucleation in Protein Crystallization. *Cryst Growth Des* **17**: 954–958.

Schubert R, Meyer A, Dierks K, Kapis S, Reimer R, Einspahr H, Perbandt M, Betzel C. 2015. Reliably distinguishing protein nanocrystals from amorphous precipitate by means of depolarized dynamic light scattering. *J Appl Crystallogr* **48**: 1476–1484.

Severinov K, Nair SK. 2012. Microcin C: biosynthesis and mechanisms of bacterial

resistance. *Future Microbiol* **7**: 281–9.

Shah U V., Williams DR, Heng JYY. 2012. Selective Crystallization of Proteins Using Engineered Nanonucleants. *Cryst Growth Des* **12**: 1362–1369.

Siddiqui KS, Cavicchioli R. 2006. Cold-Adapted Enzymes. *Annu Rev Biochem* **75**: 403–433.

Siddiqui KS, Cavicchioli R, Thomas T. 2002. Thermodynamic activation properties of elongation factor 2 (EF-2) proteins from psychrotolerant and thermophilic Archaea. *Extremophiles* **6**: 143–150.

Siddiqui KS, Williams TJ, Wilkins D, Yau S, Allen MA, Brown M V., Lauro FM, Cavicchioli R. 2013. Psychrophiles. *Annu Rev Earth Planet Sci* **41**: 87–115.

Skarzynski T. 2013. Collecting data in the home laboratory: evolution of X-ray sources, detectors and working practices. *Acta Crystallogr D Biol Crystallogr* **69**: 1283–8.

Skouri M, Delsanti M, Munch J-P, Lorber B, Giegé R. 1991. Dynamic light scattering studies of the aggregation of lysozyme under crystallization conditions. *FEBS Lett* **295**: 84–88.

Sočan J, Kazemi M, Isaksen GV, Brandsdal BO, Åqvist J. 2018. Catalytic Adaptation of Psychrophilic Elastase. *Biochemistry* **57**: 2984–2993.

Sprinzl M, Cramer F. 1979. The -C-C-A End of tRNA and Its Role in Protein Biosynthesis. *Prog Nucleic Acid Res Mol Biol* **22**: 1–69.

Stagno JR, Liu Y, Bhandari YR, Conrad CE, Panja S, Swain M, Fan L, Nelson G, Li C, Wendel DR, et al. 2017. Structures of riboswitch RNA reaction states by mix-and-inject XFEL serial crystallography. *Nature* **541**: 242–246.

Stetefeld J, McKenna SA, Patel TR. 2016. Dynamic light scattering: a practical guide and applications in biomedical sciences. *Biophys Rev* **8**: 409–427.

Stranski IN, Kaischew R. 1935. Gleichgewichtsform und Wachstumsform der Kristalle. *Ann Phys* **415**: 330–338.

Struvay C, Feller G. 2012. Optimization to low temperature activity in psychrophilic enzymes. *Int J Mol Sci* **13**: 11643–65.

Suga M, Akita F, Sugahara M, Kubo M, Nakajima Y, Nakane T, Yamashita K, Umena Y, Nakabayashi M, Yamane T, et al. 2017. Light-induced structural changes and the site of O=O bond formation in PSII caught by XFEL. *Nature* **543**: 131–135.

Tacconelli E, Magrini N. 2017. Global Priority List Of Antibiotic-Resistant Bacteria To Guide Research, Discovery, And Development Of New Antibiotics.

Tanaka Y, Hipolito CJ, Maturana AD, Ito K, Kuroda T, Higuchi T, Katoh T, Kato HE, Hattori M, Kumazaki K, et al. 2013. Structural basis for the drug extrusion mechanism by a MATE multidrug transporter. *Nature* **496**: 247–251.

Toh Y, Takeshita D, Numata T, Fukai S, Nureki O, Tomita K. 2009. Mechanism for the definition of elongation and termination by the class II CCA-adding enzyme. *EMBO J* **28**: 3353–65.

Tomita K, Fukai S, Ishitani R, Ueda T, Takeuchi N, Vassylyev DG, Nureki O. 2004. Structural basis for template-independent RNA polymerization. *Nature* **430**: 700–704.

Tomita K, Ishitani R, Fukai S, Nureki O. 2006. Complete crystallographic analysis of the dynamics of CCA sequence addition. *Nature* **443**: 956–960.

Touw WG, Baakman C, Black J, Te Beek TAH, Krieger E, Joosten RP, Vriend G. 2015. A series of PDB-related databanks for everyday needs. *Nucleic Acids Res* **43**: D364–D368.

Van De Vijver P, Vondenhoff GHM, Kazakov TS, Semenova E, Kuznedelov K, Metlitskaya A, Van Aerschot A, Severinov K. 2009. Synthetic microcin C analogs targeting different aminoacyl-tRNA synthetases. *J Bacteriol* **191**: 6273–6280.

Vergara A, Lorber B, Sauter C, Giegé R, Zagari A. 2005. Lessons from crystals grown in the Advanced Protein Crystallisation Facility for conventional crystallisation applied to structural biology. *Biophys Chem* **118**: 102–112.

Volmer M, Weber A. 1926. Keimbildung in übersättigten Gebilden. *Zeitschrift für Phys Chemie* **119U**: 277–301.

Waltersperger S, Olieric V, Pradervand C, Glettig W, Salathe M, Fuchs MR, Curtin A, Wang X, Ebner S, Panepucci E, et al. 2015. PRIGo: a new multi-axis goniometer for macromolecular crystallography. *J Synchrotron Radiat* **22**: 895–900.

WATSON JD, CRICK FHC. 1953. Molecular Structure of Nucleic Acids: A Structure for Deoxyribose Nucleic Acid. *Nature* **171**: 737–738.

Weichenberger CX, Afonine P V, Kantardjieff K, Rupp B. 2015. The solvent component of macromolecular crystals. *Acta Crystallogr D Biol Crystallogr* **71**: 1023–38.

Weichenberger CX, Rupp B, IUCr. 2014. Ten years of probabilistic estimates of biocrystal solvent content: new insights *via* nonparametric kernel density estimate. *Acta Crystallogr Sect D Biol Crystallogr* **70**: 1579–1588.

Weinert T, Olieric N, Cheng R, Brünle S, James D, Ozerov D, Gashi D, Vera L, Marsh

M, Jaeger K, et al. 2017. Serial millisecond crystallography for routine room-temperature structure determination at synchrotrons. *Nat Commun* **8**.

Weinert T, Olieric V, Waltersperger S, Panepucci E, Chen L, Zhang H, Zhou D, Rose J, Ebihara A, Kuramitsu S, et al. 2015. Fast native-SAD phasing for routine macromolecular structure determination. *Nat Methods* **12**: 131–133.

Wellner K, Betat H, Mörl M. 2018. A tRNA's fate is decided at its 3′ end: Collaborative actions of CCA-adding enzyme and RNases involved in tRNA processing and degradation. *Biochim Biophys Acta - Gene Regul Mech* **1861**: 433–441.

Wende S, Platzer EG, Jühling F, Pütz J, Florentz C, Stadler PF, Mörl M. 2014. Biological evidence for the world's smallest tRNAs. *Biochimie* **100**: 151–158.

Winn MD, Ballard CC, Cowtan KD, Dodson EJ, Emsley P, Evans PR, Keegan RM, Krissinel EB, Leslie AGW, McCoy A, et al. 2011. Overview of the CCP4 suite and current developments. *Acta Crystallogr D Biol Crystallogr* **67**: 235–42.

Yang L-L, Tang S-K, Huang Y, Zhi X-Y. 2015. Low Temperature Adaptation Is Not the Opposite Process of High Temperature Adaptation in Terms of Changes in Amino Acid Composition. *Genome Biol Evol* **7**: 3426–3433.

Zhu DW, Lorber B, Sauter C, Ng JD, Bénas P, Le Grimellec C, Giegé R. 2001. Growth kinetics, diffraction properties and effect of agarose on the stability of a novel crystal form of Thermus thermophilus aspartyl-tRNA synthetase-1. *Acta Crystallogr Sect D Biol Crystallogr* **57**: 552–558.

VIII. Annexes

16 Communication, encadrement et responsabilités

16.1 Liste des communications orales

- “Real time tracking of Xo4 crystallophore effect on protein crystal nucleation and growth”; Raphaël de Wijn, Sylvain Engilberge, Bernard Lorber, Eric Girard, Claude Sauter; congrès ICCBM17, octobre-novembre 2018, Shanghai (Chine).
- “Crystal clear drug design - Le développement de médicaments, clair comme du cristal”; Raphaël de Wijn; Soirée DupleX - La pensée complexe à 2 niveaux, mars 2018, Freiburg (Allemagne).
- “Dissecting nucleation and crystal growth processes using the Xtal-Controller X900 technology”; Raphaël de Wijn, Sylvain Engilberge, Bernard Lorber, Eric Girard, Claude Sauter; 31st Rhine-Knee Regiomeeting on Structural Biology, septembre 2017, Munster (France).
- “CCA-adding enzymes in complex: structure determination”; Raphaël de Wijn, Oliver Hennig, Bernard Lorber, Heike Betat, Mario Mörl, Claude Sauter; French-German tRNA meeting, mai 2017, Mainz (Allemagne).
- Présentation de mon projet de thèse; Raphaël de Wijn; Science Slam (équivalent allemand de “Ma Thèse en 180 sec”), juin 2016, Berlin (Allemagne).

16.2 Liste des présentations de posters

- “New microfluidic design for crystallization of biomolecules and their in situ analysis by serial crystallography”; Raphaël de Wijn, Oliver Hennig, Jennifer Roche, Sylvain Engilberge, Heike Betat, Mario Mörl, Alain Roussel, Eric Girard, Vincent Oliéric, Gavin C. Fox, Karl Brillet, Bernard Lorber, Claude Sauter; congrès ICCBM17, octobre 2018, Shanghai (Chine)
- ‘’CCA-addition in the cold : characterization of the enzyme from Planococcus halocryophilus’’; Raphaël de Wijn, Felix Ernst, Oliver Hennig, Heike Betat, Mario Mörl, Claude Sauter; 27th tRNA conference (tRNA at the crossroad), septembre 2018, Strasbourg (France)
- “New microfluidic design for crystallization of biomolecules and their in situ analysis by serial crystallography”; Raphaël de Wijn, Oliver Hennig, Jennifer Roche, Sylvain Engilberge, Heike Betat, Mario Mörl, Alain Roussel, Eric Girard, Vincent Oliéric, Gavin C. Fox, Karl Brillet, Bernard Lorber, Claude Sauter; Colloque de l'Association Française de Cristallographie, juillet 2018, Lyon (France).
- “Preparation of micro- and nano-crystals with the Xtal-Controller”; Raphaël de Wijn, Bernard Lorber, Claude Sauter; Colloque du Groupement De Recherche International Xfel, décembre 2017, Paris (France).
- “De l'imagerie 3D au Drug Design”; Raphaël de Wijn; Doctoriales, mai 2017, Munster (France).
- “Crystallogenesis studies of bacterial aminoacyl-tRNA synthetases as potential targets for drug design”; Raphaël de WIjn, Bernard Lorber, Claude Sauter; congrès ICCBM16, juillet 2016, Prague (République Tchèque).

New microfluidic design for crystallization of biomolecules and their in situ analysis by serial crystallography

Raphaël de Wijn[1], Oliver Hennig[2], Jennifer Roche[3], Sylvain Engilberge[4], Kevin Rollet[1], Heike Betat[2], Mario Mörl[2], Alain Roussel[3], Eric Girard[4], Vincent Oliéric[5], Gavin C. Fox[6], Karl Brillet[1], Bernard Lorber[1], Claude Sauter[1]

[1]Institut de Biologie Moléculaire et Cellulaire, UPR 9002 CNRS, Strasbourg, France
[2]Biochemistry and Molecular Biology, Inst. for Biochemistry, Leipzig University, Leipzig, Germany
[3]Architecture et Fonction des Macromolécules Biologiques, UMR 7257 CNRS, Marseille, France
[4]Institut de Biologie Structurale, UMR 5075 CEA-CNRS-UGA, Grenoble, France
[5]Paul Scherrer Institute, Swiss Light Source, ligne X06DA, Villigen, Switzerland
[6]Synchrotron SOLEIL, ligne PROXIMA 2A, Gif-sur-Yvette, France

r.dewijn@ibmc-cnrs.unistra.fr

Introduction

For about fifteen years, microfluidics has opened up new possibilities and brought many benefits for the crystallization of biomolecules. Indeed, microfluidic systems facilitate the manipulation of nanovolumes of sample solutions, as well as extreme miniaturization and parallelization of crystallization assays. In addition, they provide a convection-free environment that favors the growth of high-quality crystals [1]. We present a new multifunctional microchip design [2] combining: 1) search and optimization of crystallization conditions of biomolecules by the counter-diffusion method, 2) crystal identification by fluorescence microscopy, 3) microcrystalline seeding, 4) derivatization of crystals by substrate soaking, and 5) in situ crystal analysis at room temperature. This design was tested on a large panel of biomolecules including soluble or membrane proteins. Several crystal structures have been solved in situ by the serial crystallography approach under synchrotron radiation. Some are presented in this poster.

ChipX design

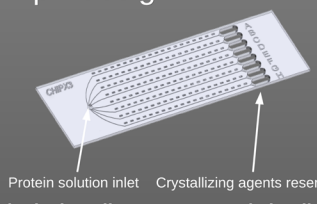

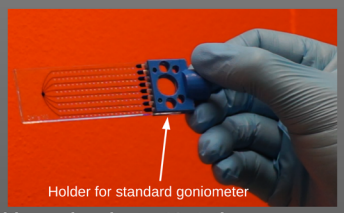

This design allows easy sample loading with regular pipets, 10µL tips and convenient use on conventional beamlines with a dedicated holder

Counter-diffusion

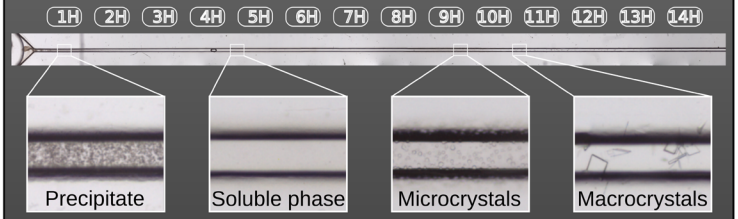

ChipX were designed to implement the counter-diffusion method which is well known for its efficiency based on a self-optimizing process: the crystallizing agent diffuses through an elongated crystallization chamber (the microfluidic channel), creates a gradient of concentration and each assay samples a broad range of supersaturation states. The longer the channel, the broader the screening.

Advanced crystallogenesis strategies

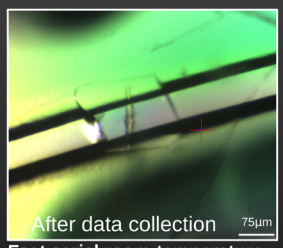

Fast serial room-temperature data collection

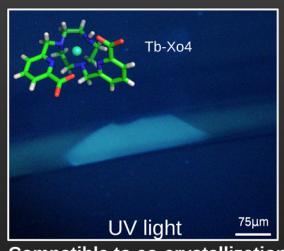

Compatible to co-crystallization with Tb-Xo4 as phasing agent, luminescent molecule and nucleating agent

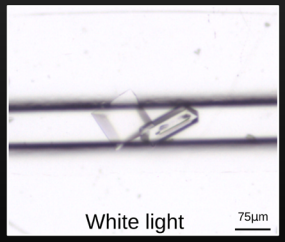

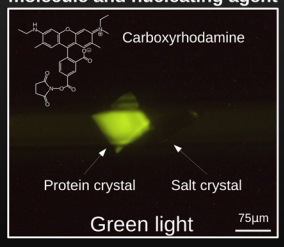

Compatible with microcrystalline seeding
→ seeds added to the protein solution before ChipX loading and soaking
→ molecules can be added to the reservoir after crystal growth

Compatible with fluo-labelling for visualization

In-situ analysis

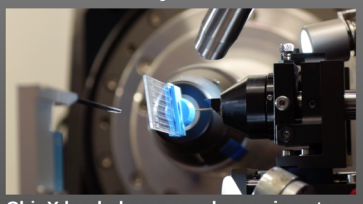

ChipX loaded on a regular goniometer head at the SLS – PXIII beamline

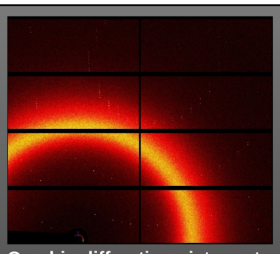

On-chip diffraction picture at room-temperature at the SLS – PXIII beamline

Table: On-chip room-temperature collections report

Protein and organism	A Camelid Nanobody	B Protease I (*Pyrococcus horikhoshii*)	C CCA-adding enzyme (*Planococcus halocryophilus*)	D CCA-adding enzyme (*P. halocryophilus*) + ligand
Beamline	SOLEIL – Proxima 2-A	SLS - PXIII	SLS - PXIII	SLS - PXII
Resolution	2.1 Å	2.15 Å	2.5 Å	2.3 Å
Space group	$P4_32_12$	$P4_12_12$	$P4_32_12$	$P4_32_12$
Crystals collected	9	12	6	14
Crystals selected	1	8	5	5
Oscillation range	0.1°	0.2 °	0.1°	0.2°
Images selected	500	1300	1000	540

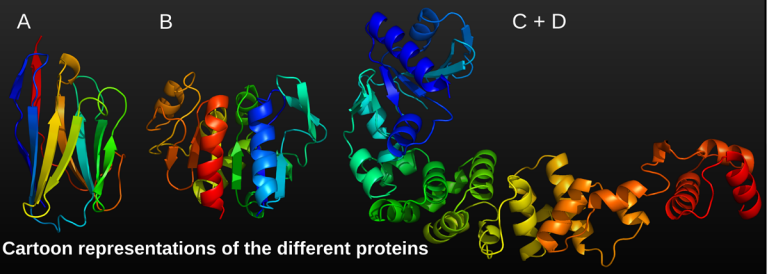

Cartoon representations of the different proteins

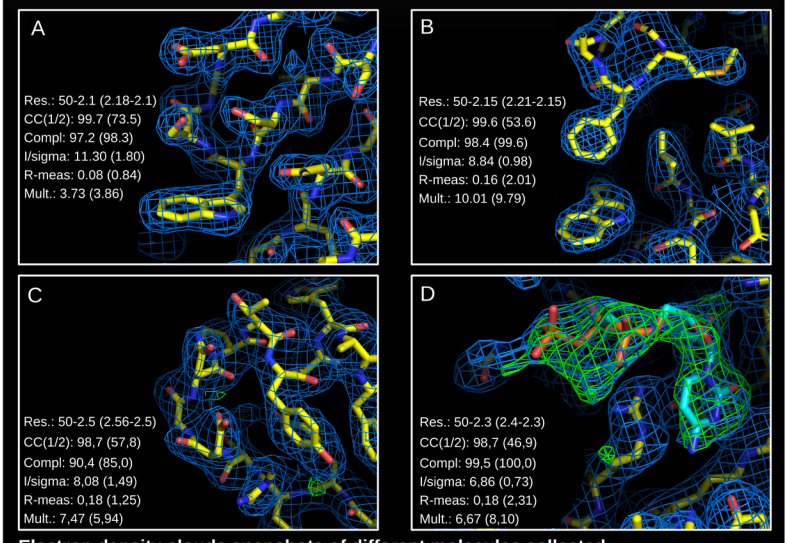

Electron density clouds snapshots of different molecules collected at room-temperature and after molecular replacement

In brief

A chip design dedicated to advanced crystallogenesis strategies:

- Crystallization by counter-diffusion
- Easy crystal visualization by fluo-labelling
- Easy crystal seeding and soaking
- Fast serial analysis at room-temperature

User-friendly, no extra equipment needed!

References

[1] Sauter C, Dhouib K, Lorber B. From macrofluidics to microfluidics in the crystallization of biological macromolecules. *Cryst. Growth Des.*, **2007**, 7, 2247-50.

[2] Pinker F, Brun M, Morin P, Deman AL, Chateaux JF, Oliéric V, Lorber B, Terrier N, Ferrigno R, Sauter C. ChipX: a novel microfluidic chip for counter-diffusion crystallization of biomolecules and in situ crystal analysis at room temperature. *Cryst. Growth Des.*, **2013**, 13: 3333–3340.

CCA-addition in the cold: characterization of the enzyme from *Planococcus halocryophilus*

Raphaël de Wijn[1], Felix Ernst[2], Oliver Hennig[2], Heike Betat[2], Mario Mörl[2], Claude Sauter[1]

[1]Institut de Biologie Moléculaire et Cellulaire, UPR 9002 CNRS, Strasbourg, France
[2]Institute for Biochemistry, Leipzig University, Leipzig, Germany

r.dewijn@ibmc-cnrs.unistra.fr

Introduction

Enzymes from psychrophilic organisms usually achieve catalysis at low temperatures by a reduction of secondary structure elements to increase their flexibility. For CCA-adding enzymes, there is a discrepancy between the need of a tightly controlled flexibility during polymerization and an increased flexibility as a strategy for cold adaptation.

Using biochemical and structural analyses, we investigated the properties of the CCA-adding enzyme (48 kDa) from *Planococcus halocryophilus*, a bacterium from the Arctic permafrost which grows at -15 °C. This enzyme is strongly cold-adapted and catalyzes CCA-addition down to 0°C in vitro.

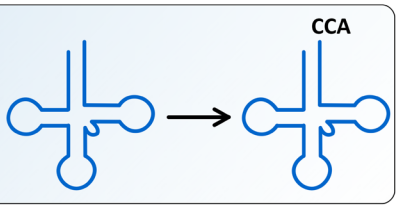

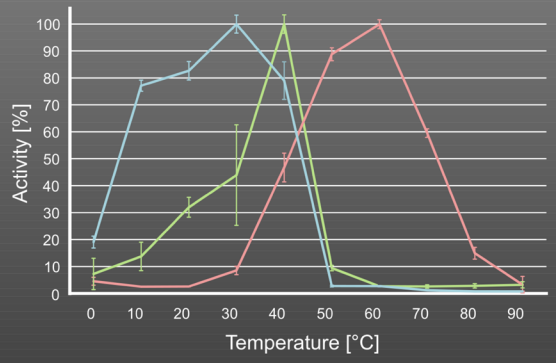

*Pha*CCA psychrophilic — *Bsu*CCA mesophilic — *Gst*CCA thermophilic

The *Pha*CCA enzyme is strongly cold-adapted and catalyzes CCA addition down to 0°C in vitro

A flexible element in *Pha*CCA contributes to cold adaptation

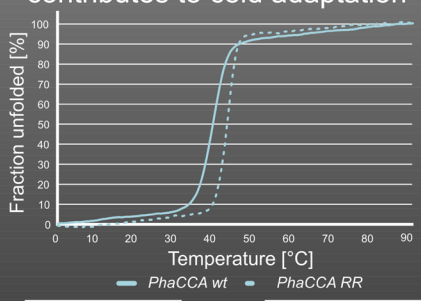

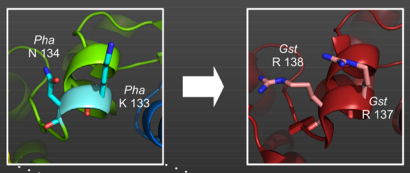

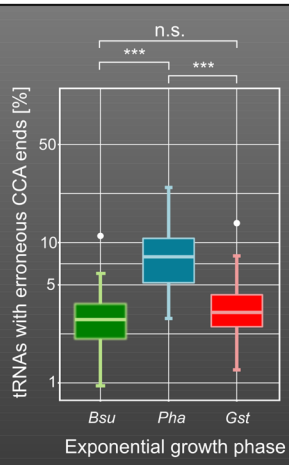

Cold-adaptation of *Pha*CCA has an impact on reaction fidelity

X-ray analysis report

Protein	*Pha*CCA SAD-phasing	*Pha*CCA Apo-form	*Pha*CCA with CTP
Beamline	SLS – PXIII	SOLEIL – Proxima 1	SOLEIL – Proxima 1
Resolution	2.14 Å	1.8 Å	1.85 Å
Space group	$P4_32_12$	$P4_32_12$	$P4_32_12$
Completeness (%)	97.3 (79.8)	99.9 (99.3)	99.8 (99.2)
CC(1/2)	99.9 (1.9)	100 (59)	100 (45.1)
R_{work} / R_{free} (%)	22.8 / 26.9	24.5 / 26.6	19.8 / 22.4

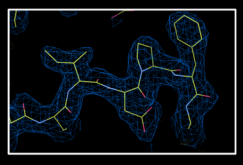

Sulfur-SAD density map

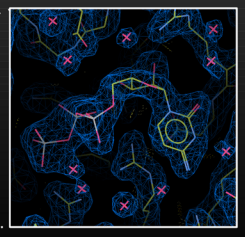

CTP density map

Reduced content of alpha-helices in *Pha*CCA

Structure	*Pha*CCA Apo-form	*Gst*CCA 1MIV	3H3A	4WC2
Source	*Planococcus halocryophilus*	*Geobacillus stearothermophilus*	*Thermotoga maritima*	*Aquifes aeolicus*
Living temp.	Psychrophilic	Thermophilic	Hyperthermo.	Thermophilic
Total helices (%)	49	50	52	56
Helices in body domain (%)	57	62	65	69

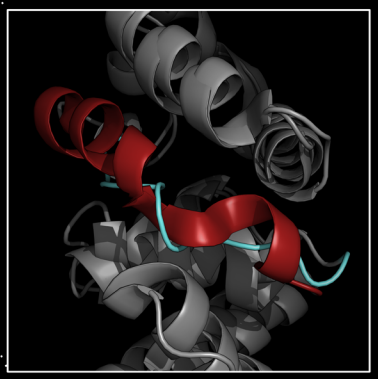

Structural alignment of the body domain of *P. halocryophilus* and *G. stearothermophilus*

Head / neck / body / tail domains

In brief

The remarkable cold adaptation of *Pha*CCA seems to be bought at the cost of a decreased stability which is a result of an increased overall flexibility of the enzyme.

(i) Compared to the thermophilic CCA-adding enzyme from *Geobacillus stearothermophilus*, the structure of the *Pha*CCA enzyme shows a **reduced content of alpha-helices**.

(ii) Residues in the flexible motif C – a region that modulates interdomain movements during CCA addition – contribute to cold adaptation. **Introduction of stabilizing helix capping amino acid residues** from the corresponding motif of a thermophilic enzyme leads to a **thermal stabilization** of *Pha*CCA, increasing the melting temperature by 5°C.

(iii) The price to be paid for such a cold-adaptation of *Pha*CCA is not only a thermal destabilization, but, importantly, a significant **reduction in polymerization fidelity**.

- Ernst F., Erber L., Sammler J., Jühling F., Betat H., Mörl M. Cold adaptation of tRNA nucleotidyltransferases: A tradeoff in a activity, stability and fidelity. *RNA BIOLOGY*, **2018**, 15, 144-155.
- Betat H., Rammelt C., Mörl M. tRNA nucleotidyltransferases: ancient catalysts with an unusual mechanism of polymerization. Cell. *Mol Life Sci.*, **2010**, 67: 1447–1463.

Preparation of micro- and nano-crystals with the Xtal-Controller

Raphaël de Wijn, Bernard Lorber, Claude Sauter
r.dewijn@ibmc-cnrs.unistra.fr

Team « Biology of tRNAs and Pathogenicity »
IBMC UPR 9002 - CNRS - Strasbourg

The Xtal-Controller is a novel instrument for real-time monitoring of nucleation and crystal growth in a closed chamber (Schubert *et al.*, 2017). It is composed of modules working in parallel including an ultra sensitive balance, a Dynamic Light Scattering (DLS) system, a microscope with a camera, a temperature and humidity control unit and two piezo-pumps to add water or crystallant to a micro droplet. This instrument allows control over precise conditions (macromolecule and crystallant concentrations, kinetics) required to grow micro- and nano-crystals of well defined size and suitable for X-FEL analysis. An example of application is reported that deals with a tRNA nucleotidyltransferase from the psychrophilic bacterium *Planococcus halocryophilus* for which crystals were grown that diffracts at high resolution.

R. Schubert, A. Meyer, D. Baitan, K. Dierks, M. Perbandt and C. Betzel. *Real-Time Observation of Protein Dense Liquid Cluster Evolution during Nucleation in Protein Crystallization. CGD.*, **17** (2017), 954-958

The Xtal-Controller instrument

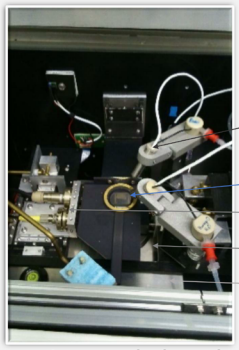

Experimental chamber

- Microscope optics
- Piezo-pump
- Humidity control
- 22 mm coverslip
- DLS optics
- Ultra sensitive balance
- Temperature control

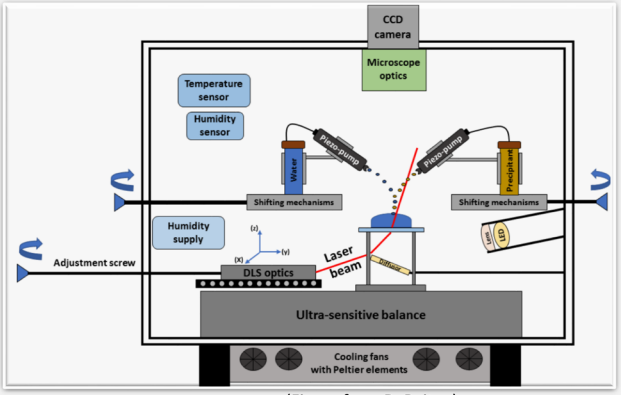

(Figure from D. Baitan)

Experimental protocol and Results

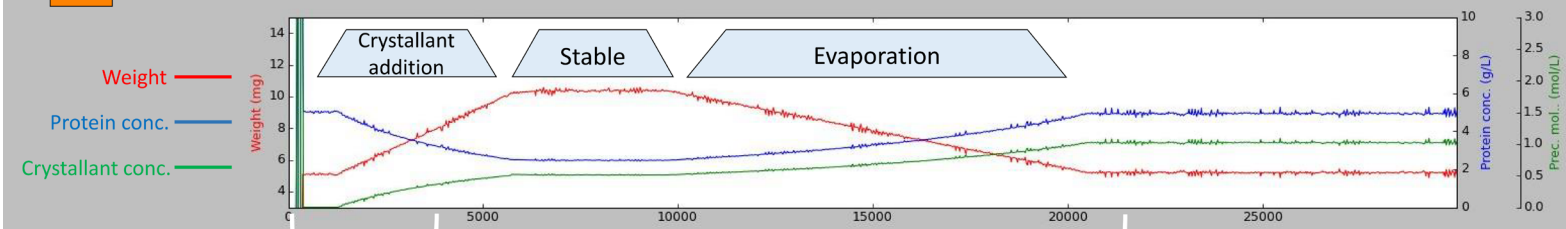

Live monitoring

Dynamic Light Scattering

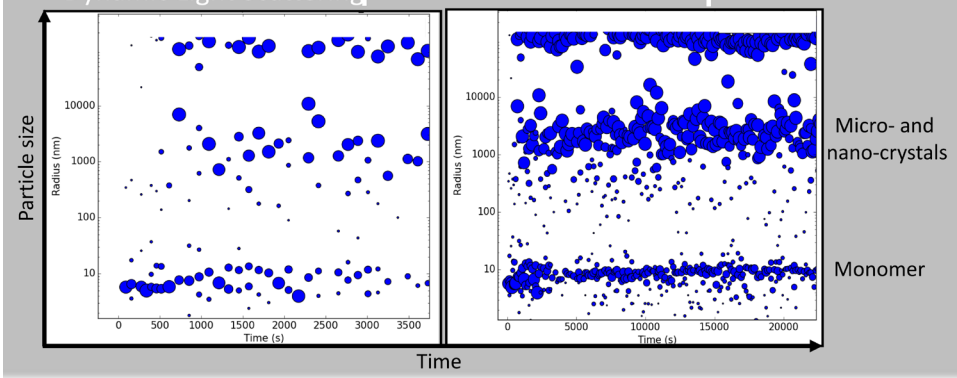

Optical microscopy (5µL drop)

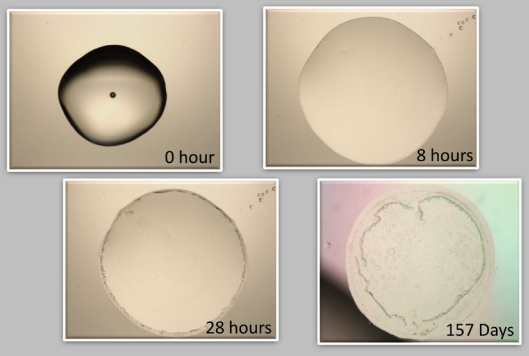

A precipitation case

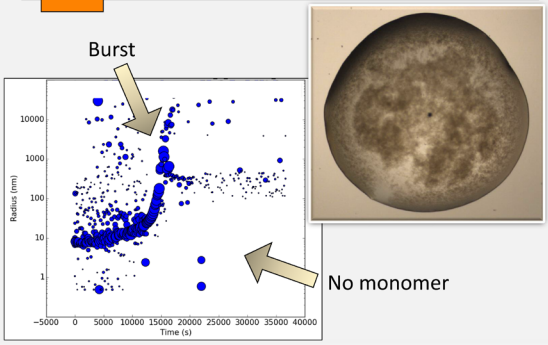

We completed the first step with the Xtal-Controller, which was the growth of quality crystals (in highly controlled conditions) of an enzyme of interest. Our next step before the preparation of samples suitable for X-FEL analysis is to characterize the different populations observed with the DLS module by electron microscopy.

The Xtal-Controller is an investment supported by the MitoCross LabEx.

X-ray diffraction

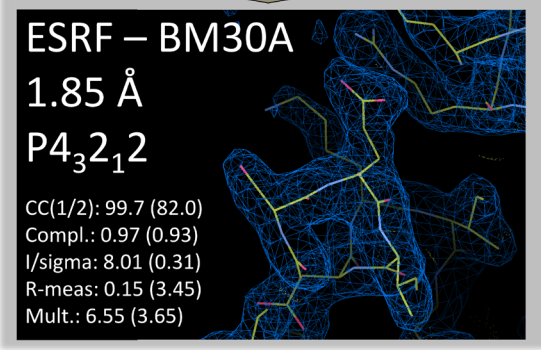

De l'imagerie 3D au Drug Design

Raphaël de Wijn
r.dewijn@ibmc-cnrs.unistra.fr

Soutien à domicile en sciences pour des élèves de collège et lycée
Tuteur de licence Franco-Allemande
Monitorat et encadrement de mémoire pour les étudiants Franco-Allemand

Stage à l'IBMC
Stage à l'Université de Tokyo
Réseau BIOTechno Stras'Air

2010 ... | 2013 | 2014 | 2015 | 2016 | 2017

Baccalauréat et Abitur
Mémoire de licence
Mémoire de master
Licence en Biologie Parcours Franco-Allemand
Master en Biochimie et Génétique Moléculaire, Parcours Franco-Allemand
Doctorat

Enseignement **Communication**
Biochimie **Biologie structurale**

L'Organisation Mondiale de la Santé a relancé un message le 27 Avril dernier pour rappeler aux communautés scientifiques et politiques que le développement de nouveaux antibiotiques est une urgence sanitaire.
La synthèse protéique est un processus nécessaire à toute vie. Une partie essentielle de cette machinerie sont les aminoacyl-ARNt synthétases qui permettent le chargement des ARNt avec leur acide aminé correspondant. De par leur essentialité et leur grande spécialisation, ces enzymes sont de très bonnes cibles pour le développement de nouveaux antibiotiques. Deux des projets de ma thèse consistent en le développement et l'étude de nouvelles molécules par des méthodes biochimiques et de biologie structurale.

Collaboration avec le Muséum National d'Histoire Naturelle, Paris

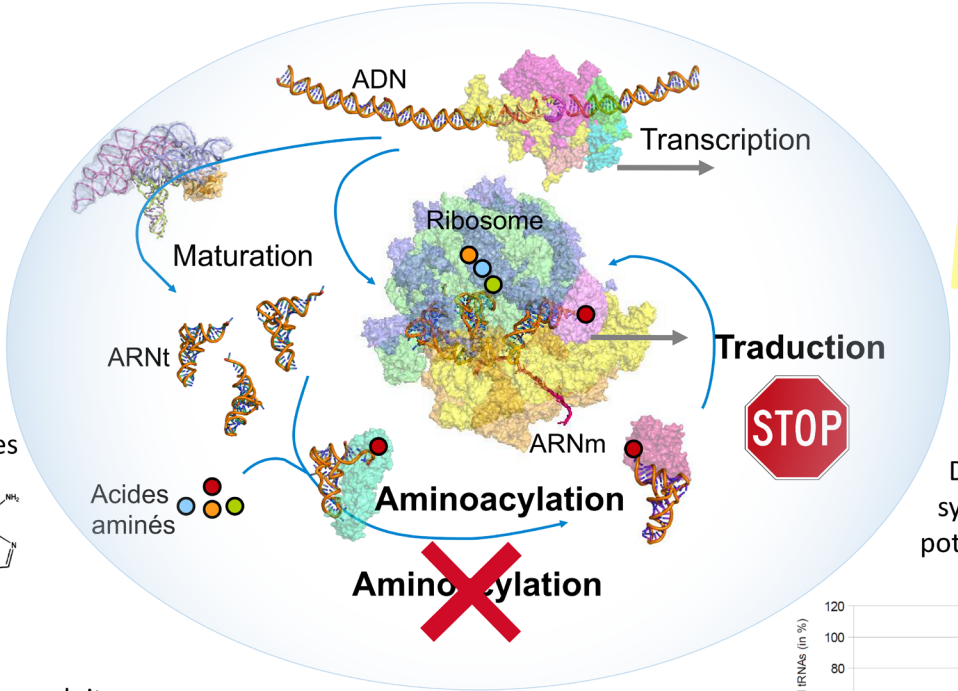

Collaboration avec l'Université de Tokyo

Substrat naturel des aspartyl-ARNt synthétases

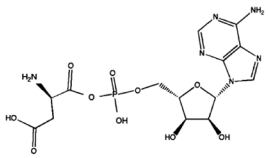

Microcine C, inhibiteur produit par une souche d'*Escherichia coli*

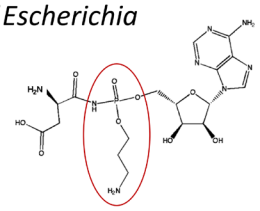

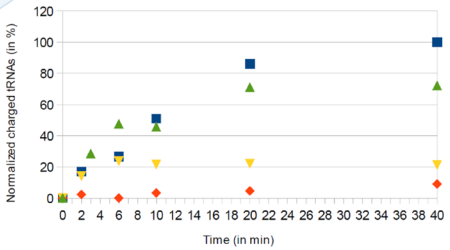

Plusieurs montrent des résultats prometteurs

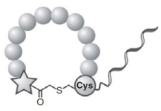

Design de peptides synthétiques comme potentiels antibiotiques

Equipe Biologie des ARNt et pathogénicité, IBMC UPR 9002 – CNRS

Université de Strasbourg
institut de biologie moléculaire et cellulaire
Les Doctoriales d'Alsace 2017
Université franco-allemande Deutsch-Französische Hochschule
INVESTISSEMENTS D'AVENIR

Crystallogenesis studies of bacterial aminoacyl-tRNA synthetases as potential targets for drug design

Raphaël de Wijn, Bernard Lorber & Claude Sauter

Architecture et Réactivité de l'ARN, Institut de Biologie Moléculaire et Cellulaire (IBMC-CNRS), Université de Strasbourg, France

Context

Aminoacyl-tRNA synthetases (aaRSs) are part of the protein synthesis machinery and catalyze the attachment of amino acids to tRNAs. Aminoacyl-tRNA are then carried to the ribosome by elongation factors to be used in translation [1]. Because aaRSs are essential enzymes with a high specificity for their substrates, they constitute good targets for drug design.
This work is focused on bacterial aspartyl-tRNA synthetases (AspRS), aaRSs specific for L-aspartate, with *E. coli* and *T. thermophilus* enzymes as bacterial models and *Pseudomonas aeruginosa* enzyme as potential drug design target. We have initiated the biochemical and structural characterization of two types of inhibitors: a natural antibiotic produced by *E. coli* strains, named Microcin C and targeting the catalytic site of AspRSs, and synthetic peptides selected against these types of enzymes. In both cases, a preliminary optimization of crystal production was necessary in the preparation of soaking experiments. Different crystallogenesis approaches have been selected to prepare suitable crystals.

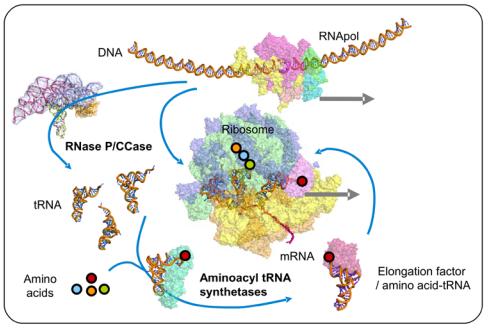

My strategy

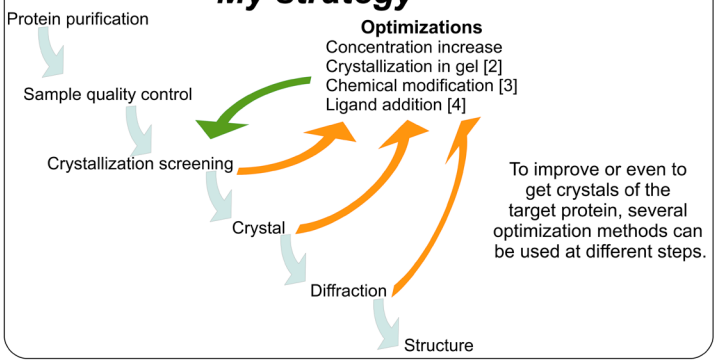

To improve or even to get crystals of the target protein, several optimization methods can be used at different steps.

Crystallization in gel

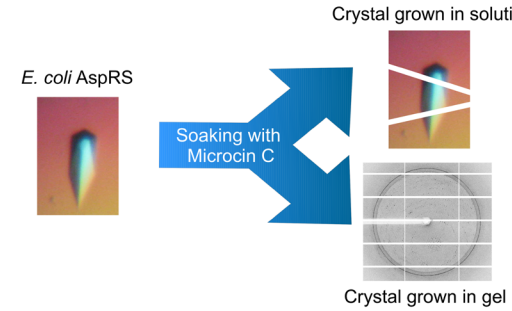

The aim and utility of this technique is to grow bigger, better ordered crystals in convection-free conditions and to protect then during soaking and freezing.

First crystals of my main target P. aeruginosa *AspRS*

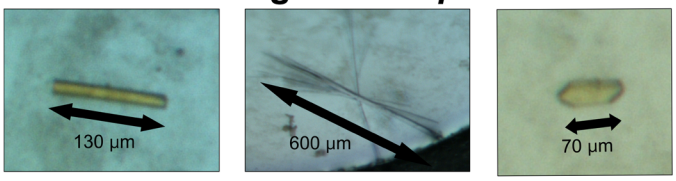

Crystals of the *P. aeruginosa* (*Pa*) enzyme before optimization

Protein methylation of the T. thermophilus *AspRS*

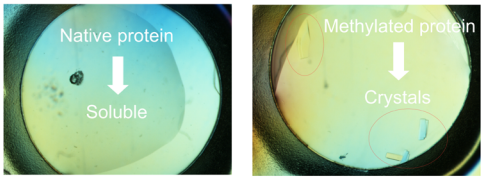

Methylation of the lysines will have as a result to change the surface properties of the protein, thus impacting solubility and crystallizability.

Looking at a natural antibiotic

Cooperation with the Muséum National d'Histoire Naturelle, Paris

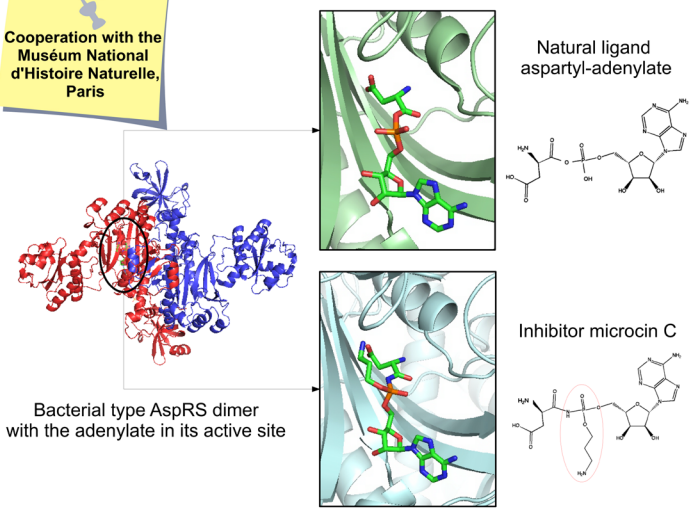

Bacterial type AspRS dimer with the adenylate in its active site

Our goal is to understand if the addition of a propylamine arm in microcine C improve the affinity compared to conventional adenylate analogs.

Designing synthetic peptides as potential antibiotics

Cooperation with the University of Tokyo, Tokyo

RaPID system: in vitro selection of synthetic macrocyclic peptide [5]

Crystal quality improvement

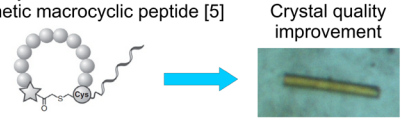

Activity tests by aminoacylation assays

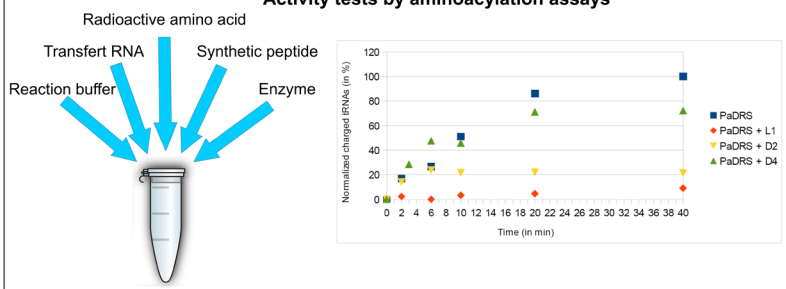

Six peptides have already been selected, three of them showing promising inhibitory activity. They will now be used for cocrystallization with the target.

References

[1] M. Ibba, C. Francklyn and S. Cusack. *Aminoacyl-tRNA Synthetases*, Goergetown, TX: Landes Biosciences. 2005.

[2] B. Lorber, C. Sauter, A. Théobald-Dietrich, A. Moreno, P. Schellenberger, M.-C. Robert, B. Capelle, S. Sanglier, N. Potier, R. Giegé. *Crystal growth of proteins, nucleic acids, and viruses in gels. Progr. Biophys. Mol. Biol.*, **101** (2009), 13-25.

[3] Y. Kim *et al. Large-scale evaluation of protein reductive methylation for improving protein crystallization. Nature Methods*, **5** (2008), 853.

[4] C.J. Hipolito, Y. Tanaka, T. Katoh, O. Nureki, H. Suga. *A macrocyclic peptide that serves as a cocrystallization ligand and inhibits the function of a MATE family transporter. Molecules*, **18** (2013), 10514-10530.

[5] T. Morioka, N.D. Loik, C.J. Hipolito, Y. Goto, H. Suga. *Selection-based discovery of macrocyclic peptides for the next generation therapeutics. Current opinion in chemical biology*, **26C** (2015), 34-41.

In brief

- Several methods are used on ongoing projects to improve crystal quality for X-ray diffraction analyses
- The characterization of microcin C binding properties is in progress
- Novel synthetic peptides have been selected as promising leads for drug design and will be used for cocrystallization assays

16.3 Liste des stagiaires encadrés

- Léa Naudet, en 2nd année de licence Franco-Allemande en Sciences de la Vie, pendant quatre semaines en stage libre.
- Nicola Thome, ERASMUS de Leipzig en 3ème année de licence, pendant sept semaines pour son mémoire de licence (« Bachelorarbeit »).
- Victor Mac, en 1ère année du master “Biologie structurale, bioinformatique et biotechnologies”, pendant trois semaines pour son stage de M1.
- Kévin Rollet, en 1ère année du master “Biologie et génétique moléculaire”, pendant sept semaines pour son stage de M1.

16.4 Organisation d’évènements scientifiques ou pour les doctorants

- The networking meet-up on transversal skills of PhD graduates, Strasbourg (France), 9 novembre 2017: membre du comité organisateur.
- 31st Rhine-Knee Regio-meeting, Munster (France), September 2017: septembre 2017: membre du comité organisateur.
- Forum BIOTechno Grand-Est 2017, Strasbourg (France), 2 juin 2017: responsable du comité en charge des intervenants, responsable de la communication internationale, membre du comité pour les levées de fonds et de la trésorerie.
- Membre du bureau de l’association des doctorants internationaux de Strasbourg STRAS’AIR pendant un an.

17 Résumé détaillé en français

Les aminoacyl-ARNt synthétases (aaRS) ainsi que les CCA ARNt nucléotidyl-transférases (ou CCases) sont des enzymes essentielles qui participent aux premières étapes de la synthèse protéique ou traduction. Les CCases utilisent du CTP et de l'ATP comme substrats lors de la maturation des ARN de transfert (ARNt) pour former la queue CCA à leur extrémité 3'. En présence d'ATP, les aaRS activent un acide aminé sous forme d'adénylate et le lient à l'extrémité 3' CCA de l'ARNt correspondant. Les aminoacyl-ARNt résultants sont ensuite transportés par les facteurs d'élongation au ribosome qui va incorporer les acides aminés aux chaînes polypeptidiques naissantes.

De par leur caractère essentiel et leur spécificité de substrat, les aaRS constituent des cibles de choix pour la conception de médicaments. Une partie de mon travail a consisté en l'étude biochimique et la caractérisation structurale du mode de liaison de deux familles d'inhibiteurs des aspartyl-ARNt synthétases (AspRS) qui lient spécifiquement le L-aspartate. La première est représentée par un antibiotique naturel produit par certaines souches d'*E. coli* pour bloquer le site catalytique de l'AspRS de souches concurrentes (collaboration avec la professeure Sylvie Rebuffat du Musée National d'Histoire Naturelle, Paris) ; la seconde est une série de peptides synthétisés chimiquement qui ont été sélectionnés contre l'AspRS de l'agent pathogène humain opportuniste *Pseudomonas aeruginosa* (collaboration avec le professeur Hiroaki Suga de l'Université de Tokyo).

Mon travail a mené à la mise au point d'un protocole de purification des AspRS de *Thermus thermophilus* et de *P. aeruginosa*, pour assurer leur qualité et leur quantité, et débuter la production de cristaux. J'ai fait le choix de travailler sur l'enzyme de *T. thermophilus,* analogue à celle d'*E. coli* mais plus stable et facile à manipuler, afin de réaliser l'étude structurale de l'antibiotique naturel produit par des souches d'*E. coli.*

En parallèle des expériences de cristallisation, j'ai également caractérisé des peptides sélectionnés pour leurs propriétés de fixation à l'AspRS de *P. aeruginosa*. Les tests enzymatiques ont indiqué que quatre des six peptides sélectionnés avaient un effet

inhibiteur intéressant, j'ai donc mené une étude cinétique plus poussée de ces inhibiteurs. Cela m'a permis de caractériser l'inhibition et de définir des conditions de cristallisation en cours d'analyse pour une future optimisation de leur mode d'action et en vue d'essais d'inhibition sur culture cellulaire.

J'ai également été impliqué dans un programme de coopération franco-allemand PROCOPE avec l'équipe du Professeur Mario Mörl (Université de Leipzig) portant sur l'étude structurale des CCases de différents organismes extrémophiles. Ceci m'a conduit à résoudre la structure cristallographique de l'enzyme de *Planococcus halocryophilus*, une bactérie psychrophile, capable de vivre à très basse température. En plus de la structure de l'apo-enzyme, j'ai également obtenu celle du complexe avec le substrat CTP. Ces structures ont été élucidées à haute résolution (1,8 – 2 Å) et par différentes méthodes cristallographiques (remplacement moléculaire et sulfur-SAD). Les tests de co-cristallisation ou de trempage des cristaux de l'enzyme avec le substrat ATP n'ont pas aboutis, ce qui montre que ce dernier ne se fixe pas seul mais nécessite très probablement la présence préalable de l'ARNt.

Pour mener à bien ces études structurales, l'équipe de recherche s'est tournée vers une technologie innovante et une technologie plus rationnelle de préparation des cristaux de molécules biologiques appelée Xtal Controller 900 (Xtal-Concepts GmbH, Hambourg) ; elle permet de manipuler une goutte de cristallisation de quelques microlitres en jouant sur les concentrations de biomolécule et d'agent cristallisant (grâce à des microinjecteurs), tout en suivant l'évolution du système en direct par diffusion de la lumière (détection d'événements d'agrégation ou de nucléation, de formation de nanocristaux) et vidéo-microscopie (suivi de la croissance cristalline), le tout dans une enceinte thermostatée et à humidité contrôlée.

L'enzyme CCase m'a aussi servi de cobaye pour la mise au point de méthodes et stratégies de cristallisation, mon objectif étant de continuer à améliorer la qualité des données structurales dont je dispose. Suite à ma participation à une école internationale, j'ai introduit au laboratoire deux méthodes qui ont montré leur efficacité : une méthode de marquage fluorescent des protéines (dite « Trace Fluorescent Labelling ») qui facilite l'identification de cristaux lors du criblage initial, ainsi qu'une méthode de microseeding (dite « Microseed Matrix Screening ») pour augmenter le nombre de conditions de cristallisation. J'ai aussi exploité un nouveau concept de puces microfluidiques développées dans l'équipe pour déterminer la structure de

plusieurs macromolécules, dont la CCase, à température ambiante par l'approche de cristallographie sérielle.

Comme je l'ai indiqué plus haut, notre équipe dispose de la dernière version du Xtal Controller. J'explore les possibilités qu'offre cette technologie pour l'étude de la cristallogenèse et un meilleur contrôle de la production de cristaux en vue de leur exploitation en biologie structurale. Ceci m'a conduit à étudier l'effet de différents agents cristallisants sur divers modèles protéiques, mais aussi d'un nouvel agent nucléant, un complexe de lanthanide facilitant la nucléation et la croissance de cristaux biologiques. Ces expériences se font sur de protéines d'intérêt biologique, dont ma CCase et des protéines fournis par nos collaborateurs (équipe du Dr Eric Girard à l'Institut de Biologie Structurale Grenoble), et j'ai pu obtenir des cristaux pour plusieurs d'entre elles et les ai étudiés sous rayonnement synchrotron.

Raphaël DE WIJN

Application des nouvelles approches de cristallisation et de cristallographie sérielle à l'étude structurale de complexes enzymes : ARNt

Résumé en français

Cette thèse porte sur deux aspects complémentaires, le développement et l'implémentation de nouvelles approches de cristallisation et de cristallographie sérielle ainsi que leur mise en oeuvre dans l'étude structurale de complexes enzymes : ARNt. La cristallographie est la méthode la plus employée en biologie structurale, mais elle présente encore des points délicats. Plusieurs méthodes avancées ont été déployées dans ce travail pour y pallier qui ont conduit à la résolution de la structure de l'ARNt nucléotidyltransférase du psychrophile *Planococcus halocryophilus* et à l'étude de son adaptation structurale au froid; des puces microfluidiques de cristallisation qui ont servi à la résolution de plusieurs structures à température ambiante par cristallographie sérielle; enfin le Xtal Controller utilisé pour l'étude d'évènements de nucléation et de croissance cristalline dans un but de préparation d'échantillons pour analyse sous rayonnement XFEL. Entre autres systèmes biologiques, cette thèse présente la caractérisation de deux familles d'inhibiteurs visant les aspartyl-ARNt synthétases, notamment du pathogène *Pseudomonas aeruginosa*.

Mots clés :
Biologie structurale ; Cristallographie sérielle ; Cristallogénèse ; Puces microfluidiques ; Xtal Controller ; Organisme psychrophile ; Organisme pathogène

English abstract

This thesis focuses on two complementary aspects, the development and implementation of new approaches of crystallization and of serial crystallography as well as their use in the structural study of enzymes/tRNA complexes. Crystallography is the most used method in structural biology, but it presents delicate points. Different methods were implemented in this work to overcome these points, which led to the resolution of the structure of the CCA-adding enzyme of the psychrophilic organism *Planococcus halocryophilus* and to the study of its structural adaptation to the cold; novel microfluidic crystallization chips that have been used for the resolution of several structures by serial crystallography at room-temperature; finally the Xtal Controller used for the study of nucleation and crystal growth events with the purpose of preparing samples for analysis under XFEL radiation. Among other biological systems, this thesis presents the study and characterization of two families of inhibitors targeting aspartyl-tRNA synthetases, including the one of the pathogenic organism *Pseudomonas aeruginosa*.

Keywords :
Structural biology ; Serial crystallography ; Crystallogenesis ; Microfluidic chips ; Xtal Controller ; Psychrophilic organism ; Pathogenic organism